
**Using zebrafish as a model to study
acute and chronic mucosal inflammation**

Fränze Progatzky

**Imperial College London
Department of Life Sciences**

**Thesis Submitted for the degree of
Doctor of Philosophy
2014**

Declaration of originality

I declare that all of the work presented in this thesis is my own, and that all else, information, data, results, figures and ideas from another source or from collaborations have been appropriately referenced or acknowledged.



Fränze Progatzky

September 2014

Copyright declaration

The copyright of this thesis rests with the author and is made available under a Creative Commons Attribution Non-Commercial No Derivatives licence. Researchers are free to copy, distribute or transmit the thesis on the condition that they attribute it, that they do not use it for commercial purposes and that they do not alter, transform or build upon it. For any reuse or redistribution, researchers must make clear to others the licence terms of this work.

Abstract

Mucosal barriers of the intestine and the lung offer the first line of protection in the host defence mechanisms against ingested and inhaled antigens. During the 20th century, the incidence of chronic mucosal inflammatory diseases of unknown aetiology such as inflammatory bowel disease, chronic obstructive pulmonary disease and pulmonary fibrosis has risen markedly in the Western World. This PhD project used zebrafish, *Danio rerio*, as a model organism to study acute and chronic mucosal inflammatory responses in the intestine and the gills induced respectively by dietary components and respiratory irritants/injury associated with human disease.

A single exposure to a diet rich in cholesterol (HCD) results in the accumulation of myeloid cells in the intestine in both zebrafish and mice. HCD-induced immune cell accumulation is dependent on NFκB activation and the microbiota and acute exposure to HCD leads to caspase-1 activation in intestinal epithelial cells. Extended HCD results in localised, inflammation-dependent, functional dysregulation. This model reveals a novel route by which dietary cholesterol can initiate intestinal inflammation.

Acute exposure to cigarette smoke and silica particles leads to an acute inflammatory response in zebrafish gills similar to that seen in mammalian lungs. Despite gill tissue remodelling following long-term exposure to these irritants, no collagen deposition, *i.e.* fibrosis, could be detected. When combined with severe tissue damage induced by cryoinjury, exposure to silica delayed wound-healing responses and again no fibrotic changes were observed. Preliminary gene expression analysis by RNA-seq showed altered gene expression of similar genes to those involved during wound-healing processes in mammals. These results provide a basis for further investigations such as extensive comparisons of gene expression with fibrosis in mammals.

Overall, these findings demonstrate that the zebrafish is a valuable and pathophysiologically relevant model in which to study mucosal inflammatory diseases.

Acknowledgements

There are several important people who substantially influenced my work throughout the past three years, made this time so enjoyable and helped me to grow and mature.

I would like to thank Maggie, for invaluable scientific and personal support, guidance and inspiration. For teaching me scientific rigour, sharing enthusiasm for science and helping me to develop my independence and confidence.

Laurence for unconditional support and guidance on a daily basis, encouragement, inspiration and enthusiasm, of both the scientific and personal kind.

Jon for guidance, support, for help obtaining funding for this project and for perspective throughout and beyond this PhD.

Terry for guidance, inspiration, expert pathologist's eyes and for the constructive early (8.30 am) Monday morning meetings.

Clare Lloyd and Cristina Lo Celso for thorough and detailed review of my progress throughout my PhD and constructive and helpful comments.

Birgit Jung and Jürgen Schymeinsky for an invaluable collaboration beyond financial support.

The present and past members of the Dallman lab for making endless hours in the fish room, in the lab and in the pub so enjoyable and memorable; in particular Navjyot Sangha for setting up the scene for such an exciting project, Rachel Vaux for deciding to go for silica, Natalie Andrews for convincing me about FLIM, Nagisa Yoshida for imaging skills, Marie-Christine Ramel for *in situ* insights and Kathryn Charlwood and Marie McBrien for taking over responsibilities.

Tobias Hildebrandt, Werner Rust and Germán Leparc for performing RNA-seq, Geraint Barton for help with RNA-seq data analysis, Julian Marchesi for performing microbiome analysis, Lorraine Lawrence for help with histology, Martin Spitaler and Stephen Rothery for support with confocal imaging, Catherine Simpson and Jane Srivastava for expertise in flow cytometry, Marie-Christine Jones for help with silica particle size characterisation and critical comments.

A special thank you to Finn, Mutti, Oma, Wolfgang and Renate for unconditional support and belief in me.

Funding

I am grateful to both the Biotechnology and Biological Science Research Council and Boehringer Ingelheim for funding this project.

Abbreviations

amy	Amylase
APC	Antigen Presenting Cell
ASC	Apoptosis-associated Speck-like Protein containing a CARD
α -SMA+	α -Smooth Muscle Actin-positive
ATI	Alveolar Type I cell
ATII	Alveolar Type II cell
CARD	Caspase Recruitment Domain
Ccr	C-C chemokine receptor
CD	Cluster of differentiation
cell	Carboxyl ester lipase 1
c/mL	Cigarettes/mL
col	Collagen
COPD	Chronic Obstructive Pulmonary Disease
CONV	Conventionally
cpa4	Carboxypeptidase A4
cpb1	Carboxypeptidase B1
CRISPR/Cas	Clustered Regularly Interspaced Short Palindromic Repeat/ CRISPR-associated
csf1ra	Colony stimulating factor 1 receptor, a
CSW	Water containing cigarette smoke extract
Ct	Cycle threshold
ctgf	Connective tissue growth factor
ctnbl	Catenin (cadherin-associated protein) β 1
CU	Cardiff University
DAMPs	Damage-Associated Molecular Pattern molecules
DAPI	4',6-diamidino-2-phenylindole
DCs	Dendritic cells
de	Differentially expressed
dH2O	Deionised water
dpf	Days post-fertilisation
dpi	Days post-injury
DSS	Dextran Sodium Sulphate

dsRed	<i>Discosoma</i> Red fluorescent protein
ECM	Extracellular Matrix
EDTA	Ethylenediaminetetraacetic acid
EGFP	Enhanced Green Fluorescent Protein
ela	Elastase
EMT	Epithelial-Mesenchymal Transition
EndoMT	Endothelial-Mesenchymal Transition
FACS	Fluorescence Activated Cell Sorting
fdr	False discovery rate
FFPE	Formalin Fixed and Paraffin Embedded
Fn1a	Fibronectin a
Fgf	Fibroblast growth factor
FITC	Fluorescein
FLICA	Fluorescent Labeled Inhibitor of Caspase Activity
FLIM	Fluorescence Life-time Imaging Microscopy
fms	(previous name for) colony stimulating factor 1 receptor, a
Foxp3	Forkhead box p3
FSC	Forward Scatter
FSC-A	Forward Scatter - Area
FSC-H	Forward Scatter - Height
GALT	Gut Associated Lymphoid Tissue
gata2	GATA binding protein 2
GF	Germ Free
GFP	Green Fluorescent Protein
GWAS	Genome-Wide Association Studies
HCD	High Cholesterol Diet
H&E	Haematoxylin and Eosin
HFD	High Fat Diet
HRP	Horseradish Peroxidase
IBD	Inflammatory Bowel Disease
ICL	Imperial College London
IECs	Intestinal Epithelial Cells
Ifabp	Intestinal fatty acid binding protein

IFN	Interferon
Ig	Immunoglobulin
IL	Interleukin
ILCs	Innate Lymphoid Cells
INKT	Invariant NKT
krt	Keratin
lck	LCK proto-oncogene, Src family tyrosine kinase
lcp1	L-plastin
LPS	Lipopolysaccharide
LTB ₄	Leukotriene B4
lyn	LYN proto-oncogene, Src family tyrosine kinase
lysC	Lysozyme C
MALT	Mucosal Associated Lymphoid Tissue
M-cells	Microfold cells
mfi	Median Fluorescence intensity
MLNs	Mesenteric Lymph Nodes
MMP	Matrix Metalloproteinase
MO	Morpholino oligonucleotides
mpf	Month post-fertilisation
mpx	Myeloperoxidase
msxb	Muscle segment homeobox B
Myd88	Myeloid differentiation factor 88
NAFLD	Non-Alcoholic Fatty Liver Disease
NASH	Nonalcoholic Steatohepatitis
NAI	NFkB activation inhibitor
NETs	Neutrophil Extracellular Traps
NFkB	Nuclear Factor Kappa-light-chain-enhancer of activated B cells
nfsB	Nitroreductase
NK cell	Natural Killer cell
NOD	Nucleotide-binding Oligomerisation Domain
NLR	NOD-like receptors
NPC1L1	Niemann-Pick C1-Like 1
n.s.	Non-significant

NTC	No Template Control
OTU	Operational Taxonomic Unit
OVA	Ovalbumin
PAMPs	Pathogen-Associated Molecular Pattern molecules
PAS	Periodic-Acid-Schiff
PBS	Phosphate Buffered Saline
PBS-T	Phosphate Buffered Saline with 0.1% Tween
PCA	Principal Component Analysis
PDGF	Platelet-Derived Growth Factor
PFA	Paraformaldehyde
PSR	Picro-Sirius-Red
PYD	Pyrin Domain
qRT-PCR	quantitative Real-Time PCR
rag2	Recombination activating gene 2
RNA-seq	RNA sequencing
postnb	Periostin b
PRR	Pattern Recognition Receptor
RegIII γ	Regenerating islet-derived 3-gamma
RIN	RNA Integrity Number
RLNs	Regional Lymph Nodes
ROS	Reactive Oxygen Species
SCFAs	Short-Chain Fatty Acids
SD	Standard Deviation
SEM	Standard Error of the Mean
SFA	Saturated fatty acids
sHCD	Sterile HCD
SNPs	Single Nucleotide Polymorphisms
spp1	Osteopontin
SSC	Side scatter
sZM	Sterile ZM
TALEN	Transcription Activator-Like Effector Nucleases
TCR	T cell receptor
Tg	Transgenic

TGF	Transforming Growth Factor
Th	T helper
TLR	Toll-like receptor
TNBS	2,4,6-trinitrobenzene sulphonic acid
tnc	Tenascin C
TNF	Tumor-Necrosis Factor
tp63	Transformation-related protein 63
Treg	Regulatory T cell
try	Trypsin
TUNEL	Terminal deoxynucleotidyl transferase mediated dUTP nick-end labelling
UFA	Unsaturated fatty acids
UC	Ulcerative Colitis
vegfaa	Vascular endothelial growth factor A a
vim	Vimentin
Vs.	Versus
WT	Wild Type
WKM	Whole kidney marrow
ZFIN	Zebrafish Model Organism Database
ZM	ZM standard zebrafish larval control diet

Table of Contents

Declaration of originality	2
Copyright declaration	2
Abstract	3
Acknowledgements	4
Funding	4
Abbreviations	5
Table of Contents	10
List of Tables	13
List of Figures	13
List of Appendices	15
Chapter 1 Introduction	17
1.1 Immune homeostasis of mucosal epithelial barriers.....	17
1.1.1 General structure and function of mucosal epithelial barriers	17
1.1.1.1 Mucus layer	19
1.1.1.2 Epithelial cell barrier	19
1.1.1.3 Microbiota	20
1.1.1.4 Mucosal immune system	22
1.1.1.4.1 Inducers: PAMPs and DAMPs	23
1.1.1.4.2 Sensor cells and PRRs at mucosal barriers.....	23
1.1.1.4.3 Pro- and anti-inflammatory mediators.....	28
1.1.1.4.4 Effector cells at mucosal barriers	28
1.1.2 Organ specific structure and function of mucosal epithelial tissues	35
1.1.2.1 Intestinal epithelium	35
1.1.2.2 Respiratory epithelium	37
1.2 Chronic inflammation of mucosal barriers	39
1.2.1 Intestinal mucosal inflammation	41
1.2.2 Respiratory mucosal inflammation	42
1.2.3 Breakdown of components of mucosal barriers during the pathogenesis of mucosal inflammatory conditions	43
1.2.3.1 Impaired mucus layer during mucosal inflammatory pathologies	44
1.2.3.2 Impaired epithelial cell integrity during mucosal inflammation	44
1.2.3.3 Role of the microbiota in mucosal inflammation	45
1.2.3.4 Exacerbated inflammatory responses during mucosal pathologies.....	46

1.3	Animal models of mucosal inflammation	47
1.3.1	Animal models of intestinal inflammatory diseases	48
1.3.2	Animal models of pulmonary inflammatory diseases.....	48
1.3.3	Limitations of current animal models of mucosal inflammation and need for alternative approaches.....	49
1.4	Zebrafish as a model of mucosal inflammation	49
1.4.1	Zebrafish intestine.....	52
1.4.1.1	Structure of mucosal intestinal tissue.....	52
1.4.1.2	Mucosal tissue responses during intestinal disease.....	53
1.4.2	Zebrafish gills.....	53
1.4.2.1	Structure of mucosal gill tissue.....	54
1.4.2.2	Mucosal tissue responses during gill disease.....	57
1.4.3	Zebrafish intestine as a model of intestinal inflammatory disease.....	58
1.4.4	Zebrafish gills as a model of lung inflammatory diseases.....	58
1.5	Aims	59
Chapter 2 Material and Methods		61
2.1	Animal maintenance	61
2.2	Feeding experiments	62
2.2.1	Preparation of experimental diets.....	62
2.2.2	Feeding of zebrafish and treatment with inhibitors.....	63
2.2.3	Analysis of food uptake and intestinal transit.....	64
2.2.4	Mouse gavage.....	64
2.3	Germ-free zebrafish	64
2.4	Morpholino treatment	65
2.5	Exposure to cigarette smoke and silica particles	65
2.6	Cryoinjury	66
2.7	Staining of zebrafish larvae	66
2.7.1	Fixation of zebrafish larvae.....	66
2.7.2	Whole mount staining of Zebrafish larvae with L-plastin antibody.....	67
2.7.3	Oil Red O staining.....	67
2.8	Histology	67
2.9	Active caspase-1 staining (FLICA)	68
2.10	Horseradish peroxidase staining	68
2.11	Cholesterol uptake assay using BODIPY-cholesterol	68
2.12	Imaging	69
2.12.1	Stereomicroscopy.....	69
2.12.2	Epifluorescence microscopy.....	69

2.12.3	Confocal microscopy	69
2.12.4	Light microscopy	69
2.12.5	Widefield microscopy and FLIM acquisition	69
2.12.6	Image analysis and quantification of cells	70
2.13	Flow cytometry.....	70
2.14	Quantitative Real-Time PCR (qRT-PCR).....	71
2.15	454-pyrosequencing	73
2.16	RNA-seq analysis	73
2.17	Statistical analysis	74
 Chapter 3 HCD-induced intestinal inflammation		76
3.1	Introduction	76
3.2	Aims	84
3.3	Results	85
3.3.1	The effect of HCD on accumulation of myeloid cells in the intestine of adult zebrafish and mice	85
3.3.2	Signal 1 of HCD-induced inflammasome activation	93
3.3.3	Examination of cellular origin of inflammasome activation consequent to HCD....	108
3.3.4	Analysis of pathologies following extended HCD.....	120
3.4	Summary	129
3.5	Discussion	130
3.5.1	Conservation of HCD-induced acute inflammation between zebrafish and mice and its relevance to humans.....	130
3.5.2	Constitutive NFkB activation delivers signal 1 of HCD-induced inflammasome activation in the intestine of larval zebrafish	132
3.5.3	HCD induces inflammasome activation in intestinal epithelial cells.....	136
3.5.4	Relevance of HCD-induced inflammation for chronic auto-inflammatory pathologies	138
3.6	Conclusion.....	141
 Chapter 4 Inflammation and tissue remodelling of zebrafish gills upon exposure to irritants and/or cryoinjury		143
4.1	Introduction	143
4.2	Aims	151
4.3	Results	152
4.3.1	Acute exposure to silica and smoke	152
4.3.2	Long-term exposure to silica and/ or smoke	165

4.3.3	Cryoinjury of zebrafish gills	171
4.3.4	Transcriptome profiling using RNA-seq analysis.....	179
4.4	Summary.....	203
4.5	Discussion.....	204
4.5.1	Conserved pathways of immune activation upon silica and smoke exposure	204
4.5.2	Chronic exposure to irritants leads to tissue remodelling but no scarring	207
4.5.3	Zebrafish heal without scarring following cryoinjury and/ or exposure to silica	209
4.5.4	Preliminary RNA-seq analysis reveals conserved mechanism of wound-healing between mammals and zebrafish	210
4.6	Conclusion.....	218
Chapter 5 Final discussion.....		220
5.1	Significance of the study and key findings.....	220
5.2	Future work	221
5.3	Implications and future directions	227
Bibliography.....		229
Appendices		252

List of Tables

Table 1:	Overview of zebrafish lines used in this study.....	62
Table 2:	List of morpholino sequences.	65
Table 3:	List of Taqman assays and SYBR primer sequences used in this study.	73
Table 4:	Summary of key findings of N. Sangha’s PhD thesis	79

List of Figures

Fig. 1.1	Schematic representation of mucosal barriers.....	18
Fig. 1.2	Schematic representation of the two-signal model of NLRP3 inflammasome activation. .	27
Fig. 1.3	Schematic representation of immune responses at mucosal barriers that promote mucosal immune homeostasis.....	34
Fig. 1.4	Schematic representation of intestinal epithelium.	36
Fig. 1.5	Schematic representation of the lung epithelium.	38
Fig. 1.6	Breakdown of mucosal immune homeostasis during mucosal inflammation.....	40
Fig. 1.7	Overview of the intestinal structure of zebrafish.	53

Fig. 1.8 Overview of the gill structure of zebrafish.....	55
Fig. 1.9 Overview of lamellar gill respiratory epithelium.....	56
Fig. 3.1 Zebrafish model of HCD-induced intestinal inflammation.	80
Fig. 3.2 Two-signal model of HCD-induced inflammasome activation.	83
Fig. 3.3 Analysis of immune cell accumulation following acute HCD in adult zebrafish.....	87
Fig. 3.4 Analysis of myeloid cell accumulation in intestine of Balb/C mice following butter gavage.	89
Fig. 3.5 Effect of cholesterol gavage on inflammation in small intestine of Balb/C mice.....	92
Fig. 3.6 Time-line of experimental procedure.....	93
Fig. 3.7 Effect of NFkB-inhibition on HCD-induced intestinal inflammation.	96
Fig. 3.8 HCD-induced intestinal inflammation is dependent on the microbiota.....	98
Fig. 3.9 Food uptake and transit of zebrafish raised under germ free conditions.	100
Fig. 3.10 Cholesterol uptake by intestinal epithelial cells of zebrafish raised under germ free conditions.....	102
Fig. 3.11 Effect of HCD on the load of the commensal microbiota.....	104
Fig. 3.12 Analysis of NFkB expression in the intestine of <i>Tg(NFkB:EGFP)</i> following HCD.	105
Fig. 3.13 Analysis of NFkB activation in the intestine of <i>Tg(NFkB:EGFP)xTg(fms:mCherry)</i> following HCD.	107
Fig. 3.14 Analysis of caspase-1 activity in intestinal cells following HCD.....	110
Fig. 3.15 Confocal analysis of MO uptake into intestinal cells.....	113
Fig. 3.16 Analysis of ASC transcripts in intestinal cells following treatment with ASC MO.....	115
Fig. 3.17 Flow cytometry analysis of MO uptake into intestinal cells.....	117
Fig. 3.18 Effect of GFP MO treatment on EGFP fluorescence intensity in intestinal cells of <i>Tg(ubi:EGFP)</i>	119
Fig. 3.19 Effect of IL-1 β MO treatment on HCD-induced myeloid cell accumulation.....	119
Fig. 3.20 Analysis of intestinal L-Plastin cell accumulation following extended feeding.....	122
Fig. 3.21 Analysis of intestinal motility following extended HCD.....	123
Fig. 3.22 Severity of impairments in peristalsis following extended HCD correlates with degree of inflammation.....	124
Fig. 3.23 Slight changes in intestinal architecture following extended HCD feeding.	126
Fig. 3.24 Steatosis in liver following extended HCD.....	128
Fig. 4.1 Schematic representation of lung fibrosis.....	145
Fig. 4.2 Schematic representation of experimental procedure.....	153
Fig. 4.3 Localisation of immune cells in zebrafish gill tissue.....	153
Fig. 4.4 Analysis of immune cell accumulation following acute silica exposure.....	155
Fig. 4.5 Analysis of inflammatory status following acute silica exposure.....	158
Fig. 4.6 Analysis of immune cells accumulation following acute smoke exposure.....	160

Fig. 4.7 Pro-inflammatory cytokine expression following acute smoke exposure.	162
Fig. 4.8 Analysis of inflammatory status following combined treatment of silica + smoke.....	164
Fig. 4.9 Analysis of immune cell accumulation following long-term exposure to silica and/ or smoke.	166
Fig. 4.10 Histological analysis of gill tissue after long-term exposure to silica and/ or cigarette smoke.	168
Fig. 4.11 Analysis of collagen deposition following long-term exposure to silica.....	170
Fig. 4.12 Detailed description of gill cryoinjury in an adult zebrafish.....	171
Fig. 4.13 Inflammatory response after gill cryoinjury in an adult zebrafish.	173
Fig. 4.14 Histological analysis of zebrafish gill tissue after cryoinjury.....	175
Fig. 4.15 Inflammatory and wound-healing response after cryoinjury followed by continuous exposure to silica.	178
Fig. 4.16 Sample preparation for RNA-seq analysis.	181
Fig. 4.17 Workflow of RNA-seq analysis and Principal Component Analysis of samples.....	183
Fig. 4.18 Venn analysis of differentially expressed genes.	185
Fig. 4.19 Validation and correlation of <i>collala</i> mRNA expression values between RNA-seq and qRT-PCR.	187
Fig. 4.20 Examples of most significantly differentially expressed genes following silica and cryoinjury.....	189
Fig. 4.21 Regression analysis between gene expression and gill tissue-damage.	191
Fig. 4.22 Quantification of gill tissue damage and validation of <i>collala</i> mRNA expression values.	194
Fig. 4.23 Venn analysis of differentially expressed genes between experiments.	196
Fig. 4.24 Temporal profiles of example genes following silica and cryoinjury.....	198
Fig. 4.25 Temporal profiles of example genes involved in inflammatory processes following injury.	201
Fig. 4.26 Temporal profiles of example genes involved in lung repair processes.	202

List of Appendices

Appendix 1 Effect of HCD on the composition of the commensal microbiota.....	252
Appendix 2 Analysis of NFkB activation in zebrafish gill at steady state.....	253
Appendix 3 Trichrome staining of gill tissue after long-term exposure to silica and cigarette smoke	254
Appendix 4 Histological analysis of gill tissue after recovery following long-term exposure to silica and cigarette smoke.....	255

Chapter 1

Introduction

Chapter 1 | Introduction

The purpose of the PhD project was to investigate the potential of zebrafish, *Danio rerio*, to study mechanisms mediating acute and chronic inflammation of mucosal tissues. This investigation was carried out on two mucosal tissues, the gastrointestinal and the pulmonary system, that are both prone to chronic inflammatory diseases in humans. Thus, this introduction is only focused on mucosal epithelial barriers of the intestine and the lung and not on other mucosal organs such as the olfactory and the urogenital systems.

1.1 Immune homeostasis of mucosal epithelial barriers

1.1.1 General structure and function of mucosal epithelial barriers

Mucosal tissues are mucus-covered epithelial cells that cover the surfaces and cavities of structures and organs throughout the body. At the interface between the host and microorganism-rich external environments, mucosal surfaces of the lung and the gastrointestinal tract are the first line of defence against invading pathogens and other ingested or inhaled infectious agents or tissue irritants [1, 2]. Additionally, mucosal barriers serve the physiological function of the gastrointestinal and respiratory system by remaining highly permeable to allow controlled passage of nutrients, gases, ions and solutes. In order to fulfill these seemingly contradictory roles mucosal surfaces possess a closely associated complex immune system that keeps the external environment under constant surveillance through antigen sampling [1, 2]. The mucosal immune system performs a balancing act of discrimination between highly immunogenic but harmless and beneficial microbes and potentially detrimental pathogen-associated antigens to ensure rapid, but highly regulated, immune responses to local infection and injury to minimise damage to local epithelial cell surfaces. Thus, daily function, immune homeostasis and hence the integrity of respiratory and intestinal mucosal surfaces is achieved by a complex interplay between the mucosal immune system, the microbiota that promotes mucosal health and function and the mucosal epithelium itself (Fig. 1.1).

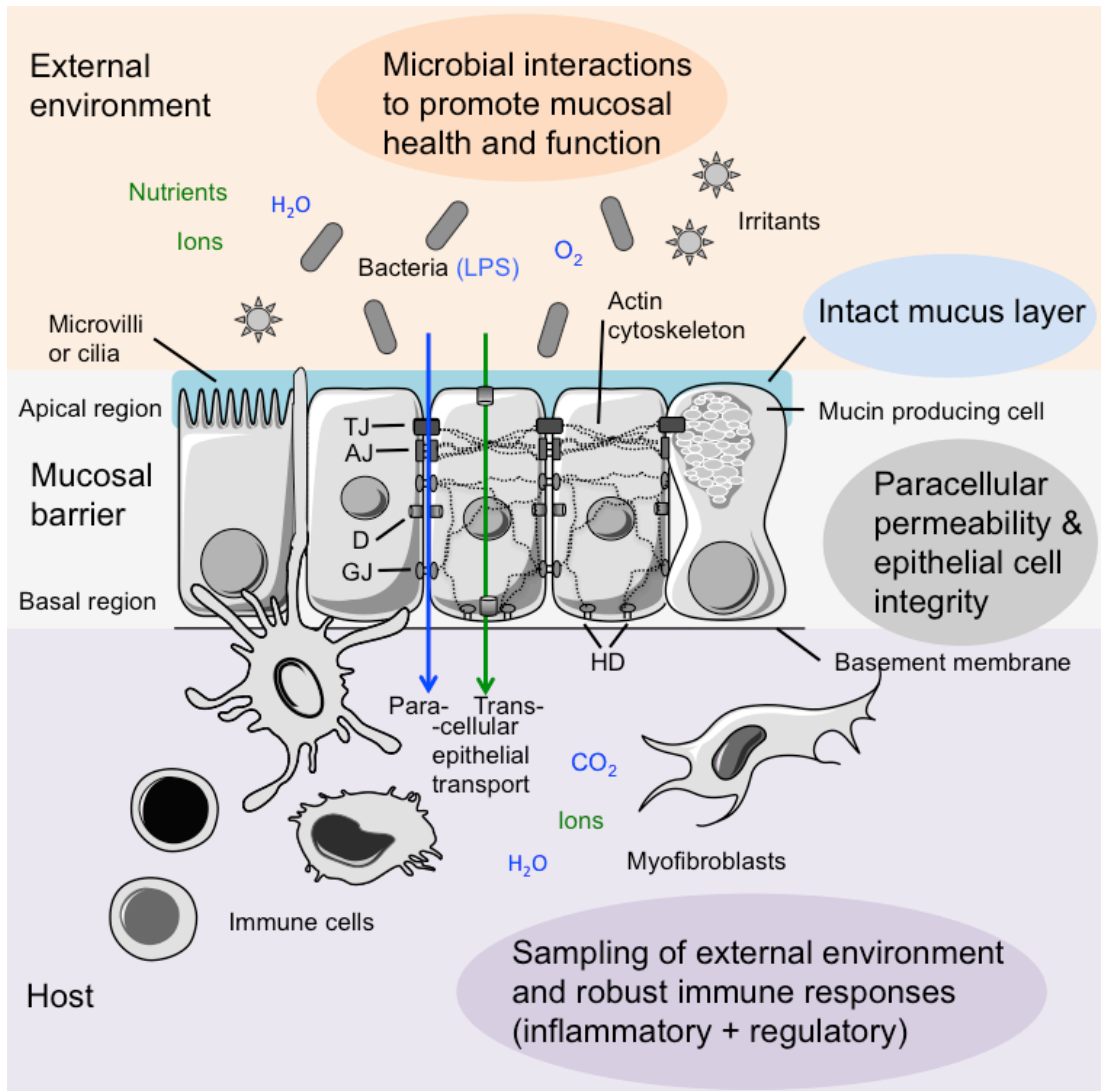


Fig. 1.1 Schematic representation of mucosal barriers.

Mucosal surfaces form a physical barrier between the external environment and the host. Four key components of mucosal barriers contribute to the maintenance of immune homeostasis and integrity: an intact mucus layer that forms a physical protection, balanced interaction with the microbiota which contribute to a healthy function of mucosal tissues, sampling of bacterial products and robust immune responses (well balanced between inflammatory and regulatory responses) and the maintenance of paracellular permeability and epithelial barrier integrity to fulfill the physiological organ requirements. Epithelial cell connections are TJ=tight junctions, AJ=adherens junctions, GJ=gap junctions, D=desmosomes and HD=hemidesmosomes. Epithelial barriers facilitate uptake of nutrients and perform gas exchange via paracellular transport (blue arrow) and transcellular transport (green arrow) route to fulfill physiological organ function.

1.1.1.1 Mucus layer

An intact mucus layer is key to the maintenance of immune homeostasis of mucosal barriers as the mucus physically protects the epithelial layer as it is semipermeable and enables nutrient and gas exchange while being impermeable to most bacteria, large particles and irritants [3]. The first layer that covers epithelial cells forming a connection with the mucus layer is the glycocalyx [4]. The glycocalyx is comprised of cell-membrane-anchored mucin glycoproteins together with secreted mucins and is only between 10-500 nm thick [3, 4]. The mucus layer is a viscous gel that is made of mucins that are secreted by specialised mucin-producing epithelial cells (goblet cells) and that are packed more loosely than in the glycocalyx. The major structural component of the intestinal mucus layer is the mucin Muc2 [5]. In the small intestine the loosely attached mucus layer has a thickness of about 50 μm , which is huge compared to bacteria of about 1 μm [5, 6]. In the colon the mucus consists of both a firmly attached inner layer that is about 50 μm thick and devoid of bacteria and an overlaying loosely attached mucus layer that can vary in thickness up to 100 μm [3, 5]. In the lung, the mucus layer of the respiratory epithelium is only 1-10 μm thick [3] and one of the major structural component is the glycoprotein Muc5ac [7]. In addition to mucins, the mucus layers of the intestine and the lung also contains other secreted proteins, such as secreted immunoglobulin (Ig) A and antiseptic enzymes. In the intestine, these are defensins, lysozymes, phospholipases, cathelicidins, lipocalins and the C-type lectin regenerating islet-derived 3-gamma (RegIII γ) [8], while those of the lung are defensins, lysozymes, cathelicidins, histatins and lactoferrin [9]. The lung also expresses complement as additional opsonin to IgA [1] and several surfactant proteins that directly bind to pathogens and other particles and thereby enhance their uptake by immune cells [10, 11].

1.1.1.2 Epithelial cell barrier

The epithelium is one of the four basic cell types of mammalian tissues (amongst connective, muscle and nervous tissue) and in mucosal tissues is organised as simple epithelium (one cell thick). Depending on tissue and function, epithelial cells can be ciliated or exhibit microvilli at their apical region (see further description below). Epithelial barrier integrity is essential for immune homeostasis at mucosal barriers and it is maintained through highly organised intercellular junctions such as tight junctions, adherens junctions, desmosomes, and gap junctions that connect epithelial cells with each

other (Fig. 1.1) [12]. Formation and maintenance of the epithelial barrier is mainly facilitated by the junctional complex, which is located at the most apical (luminal) region and includes adherens and tight junctions and desmosomes. Adherens junctions and desmosomes simply act as mechanical links between adjacent cells, whereas tight junctions, in addition to cell-cell-adhesion, also control ion and solute diffusion through the intercellular space (paracellular transport) [12, 13]. Although, tight and adherens junctions are comprised of different proteins, both are formed of transmembrane and peripheral membrane protein complexes. Transmembrane proteins provide the mechanical link between cells whereas peripheral membrane proteins associate with the actin cytoskeleton, which is reorganised upon formation and maturation of cell-cell-contacts. Key transmembrane proteins of tight junctions are occludin, claudin and the junction adhesion molecule A, whereas adherens junctions are made of the transmembrane glycoprotein protein E-cadherin. Key peripheral membrane proteins of tight junctions are the cytoplasmic scaffolding proteins zonula occludens ZO-1, -2 and -3, whereas the intracellular components of adherens junctions are p120-catenin, β -catenin and α -catenin [13].

Transport of solutes across the epithelium occurs transcellularly or paracellularly (Fig. 1.1), the paracellular pathway allowing faster transport and being the key factor in determining mucosal permeability. In the intestine, tight junctions regulate the paracellular transport by at least two potential routes, the “leak” and the “pore” pathway. Differences in selectivity of these pathways are based on size and charge of the solutes [14, 15] and both can be regulated by physiological or pathophysiological stimuli. The leak pathway allows passage of large solutes, including some proteins and bacterial lipopolysaccharide (LPS) but does not show any charge selectivity [14]. The pore pathway is characterised by small pores, which have a size limitation of 4 Å and are formed by claudin proteins that define the charge selectivity of the tight junction. Transcellular transport of nutrients within the intestine occurs via specific receptors, such as the cluster of differentiation (CD) 36, the plasma membrane fatty acid-binding protein and the fatty acid transport protein 4 which mediate the uptake of fatty acids and Niemann-Pick C1-Like 1 (NPC1L1) through which cholesterol is taken up [16, 17].

1.1.1.3 Microbiota

A healthy commensal microbiota that lives in symbiosis with its host is key to promote health and function of mucosal tissues, however, both beneficial microbes and potential

pathogens form a daily threat to the host. Thus, the mucosal immune system is required to maintain a homeostatic balance between tolerance and immunity in order to benefit from this colonisation and to protect the organism from infectious diseases [18].

The human gut microbiota has been widely characterised and their function during health and disease has been studied in depth [18-20]. One of the main roles of commensals is to compete with pathogenic bacteria for the ecological niche and therefore prevent their colonisation. In the past, treatment of mice with antibiotics and comparisons of mice that were raised germ-free, mice that were raised conventionally and mice that have been colonised with specific microbial phyla (gnotobiotic) have revealed a number of effects of microbial communities on host functions [21-23]. For example, it has been shown that the anaerobe *Bacteroides thetaiotaomicron* degrade large otherwise non-digestible starch polymers into absorbable oligosaccharides [24, 25]. This demonstrates that the microbiota can aid nutrient processing in the intestine. Likewise, the microbiota synthesises Vitamin K and parts of the Vitamin B complex and ferments non-digestible fibers [18]. The main metabolic products of this anaerobic fermentation of commensal microbiota are the short-chain fatty acids (SCFAs) acetate (C2), propionate (C3) and butyrate (C4). SCFAs are important energy sources for the host that shape the intestinal immune system. Indeed, SCFAs induce forkhead box p3 (Foxp3)⁺IL10-producing regulatory T cells (T_{regs}) [26]. Further, the otherwise toxic by-product of fermentation D-lactate is converted by lactate-utilising bacteria to butyrate and therefore prevents its accumulation and potential toxic effects in the intestine [27, 28]. Commensal bacteria can also directly affect intestinal mucosal barrier integrity. For example, the enterotoxigenic *Bacteroides fragilis* produces *B. fragilis* toxins that induce epithelial damage to improve their colonisation [29]. Beyond the epithelium, the microbiota can control angiogenesis; Stappenbeck *et al.* showed that bacterial colonisation of germ-free mice results in *de novo* formation of the villus capillary network [30]. Until recently, the diversity of the intestinal mucosal ecosystem was incompletely defined, owing to limitations in methodology for bacterial identification. The development of novel sensitive and rapid high-throughput sequencing techniques of 16S rRNA genes and advanced metagenomics has allowed characterisation of the human gut microbiota in detail and established that intestinal commensals are heterogeneous and occur with increasing numbers and increasing diversity from the proximal to the distal GI tract [18]. With a total number of about 10¹⁴ bacterial cells, the human intestinal microbiota is estimated to outnumber human cells 10 to 1 [18].

Of note, these technical advances have allowed the characterisation of the respiratory microbiome of the healthy human lung, which had historically been considered sterile. Indeed, it was recently established that the airways are replete with diverse bacterial communities contributing to both health and disease [31]. Although the origin of the lung microbiota (*i.e.* whether it is acquired through inhalation or whether its composition correlates with the intestinal microbiota) has not yet been determined, its crucial role in shaping the immune responses in mammalian lungs has recently started to be explored (reviewed in [32]). For instance, the microbiota is essential for mediating tolerance in the respiratory system, as germ-free mice are more susceptible to experimental allergic inflammatory airway disease [33].

The microbiome however not only comprises bacteria but also viruses and recent viral metagenomic studies have explored the viral community of the human gut and revealed that it is dominated by bacteriophages [34, 35]. Originally, the intestinal virome was considered to be unique to each individual as a result of the rapid sequence evolution of bacteriophages within the dynamic microbial ecosystem in the intestine [35]. In contrast, recent technical advances helped the discovery of a previously unidentified bacteriophage, referred to as crAssphage, that is present in the majority of published human fecal metagenomes [34]. *Bacteroides*, which is one of the major bacterial taxa inhabiting this human intestine, has been identified as host for crAssphage, however, the role of this bacteriophage in the microbial ecosystem is yet to be explored [34].

1.1.1.4 Mucosal immune system

Mucosal barriers allow interaction between the closely connected mucosa-associated lymphoid tissue (MALT) and the external environment, rich in antigens and microbes, to ensure mucosal immune homeostasis [15]. The MALT is a collection of cells of the innate and the adaptive immune system such as macrophages, neutrophils, mast cells, innate lymphoid cells, NK cells, dendritic cells, T cells, B cells, plasma cells and NKT cells that are well poised to encounter any antigens passing through the mucosal barrier [1, 2]. Especially in the intestine the importance of immune modulation becomes apparent by the fact that 70% of all lymphocytes in the human body are located within the mucosal immune system [18].

Bacterial sensing and sampling of antigens of the external environment by the MALT results in ‘default’, often non-inflammatory, low-level immune responses that mediate

mucosal immune homeostasis. In the case of epithelial tissue damage, which is caused either through injury or from infection, acute inflammation causes the activation of pro-inflammatory immune responses to restore mucosal barrier integrity and subsequently mucosal immune homeostasis. A step-by-step guide of the immune responses that mediate intestinal homeostasis is explained below.

1.1.1.4.1 Inducers: PAMPs and DAMPs

Pattern recognition receptor (PRRs) are the sentinels of microbial and viral motifs known as pathogen-associated molecular pattern molecules (PAMPs), non-infectious agents/antigens and host-derived danger signals known as damage-associated molecular pattern molecules (DAMPs) throughout the intestinal and respiratory tract and are expressed on cells within mucosal tissues. Amongst others, Toll-like receptors (TLRs) and nucleotide-binding oligomerisation domain receptors (in short NOD-like receptors, NLRs) are the main members of PRRs present at mucosal surfaces.

1.1.1.4.2 Sensor cells and PRRs at mucosal barriers

Intestinal and alveolar macrophages and dendritic cells possess PRRs and it is well established that they play key roles in recognising PAMPs and DAMPs during intestinal and pulmonary immune homeostasis [1, 2]. Antigen sensing by dendritic cells (DCs) is considered as key component of immune homeostasis and through their release of distinct cytokines (see below) or through antigen-presentation they drive T cell responses therefore forming a bridge between the innate and the adaptive immune system [36, 37]. Intestinal myeloid antigen-presenting cell (APC) populations exhibit distinct functions. $CD11c^+CD103^+CX_3CR1^-$ dendritic cells take up bacteria in the lamina propria and migrate to the mesenteric lymph nodes (MLNs) where they initiate adaptive response pathways, predominantly those mediating tolerance ($FoxP3^+ CD4^+ T_{reg}$ cells) [38]. However, during acute inflammation these $CD103^+$ dendritic cells acquire pro-inflammatory properties and drive T_H1 -responses through the release of IL-6 [39]. $CD11c^+CD103^-CX_3CR1^+$ DCs sample antigens and bacteria through extending transepithelial dendrites into the gut lumen, but fail to migrate to the MLNs and do not prime naïve T cells, thus contributing to local adaptive responses through the release of cytokines [38]. Local $CD103^- CD11b^+CX_3CR1^+$ intestinal macrophages sense bacteria within the lamina propria upon which they release cytokines or migrate to MLNs where they contribute to adaptive T_{reg} responses [40].

Analogous to intestinal dendritic cells, resident airway mucosal CD11c⁺CD103⁺ dendritic cells transport antigen to the regional lymph nodes (RLNs) where they initiate adaptive responses [41]. In contrast, CD11c⁺ alveolar macrophages within the alveoli do not migrate to the RLNs or seem to perform antigen presentation, thus shaping immune responses through the release of mediators [42, 43].

In addition to innate immune cells, resident fibroblasts in the lung and in the intestine express PRRs through which they can directly sense pathogens and produce cytokines that activate myofibroblasts [44]. Thus, their involvement in immune homeostasis at mucosal barriers can be hypothesised, although the myofibroblast activation has so far mainly been implicated with pathologies [45-47].

Further, epithelial cells have long been considered as innocent bystanders during mucosal health and disease, simply forming a barrier between the host and the microbe and antigen-rich environment of mucosal tissues. However, there is emerging evidence that epithelial cells are themselves equipped with PRRs, can produce inflammatory mediators and play key roles in mediating mucosal immune homeostasis and inflammation [48]. For instance, Paneth cells in the intestinal epithelium can detect commensals directly through MyD88-dependent TLR activation, triggering expression of antimicrobial peptides and therefore directly limiting bacterial translocation across the intestinal epithelial barrier [49]. Further, inflammasome components are expressed in epithelial cells of the intestine to repair tissue following injury [50, 51] and promote protection from bacterial infection [52, 53]. However, to date there are only very few *in vivo* reports that innate immune recognition within the epithelium plays essential roles during health and disease of mucosal tissues. Thus, in order to understand the exact aetiology and pathogenesis of mucosal inflammatory disease it is critical to define the specific role of each of these sensor cells, their receptors and signalling pathways.

TLRs at mucosal surfaces

TLRs are membrane-spanning PRRs that play a key role in innate immune recognition [54]. TLR activation occurs through an adaptor molecule, which for most members of the TLR family is myeloid differentiation factor 88 (Myd88) [54]. Signal transduction following TLR activation occurs through the nuclear factor kappa-light-chain-enhancer of activated B cells (NFκB) pathway, which activates a wide array of pro-inflammatory cytokines. Various members of the TLR family are expressed in cells at mucosal surfaces. For instance, intestinal epithelial cells express TLR2 and TLR4 on the apical and the

basolateral border, whilst TLR3 and TLR5 expression is restricted to the basolateral region and border, respectively [55]. TLR1/2 recognises components of Gram⁺ bacteria, such as peptidoglycan, TLR4 binds to endotoxin from Gram⁻ bacteria, *i.e.* lipopolysaccharide (LPS), and TLR3 is a receptor for viral double-stranded RNA, while TLR5 recognises bacterial flagellin. The different spatial distribution of the various TLR members suggest complementary functions of TLRs: while in steady state conditions commensals do not cross the epithelium apical TLR signalling might contribute to mucosal immune homeostasis and tolerance, while pathogenic bacteria that penetrate epithelial barriers upon injury will be recognised by basolateral TLRs resulting in immune responses to restore homeostasis [55].

NLRs at mucosal surfaces

NLRs are cytoplasmic PRRs that are like TLRs highly evolutionarily conserved [56]. Several NLRs are expressed in epithelial and haematopoietic cells of respiratory and intestinal mucosal surfaces and there is emerging evidence that inflammasomes in the intestine and lungs protect from invading pathogens [52, 53, 57, 58]. The NLRP3 family member recently gained increasing scientific interest since single nucleotide polymorphisms (SNPs) were linked to IBD susceptibility [59]. NLRP3, together with the adaptor apoptosis-associated speck-like protein containing a caspase-recruitment domain (ASC) and procaspase-1 forms the NLRP3 inflammasome. NLRP3 is comprised of a central nucleotide-binding and oligomerisation domain that is flanked with leucine-rich repeats on the C-terminus and with a pyrin domain (PYD) on the N-terminus (Fig. 1.2). Upon activation, NLRP3 oligomerises with the PYD of ASC via PYD-PYD interaction, which subsequently interacts with procaspase-1 via caspase-recruitment domain (CARD)-CARD interaction (Fig. 1.2). Upon successful assembly, caspase-1 is activated which results in subsequent cleavage of pro-interleukin (IL)-1 β and therefore activation and secretion of mature IL-1 β [56]. The expression of the pro-form of IL-1 β requires prior induction via TLR-NF κ B signalling [60], which is achieved *in vitro* by LPS. Thus, successful inflammasome activation requires two distinct signals: the priming signal 1, which induces expression of NLRP3 itself and pro-IL-1 β and the activation signal 2, which leads to activation of caspase-1 and processing of pro-IL-1 β into its active form (Fig. 1.2). Various danger signals, mainly of crystalline structure, have been shown to activate the NLRP3 inflammasome in *in vitro* set-ups. For instance, cholesterol crystals, fatty acids, silica particles, asbestos and ATP activate the NLRP3 inflammasome in macrophage

cultures leading to the release of mature IL-1 β [61-65]. Activation of the inflammasome is thought to occur following internalisation of these compounds into lysosomes where they induce destabilisation of the lysosomal membrane. This process subsequently leads to the release of the lysosomal protease cathepsin B into the cytoplasm, which appears to activate the NLRP3 through, so far, unexplained mechanisms [56, 65]. A second route of NLRP3 inflammasome activation is the production of reactive oxygen species (ROS), although the source of ROS release and the mechanism are only partly understood [56] (Fig. 1.2). Of note, most of these results and observations derive from *in vitro* studies where signal 1 was achieved by LPS stimulation. Thus, whether the same mechanisms lead to inflammasome activation and how signal 1 is provided *in vivo* is still debatable. In particular, most of these danger signals are encountered at mucosal surfaces on a daily basis; for instance cholesterol and fatty acids in their dietary forms or by occupational exposure to silica and asbestos. However whether these compounds can activate the inflammasome in mucosal tissues following exposure has not yet been investigated.

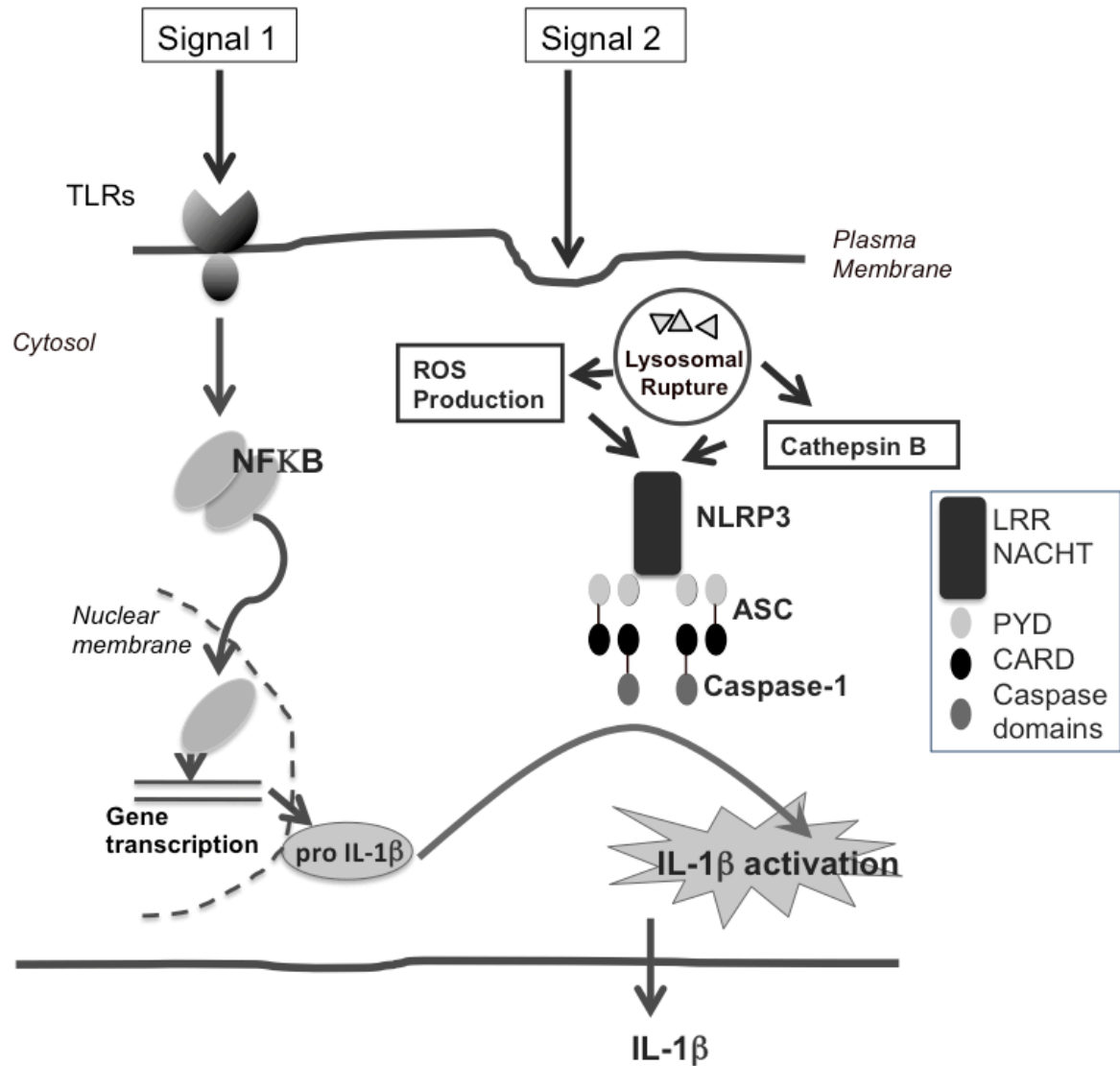


Fig. 1.2 Schematic representation of the two-signal model of NLRP3 inflammasome activation.

Signal 1 (priming signal) induces pro-IL-1 β expression through TLR signalling in an NF κ B-dependent manner. Signal 2 stimulates ROS production and cathepsin B release following lysosomal destabilisation resulting in inflammasome activation. This activation triggers NLRP3 inflammasome complex formation involving ASC and procaspase-1. Procaspase-1 is a zymogen that is cleaved following inflammasome assembly into the 20 kDa (p20) and 10 kDa (p10) subunits that form the active caspase-1 p10/p20 tetramer. Subsequently, activate caspase-1 mediates pro-IL-1 β processing and mature IL-1 β release. Relevant domains are indicated: LRR=leucine-rich repeat, NACHT=nucleotide-binding and oligomerisation domain and caspase domains=p20 & p10. Adapted from Schroder and Tschopp [56].

1.1.1.4.3 Pro- and anti-inflammatory mediators

Innate immune recognition at mucosal surfaces of PAMPs, DAMPs and other agents by PRRs (TLRs and NLRs) triggers the above described signalling cascades which lead to the induction of pro-inflammatory mediators such as cytokines and chemokines (Fig. 1.3). Key pro-inflammatory cytokines involved in mucosal immune responses are tumor-necrosis factor-alpha (TNF- α), IL-6, and IL-1 β [45, 66]. All of these cytokines are pleiotropic and exert their effects in both physiological and pathological processes [67-69]. Cytokines released by dendritic cells direct different T helper (T_h)-effector cell responses: IL-12 and IL-23 activate T_h1 responses and natural killer cells, IL-23 and IL-6 initiate T_h-17 responses, transforming growth factor (TGF)- β and retinoic acid activate T_{reg} cells and IL-4 activates T_h2 responses [70, 71]. Those cells in turn release a different set of cytokines through which they drive different immune responses: T_h1 cells, which produce interferon- γ (IFN- γ) and IL-2 and drive type I immune responses, T_h17 release IL-17 and IL-22 and contribute to immune homeostasis, T_{reg} cells release the anti-inflammatory cytokine IL-10 and promote tolerance and T_h2 cells, which produce IL-13 and IL-4 and drive type II immune responses. In addition to cytokines, chemokines play a critical role in orchestrating immune responses in mucosal tissues by controlling the traffic of inflammatory leukocytes to sites of epithelial injury [72]. Key chemokines involved in mucosal immune responses are chemokines of the CXC family that recruit neutrophils, such as CXCL8 (IL-8) and CXCL1 (growth-related oncogene- α , GRO- α) and chemokines of the CC family that recruit monocytes, such as CCL2 (monocyte chemoattractant protein-1) [73, 74]. Other mediators that play a role in mucosal inflammatory responses are lipid mediators (eicosanoids), such as leukotriene LTB₄, which drives acute inflammation by promoting neutrophil chemotaxis, the release of ROS and granule enzymes by neutrophils [75].

1.1.1.4.4 Effector cells at mucosal barriers

There is an array of effector cells contributing to mucosal immune homeostasis at mucosal barriers (Fig. 1.3). These cells originate mainly from either the innate or the adaptive immune system, however, other resident cell, such as epithelial- or endothelial cells or myo-/fibroblasts are also involved in mucosal immune responses (Fig. 1.3). Different pro- and anti-/regulatory inflammatory processes when in balance maintain immune homeostasis. However, during mucosal inflammatory conditions in the human lung and

intestine chronic inflammation and persistent epithelial damage occurs, thus the precise role of these effector cells needs to be characterised to understand mucosal disease pathology.

Cells of the innate immune system

Neutrophils

Neutrophils are the first cell type that is recruited from the circulation to the site of mucosal infection and injury upon sensing neutrophil attractants (LTB₄, CXCL8 and CXCL1) and danger signals (TNF- α and IL-6) [73]. Neutrophils clear up infections through three main mechanisms: phagocytosis of particles or microorganism, the release of granules or the formation of neutrophil extracellular traps (NETs). Neutrophil granules are classified in three groups: primary (azurophilic) granules, such as myeloperoxidase, proteinase, cathepsin G and neutrophil elastase; secondary (specific) granules, such as lysozyme, NADPH oxidase and collagenase; and tertiary granules, such as gelatinase [73]. Apart from their direct microbicidal properties, all three forms of granules contribute to the formation of NETs in conjunction with chromatin, which are extracellular traps that bind pathogens [76]. To limit excessive inflammation, neutrophils produce anti-inflammatory lipid mediators such as lipoxins, which in turn inhibit further entry neutrophils to inflammatory sites and their release of ROS and inflammatory mediators [77]. However, neutrophil granules also degrade the extracellular matrix (ECM) of mucosal tissues, which has been implicated in persistent tissue injury and chronic mucosal inflammatory conditions [78]. Thus, neutrophils are key to immune homeostasis by controlling infection, however, can also be detrimental during mucosal inflammatory processes if their responses are not switched off correctly.

Macrophages

Macrophages are key cells in mucosal tissues where they exert pleiotropic functions. On one hand they contribute to mucosal immune homeostasis by surveying mucosal tissues, clearing apoptotic debris through phagocytosis and helping repair after epithelial injury [79]. On the other hand they drive acute and chronic inflammation through the release of pro-inflammatory cytokines and their communication with the adaptive immune system via antigen-presentation [74]. Macrophages exhibit a noteworthy plasticity that enables them to adapt to external signals and exert their function accordingly. Although several anti- and pro-inflammatory macrophage subtypes have been classified and characterised so

far, the consensus is that when classified simplistically there are two main different macrophage subtypes: the classically activated M1 macrophage and the alternatively activated M2 macrophages [80]. M1 macrophages require both IFN- γ and TNF- α for their activation upon which they drive inflammatory responses through the production of pro-inflammatory mediators such as TNF- α , IL-1 β , IL-6, IL-12. M1 macrophage numbers are increased in the inflamed intestinal and respiratory mucosa during chronic inflammatory pathologies [1, 2]. M2 macrophages comprise macrophages with a wide spectrum of functions ranging from wound healing to anti-inflammatory. IL-10 and TGF- β lead to a regulatory macrophage phenotype that dampens inflammation through the subsequent production of IL-10, TGF- β and the lipid mediator prostaglandin PGE₂ [74, 80]. IL-4 and IL-13 cytokines that are released in response to injury lead to a wound-healing M2 macrophage phenotype that promotes ECM production by myofibroblasts [46]. However, since excess ECM deposition leads to fibrosis, this macrophage phenotype can have detrimental properties [46, 47].

Innate lymphoid cells

Innate lymphoid cells (ILCs) lack T cell receptors but produce T_h cell-associated cytokines and are divided into three subsets according to their ability to secrete T_h1, T_h2 and T_h17-cell associated cytokines [81]. ILCs are prevalent at mucosal surfaces where they rapidly produce these immunoregulatory cytokines, therefore contributing in the orchestration of adaptive immune responses during health and disease of mucosal tissues [82, 83].

Natural killer cells

The lamina propria of the intestine and the lung as well as the lung parenchyma also contains Natural killer cells (NK cells). While the presence of NK cells is mainly associated with mucosal inflammation, there is emerging evidence that they play distinct roles in mediating immune homeostasis. NK cells control infections of intracellular pathogens and NK cell deficiency is associated with increased susceptibility to viral infections [84].

Invariant natural killer T cells

Invariant natural killer T (iNKT) cells are a subpopulation of CD1d-restricted T lymphocytes expressing an invariant T-cell receptor (TCR) and NK cell associated markers such as NK1.1 [85]. iNKT cells are thought to form a bridge between innate and adaptive

immune responses [86]. Like mast cells and NK cells, invariant NKT cells are increased during and therefore associated with inflammatory conditions of the lung and the intestine [66, 87]. However, since NKT-deficient mice show an inability to maintain protection from bacterial and viral pathogens and parasites, their critical role in mucosal immune homeostasis can be hypothesised [88, 89].

Mast cells

Mast cells are very prominent at mucosal tissues compared to their distribution in other tissues. Mainly detrimental roles have been associated with mast cells as their numbers are highly increased during mucosal inflammatory conditions of the lung and the intestine [90, 91]. However, there is some evidence that mast cells may have protective roles during inflammatory responses and that the increased numbers is a sign that mast cells are trying to ameliorate the condition [92]. Further, there is evidence, however mainly from *in vitro* experiments, suggesting that mast cells perform a wide array of functions that contribute to immune homeostasis, such as promotion of T-cell proliferation and polarisation, T_{reg}-mediated tolerance and neutrophil recruitment, potentially through the release of histamine, prostaglandins, cytokines and chemokines [93-95].

Eosinophils/Basophils

The presence of eosinophils and basophils in the lung is considered as detrimental as they are absent in the healthy state but increased during inflammatory conditions [96, 97]. Basophils and eosinophils are thought to exacerbate ongoing airway inflammation through enhancement of T_H2 cytokine production by effector CD4⁺ T cells [98] and release of IL-4 [99], respectively. Their role in the intestine is more controversial as eosinophils and basophils reside in the intestine at steady state, thus potentially contributing to immune homeostasis, although their prime roles have been associated with detrimental inflammatory conditions of the intestine and the lung [95, 100].

Cells of the adaptive immune system

B cells

The main role of B cells in mucosal tissues is their release of protective secretory IgA following maturation into plasma cells [101, 102]. Secreted IgA binds to and neutralises pathogens and their toxic products. An additional role for B cells in local antigen presentation in the lung mucosa has been suggested but needs further investigation [103].

T cells

In the intestine as well as in the lung most CD8⁺ T cells exhibit an intraepithelial location, whereas CD4⁺ T cells are predominantly found in the lamina propria and within the parenchyma, respectively [1]. Following priming of T cell in the MLNs, intestinal T and B cells express the homing receptors chemokine receptor (CCR) type 9 and $\alpha_4\beta_7$ -integrin [104, 105]. Distinct homing phenotypes of T and B cells in the lung have yet to be defined [106], but CCR10 and $\alpha_4\beta_1$ -integrin have been suggested as potential homing factors [105]. Depending on their activation state, T cells can fight invading intracellular pathogens (T_h1 responses), act against extracellular bacteria and fungi (T_h17), tolerate commensals (T_{reg}) and fight extracellular parasites (T_h2) [70, 71]. Together these different T cell responses contribute to immune homeostasis, provided they are in balance. In particular, IL-10 and TGF- β producing Foxp3⁺CD4⁺CD25⁺ T_{reg} cells are central to the control of mucosal immune homeostasis in the lung and in the intestine [107].

 $\gamma\delta$ T cells

$\gamma\delta$ T cells are highly abundant as intraepithelial lymphocytes within the intestinal mucosa where they contribute to autoimmune responses mainly through the release of IL-17 and IL-22 [108, 109]. Although less abundant, $\gamma\delta$ T cells are also associated with Th17 responses towards bacterial infection in the lung [110].

Epithelial cells

Upon tissue injury, the epithelium undergoes apoptosis or necrosis and a lesion occurs that needs to be closed rapidly to restore immune homeostasis of mucosal tissues by limiting bacterial translocation. During the first wound healing step that has been termed “epithelial restitution”, surviving epithelial cells surrounding the injured area lose their columnar polarity and change to a flattened morphology, which allows them to migrate into the denuded area [111]. This process does not involve epithelial cell proliferation, but it is highly coordinated and under physiological circumstances can last between minutes and hours depending on the severity of injury. Then, replication of epithelial cells takes place to replenish the lost cell pool. Following proliferation, maturation and differentiation of these undifferentiated epithelial cells occurs to provide all different epithelial cell types that restore functional barrier integrity [111]. These processes are controlled and stimulated by cellular mediators, such as cytokines and growth factors.

When the injury is more severe or persistent and involves non-resolving inflammation, deeper lesions occur and inflammatory processes interfere with healing processes of epithelial barriers. Thus, in some cases, additional repair mechanisms are required that involve non-epithelial cell populations, such as myofibroblasts.

Myofibroblasts

Myofibroblasts, the collagen and ECM producing cells of mucosal tissues, are α -smooth muscle actin-positive (α -SMA+) cells that promote wound healing following mucosal injury [45-47, 112]. These fibroblast-like cells within the intestinal lamina propria and lung interstitium are often of mesenchymal origin and so far three mechanisms for their generation have been proposed: transdifferentiation of resident fibroblast or pericytes, origination from bone marrow fibrocytes or transition from epithelial or endothelial cells via epithelial-mesenchymal transition (EMT) or endothelial-mesenchymal transition (EndoMT) [46]. Myofibroblasts are thought to be the drivers of pulmonary fibrosis when their production of ECM is de-regulated and leads to excessive deposition of scar tissue resulting in the impairment of the underlying tissue function [45-47, 112].

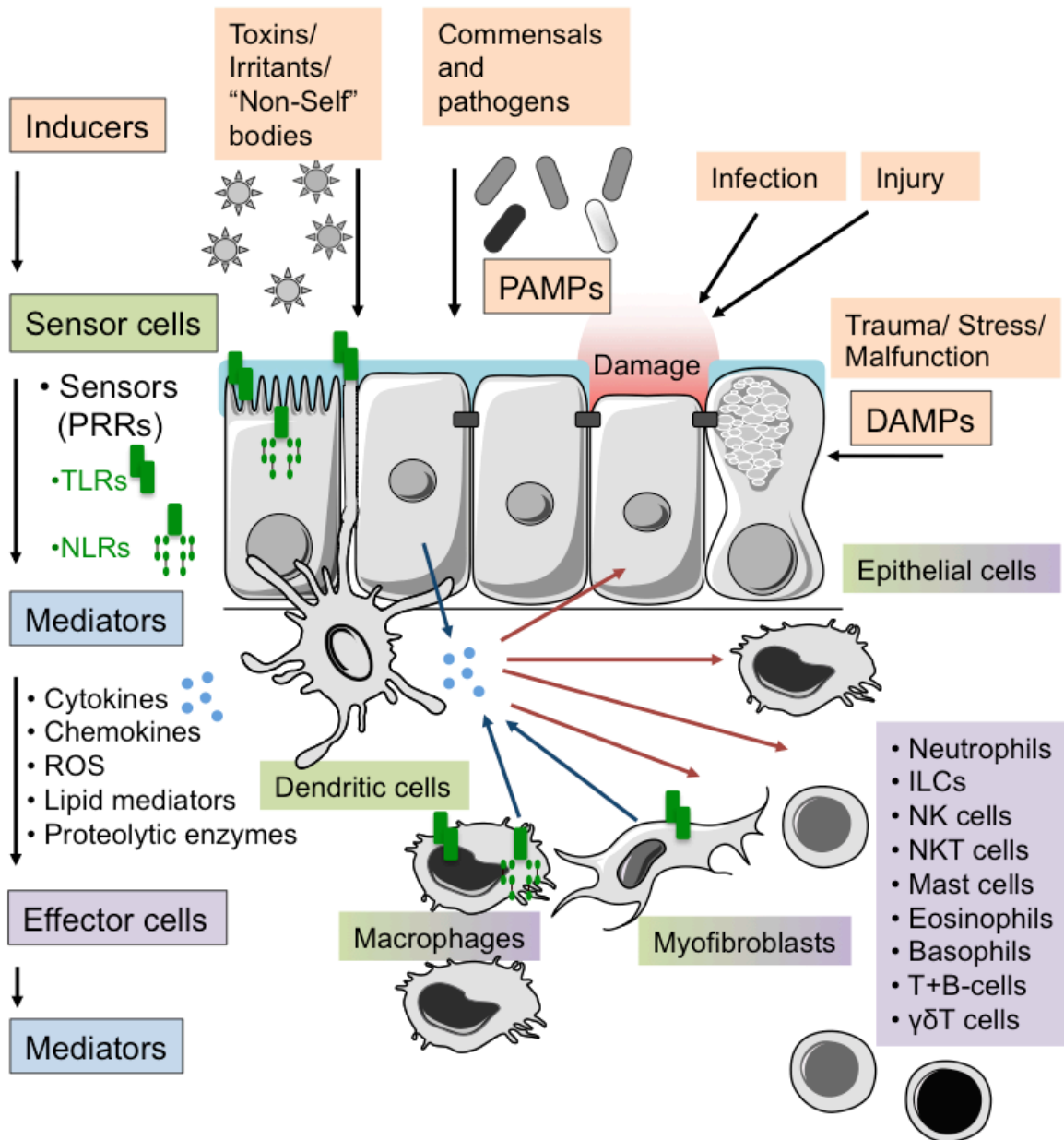


Fig. 1.3 Schematic representation of immune responses at mucosal barriers that promote mucosal immune homeostasis.

Epithelial cells, immune cells (macrophages and dendritic cells) and (myo)fibroblasts exhibit sensors (PRRs) that recognise external microbial, non-microbial or internal host-derived inducers upon which they release mediators to attract and activate effector cells. These effector cells in turn release more mediators to further activate more effector cells to raise an adequate immune response to maintain or restore mucosal immune homeostasis.

1.1.2 Organ specific structure and function of mucosal epithelial tissues

1.1.2.1 Intestinal epithelium

The major function of the intestine is to absorb nutrients. The intestinal mucosa is organised into two distinct structures: villi that are projections into the intestinal lumen and crypts (of Lieberkühn) that are invaginations around the villi into the underlying connective tissue (Fig. 1.4). Villi and crypts are comprised of multiple types of epithelial cells exhibiting different functions (absorption and secretion). Villi are mainly covered with absorptive enterocytes that absorb nutrients in the small intestine and water in the colon [6, 55]. Enterocytes exhibit cellular membrane protrusions (microvilli) to increase the surface area available for nutrient absorption. Together the folded intestinal structure of the human intestine would cover the surface area of a tennis court of around 200 m² [2, 18]. Mucin-secreting goblet cells are located on the villi, while the hormone-secreting enteroendocrine cells and the anti-microbial peptide secreting Paneth cells are located in the crypts (Fig. 1.4). At the base of the crypts of the small intestine are proliferative epithelial stem cells that give rise to all epithelial subtypes in the intestinal epithelium [113]. The epithelium is renewed every 4-5 days with newly generated cells migrating upwards to the tip of villus where they undergo apoptosis and are shed into the lumen [113].

Myofibroblasts (stromal cells) and the MALT, or in case of the intestine also referred to as gut-associated lymphoid tissue (GALT), are located beneath the intestinal epithelial cells within the lamina propria (Fig. 1.4). Antigen recognition is primarily carried out by dendritic cells that are located between the intestinal epithelial cells or within specialised regions of the epithelium such as follicle-associated epithelium and microfold cells (M cells) that overlie the Peyer's patches of the small intestine and take up external particles through transcytosis [55]. M cells are not covered in mucus and only exhibit a very thin glycocalyx layer (20 - 30 nm) [3, 6]. Antigen-presentation and T cell priming is primarily carried out within the Peyer's patches or within the mesenteric lymph nodes [38-40].

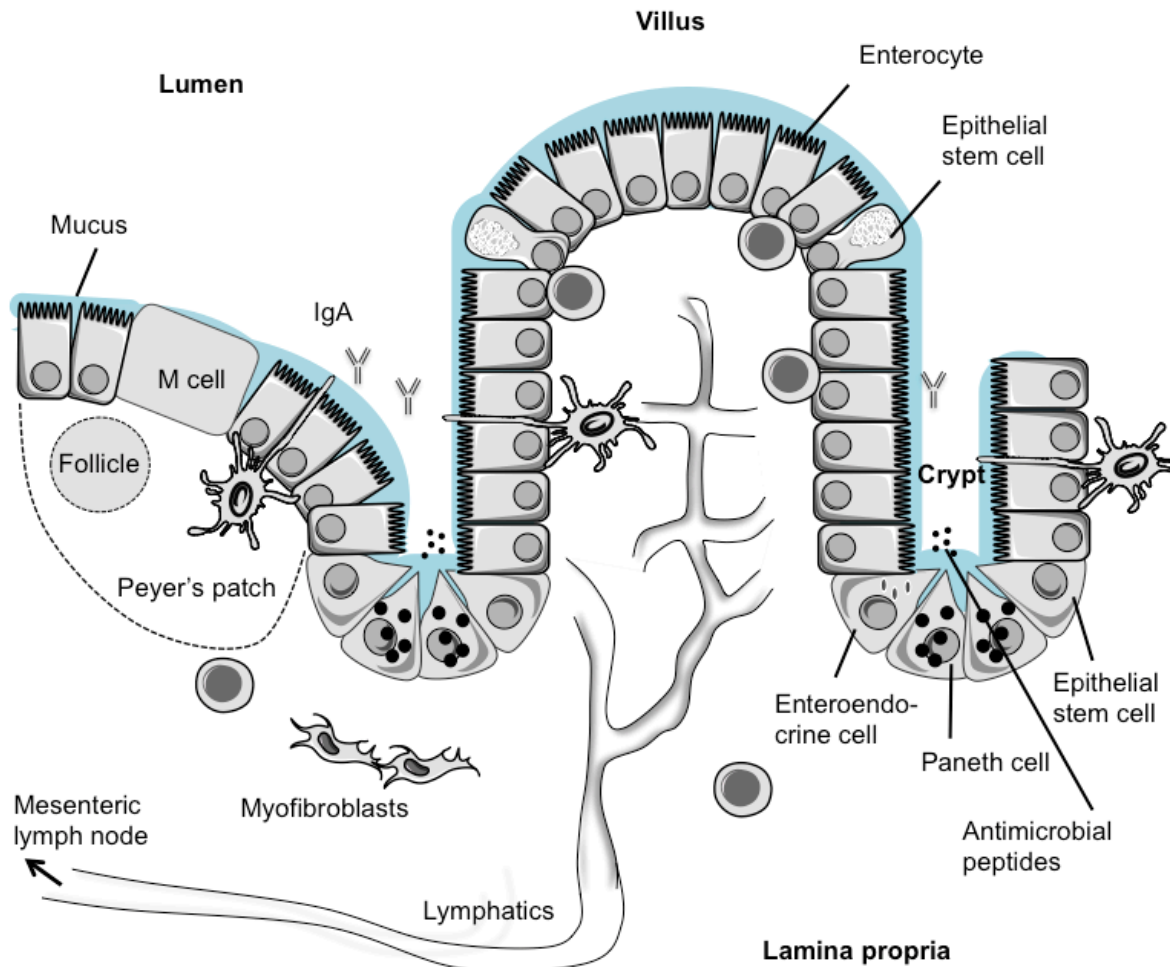


Fig. 1.4 Schematic representation of intestinal epithelium.

The human intestinal epithelium is organised in villi and crypts and is comprised of four main different epithelial cell types: goblet cells, absorptive enterocytes with microvilli, Paneth cells, enteroendocrine cell. The epithelial barrier separates the mucosal immune system of the lamina propria (which is comprised of B cells, T cells, macrophages, intraepithelial lymphocytes and plasma cells) from the external environment rich in commensal bacteria. A mucus layer covers the epithelium, which also contains IgA and antimicrobial peptides. The epithelial stem cell pool is located in the crypts. In the small intestine, specialised M cells sample external antigens directly from the lumen through transcytosis and deliver it to APCs within the Peyer's patches. Figure adapted from M.T. Abreu [55].

1.1.2.2 Respiratory epithelium

The primary function of the mammalian lung is oxygen and carbon dioxide exchange that takes place in the alveoli. The respiratory mucosa lines the entire network of branching bronchi and bronchioles and the alveoli, but shows location dependent anatomical differences [114]. In the upper airways the epithelium is ciliated and coated in mucus produced by goblet cells (Fig. 1.5). These two features together with locally produced secreted IgA form the ‘mucociliary escalator’, which represents the main protective barrier of the respiratory tract as it continually moves particles up and out into the throat [1]. In the small airways, goblet cells gradually decrease in number as the number of surfactant-synthesising Clara cells (now termed Club cells [115]) increase (Fig. 1.5) [116]. Surfactants are composed of surfactant proteins SP-A, SP-B, SP-C and SP-D and phospholipids that together are essential for reducing the surface tension at the air-liquid interface. Further, surfactant proteins have been shown to bind a variety of bacteria, viruses, apoptotic cells and allergens and thereby aid subsequent immune responses (reviewed in [11]). The alveoli in the terminal airways are lined with squamous alveolar type I (ATI) and cuboidal alveolar type II (ATII), the latter synthesising surfactant. Similar to the intestine, the airways are lined with a dense network of subepithelial macrophages, plasma cells, T cells and B cells that together with intraepithelial DCs protruding into the airway lumen perform immune surveillance (Fig. 1.5) [41, 42]. In contrast to the intestine, immune cells in the alveoli are located both above (mainly alveolar macrophages, but also a few DCs and T cells) and below the epithelium (macrophages, DCs, T cells, B cells and mast cells but no plasma cells) in the underlying parenchyma [43]. To facilitate gaseous diffusion, the alveolar space is in close contact with pulmonary capillaries located within the stromal cells containing interstitium. The respiratory mucosal epithelium regenerates very slowly (more than 100 days) under steady state conditions with the basal cells giving rise to ciliated epithelial cells, goblet cells and neuroendocrine cells [117]. Club cells have self-renewing capacities and can also differentiate into the other epithelial sub types following injury [118]. At the alveolar level, the ATII cell is the putative progenitor cell that has capacities to differentiate into ATI cells in response to lung injury [118].

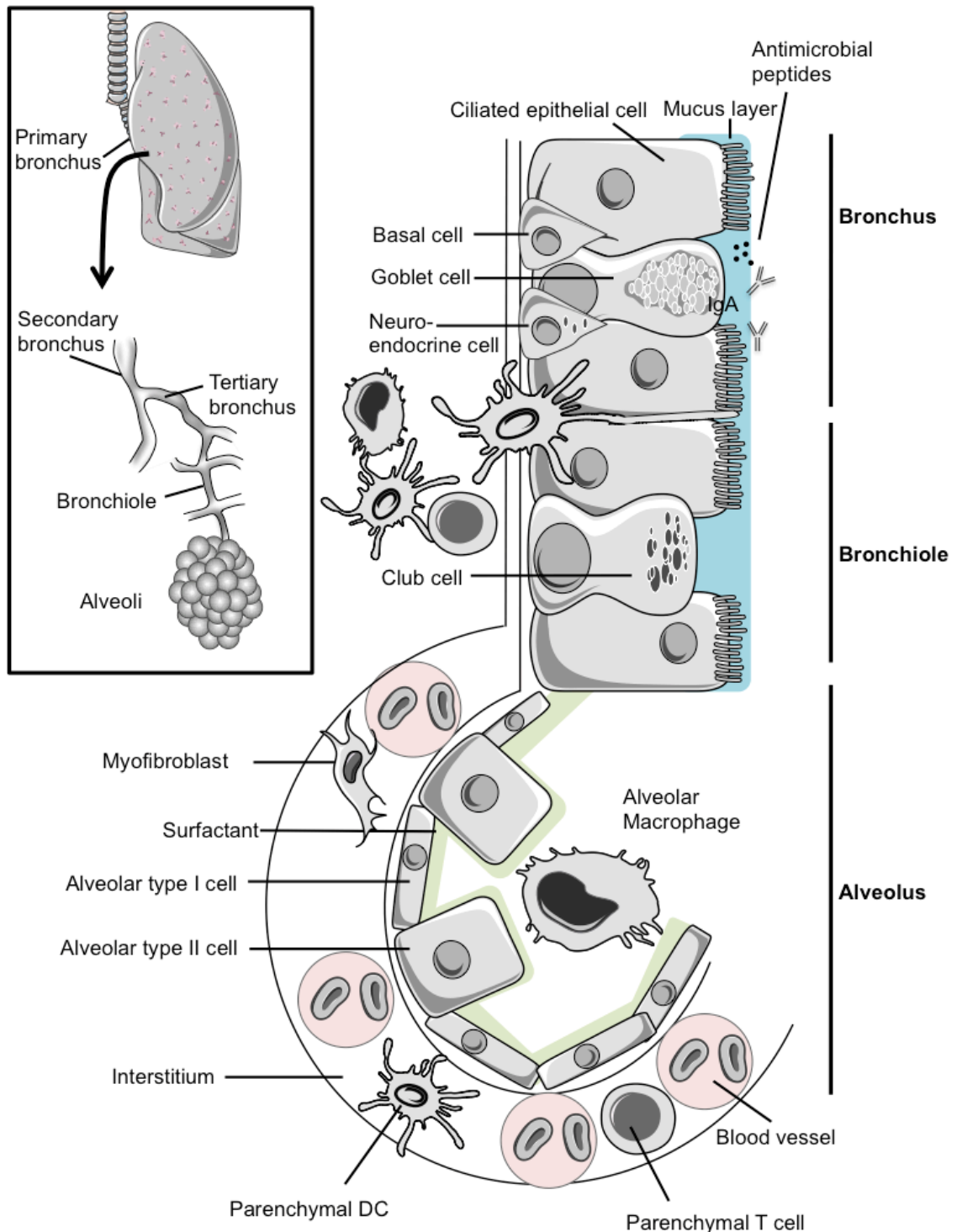


Fig. 1.5 Schematic representation of the lung epithelium.

The respiratory epithelium shows structural and functional differences in different parts of the airways. The epithelium in the upper airways are covered with mucus and consist of ciliated epithelial cells, goblet cells, stem cells and neuroendocrine cells, while the lower airways mainly exhibit Clara cells instead of goblet cells. The alveoli facilitate the respiratory gas exchange and are lined with type I and type II alveolar epithelial cells covered in surfactant. In the upper airways, immune cells are located beneath the lung epithelium, while in the alveoli, immune cells, mainly macrophages, are contained within the alveolar space. Figure adapted from Sun *et al.* [114] and Holt *et al.* [1].

1.2 Chronic inflammation of mucosal barriers

Chronic inflammation of mucosal barriers is defined by the inability of the mucosal tissue to maintain immune homeostasis. This occurs when pro-inflammatory immune responses towards a persistent injury or persistent infection cause the progressive or recurrent destruction of the mucosal tissue that impairs the normal physiological function of the underlying organ, ultimately leading to disease. The necessity for permeability of mucosal sites in microbial and immune cell rich environments means that the gastrointestinal and pulmonary systems are particularly prone to the development of chronic inflammatory diseases [48]. All of the above-described components of mucosal tissues, *i.e.* an intact mucus layer, epithelial barrier integrity, controlled immune responses and interaction with the microbiota, are important in maintaining immune homeostasis on mucosal barriers, while dysfunction of one component starts a cascade of events that affects the others and leads to inflammation (Fig. 1.6). During chronic inflammation, various persistent stimuli on both sides of the epithelium compromise the defence mechanism of the epithelium leading to epithelial barrier-disruption, increased epithelial permeability and increased exposure to external pathogens or antigens/irritants [119] (Fig. 1.6). Chronic mucosal inflammation in the intestine is established as inflammatory bowel disease (IBD) [15], irritable bowel syndrome (IBS) [120] or gastroenteritis and in the lung manifested as asthma [121], chronic-obstructive pulmonary disease (COPD) [122] or pneumonitis, all of which can lead to irreversible scarring of the lung tissue termed pulmonary fibrosis [123].

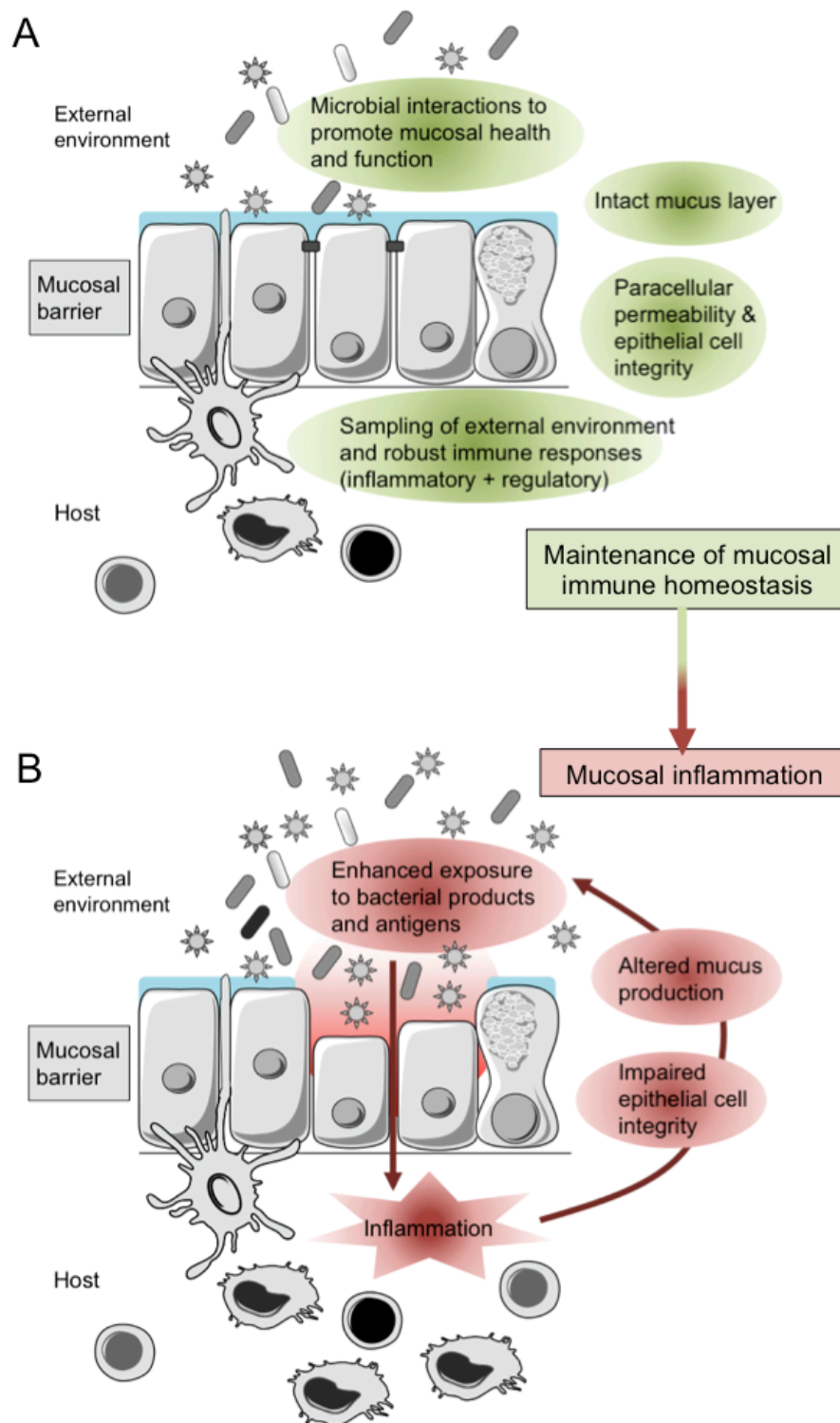


Fig. 1.6 Breakdown of mucosal immune homeostasis during mucosal inflammation.

(A) Epithelial barrier under steady state conditions and (B) epithelial barrier during chronic mucosal inflammation. (A) Four key components of mucosal barriers contribute to the maintenance of immune homeostasis of mucosal barriers: an intact mucus layer that forms a physical protection, balanced interaction and sampling of bacterial products which contribute to a healthy function of mucosal tissues, robust immune responses (well balanced between inflammatory and regulatory responses) and the maintenance of paracellular permeability and epithelial barrier integrity to fulfil the physiological organ requirements. (B) During mucosal inflammation immune homeostasis becomes impaired which affects the mucus layer, impairs epithelial barrier integrity and leads to an enhanced exposure to bacterial products and antigens.

1.2.1 Intestinal mucosal inflammation

IBD

The incidence and prevalence of IBD is significantly more common in industrialised than in non-industrialised countries affecting an estimated 2.5-3 million individuals in Europe each year [124]. IBD is a general term for a group of intestinal inflammatory conditions with Crohn's disease (often referred to as Crohn's) and ulcerative colitis (UC) as the two most common forms. Whilst Crohn's may affect any part of the gastrointestinal tract from the mouth to the anus, UC pathology is restricted to the colon [124]. Chronic intestinal inflammation results in abdominal pain/discomfort, diarrhea and defecation rich in mucus and blood leading to anemia. Current treatments for IBD involve anti-inflammatory drugs, immunosuppression or anti-TNF antibody therapy [125, 126]. Not all patients respond to these therapies however, and some may need to undergo colectomy in case of UC or surgical removal of parts of the intestine in case of Crohn's [127]. To date, the causative factors of IBD are unknown; however, several factors have been implicated in the disease pathogenesis, including genetic predisposition, defects/imbalance of the host immune responses, altered interaction with intestinal microbial communities and environmental risk factors [66]. Risk factors can be external such as diet, hygiene, enteropathogens, antibiotics or internal such as stress and even smoking [128, 129].

IBS

IBS is a functional gastrointestinal disorder of no known origin but with a high prevalence (5-20 % of the population) [130]. Patients suffer from chronic abdominal discomfort, bloating and impaired bowel movements leading to constipation [131]. As IBS has been linked to stressful life style/events, current treatment involve targeting the brain-gut regulation, however, recent studies have linked alterations in the microbiota and intestinal inflammation to altered bowel function [130, 132, 133]. Underlying conditions of IBS are sometimes other enteropathies such as celiac disease or food allergies [130].

Bacterial and viral gastroenteritis

Intestinal inflammatory conditions caused by bacterial or viral infections result in diarrhea, vomiting and sometimes fever. The major types of viral intestinal infections are caused by rotaviruses or other enteroviruses [134]. Common bacteria that lead to gastroenteritis are *Campylobacter*, *Shigella*, *Escherichia coli*, *Clostridium difficile*, *Listeria* or

Staphylococcus aureus [134]. Most infections only last a few days and often people recover without treatments or in some cases are treated with antibiotics. However, some infections are chronic and require attention. A novel treatment that has proven particular successful for *Clostridium difficile* infections are fecal microbiota transplantations [135].

1.2.2 Respiratory mucosal inflammation

Asthma

Like IBD, the incidence and prevalence of asthma is significantly more common in industrialised than in non-industrialised countries and asthma is considered one of the most common respiratory diseases worldwide affecting about 30 million in Europe [136] and around 300 million people globally [137]. Asthma is a chronic inflammatory condition affecting the airways leading to airflow obstruction and bronchospasm, which is reflected in symptoms such as wheezing, coughing, shortness of breath [96, 97, 121, 138]. Asthma remains a poorly understood condition with current treatments involving predominantly the use of anti-inflammatory corticosteroids [139].

COPD

COPD affects about 65 million people globally [140] and is like asthma an obstructive lung disease that results in shortness of breath, coughing and sputum production [141, 142]. One of the major phenotypes of COPD is emphysema [141]. The prevalence of COPD is linked to tobacco smoke and air pollution, which provoke an inflammatory response in the lungs. Nevertheless, the full pathogenic factors are yet to be elucidated [122]. Current treatments involve the use of anti-inflammatory corticosteroids to reduce symptoms and patients are advised to quit smoking to help slow the progression of the condition; however there is no cure for COPD [122].

Bacterial and viral pneumonitis

Pneumonitis comprises pulmonary inflammatory conditions caused by viral or bacterial infections (e.g. pneumonia caused by *Streptococcus pneumoniae* [143] or by *influenza A* [144]), prolonged exposure to inhaled particulates (farmer's lung, bird fancier's lung, silicosis, asbestosis or pneumoconiosis) or radiation therapy [46, 47, 145]. Clinical features include shortness of breath and cough. Bacterial infections often require treatment with

antibiotics but healthy individuals usually recover [143]. In contrast, chronic inflammation of the lung tissue caused by inhaled particulates or following radiotherapy can lead to pulmonary fibrosis [47].

Pulmonary fibrosis

Pulmonary fibrosis is a serious disease during which excess fibrous connective tissue is formed, which progressively impairs the efficiency of gas exchange. Although the exact incidence and prevalence of pulmonary fibrosis is unknown, it is estimated that fibrotic diseases in general contribute to about 45% of all deaths in the industrialised world [146]. Pulmonary fibrosis has been implicated in chronic pneumonitis, chronic asthma, COPD and other insults to the lungs which cause them to react with scarring, *e.g.* first or second-hand cigarette smoke, environmental pollutants and persistent irritants, *e.g.* silica and asbestos [147]. However, the exact cause and evolution of this chronic disease in humans is difficult to study and remains poorly understood since patients seek medical care only at a stage of advanced disease. Consequently, the resulting disease is clinically termed “idiopathic” as the aetiology is unexplained [123] and is often fatal with no effective therapy available. Until now, a poor prognosis of only approximately 3 years survival after diagnosis demonstrates the lack of understanding of interstitial pulmonary fibrosis and the need for novel and efficient therapies [46].

1.2.3 Breakdown of components of mucosal barriers during the pathogenesis of mucosal inflammatory conditions

It is established that truly pathogenic bacteria or viruses can cause gastroenteritis and pneumonitis, even in healthy individuals. Therefore, bacterial or viral infections of mucosal tissues are not further discussed in this study. In contrast, the disease aetiology of IBD, asthma, COPD and pulmonary fibrosis is unknown. These mucosal inflammatory conditions, which represent central causes of morbidity and mortality worldwide, have led to intense research efforts to understand their pathogenesis. Currently, treatments are limited due to the lack of understanding of disease aetiologies and the occurrence of most of these inflammatory conditions has increased in recent decades progressively placing an economic burden on the health care systems.

It is generally believed that in genetically predisposed individuals one of the essential components of mucosal tissues is compromised which leads to a breakdown of immune homeostasis and chronic inflammation (Fig. 1.6). However, as the occurrence of mucosal

inflammatory diseases has dramatically increased in the last few decades, especially in highly developed countries [136, 140], additional non-genetic factors are thought to interfere with mucosal immune homeostasis [66, 122, 137]. Whilst it is well accepted that epithelial barrier dysfunction is associated with the development of inflammatory diseases [15, 116, 118, 121, 123, 148-150], controversies still exist as to what is the driving force of mucosal inflammation. Is it primarily a leukocyte-driven response that got out of control, leading to tissue injury and subsequent loss of epithelial barrier function? Or is the mucosa itself the primary conductor of local immune responses that has somehow lost its capacity to orchestrate?

1.2.3.1 Impaired mucus layer during mucosal inflammatory pathologies

Inflammatory pathologies of the lung are marked by goblet cell hyperplasia in the larger airways and metaplasia in the smaller airways, while inflammatory conditions of the intestine show a decrease in mucin-producing cells. Correspondingly, overexpression of mucins and increased mucin production has been linked to asthma, COPD and cystic fibrosis [116, 151, 152] and deficiency in mucin production is a key pathology in spontaneous colitis [2, 6]. Human inflammatory bowel diseases are accompanied by aberrant MUC2 expression and *Muc2*^{-/-} mice develop spontaneous colitis [153]. Human airway inflammatory conditions show increased levels of MUC5AC and its overexpression in mice leads to increased mucus production and protection from influenza infection [7]. Alongside increased mucus production, patients with pulmonary inflammatory pathologies also exhibit increased serum levels of surfactant protein such as SP-D [154, 155].

1.2.3.2 Impaired epithelial cell integrity during mucosal inflammation

Epithelial barrier disruption and increased epithelial permeability are well-accepted contributors to the pathogenesis of intestinal and respiratory inflammation [116, 120]. Both, epithelial barrier-disrupting agents and cytoskeleton-modifying proteins released by pathogens on the apical side and pro-inflammatory cytokines, proteases and ROS secreted by mucosal immune cells on the basal (tissue) side contribute to the disruption of the epithelial layer [119].

A defective ('leaky') intestinal epithelial barrier has been widely reported in the acutely and chronically inflamed and damaged intestinal mucosa of patients with IBD and IBS [15, 119, 120]. Indeed, decreased expression and differential distribution of tight junction

proteins is commonly observed within mucosal epithelial cells of IBD patients [120]. Induced defects in the intestinal epithelium of otherwise healthy animals leads to the initiation of colitis [153] and conversely reducing epithelial permeability using a zonulin peptide inhibitor attenuates colitis and ameliorates mucosal inflammation in colitis-prone *IL10*^{-/-} mice [156]. Further, disruption of the epithelial barrier has been implicated not only in other enteropathies such as food allergies, celiac disease and various infections with enteric pathogens, but also in systemic, extraintestinal inflammatory diseases such as sepsis and type I diabetes [148]. The contribution of barrier dysfunction to inflammation of the airways has not been characterised as intensively as in the intestine, however, increased airway epithelium permeability has been implicated in respiratory disorders such as asthma [121], pulmonary edema [157], acute lung failure [149], pulmonary inflammation and fibrosis [150]. Cytokines, such as TNF and IFN- γ , that are central to the pathogenesis of mucosal inflammatory conditions in the lungs [46] and the intestine [125], can affect the intestinal permeability by directly increasing the flux across the leak pathway [15]. Further, the increased number of mast cells in mucosal inflammatory pathologies has been linked to epithelial barrier disruption through the release of inflammatory mediators and mast cell tryptase [120].

1.2.3.3 Role of the microbiota in mucosal inflammation

Altered interactions between the intestinal microbiota and the host have been implicated in IBD [18, 66, 158-160]. For example, an impaired SCFA metabolism has been linked to intestinal inflammatory diseases [161]. Phylogenetic study of IBD-associated intestinal microbiota has revealed a reduced diversity of the microbiota in IBD-patients in comparison with non-IBD controls, in particular the depletion in certain types of commensals such as *Lachnospiraceae* and *Bacteroidetes* and the enrichment in *Proteobacteria* [162]. Similarly, the abundance of certain bacterial types such as *Firmicutes* and *Gammaproteobacteria* in human and mouse airways determine an asthmatic phenotype [163, 164]. This is consistent with studies analysing the lung microbiome of never-smokers, healthy smokers, smokers with COPD and COPD patients in general, which showed that a change in bacterial diversity, rather than overall microbial load, was associated with disease severity [165, 166]. In addition, Erb-Downward *et al.* demonstrated that the microbial composition differed in distinct areas of the lungs [165] suggesting that the heterogeneity observed during COPD and lung fibrosis (*i.e.* areas of

normal healthy lung tissue adjacent to localised foci of inflammation and tissue-damage) might be associated with a certain type of microbiota.

1.2.3.4 Exacerbated inflammatory responses during mucosal pathologies

It is clearly established that mucosal inflammatory diseases of both the intestine and the lung are the consequence of dysregulated adaptive immune responses. Whilst IBD is considered a T_H1 -type T-lymphocyte-driven disease [167] accompanied by impaired T_{reg} and T_H17 responses [168], asthma is driven by T_H2 -type T-lymphocyte mediated immunity [96, 121], COPD is characterised by an imbalance of $CD4^+$ / $CD8^+$ T cells [122, 169] and pulmonary fibrosis is associated with T_H2 and T_H17 responses [91]. Hence, extensive research has been undertaken to understand the underlying mechanisms of the complex and heterogeneous functions of T cells during mucosal inflammation. However, it is becoming increasingly evident that innate immune recognition at mucosal barriers might be considerably more important than originally envisaged and that inappropriate activation of mucosal immune responses leads to continuous antigen stimulation, ultimately activating pathogenic T cells and causing chronic mucosal inflammation [2, 122, 138]. Indeed, accumulating evidence suggests that PRR signalling in the intestine elicits complementary responses in mucosal epithelial and immune cells: whilst basal PRR signalling elicits immune responses that contribute to mucosal barrier function and mucosal immune homeostasis [55], aberrant PRR activation has been associated with persistent pro-inflammatory responses and chronic inflammation that is central to the pathophysiology of mucosal inflammatory diseases [170]. The latter point has received great attention in genome-wide association studies (GWAS) and has led to the discovery of the genes associated with susceptibility to IBD in humans, such as *NOD2/CARD15*, *NLRP3* and various TLR components [59, 171, 172]; although the exact role of these PRR genes in different cells of mucosal tissues and in disease aetiology remains unclear. Similar observations have been made in asthma where the importance of innate immune recognition of mucosal commensals and pathogenic microbes and their interaction with the respiratory epithelium during the development of asthma is becoming increasingly relevant [138].

Aberrant PRR signalling leads to a constant production of pro-inflammatory cytokines. $TNF-\alpha$ and IL-6 are increased in the inflamed intestinal mucosa in patients with IBD [66] and blockade of both using antibody therapies, anti- $TNF-\alpha$ (Infliximab, Adalimumab and

Certolizumab) and anti-IL-6R (Atlizumab/Tocilizumab), had ameliorating effects in clinical trials of IBD patients [125]. Hence, IBD patients are routinely treated with anti-TNF therapies, but the responsiveness varies between patients. In fact, in some cases patients show increased disease severity primarily mediated by infections [126]. TNF- α inhibitors (Infliximab, Golimumab and Etanercept) also show promising, but variable efficacy, for the treatment of lung inflammatory disease such as asthma, COPD and pulmonary fibrosis [46, 47, 173]. The main reason for the varying effects on disease outcomes of these anti-cytokine treatments is the fact that both cytokines are pleiotropic and exert their effects in both physiological and pathological processes [67, 69]. For instance, whilst under physiological homeostatic conditions TNF- α is key for haematopoiesis, cellular proliferation and regulating innate immune responses to control small infections at mucosal sides, this potent cytokine also drives chronic inflammation by recruiting and activating neutrophils and macrophages [69].

Although the pro-inflammatory mediator IL-1 β has been implicated in mucosal inflammation for some time, it is only recently that studies exploring inflammasome-dependent IL-1 β production have reinvigorated interest in the relationship of IL-1 β to mucosal inflammatory disease. In murine models, several pathologies, such as intestinal inflammation, lung inflammation and pulmonary fibrosis are prevented in mice lacking inflammasome components, such as *Asc*^{-/-}, *Caspase-1*^{-/-}, and *Nlrp3*^{-/-}, whereupon key role for inflammasome-dependent IL-1 β production in mucosal disease pathologies have been suggested [174]. However, there is emerging evidence that caspase-1 can also act as cell death enzyme [175] which might imply that inflammasome activation could represent an IL-1 β -independent mechanism that drives mucosal inflammatory diseases. Therefore, more research needs to be undertaken to specifically dissect the tissue/cell-related roles of inflammasomes in mucosal inflammatory diseases to be able to target mucosal inflammation more specifically than previously done with broad anti-TNF- α and IL-6 therapies.

1.3 Animal models of mucosal inflammation

Current treatments for mucosal inflammatory conditions often do not cure the disease but rather only treat symptoms [47, 122, 126, 137, 139, 146]. Thus, the incompletely understood pathogenesis and the clinical need for effective treatments of mucosal

inflammatory conditions are the main driving force behind the study of mucosal immunity in the intestine and in the lung and the continuous emergence of new animal models. Insights in the mechanisms mediating mucosal inflammatory diseases have commonly been obtained from studies in mammalian animal models that aim to recapitulate disease pathology in man [168, 176]. Animal models of mucosal inflammatory disease of both the intestine and the lung are fundamentally similar. Firstly, they are all aimed at trying to recreate the exact disease pathologies of humans. Secondly, all of them are aimed at inducing inflammation by interfering with immune homeostasis of the mucosal barrier.

1.3.1 Animal models of intestinal inflammatory diseases

The most prevalent models for recapitulating human IBD have been established in mice [168]. Since the aetiology of IBD has been explained by several mechanisms (Fig. 1.6) different approaches have been established to induce conditions reminiscent of IBD in mice: (i) administration of colitogenic chemicals, (ii) colonisation by colitogenic microbiota, (iii) genetically modified animals that develop spontaneous colitis and (iv) transfer of pathogenic T-cells into Treg-lacking recipient mice [168]. Chemically induced models of IBD are the most frequently used models since they allow testing for efficacy of genetic interventions to ameliorate inflammation without introducing further genetic manipulation and other caveats. Treatment of mice with dextran sodium sulphate (DSS), 2,4,6-trinitrobenzene sulphonic acid (TNBS) or oxazolone induces destruction of the epithelial layer of the mucosal barrier, subsequent bacterial translocation followed by immune cell infiltration [177]. In contrast, mice with a deficiency in their ability to recognise translocating antigens, such as *Tlr5*^{-/-} mice, develop spontaneous colitis, originating from altered gut-microbial homeostasis [178]. Powrie's model of IBD induced by transfer of CD45RB^{hi} CD4⁺ T cells into immunodeficient recipients mice is the most widely used model for studying effector T cell mechanisms in IBD [167]. All of these models confirmed the previously described interdependency of different host-derived and environmental factors contributing to mucosal immune homeostasis, while impairment of one of these factors leads to imbalance resulting in mucosal inflammation (see Fig. 1.6).

1.3.2 Animal models of pulmonary inflammatory diseases

As for the intestine, the most popular animal models for lung inflammatory conditions are established in mice [176, 179, 180]. Animal models of COPD and fibrosis mainly aim to

induce airway epithelial damage by exposing mice to pulmonary irritants associated with these conditions in humans, such as cigarette smoke, silica and asbestos, all of which induce inflammation and epithelial damage [179, 180]. The most widely used model of fibrosis is the bleomycin model, where lung epithelial damage induces excessive scarring [181]. Since asthma has long been considered a disease predominantly driven by T_H2 responses, the majority of animal models of asthma have been designed to recapitulate the classic T_H2 asthmatic eosinophilic airway inflammatory phenotype characterised by IgE production and T_H2 cytokines (IL-4, IL-5 and IL-13) [176]. The most common mouse models of allergic airway inflammation are the OVA and house dust mite sensitisation and challenge models [176]. However, there is a growing body of evidence suggesting that asthma is a result of aberrant innate immune recognition of viruses and bacteria at mucosal barriers [138], highlighting the need for novel and alternative approaches to study the mechanisms behind this condition.

1.3.3 Limitations of current animal models of mucosal inflammation and need for alternative approaches

There are several drawbacks of the above-mentioned animal models of mucosal inflammatory conditions of the intestine and the lung. Firstly, one of the major criticisms is that all models lack the chronicity or progressive nature of mucosal inflammatory diseases in humans [47, 137, 177]. Thus, while all of these models have contributed to understanding aspects of mucosal inflammatory diseases, not many of them might actually be physiologically relevant. Hence, so far the exact disease aetiology of mucosal inflammatory conditions is unknown and only very few promising drug candidates have been adopted for clinic use. Mucosal inflammatory disease is on the rise globally and remains an area of considerable unmet medical need [140]. Therefore, there is a need for a better understanding of the initiation and the mechanisms within different cellular components of mucosal tissues that drive mucosal inflammation and the development of new *in vivo* models to ensure the generation of new treatments that will go beyond symptomatic relief and potentially help to prevent mucosal inflammatory conditions.

1.4 Zebrafish as a model of mucosal inflammation

Zebrafish (*Danio rerio*) is the laboratory model of choice for studying many aspects of vertebrate biology. Compared with rodents they are inexpensive to maintain in large

numbers. Their permeability, at least during larval stages, allows targeting of biological processes by non-invasive administration of small molecule pharmacological inhibitors to the fish water, therefore facilitating high-throughput screening of therapeutic compounds. Zebrafish are amenable to genetic manipulation and microinjection of morpholino oligonucleotides into zebrafish embryos allows transient knock-down of target genes through interference with either splicing or translation [182]. Recent advances in the field of genome editing technologies such as the development of transcription activator-like effector nucleases (TALENs) and the clustered regularly interspaced short palindromic repeat/CRISPR-associated (CRISPR-Cas) system [183, 184] allow knock-down of target genes up to adulthood. The translucency of zebrafish embryos together with the availability of transparent mutants allows *in vivo* visualisation of biological processes of mucosal organs in an intact organism [185].

The immune system of zebrafish closely resembles that of mammals with the conserved presence of the major components involved [186-188]. Since the adaptive immune system is not fully functional until 4-6 wpf [189], the zebrafish offers the possibility to dissect innate immune responses in the presence or absence of responses of the adaptive immune system. However, the absence of the adaptive immune system during early stages of zebrafish development makes their use for mucosal immunology studies questionable.

The behaviour and activity of macrophages and neutrophils, cell types of particular importance in chronic mucosal inflammatory disease, is strikingly similar in human and zebrafish [186, 188, 190]. To study the involvement of these cells in mucosal inflammation *in vivo*, many transgenic (*Tg*) zebrafish lines are available with fluorescently labelled cells of the innate and immune system. For instance, in the *Tg(mpx:GFP)* labelling neutrophils green fluorescent protein (GFP) is expressed under control of the *myeloperoxidase* (*mpx*) promoter [191]. The transgenic line *Tg(lyz:dsRed)* in which *Discosoma* red fluorescent protein (*dsRed*) is expressed under the *lysozyme C* (*lyz*) promoter marks myeloid cells [192]. Both the transgenic lines *Tg(fms:mCherry)* and *Tg(mpeg1:EGFP)* mark macrophages while mCherry expression is controlled by the *colony stimulating factor 1 receptor*, a (*csf1ra* or *fms*) promoter and enhanced GFP expression (EGFP) is driven by the *macrophage expressed 1* (*mpeg1*) promoter [193, 194]. The transgenic line *Tg(gata2:EGFP)* labels eosinophils (*gata2* = *GATA binding protein 2*) [195], *Tg(lck:EGFP)* labels T cells (*lck* = *LCK proto-oncogene*, *Src family tyrosine kinase*) [196], *Tg(rag2:EGFP)* marks T and B cells (*rag2* = *recombination activating gene 2*) [197] and the *Tg(IgM1:EGFP)* labels B cells [198]. Further, mast cells seem to be conserved in

zebrafish [199, 200], but a transgenic line allowing the study of these cells in *in vivo* is yet to be generated. Hence, zebrafish appear to be a suitable model to study mechanisms of mucosal inflammation *in vivo*. However, there are key components of mucosal inflammatory conditions that are present in zebrafish but require functional validation [187, 188, 196, 201, 202]. For instance, despite genetic evidence true dendritic cells and NK cells are still elusive and conservation of the functional role of T cells and their subtypes in inflammatory set ups are yet to be investigated [203-207]. In addition, despite indication of the presence of different macrophage subtypes (M1 and M2) in zebrafish embryos [208], their functional specialisation is not clear. The same is the case for innate lymphoid cells: although genetic evidence of their conservation in zebrafish exists, their functional characterisation is still missing [81]. Zebrafish also lack lymph nodes, hence APC-lymphocyte interactions have been suggested to take place in the spleen [206]. Further, despite the presence of several immunoglobulin isotypes in zebrafish [209, 210], class switch recombination seems to be absent in zebrafish [211] and zebrafish do not produce IgA [212].

Despite these fundamental differences, the PRRs involved in mediating inflammation at mucosal barriers, such as TLRs and NLRs, are conserved in human and zebrafish [213-217]. Further, inflammatory mediators implicated in mucosal inflammation (such as Tnf- α , IL-1 β , IL-8, etc...) are not only present in zebrafish, but seem to fulfill similar pro-inflammatory functions [186, 188, 218-221]. The *Tg(NFkB:EGFP)* reporter line in which cells express EGFP following NFkB activation, represents a valuable tool to study NFkB signalling during mucosal inflammatory responses [222]. A characteristic of zebrafish that is generally regarded as disadvantage over mouse models is the fact that inbred lines cannot be generated [223]; thus making studies involving transplants or chimeras difficult [224]. However, when trying to understand mechanisms of mucosal inflammation, more-or-less outbred zebrafish could potentially better represent the variability seen in humans compared to inbred mice. Further, zebrafish are exposed to many more pathogens and diseases than laboratory mice, as their environments are more conducive to growth of microorganisms. In comparison to relatively sterile kept mice, this might actually represent a benefit of zebrafish when studying mucosal inflammation. With these unique features, zebrafish might be an attractive model with which to study aspects involved responses mediated by the innate immune system of acute and chronic inflammation within the mucosal intestinal and respiratory tissues.

1.4.1 Zebrafish intestine

Zebrafish, like other *cyprinids*, are stomachless and their intestinal tracts are comprised of three contiguous regions [225]. The anterior intestine (often referred to as the intestinal bulb), the mid intestine and the posterior intestine essentially carry out distinct roles similar to the small and large intestine of mammals [225, 226]. The anterior intestine is the principal site of digestion and nutrient absorption, such as fatty acids, which is reflected in the expression of the intestinal fatty acid binding protein (ifabp) in this region [227]. The mid and posterior regions of the intestine allow water absorption and ion uptake [228]. The intestine of larval zebrafish is fully functional by 5 dpf [226].

1.4.1.1 Structure of mucosal intestinal tissue

The mucosal epithelium of the zebrafish intestine is structurally similar to that of mammals, but less complex. The distinct crypt compartments are absent but the intestinal epithelium is multi-folded resembling the intestinal villi of mammals (Fig. 1.7). The stem cells are maintained in the intervillus pockets [225, 228, 229]. Additionally, zebrafish seem to be lacking Paneth cells and M-cells, but exhibit the other secretory cells (goblet and enteroendocrine cells) and absorptive enterocytes [228]. As in mammals, the zebrafish intestinal epithelial cells exhibit microvilli and are covered by a thick mucus layer. By 3 dpf, the zebrafish mouth has fully opened [226] and the intestine is colonised with the microbiota of the surrounding water [222]. The microbiota of the zebrafish larval intestine has recently been explored using modern 16S rRNA gene pyrosequence-based surveys, which revealed similarities to mammals in the main phyla present in the intestine, such as *Firmicutes*, *Proteobacteria* and *Bacteroidetes* [230, 231]. Techniques to generate germ-free and gnotobiotic zebrafish have been established [232] and revealed that the microbiota is key for the development and function of the intestinal mucosa [230, 233]. Further, although structurally different, teleosts possess a phylogenetically early form of GALT that is diffusely distributed and consists of innate immune cells (macrophages and granulocytes), lymphocytes and plasma cells, although the latter cells do not produce IgA [212].

1.4.1.2 Mucosal tissue responses during intestinal disease

In contrast to gills, which are routinely analysed during histopathological examination (see below), the intestinal tract is more difficult to examine due to technical issues with ensuring that the fixative properly penetrates the intestinal lumen and structural epithelial changes observed are not just artifacts from tissue autolysis [234]. Consistent with inflammatory disease of the mammalian intestine, the intestinal mucosa responds to infection with altered goblet cell physiology, intestinal epithelial cell damage and necrosis and infiltration of immune cells [234]. Therefore, the zebrafish intestine could potentially be a good model to study mucosal inflammatory diseases of the intestine.

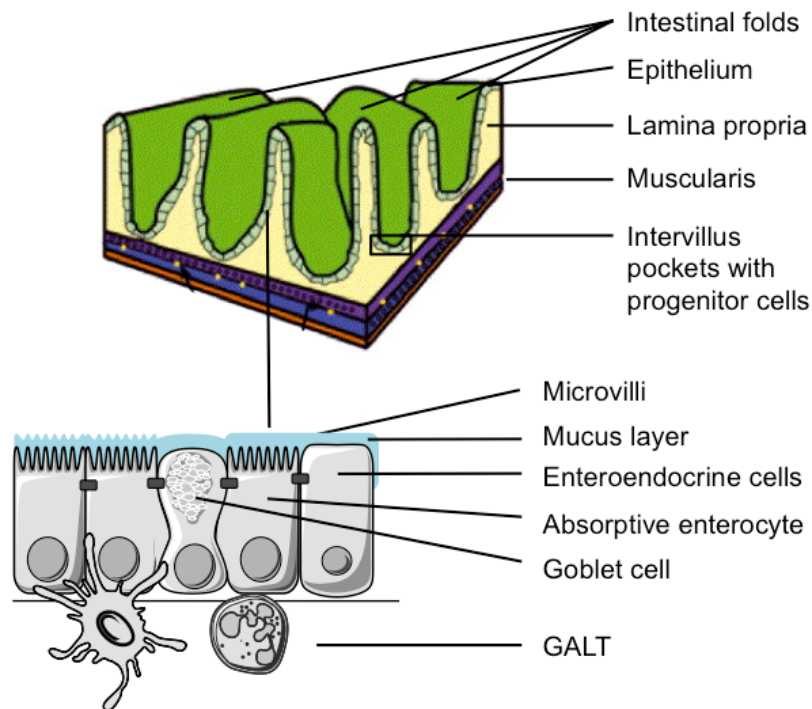


Fig. 1.7 Overview of the intestinal structure of zebrafish.

The intestine is organised in folds and lacks crypts. The progenitor zones that give rise to epithelial cells are located in the intervillus pockets. The composition of the intestinal epithelium resembles that of mammals with enteroendocrine cells, absorptive enterocytes and goblet cells that produce a protective mucus layer. The GALT is located in the lamina propria. Illustration above adapted from Wallace *et al.* [225].

1.4.2 Zebrafish gills

In zebrafish, the gill epithelium is the major route of oxygen uptake, as are mammalian lungs. They are directly exposed to ambient water and due to their lamellar and filamentous structure able to filter water in great volume [235], making them easily targetable with any waterborne substances. From 14 days post-fertilisation (dpf), zebrafish

fully depend on their gills to fulfill their oxygen requirements [236], considerably earlier than mice [237]. However, in addition to gas exchange, fish gills are a multipurpose organ that also carry out ionic diffusion to provide acid-base balance, osmoregulation and the excretion of nitrogenous wastes [234]. Teleost gills are comprised of four pairs of arches from which two rows of posteriolaterally oriented filaments diverge [234]. Filaments are supported by connective and muscle tissue. Each filament bears plate-like lamellae on both sides where the gas exchange occurs by a countercurrent exchange mechanism (Fig. 1.8).

1.4.2.1 Structure of mucosal gill tissue

The respiratory epithelium that lines the lamellae is microridged to increase the surface area for oxygen exchange (Fig. 1.9) [238]. The mucosa forms a physical barrier between the host and the aqueous external environment. Epithelial cells are interconnected with tight-junctions and desmosomes [238]. Goblet cells and osmo-regulatory chloride cells that are responsible for salt secretion of the gills are part of the respiratory epithelium that is covered with a layer of mucus and glycocalyx (Fig. 1.9) [239]. Each lamella is held together by pillar cells that form pillar channels or pillar capillaries through which the blood flows [240]. Additionally, there is data suggesting that pillar cells may constitute part of the mucosal immune system as they have been shown to phagocytose particles [241]. Similar to the mammalian intestine, the gill epithelium constantly regenerates with fast turnover times [234]. The progenitor zone that gives rise to mature epithelial cells is located at the base of the lamella beneath the epithelium from which new cells migrate up to the lamellar tip. Although a respiratory mucosa-associated lymphoid tissue seems to be lacking [242], the presence of immune cells such as macrophages and neutrophils within the intercellular spaces has been observed (Fig. 1.9) [234]. In addition, an interbranchial lymphoid tissue has been described in the gills of salmonids, which is located at the bottom of the filaments evenly distributed throughout the length of the gill arch [242]. However, whether the same is true for zebrafish is not established.

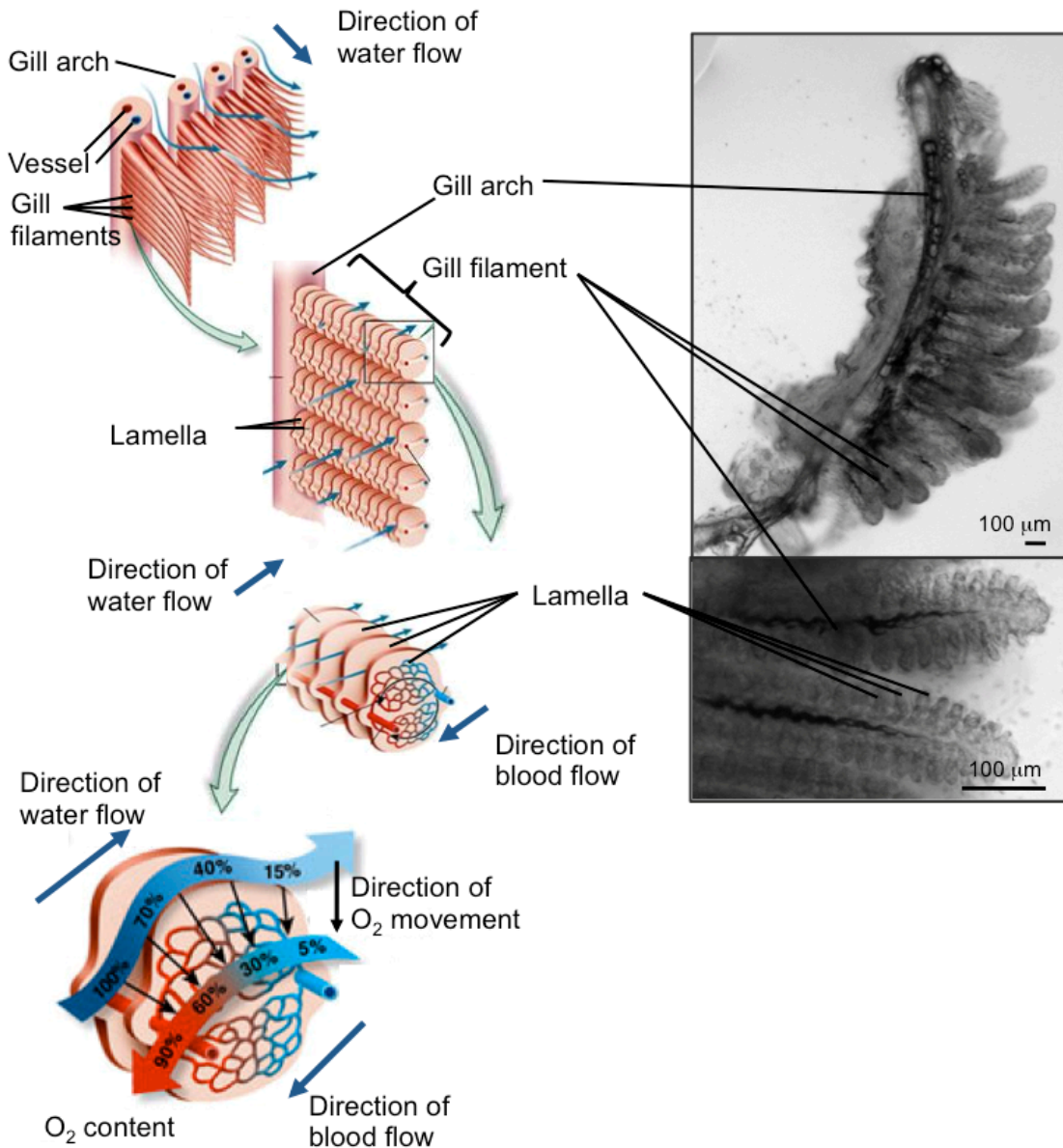


Fig. 1.8 Overview of the gill structure of zebrafish.

Gills are comprised of four pairs of arches on each side, diverging rows of filament bearing plate-like lamellae where the gas exchange occurs by a countercurrent exchange mechanism. Water flow occurs in the opposite direction of blood flow through lamellae resulting in a gradient for oxygen (O₂) saturation along the full length of the capillaries. Schematic was taken and adapted from R.J. Brooker [243]. Bright field images of one dissected gill arch from an adult zebrafish showing individual gill filaments (top) and individual lamellae (bottom).

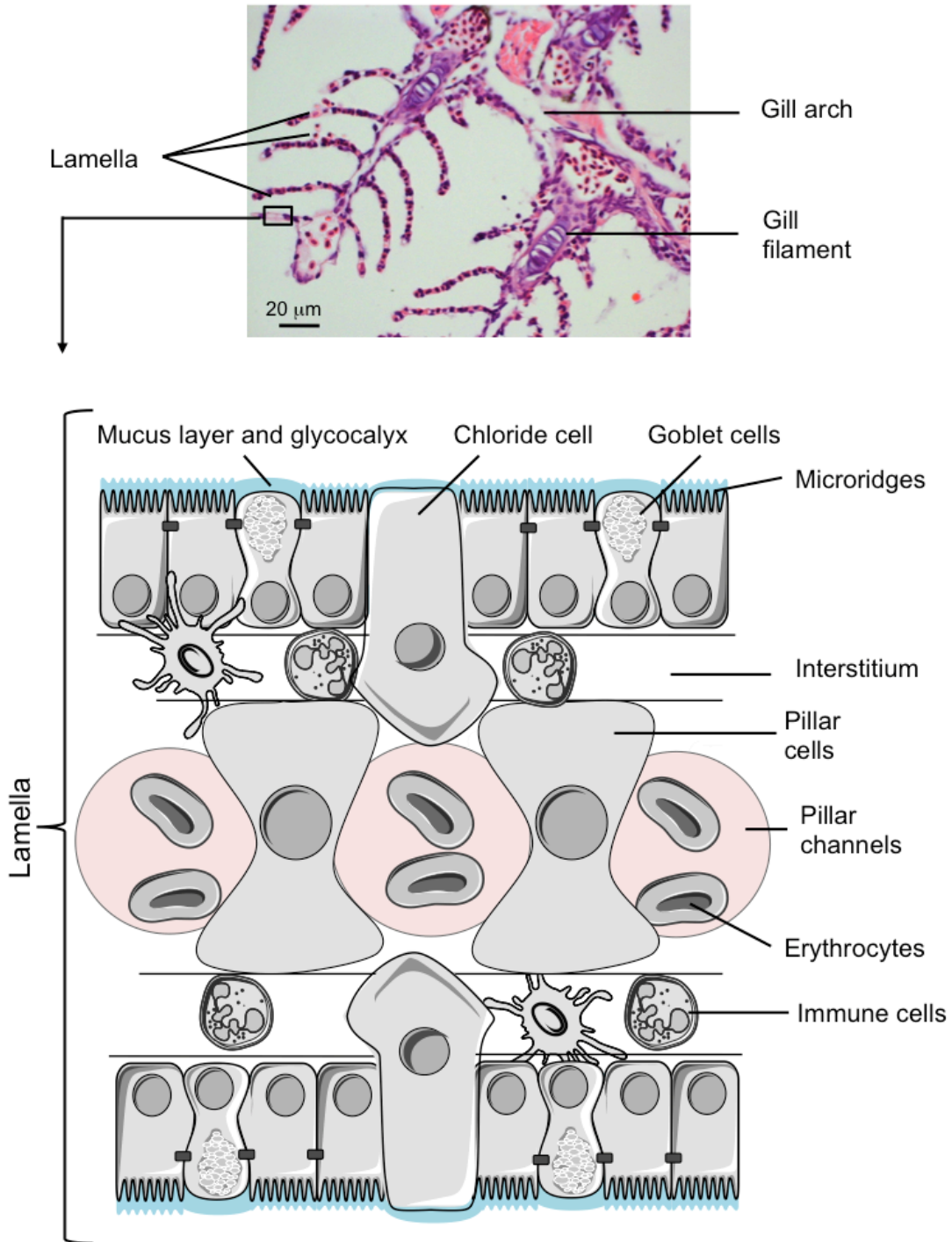


Fig. 1.9 Overview of lamellar gill respiratory epithelium.

Transversal section of a formalin fixed and paraffin embedded (FFPE) adult zebrafish head stained with haematoxylin & eosin (H&E) showing a gill arch with filaments and lamellae. The graphic at the bottom illustrates the structure of the respiratory epithelium of the lamellae. Epithelial cells are microridged and covered with a layer of mucus and glycocalyx. Chloride cells facilitate the osmoregulation and goblet cells produce mucus. Pillar cells maintain the structure of the lamellae and forms channels for erythrocytes to flow through.

1.4.2.2 Mucosal tissue responses during gill disease

Histopathological alterations in fish gills are often used as biomarkers of environmental water quality, and hence are commonly examined for diagnosis of fish health and toxicology, mainly during fish farming [234]. They are one of the first organs targeted by infectious and non-infectious processes and easily damaged. The type of response to injury of the complex and delicate gill structure (classified as lesions) depends on the length of exposure and severity of the causative agent [234]. There are an array of gill lesions commonly described, such as epithelial hyperplasia, lamellar fusion, lamellar oedema, epithelial lifting, flattening of secondary lamella, epithelial structure changes, vacuolisation, hypertrophy of secretory cells and infiltration of immune cells [238, 244-246]. Consistent with mammalian lungs, an increase in the number of goblet cells as well as mucus production is commonly reported when pollutants or pathogens irritate gills [247]. Remarkably, even after complete destruction or after severe damage [245], gills recover rapidly and often completely, but the mechanisms of repair in fish gills are unknown [234]. Although very common and histologically well characterised, the pathobiology of gill disease is poorly understood; the cell types acting as inflammatory mediators and the involvement of the innate immune system, the role of selected inflammatory cells and mediators and specific signalling pathways have yet to be elucidated. Only recent studies in the salt water fish salmon and cod have suggested that fish gills respond to infection with transcriptional responses of immune genes similar to that seen in mammalian lungs, such as the induction of IL-1 β , IL-8 and IFN- γ [248, 249].

1.4.3 Zebrafish intestine as a model of intestinal inflammatory disease

Due to the structural and functional similarities of the zebrafish and mammalian intestine, some of the above-mentioned models of chemical-induced intestinal damage have recently been adopted for zebrafish [250]. For instance, systemic exposure of zebrafish larvae to TNBS and DSS and zebrafish adults to oxazolone induces intestinal inflammation reminiscent of IBD characterised by intestinal immune cell accumulation in zebrafish, pro-inflammatory cytokine production and altered goblet cell physiology and mucus production [251-254]. Similar, glafenine treatment of zebrafish larvae induces intestinal inflammation through endoplasmic reticulum and mitochondrial stress leading to damage and apoptosis of intestinal epithelial cells and disrupted intestinal architecture [255]. Although the physiological relevance of these models is questionable, the zebrafish is a promising model organism in which to study aspects of IBD opening up new potential platforms for IBD drug discovery. Further, the developed germ-free and gnotobiotic techniques and modern sequencing technologies that allow determination of the intestinal microbial diversity offer valuable tools to complement the use of zebrafish as a model for dissecting host-microbial interactions in the vertebrate digestive tract implicated in IBD [230].

1.4.4 Zebrafish gills as a model of lung inflammatory diseases

Due to the absence of lungs and the obvious anatomical differences between the mammalian and the fish respiratory organ, so far researchers have not used zebrafish gills to model human lung inflammatory diseases [256]. However, there are some zebrafish models established in embryos to allow investigation of the genetic control of fundamental pathophysiological processes of lung inflammation.

For instance, Renshaw *et al.* developed a tail-transection model in *Tg(mpx:GFP)* zebrafish embryos which allows the study of mechanisms of neutrophil inflammation [190, 191], *i.e.* neutrophil accumulation, a key characteristic of lung inflammatory diseases, and reverse migration of neutrophils, which probably fails to take place during chronic lung inflammatory disease. This model is now widely used to study mechanisms of leukocyte recruitment towards a tissue injury [193, 194]. In the developing embryo the swimbladder epithelium is structurally, functionally and transcriptionally similar to the lung [257]. It represents an air-mucosal interface that performs gas exchange and consists of a single layer of epithelial cells [219]. Thus, Gratacap *et al.* established a mucosal zebrafish

swimbladder infection model using the human commensal fungus *Candida albicans* that can infect mucosal tissues as an opportunistic pathogen [219]. However, the physiological relevance of these models to study mucosal inflammation in the human lung is questionable.

Given the similarities of the basic components and structure of mucosal epithelial tissues of the zebrafish gill and the mammalian lung, it can be hypothesised that zebrafish gills could be used as a model to study mechanisms of mucosal inflammation in the human lung.

1.5 Aims

The main aim of this thesis was to use zebrafish as a model organism to study acute and chronic mucosal inflammatory responses in the intestine and the gills induced respectively by dietary components and respiratory irritants/injury associated with human disease.

Aim of chapter 1: To determine the mechanisms and cellular origin of intestinal inflammation induced by the dietary component, cholesterol, using larval zebrafish.

Aim of chapter 2: To develop a model of mucosal gill tissue injury in adult zebrafish in which to study the mechanism of wound healing versus fibrosis

The specific background and detailed aims are described in the two results chapters.

Chapter 2

Material and Methods

Chapter 2 | Material and Methods

2.1 Animal maintenance

Zebrafish

Wild type (WT), mutant and transgenic zebrafish strains used in this study (summarised in Table 1) were maintained according to standard practices and all procedures conformed to UK Home Office requirements (ASPA 1986). The following classification was used for the different fish life-stages: embryo stage after fertilisation to 5 days post-fertilisation (dpf), larval stage between 6 dpf - 1 month pf (mpf), juvenile stage 1-2 mpf and adult stage over 2 mpf. Larvae were initially reared at a density of 50 larvae per Petri dish in system water containing 3×10^{-5} % methylene blue (M9140; *Sigma*) as an antifungal agent and then transferred into 3-liter tanks with standard E2 media containing 15 mM sodium chloride (S7653; *Sigma*), 0.5 mM potassium chloride (P9333; *Sigma*), 1 mM magnesium sulfate (M7506; *Sigma*), 150 μ M potassium phosphate monobasic (P5655; *Sigma*), 50 μ M sodium phosphate dibasic (S7907; *Sigma*), 1mM calcium chloride (C5670; *Sigma*), 0.7 mM sodium bicarbonate (S6297; *Sigma*) and 10 U/mL penicillin/ streptomycin (15070-063; *Life Technologies*).

Fish were reared and maintained at 28.5°C on a 14 hours light / 10 hours dark cycle and fed twice a day using a combination of brine shrimp and dry food (standard zebrafish larval food (ZM; *ZM System*; ingredients: protein 52%, oil 12%, ash 8%, moisture 7%, fibre 3%) for larvae aged 6 dpf – 8 dpf (ZM000), larvae aged 9 dpf – 14 dpf (ZM100) and juveniles aged 2 wpi – 2 mpf (ZM200) and standard adult food (Hikari Tropical Micro Pellets, *Hikari*; ingredients: protein 49%, oil 7.8%, ash 11%, moisture > 10%, fibre 0.9%, phosphorus 1.7%) for adult zebrafish). System water used in all experiments is a combination of dechlorinated tap and reverse osmosis water at a ratio of 1:5.

Mice

Mice used in this study were maintained according to standard practices and all procedures conformed to UK Home Office requirements (ASPA 1986). Female Balb/c mice were obtained from Charles River UK at an age of 8-10 weeks and were maintained on a 12

hours light / 12 hours dark cycle. Drinking water and standard mouse diet (RM1, *Special Diet Service*) were provided continuously.

Name of strain		Original/ other name	Reference
Wild Type (WT)		AB	
Mutants	Genes affected		
<i>Tra^{-/-}/Nac^{-/-}</i>	<i>transparent (microphthalmia-associated transcription factor a, mitfa) and nacre</i>	<i>mitfa^{w2/w2};tra^{b18/b18}</i>	
Transgenics	Gene promoter	Labeled cells	
<i>Tg(lyz:dsRed)</i>	<i>Lysozyme C</i>	Mainly neutrophils	[192]
<i>Tg(mpx:GFP)</i>	<i>Myeloperoxidase</i>	Mainly neutrophils	<i>Tg(mpx:GFP)i114</i> [191]
<i>Tg(fms:nfsB.mCherry)</i>	<i>Colony stimulating factor 1 receptor</i>	Macrophages	<i>Tg(fms:Gal4.VP16)i186;Tg(UAs:nfsB.mCherry)i149</i> [193]
<i>Tg(NFkB:EGFP)</i>	NFkB transcription factor	Cells with activation of the NFkB pathway	<i>Tg(pNF-κB:EGFP)sh235</i> [222]
<i>Tg(ubi:EGFP)</i>	Ubiquitin B	All cells	<i>Tg(-3.5ubb:EGFP)</i> [258]

Table 1: Overview of zebrafish lines used in this study.

2.2 Feeding experiments

2.2.1 Preparation of experimental diets

50 mg or 100 mg cholesterol (C75209; *Sigma*) was dissolved in 1 ml diethyl ether (309966; *Sigma*) to create a 5% or a 10% solution, respectively, of which 400 µl were added to 0.5 g of standard zebrafish larval food (ZM000 and ZM100) or adult food (Hikari) to create a 4% or 8% diet. 400µl of diethyl ether was added to 0.5 g of ZM or Hikari to serve as a control diet. The larval diets were left in the fume cupboard overnight for the ether to evaporate and were ground up the following day into fine particles using a pestle and mortar (adapted from [259]). For the preparation of sterile food, ZM000 was autoclaved prior to the supplementation with cholesterol as described above, which was performed under sterile conditions.

Assuming that during the preparation process of an HCD all of the supplemented cholesterol is absorbed into the zebrafish food, the final percentage of cholesterol used for the short-term experiments in this study would be 8 %. However, this is unlikely to be the case due to residual amounts of cholesterol remaining on the preparation dish. Attempts to quantify the exact amount of cholesterol bound to the diet in HCD using ^3H -Cholesterol trace labelling failed since more than 90% activity was quenched by the food. Thus, cholesterol that was left on the pipette and the preparation dish was quantified instead and a loss of about 25% of cholesterol during the preparation process was estimated. This results in a final concentration of about 6% cholesterol instead of 8% for the acute feeding experiments and about 3% instead of 4% for the extended HCD experiments. This concentration of cholesterol is similar to that routinely used in used in atherogenic diets in inbred mice [260].

2.2.2 Feeding of zebrafish and treatment with inhibitors

All short term feeding experiments were performed at 6 dpf, or 7 dpf for MO feeding experiments (illustrated in Fig. 3.1A and Fig. 3.6), on zebrafish larvae that have not been fed prior the start of the experiment. Adult zebrafish were starved for 48 hours prior feeding. Larvae and adult zebrafish were placed in system water containing either 8% cholesterol (HCD) or a standard diet (control) for 6 hours at 28.5°C. For inhibitor treatment, zebrafish larvae were pre-treated with 200 nM NFkB activation inhibitor (NAI; 6-Amino-4-(4-phenoxyphenylethylamino)quinazoline; 481407; *Merck*) which was administered into system water 30 min prior the start of the 6 hours feeding period and was present for the duration of the feeding.

For long-term feeding, zebrafish larvae were kept in E2 media and were fed from 6 dpf twice a day with daily media changes for 10 days with 4% HCD or a control diet (illustrated in Fig. 3.20A). All inhibitor treatments were carried out using appropriate vehicle controls as indicated in the figure legends. For inhibitor treatments, 25 μM ezetimibe (SRP04000e; *Sequoia Research Ltd*) and 10 μM cathepsin B inhibitor Ca-074-Me (CA-074 methyl ester; C5857; *Sigma*) were administered to the E2 media before the first feed and were replaced daily with fresh E2 always prior to the first of the day.

For all experiments, zebrafish were randomly assigned to the various treatment groups. After randomised allocation of animals, treatments were coded until the experiment was finished and data was analysed.

Some of the long-term feeding experiments were performed with Nagisa Yoshida (Department of Life Sciences, Imperial College London (ICL), UK) as part of her Master's project. Therefore, Nagisa contributed to the data shown in Fig. 3.20B.

2.2.3 Analysis of food uptake and intestinal transit

According to the previously published technique for measuring intestinal motility and transit in zebrafish larvae [261], HCD or sHCD were supplemented with nonmetabolisable 2 µm yellow-green or red fluorescent polystyrene microspheres (F8827 or F8826; *Invitrogen*) and fed to zebrafish larvae in the presence of indicated inhibitors, morpholinos or under germ-free conditions. To assess the amount of ingested food at 2 hours, thresholded binary patterns of the area of the anterior bulb filled with fluorescent microspheres-labelled HCD were quantified using ImageJ (Fig. 3.7B). Additionally, the number of fish that have ingested food at 2 hours and 6 hours was recorded. To assess kinetics of microsphere movement through the intestine the transit zones and scoring system established by Field *et al.* [261] was followed (Fig. 3.7E) and larvae were analysed directly after the feeding period (6 hours) and after 24 hours (=6 hours feeding + 18 hours).

2.2.4 Mouse gavage

Female Balb/c mice (group of 3) were starved during the day and gavaged in the evening with 200 µl of either melted butter (unsalted, 82.2 g of fat/ 213 mg of cholesterol/ 100 g), corn oil, corn oil with cholesterol (40 mg/ml) or water control. Mouse gavage and dissection of intestines was performed by Dr Laurence Bugeon (Department of Life Sciences, ICL, UK).

2.3 Germ-free zebrafish

Zebrafish larvae were raised under germ-free condition as established by Pham *et al.* [232] with a few modifications. Adult zebrafish were bred either by setting up individual breeding pairs (one male and one female) in autoclaved system water or by in tank spawning trays. Embryos were collected no longer than one hour after the beginning of the light cycle and directly transferred into sterile E2 containing a mixture of antibiotics (100 µg/ml ampicillin (A9518; *Sigma*), 5 µg/ml kanamycin (K4000; *Sigma*), and 250 ng/ml amphotericin B (A2949; *Sigma*)). Both breeding methods were suitable to obtain germ-free embryos using the following treatment. Freshly fertilised zebrafish eggs were maintained at 28.5°C in sterile E2 antibiotic medium until 6 hpf when they were washed in 0.1%

polyvinylpyrrolidone-iodine complex (PVP1; *Sigma*), rinsed three times with the E2 antibiotic medium, incubated in 0.003% sodium hypochlorite for 20 min at room temperature and washed again three times with the E2 antibiotic medium. Subsequently, embryos were transferred into tissue culture flasks at a density of 5 embryos/ 10 ml of sterile E2 antibiotic medium and raised at 28.5°C with daily media changes but without any food supplementation until 6 dpf. Sterility of embryos was monitored routinely by either spotting 100 µl of embryo media or pestle-and-mortar-lysed embryos on tryptic soy agar plates (22091; *Sigma*) and was further confirmed by qRT-PCR using primers targeting 16S ribosomal RNA genes. For each experiment, conventionally raised zebrafish were maintained using standard conditions as described above in absence of any antibiotics or sterilisation by bleaching.

2.4 Morpholino treatment

Morpholino oligonucleotides (MO) were purchased from GeneTools, LLC (Philomath, OR, USA) and tagged 3'-carboxyfluorescein (FITC) or not (Table 2). 6 dpf zebrafish larvae were exposed to 20 µM MO solution for 24 h prior to feeding at 7 dpf (Fig. 3.15) or for 48 h before analysis of EGFP knock-down by flow cytometry (Fig. 3.16E).

Morpholino	Sequence (5'-3')	3' Modification
Standard control	CCCACAAACTGCAAAATATCAGCTT	- or FITC
ASC splice blocking	CAATTGCACTTACATTGCCCTGTGT	FITC
ASC specific control (mismatch)	CAATCCAGTTAGATTGCCGTGTCT	FITC
IL-1 β splice blocking	CCTCTTACCTCAGTTACAATTATA	FITC
GFP translation blocking	ACAGCTCCTCGCCCTTGCTCACCAT	-

Table 2: List of morpholino sequences.

2.5 Exposure to cigarette smoke and silica particles

Water containing cigarette smoke extract (CSW) was freshly prepared for each experiment (unless otherwise indicated) by bubbling smoke from one standard reference research cigarette (3R4F; *Kentucky Tobacco Research & Development Centre*) through 5 mL system water using an electrical pump to standardise the pressure applied. The solution was filtered through a 0.45 µm filter (*Nalgene*). The resulting concentration of CSW was 0.2 cigarettes/mL (c/mL). CSW was then further diluted in system water to obtain concentrations described elsewhere.

Silica nanoparticles (718483; *Sigma*) were suspended in system water at 0.5 mg/mL and dispersed by vortexing and sonication. Free-swimming larvae, typically 10-20 in number, or juvenile/ adult zebrafish, 3-5 in number, were exposed in either 20 mL (universal) or 250 mL (plastic containment), respectively, and rotated on a hybridiser (HB-1D; *Techne Hybridiser*) or on a shaker to prevent silica particle settlement during exposure. Dynamic light scatter measurements to determine size of silica nanoparticles were performed on a Zetasizer Nano (*Malvern*) with an average of 15 readings per particle suspension demonstrating an average silica particles size range of 100-1000 nm in system water. The set-up of the silica exposure experiment was carried out together with Rachel Vaux (Department of Life Sciences, ICL, UK) as part of her Master's project. Therefore, Rachel contributed to the data shown in Fig. 4.4E&F.

2.6 Cryoinjury

The experimental design for cryoinjury performed on gills of adult zebrafish is depicted in figure 8 and was performed as follows. Zebrafish were anaesthetised with 4.2% MS222 and positioned laterally under a dissecting microscope on a Petri dish. In order to facilitate the application of the cryoprobe the gill operculum was resected unilaterally with clean microdissection scissors. A deformed paperclip linked to a polyamide tube was cooled in liquid nitrogen and placed central on the gill tissue covering about 50% of the tissue. The cryoprobe was applied for 10 seconds after which fish were placed in a tank of fresh system water. Fish were swimming normally after 5 minutes. No fatality occurred during this procedure. Gill tissue damage was quantified using a qualitative score ranging from 0 to 3 was given where 3 reflects an injury affecting all four gill arches and 0 represents the absence of any detectable injury.

2.7 Staining of zebrafish larvae

2.7.1 Fixation of zebrafish larvae

Zebrafish larvae were euthanised with a lethal dose of MS222 (4 mg/ml; E10521; *Sigma*) and fixed in 4% paraformaldehyde over night at 4°C (PFA; 18814; *Polysciences Inc*). Following fixation larvae were washed twice in phosphate buffered saline (PBS) and stored no longer than 1 month at 4°C in PBS before being stained or sectioned as described below. Fixations as well as the all of the staining protocols were performed in 1.5 ml or 2 ml microcentrifuge tubes.

2.7.2 Whole mount staining of Zebrafish larvae with L-plastin antibody

Larvae were washed twice in PBS and deionised water (dH₂O), transferred to acetone (*Sigma*) for 7 minutes at -20°C, rinsed in dH₂O and then incubated in blocking solution (5% donkey serum (D9663; *Sigma*), 1% DMSO (D2650; *Sigma*) and 0.1% Tween (P1379; *Sigma*) in PBS) for 30 minutes. All the following steps were performed in blocking solution: embryos were incubated with a polyclonal rabbit anti zebrafish L-plastin antibody (1:500, kind gift of Paul Martin, University of Bristol, UK) at 4 °C overnight, washed four times for 20 min, incubated with a donkey anti-rabbit-TRITC antibody (1:100 diluted in blocking solution, 711-025-152; *Jackson ImmunoResearch Laboratories*) for 4 h at RT, washed four times for 20 min, rinsed briefly with PBS-Tween (0.1%; PBS-T) and imaged. Larvae were then imaged using an epifluorescent microscope and cell numbers were counted in a blinded manner.

2.7.3 Oil Red O staining

Fixed larvae were washed twice in PBS, once in 30% isopropanol, incubated in 60% isopropanol for 1 hour followed by incubation with freshly prepared Oil Red O staining solution for 2 hours. To prepare the final Oil Red O staining solution (0.3% Oil Red O (O9755; *Sigma*) in 60% isopropanol) a stock solution of 0.5% (w/v) Oil Red O was made up in 100% isopropanol (stable for 1 year), which was then diluted with dH₂O, incubated for 10 min at RT and filtered twice using Whatman Paper. After staining, samples were washed twice for 30 min in 60% isopropanol before being transferred to PBS.

2.8 Histology

Whole zebrafish heads were fixed in 10% neutral-buffered formalin overnight at room temperature. Samples were then washed in PBS and decalcified in ethylenediaminetetraacetic acid (EDTA, E5134; *Sigma*) solution containing 8% EDTA and 0.8% sodium hydroxide (S5881; *Sigma*) for 7-10 days. After decalcification specimens were washed with tap water, dehydrated and paraffin wax embedded. Larval zebrafish were fixed in PFA at 4°C overnight, washed in PBS, mounted in 3% agar (A1296; *Sigma*) and wax embedded. Sections (4 µm) were cut on a Leica rotary microtome RM2235 and mounted on slides. Slides were dried, deparaffinised in xylol, rehydrated and stained with either H&E, Alcian blue/Periodic-Acid-Schiff (PAS), trichrome or picro-sirius-red (PSR). Staining and coverslipping was performed on a Leica ST5020-CV5030 workstation operated by Lorraine Lawrence (Department of Medicine, ICL, UK). Lamellar fusion of

gill tissue was quantified using a qualitative score ranging from 0 to 3 where severe lamellar fusion affecting all lamella was scored with 3 and the absence of lamellar fusion was scored with 0.

2.9 Active caspase-1 staining (FLICA)

To assess caspase I activity in larval zebrafish, 19 dpf live zebrafish were incubated in system water containing 1xFLICA using the FAM FLICA™ Caspase 1 Assay Kit (ImmunoChemistry Technologies) for 30 min at 28.5°C. Following incubation larvae were washed twice for 5 min in washing buffer (included in the kit) diluted 1:20 in system water before analysis using fluorescence life-time imaging microscopy (FLIM).

2.10 Horseradish peroxidase staining

To assess horseradish peroxidase (HRP) uptake into intestinal cells, 7 dpf larval zebrafish were incubated in system water containing 10 mg/mL HRP (77332; *Sigma*) for 2 hours at 28.5°C. Following incubation larvae were washed once in system water and fixed in 4% PFA for 2 hours at room temperature. Following fixation, larvae were washed twice in PBS, twice in dH₂O, transferred to acetone for 7 minutes at -20°C, rinsed in dH₂O and incubated at room temperature for 10 minutes with the AEC Peroxidase Substrate Kit (SKH200; *Vector Laboratories*).

2.11 Cholesterol uptake assay using BODIPY-cholesterol

BODIPY-cholesterol (81255P; *Avanti Polar Lipids*) solutions were prepared according to Walters *et al.* with a few modifications [262]. In brief, BODIPY-cholesterol was dissolved in sterile DMSO to obtain a 1.5 mg/ml stock solution, which was subsequently diluted in 1 % fatty acid free BSA in either system water or sterile E2 antibiotic medium. This suspension was further diluted directly by addition to larvae in system water or sterile E2 antibiotic medium to obtain a final concentration of 1.5 µg/ml BODIPY-cholesterol. Larvae were fed for 6 hours with sterile HCD before the uptake of BODIPY-cholesterol in intestinal epithelial cells was analysed by live confocal microscopy. A qualitative score of presence of BODIPY-cholesterol in cytoplasm of intestinal cells was given where the presence of strong fluorescence intensity and an abundant signal was scored with 3 and the absence of a signal was scored with 0.

2.12 Imaging

To perform of *in vivo* imaging zebrafish larvae or adults, fish were anaesthetised in 0.17 mg/ml MS222 and positioned laterally in either PBS or 0.5% low melt agarose (NuSieve™ GTG™ Agarose, 50080, Lonza).

2.12.1 Stereomicroscopy

Routine handling of zebrafish larvae and adults was performed using a manual stereomicroscope Zeiss Stemi 2000, Nikon SMZ1000 or fluorescent stereomicroscope Leica MZ10F.

2.12.2 Epifluorescence microscopy

Zebrafish larvae were imaged on an Olympus CKX41 fluorescent microscope (Olympus UR FLT50) fitted with a QImaging QICAM camera using the software Q Capture-Pro. Image analysis was performed using ImageJ or Photoshop CS4 software. The brightness and contrast were adjusted if required to improve the visibility of fluorescence and picture quality.

2.12.3 Confocal microscopy

Analysis of BODIPY-cholesterol and ASC-FITC-MO uptake in intestinal epithelial cells of zebrafish larvae was performed using an inverted Leica SP5 confocal microscope.

2.12.4 Light microscopy

Stained histological sections were imaged using Axiovision Rel 4.7 software on a Leica MPS 60 inverted microscope fitted with an AxioCam HRc camera.

2.12.5 Widefield microscopy and FLIM acquisition

Wide-field fluorescence microscopy was performed recording a series of Z-plane images (every 10 µm) on a Zeiss Axiovert 200 microscope with Compix SimplePCI imaging software. FLIM data were obtained from FLIM images recorded on a wide-field microscope (IX-71; *Olympus UK Ltd*) and a filter cube for GFP (GFP-3035B-OMF; *Laser 2000 Ltd*) using an in-house program Lab View. Natalie Andrews (Department of Chemistry, ICL, UK) performed FLIM acquisition and the analysis of the data shown in Fig. 4.5C.

2.12.6 Image analysis and quantification of cells

To quantify fluorescent cells following widefield microscopy images were merged and the area of interest selected using the image software Volocity. Blind counts were carried out to assess the number of cells.

2.13 Flow cytometry

All samples were processed on a LSRFortessa (*BD Biosciences*) and analysed using FlowJo software (*Tree Star*) or sorted using fluorescence activated cell sorting (FACS) on a FACS Aria (*BD Biosciences*).

Zebrafish

For analysis of cell accumulation, distal portions of adult zebrafish intestines or zebrafish whole gill tissues were dissected, dissociated into single cell suspensions by digestion for 15 min at 37°C with PBS containing 0.25% trypsin, 1 mM EDTA, 5 mg/mL collagenase P (*Roche*) and subjected to flow cytometry analysis. For analysis of neutrophils, cells from *Tg(mpx:GFP)* transgenics were analysed as live cells, whereas for analysis of leukocytes, dissociated cells were fixed for 30 min at room temperature in 4% PFA and stained for 1 hour at room temperature with an rabbit anti-zebrafish L-plastin antibody (diluted 1:500 in blocking solution containing 5% donkey serum in PBS), then for 30 min at room temperature with the secondary donkey anti-rabbit IgG conjugated to TRITC (diluted 1:500 in blocking solution) and then analysed by flow cytometry. For analysis of fluorescence intensity and EGFP⁺ cell number, intestines of larval *Tg(NFkB:EGFP)* transgenic zebrafish were dissected out, pooled (n=3), filtered through a 100 µm strainer, and analysed by flow cytometry. For analysis of fluorescence intensity and mCherry⁺/EGFP⁺ cell number, intestines of larval *Tg(fms:mCherry)xTg(NFkB:EGFP)* transgenic zebrafish were dissected out, pooled (n=5), filtered through a 100 µm strainer, and analysed by flow cytometry. For analysis of caspase 1 activation, distal portions of adult zebrafish intestines or adult gill tissues were strained through a 100 µm strainer to prepare single cell suspensions which were then incubated for 30 min at 28.5°C in 1xFLICA using the FAM FLICA™ Caspase 1 Assay Kit (ImmunoChemistry Technologies) according to the manufacturer's instructions, washed in wash buffer and analysed by flow cytometry in presence of 1 µg/ml DAPI (Sigma) for live/ dead cell discrimination. For co-labelling with cytokeratin, single cell suspensions were fixed after incubation with FLICA according to the manufacturer's instructions, washed twice in

PBS-Triton-X (0.5%), stained for 1 hour at room temperature with a mouse anti-pan-cytokeratin antibody (MA1-82041; Thermo Scientific, diluted 1:100 in blocking solution containing 5% goat serum in PBS) and then washed and stained for 30 min at room temperature with the secondary goat anti-mouse-IgG-AF633 (A21052; Life Technologies; 1:1000 in blocking solution). To control for potential unspecific staining of the secondary antibody and to assign the gates for truly AF633+ cells, a secondary only staining control was performed. For analysis and sorting of FITC+ intestinal cells following treatment with indicated FITC-conjugated MO, pools of dissected intestines were strained through a 100 μm strainer to prepare single cell suspensions and analysed in presence of presence of 1 $\mu\text{g/ml}$ DAPI (Sigma) or fixed and co-labelled with a cytokeratin antibody as described above.

Mouse

For flow cytometry analysis, intestinal tract was dissected after 12 h and separated in 3 sections, upper and lower part of small intestine and colon (illustrated in Fig. 3.4). Tissue was cut into small pieces and incubated in PBS supplemented with 10 mM EDTA and 10% FCS for 10 min at 37°C. This step was repeated 4 times followed by incubation in RPMI containing 10% FCS, 15 mM HEPES (5630-056; *Gibco*), 100 U/ml collagenase VIII (C2139; *Sigma*) and 50 U/ml DNase (DN25; *Sigma*) for 45 min at 37°C. The suspension was filtered (100 μm strainer) and cells separated using percoll (P1644; *Sigma*). For flow cytometry analysis, cells were blocked with 0.5 $\mu\text{g/ml}$ anti-FC γ RII/FC γ RIII antibody (1:100; 553141; *BD*) for 20min at 4°C followed by an incubation with CD11b-FITC (1:100; 553310; *BD*) or a CD11c-FITC (557400; *BD*) antibody in PBS containing 3% bovine serum albumin (BSA, A8806; *Sigma*) and 0.09% sodium azide (08591; *Fluka*). Samples were washed twice in PBS before resuspension in PBS + 1 $\mu\text{g/ml}$ DAPI (4',6-Diamidino-2-phenylindole dihydrochloride, D9542; *Sigma*) for flow cytometry analysis.

2.14 Quantitative Real-Time PCR (qRT-PCR)

RNA extraction and cDNA synthesis

Dissected guts from larvae (pool of 20), dissected distal intestinal tissues from individual adult zebrafish, FACS-sorted FITC+ cells of dissected intestinal zebrafish, dissected gill tissue from adult zebrafish or dissected intestinal tissues from mice were homogenised using a pestle in lysis buffer and processed for RNA using the MagMAX™-96 Total RNA

Isolation Kit (*Life Technologies*) according to the manufacturer's instructions. The quantity and quality of RNA was assessed spectrophotometrically using a Thermo Scientific Nanodrop™1000. Dissected gill tissue for RNA sequencing (RNA-seq) analysis was lysed and homogenised in Trizol and processed using the PureLink™ RNA Mini Kit (*Life Technologies*) according to the manufacturer's instructions following the manufacturers protocol on a PTC-100™ programmable thermal converter (*MJ Research Inc*). The quantity and quality of the RNA was assessed using a 2100 Bioanalyser Instrument (*Agilent Technologies*). 85 ng of total RNA was used for reverse transcription using High-Capacity cDNA Archive Kit (*Applied Biosystems*) according to the manufacturer's instructions.

qRT-PCR

qRT-PCR was performed with 2% of cDNA generated using Taq fast universal 2x PCR Master Mix (*Applied Biosystems*) and Taqman primer and probes assays (*Applied Biosystems*, Table 3) or SYBR Green fast universal 2x PCR Master Mix (*Applied Biosystems*) and primers as listed in Table 3. All reactions were performed in duplicate or triplicate using a 7500 Fast Real-time PCR system (*Applied Biosystems*). Cycle thresholds obtained were normalised to 18S. For relative quantification, samples were calibrated to one control sample and using the standard $\Delta\Delta C_t$ method expressed as fold change relative to that sample.

Gene name	Organism	Type of assay	Taqman assay identification code/ SYBR primer sequences
18S rRNA	Eukaryote	Taqman	4319413E
16S rRNA	Prokaryote	SYBR	F: 5'-TCCTACGGGAGGCAGCAGT-3' R: 5'-GGACTACCAGGGTATCTAATCCTGTT-3'
	Species		
<i>Il1β</i>	Mouse	Taqman	Mm01336189_m1
<i>IL18</i>	Mouse	Taqman	Mm00434225_m1
<i>Nlrp3</i>	Mouse	Taqman	Mm00840904_m1
<i>Nlr4</i>	Mouse	Taqman	Mm01233151_m1
<i>Nlrp6</i>	Mouse	Taqman	Mm00460229_m1
<i>pycard (ASC)</i>	Zebrafish	Taqman	Dr03125114_m1 (exon spanning 1-2)
<i>il1b</i>	Zebrafish	Taqman	Dr03114368_m1
<i>tnfa</i>	Zebrafish	Taqman	Dr03126850_m1
<i>l-plastin (lcp1)</i>	Zebrafish	Taqman	Dr03099284_m1

<i>mpx</i>	Zebrafish	Taqman	Dr03075659_m1
<i>m17 (il6-like)</i>	Zebrafish	Taqman	Dr03098117_g1
<i>il8</i>	Zebrafish	SYBR	F: 5'- TGTGTTATTGTTTTCTGGCATTTC -3' R: 5'- CTGTAGATCCACGCTGTCGC -3'

Table 3: List of Taqman assays and SYBR primer sequences used in this study.

2.15 454-pyrosequencing

To analyse the microbial composition of zebrafish larval intestines 454-pyrosequencing was performed. cDNA was used as described above and from this source material 16S rRNA gene amplicons were generated for the V3-V5 variable regions using primer pair 357F and 926R. The amplicons were prepared by Research and Testing Laboratories Ltd. (Austin, Texas, USA) and were run on a Roche 454 GS FLX+. Once the sequence data had been obtained Dr Julian Marchesi (School of Biosciences, Cardiff University (CU), UK and Centre for Digestive and Gut Health, ICL, UK) performed all of data analysis. The raw data was pre-processed using the RDP's pyrosequencing pipeline using the default filtering criteria (Q score >20, max number of N's = 0, >200 and <600 nt). Once the sequences had been processed they were run through Mothur using the Schloss SOP [263]. Additionally the shared OTU data set was edited to compress all singletons and OTUs for which there were <10 reads in a sample, into a holding OTU, called OTU_X, in order to preserve the same reads numbers for each sample. Heatmaps of shared OTU data were generated in R using the packages NMF, RColorBrewer and Ggplots. All gut microbiota were sampled to >97% coverage with reads between 603-1965 per sample. Statistical analysis of the changes in the bacterial OTUs was undertaken in STAMP [264] using Welch's t-test and using a Bonferroni correction for multiple testing.

2.16 RNA-seq analysis

RNA samples for RNA-seq were sent to Boehringer Ingelheim where the subsequent steps were carried out. The library preparation for sequencing was performed using 200ng of total RNA input with the TrueSeq RNA Sample Prep Kit v2-Set B (RS-122-2002, *Illumina Inc, San Diego, CA*) producing a 275bp Fragment including Adapters in average size. In the final step before sequencing, 8 individual libraries were normalised and pooled together using the adapter indices supplied by the manufacturer. Pooled libraries were clustered on the cBot Instrument (*Illumina Inc*) using the TruSeq SR Cluster Kit v3 - cBot – HS (GD-401-3001, *Illumina Inc, San Diego, CA*). Sequencing was performed as 50 bp, single reads and 7 bases index read on an Illumina HiSeq2000 instrument using the TruSeq

SBS Kit HS- v3 (50-cycle, FC-401-3002, *Illumina Inc*). The raw sequencing data were then transferred to ICL where Geraint Barton (Bioinformatic Support Service, ICL, UK) performed the subsequent data analysis. RNA-seq data in FASTQ form from each sample were first quality assessed using fastQC. Reads were mapped using Bowtie [265] to the *Danio rerio* genome sequence v9 release 73 retrieved from Ensembl. Read counts for each exon and gene were generated in R using the GenomicRanges and Samtools Bioconductor packages against the *Danio rerio* v9 release 73 gtf file. Read counts were normalised to generate pseudo counts, followed by differential expression analysis using the edgeR [266] Bioconductor package which utilises empirical Bayes estimation and exact tests based on the negative binomial distribution. In addition the Bioconductor package mmseq was used to obtain differentially expressed transcripts. Genes were deemed statistically differentially expressed using 0.01 as cutoff for the false discovery rate (fdr).

2.17 Statistical analysis

All statistical analysis was carried out using GraphPad Prism 4.0 software (GraphPad software, CA, USA). Normality distribution was tested with the D'Agostino–Pearson omnibus test. When comparing two groups unpaired two-tailed t-tests (followed by Welch's correction test for non-equal standard deviations) and Mann-Whitney tests were used for parametric and non-parametric datasets, respectively. When comparing more than two groups, One-way ANOVA followed by Tukey's or Bonferroni's multiple comparison test and Kruskal Wallis test followed by a Dunn's multiple comparison test were used for parametric and non-parametric datasets, respectively. Two-way ANOVA was used to compare time-course curves followed by Bonferroni's multiple comparison test to determine the significance (Fig. 4.15C, Fig. 4.22C&D, Fig. 4.24, Fig. 4.25 and Fig. 4.26). P values of less than 0.05 were deemed statistically significant with *** $p < 0.001$, ** $p < 0.01$ and * $p < 0.05$. Pearson's correlation coefficient was used to assess the significance of the correlation shown in Fig. 3.22B, Fig. 4.19C, Fig. 4.21C-F and Fig. 4.22E. Error bars represent either standard error of the mean (SEM) or standard deviation (SD) as indicated in the figure legends.

Chapter 3

HCD-induced intestinal inflammation

Chapter 3 | HCD-induced intestinal inflammation

This chapter presents the work on the zebrafish intestine as a model to study mechanisms of diet-induced acute and longer-term intestinal inflammation. The work presented and discussed in this chapter builds on a previously established model in the Dallman lab of acute intestinal inflammation in zebrafish larvae following a high-cholesterol diet (HCD). The work leading up to this project is published in the PhD thesis of Navjyot J. Sangha [267] and key results that formed the starting basis of this project are explained in the introduction below (3.1) and summarised in Table 4 and Fig. 3.1. Together, our work has led to a publication entitled “Dietary cholesterol induces acute inflammasome-dependent intestinal inflammation” [Nature Communications, under review].

3.1 Introduction

Homeostasis of the intestinal mucosal immune system and its breakdown in local and systemic conditions

The gastrointestinal tract has to fulfill seemingly opposing tasks daily: to absorb nutrients and at the same time to defend the host from harmful pathogens/antigens. The gut microbiota poses a challenge for the mucosal immune system which has therefore evolved a sophisticated regulatory system to maintain a cooperative relationship. Whilst remaining relatively unresponsive during nutrient digestion and absorption, the mucosal immune system needs to be able to raise adequate host defence mechanisms against invading pathogens. These divergent roles of the mucosa are achieved by complex interactions between mucosal epithelial, immune cells and the commensal microbiota in a mutual effort to maintain intestinal immune homeostasis [2]. Homeostatic imbalance has adverse consequences both locally in the intestine, where it leads to immune-mediated conditions such as IBD [51] and systemically, where a compromised intestinal barrier has been implicated in the pathogenesis of systemic conditions such as obesity, diabetes, nonalcoholic steatohepatitis (NASH) and cardiovascular diseases [160, 268, 269]. Since patients suffering from these systemic conditions show markedly increased levels of circulating LPS, the prevailing notion is that physical impairment of the mucosal barrier allows translocation of bacterial products leading to metabolic endotoxemia and systemic

auto-inflammatory responses [160, 269]. The occurrence of these local and systemic immune-related disorders has dramatically increased in the last decades, coincidentally with the development of cultural westernisation and the consumption of diets rich in cholesterol and saturated fatty acids [129, 270]. Although the mechanism of dietary influence on intestinal homeostatic balance is only beginning to be understood, the microbiota is now considered a main cause of homeostatic perturbations (reviewed in [18]). For example, recent studies have demonstrated that long-term ingestion of a high fat diet (HFD) alters the microbiota [271, 272] which has been suggested to lead to dysbiosis, perturbation of immune homeostasis and a compromised mucosal barrier function resulting in intestinal inflammation [158, 159], which precedes systemic conditions [159]. In contrast, whether or not daily events such as changes in dietary components or nutrient absorption can directly induce acute inflammation in intestinal cells has been relatively understudied, apart from some earlier isolated reports suggesting the concept of nutrient-induced inflammation in intestinal cells, mainly introduced by fatty acids [273, 274].

The concept of nutrient-induced intestinal inflammation

Fatty acids

From *in vitro* studies in monocytes and macrophages, it is now established that saturated fatty acids have acute pro-inflammatory properties [275], while anti-inflammatory characteristics have been assigned to ω 3-unsaturated fatty acids [276, 277]. However the pro-inflammatory effect of saturated fatty acids on intestinal cells has not been explored in great detail. There are only two *in vitro* studies suggesting that fatty acids directly initiate inflammatory responses in the intestine. Fatty acid-exposure of IEC-6 cells, a cell line established from rat small intestine epithelial cells, induces the secretion of growth-regulated oncogene/cytokine-induced neutrophil chemoattractant-1 and IL-6 [274]. Further, intraepithelial lymphocytes isolated from mice produce less IFN- γ following TCR/CD3-mediated activation when treated with long chain fatty acids compared to untreated controls [273]. The direct link between fatty acids and intestinal immune responses has been explored further by two *in vivo* studies, which demonstrated that acute feeding of fat in mice increases the production of pro-inflammatory cytokines such as TNF- α , IFN and IL-6 by myeloid cells [278] and mast cell mediators such as histamines, proteases and lipid mediator prostaglandin D2 in mast cells [279]. However, the mechanism of initiation of inflammation in these studies is not dissected in detail and inflammatory effects indirectly

mediated via the microbiota were not excluded. Thus, *in vivo* evidence regarding a direct pro-inflammatory effect of dietary components on intestinal cells is lacking.

Cholesterol

Another component of Western type diets is cholesterol. Cholesterol crystals have been shown to activate the NLRP3 inflammasome complex in macrophages *in vitro* [61]. Successful assembly of the inflammasome and activation of caspase-1 in macrophages is thought to require two distinct signals (at least *in vitro*): priming (signal 1) and activation (signal 2) of the inflammasome complex [60]. Macrophages can be primed with LPS (signal 1) prior to exposure to cholesterol [61]. Cholesterol is engulfed by macrophages which perturbs cytoplasmic homeostasis and triggers lysosome destabilisation providing signal 2 of inflammasome activation [174]. The fatty acid palmitate has also been shown to activate the NLRP3 inflammasome in macrophages *in vitro* [62]. Components of the inflammasome machinery are expressed in intestinal cells where they exert essential functions such as sensing danger and triggering immune and repair responses thereby orchestrating mucosal immunity [50, 51, 174]. However, whether dietary fatty acids or cholesterol can directly engage with inflammasomes in intestinal cells and induce inflammatory processes in the intestine is an important but unanswered question.

A zebrafish model of HCD-induced intestinal inflammation

To study the potential pro-inflammatory effects of dietary components on intestinal cells *in vivo*, prior to this project, the Dallman lab established a model of acute intestinal inflammation in zebrafish larvae [267]. The zebrafish has been chosen as experimental model since nutrient- and pathogen-sensing systems are evolutionarily conserved between species [213, 214] and with their optical translucency and the availability of transgenic immune cell reporter lines [191, 193], the zebrafish allows an integrative multi-organ analysis of the short and long term diet-induced pathophysiological responses locally in the intestine as well as systemically. A single (6 hours) exposure to a high-fat diet (HFD) in the form of cream resulted in a significant, transient accumulation of myeloid cells in the zebrafish intestine. Subsequent experiments were performed to determine which component of the HFD mediated the inflammatory effect. In view of reported pro-inflammatory properties of cholesterol in cultured macrophages [61], cholesterol was introduced in the diet, which also resulted in the accumulation of myeloid cells in the larval intestine when compared to ZM control diet (Fig. 3.1A&B). Since this high-

cholesterol diet (HCD) also induced the accumulation of myeloid precursor cells, neutrophils and macrophages, the induction of generalised myeloid cell inflammation was concluded (Table 4). Pre-treatment with the pharmacological inhibitor ezetimibe, which inhibits cholesterol uptake/binding via NPC1L1 [280], blocked HCD-induced myeloid cell accumulation in the intestine (Table 4, Fig. 3.1C). This result demonstrated a direct pro-inflammatory effect of cholesterol on intestinal cells [267]. To our knowledge, this is the first *in vivo* report of an acute immune response induced by dietary components directly in intestinal cells.

In view of the recent discovery that cholesterol crystals activate the inflammasome [61], inflammasome-dependency was investigated in the model of HCD-induced intestinal inflammation in zebrafish larvae. Various pharmacological and genetic perturbations of signal 2 of inflammasome activation, such as chemical inhibitors targeting cathepsin B (Ca-074-Me), NADPH oxidase (VAS-2870) and caspase-1 (N-Acetyl WEHD-al) as well as morpholino oligonucleotides targeting ASC, inhibited HCD-dependent myeloid cell accumulation in the zebrafish intestine (Table 4, Fig. 3.1C). These results clearly demonstrated that HCD-induced intestinal inflammation depends on inflammasome activation and suggest that signal 2 of inflammasome activation is delivered by cholesterol engagement with NPC1L1 subsequently leading to lysosomal destabilisation involving ROS and cathepsin B [267]. These results prompted questions about the exact mechanism of action, *i.e.* how and where was signal 1 delivered.

Zebrafish larvae fed an HCD showed an accumulation of:		Peak of accumulation post feeding
Myeloid precursors	GFP+ cells in <i>Tg(pu.1:GFP)</i> [281]	12 hours
Neutrophils	dsRed+ cells in <i>Tg(lyz:dsRed)</i>	15 hours
Neutrophils	Cells stained for myeloperoxidase activity	12 hours
Macrophages	mCherry+ cells in <i>Tg(fms:mCherry)</i>	24 hours
Myeloid cells	L-Plastin+ cells	18 hours

Perturbations that abrogated the HCD-induced accumulation of L-Plastin+ cells in the intestine

Inhibitor/ Morpholino	Conclusion: HCD-induced accumulation of myeloid cells is dependent on:
Ezetimibe	Cholesterol binding/ uptake via NPC1L1
Ca-074-Me	Cathepsin B
VAS-2870	NADPH oxidase and ROS
N-Acetyl WEHD-al	Caspase 1 & 5
Splice- and translation blocking MO targeting ASC	ASC (<i>pycard</i>)

Table 4: Summary of key findings of N. Sangha's PhD thesis [267].

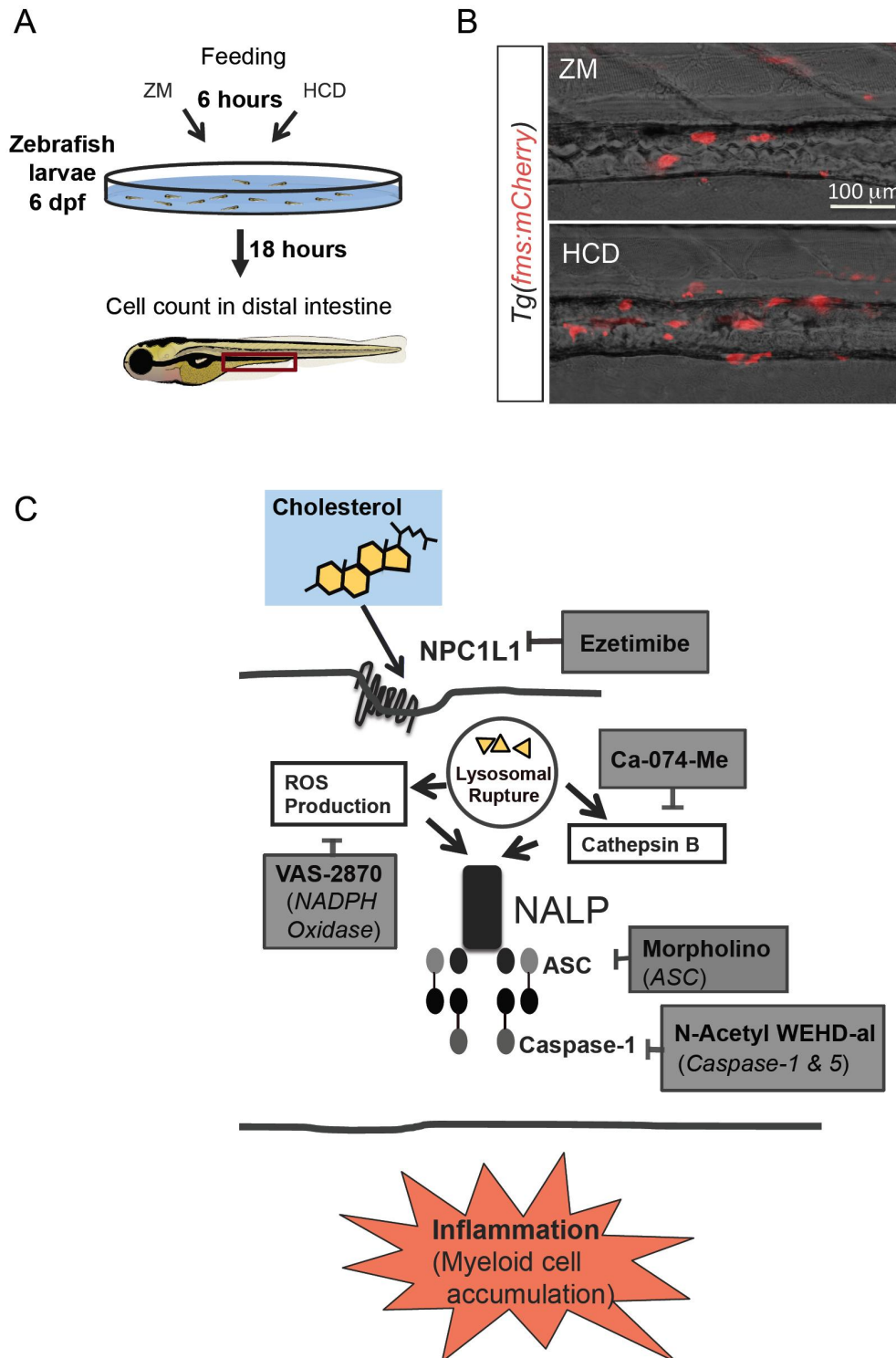


Fig. 3.1 Zebrafish model of HCD-induced intestinal inflammation.

(A) Schematic representation of experimental procedure. Zebrafish larvae (6 dpf) were treated with ZM control diet or HCD for 6 hours. 18 hours after feeding intestinal cells were quantified by cell counts in the distal intestine. (B) Representative fluorescent image of the distal intestine of *Tg(fms:mCherry)* zebrafish larvae showing accumulation of macrophages following HCD. (C) Schematic representation of components of inflammasome pathway investigated by N. Sangha [267]. Grey shaded boxes indicate inhibitory tools used.

Cellular origin of HCD-induced intestinal inflammation

Dietary cholesterol in its ingested form is esterified and needs to be hydrolysed by intestinal pancreatic cholesterol esterase [282, 283], following which it is incorporated into mixed micelles to enhance solubility in the intestinal lumen and to facilitate its diffusion to the boundary layer through the brush border of the mucosa [282]. Cholesterol uptake into enterocytes via their apical domain occurs via NPC1L1, likely through clathrin-mediated endocytosis [284, 285]. HCD-induced intestinal inflammation in zebrafish larvae is dependent on cholesterol binding/uptake via NPC1L1. Both haematopoietic and non-haematopoietic cells express NPC1L1 [286]. Thus, the cellular location of cholesterol-induced intestinal inflammation is unknown and could potentially be either haematopoietic or intestinal epithelial cells (IECs).

Apart from regulating absorption and metabolism of nutrients, IECs are equipped with innate immune sensors, PRRs, such as TLRs and inflammasomes [51, 55, 56]. Hence, IECs are well poised to act as sentinels and form the first line of protection in the armory of defence mechanism of the intestinal immune system. Indeed, there is growing evidence for a role for inflammasomes in IECs in defending the organism from harmful pathogens [52, 53], however, whether inflammasomes expressed in IECs can detect non-pathogen derived danger signals such as cholesterol is unknown.

Signal 1 of HCD-induced inflammasome activation

To achieve inflammasome activation *in vitro*, bacterial products such as LPS, through ligation of TLRs and NF κ B activation, typically deliver the cellular priming signal 1 leading to increased expression of both pro-IL-1 β and NLRP3 itself [60]. Since previous studies reported cholesterol-induced inflammasome activation in the context of inflammation in ‘sterile’ atherosclerotic lesions (in the absence of LPS), phagocytosis by macrophages was suggested to deliver signal 1 [61]. In contrast, a recent study hypothesised an alternative mechanism for signal 1 provision in the sterile environment: priming through the activation of a TLR4/6 homodimer and CD36 [287]. In fact, recognition and endocytosis of oxLDL by CD36 has also been described as 0’, which precedes upregulation of pro-IL-1 β expression by CD36-mediated interaction with the TLR4-TLR6 heterodimer (signal 1) and CD36-mediated intralysosomal conversion of oxLDL into cholesterol crystals, inducing lysosomal membrane rupture (signal 2) [288]. Whether common mechanisms provide signal 1 and signal 2 in the context of non-sterile

cholesterol-induced inflammation in the intestine *in vivo* or whether they are unrelated remains undefined.

Based on published data, three possible mechanisms of signal 1 delivery could be suggested: (i) direct stimulation of NF κ B and PRR signalling by the commensal microbiota, (ii) indirect activation by HCD-induced alterations of the microbiome and/ or (iii) direct PRR receptor engagement by cholesterol (Fig. 3.2). Colonisation of germ-free NF κ B reporter zebrafish [222] and mice [289] induces reporter activity in intestinal cells demonstrating that the microbiota activates NF κ B in the intestine. Indeed, intestinal paneth cells can directly sense gut bacteria MyD88-dependent toll-like receptor (TLR) activation [49]. Changes in the intestinal microbiome induced by dietary-changes have been detected as early as 24 hours [290, 291] and diet-mediated changes of the microbiota have been shown to induce intestinal inflammation [158, 159]. There is also a possibility that cholesterol can directly engage with PRRs inducing NF κ B activation *in vivo*, since free cholesterol in either plasma or endosomal membranes in macrophages can lead to activation of signalling via various TLRs *in vitro* [292].

Inflammatory mediator of HCD-induced intestinal inflammation

Whilst the results of N. Sangha suggested that HCD-induced myeloid cell accumulation is dependent on the inflammasome pathway, the mechanism linking inflammasome activation and myeloid cell accumulation is yet to be defined. In mammals, the IL-1 family members IL-1 β and IL-18 are processed by inflammasomes [61, 174]. Whilst *il18* has not yet been identified in zebrafish (ZFIN), IL-1 β processing by inflammasomes in zebrafish is controversial, as IL-1 β in zebrafish lacks the conserved caspase-1 proteolytic cleavage site [293]. However, in a tail transection injury model in zebrafish larvae *il1b* transcripts are increased followed by subsequent myeloid cell recruitment [294]. This accumulation of myeloid cells is abrogated using a caspase-1 inhibitor YVAD or a MO targeting IL-1 β , suggesting that inflammasome activation and IL-1 β function may be similar in zebrafish and mammals. Further, IL-1 β -processing by zebrafish caspase 1 orthologues (caspase a and b) has been demonstrated *ex vivo* [218] suggesting that IL-1 β in zebrafish can be proteolytically activated, although whether the same is true in an *in vivo* set-up is still elusive. Further, there is a possibility that the mechanism linking caspase-1 activation and inflammation is independent of IL-1 β processing [175]. Indeed, Angosto *et al.* show that infection-induced cell death of seabream macrophages is prevented when using a caspase-1 inhibitor, while IL-1 β processing is not affected [295]. These results support observations

showing that caspase-1 activation leads to cell death (termed pyroptosis) [296], but additionally suggest that pyroptosis may occur independent of IL-1 β processing.

In the present study, the previously established model of HCD-induced intestinal inflammation in zebrafish [267] was used to further investigate mechanisms underlying acute local inflammatory responses induced by dietary cholesterol and their relevance for extended local and systemic pathologies were investigated.

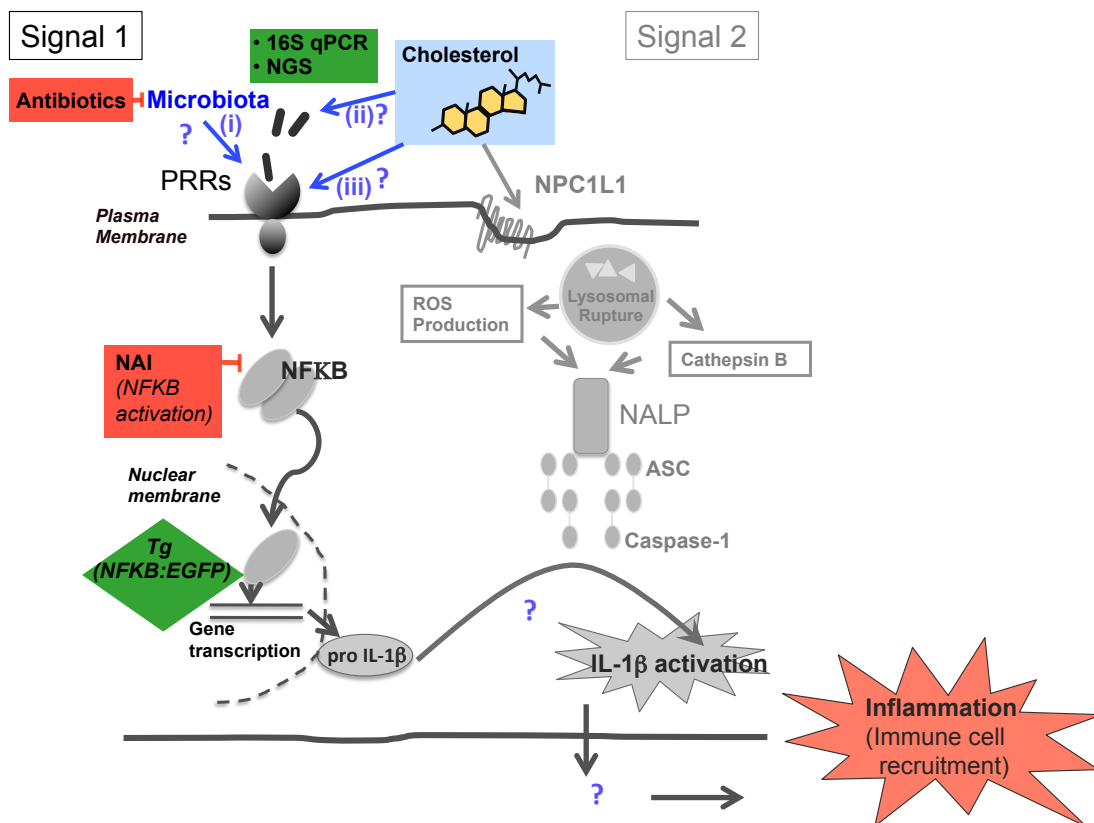


Fig. 3.2 Two-signal model of HCD-induced inflammasome activation.

Schematic representation of signal 1 of the two-signal-model of activation of the inflammasome investigated in this study. Red boxes indicate inhibitory tools, green diamonds highlight reporter activity tools and green rectangle experiments performed. Components of signal 2 of inflammasome activation were previously dissected by N. Sangha (see also Table 4 and Fig. 3.1C) and are coloured light grey [267].

3.2 Aims

Given the fact that cholesterol was able to deliver signal 2 of inflammasome activation, it was hypothesised that signal 1 might be delivered by the microbiota and that this activation would take place within intestinal epithelial cells.

More specifically, the aims of this chapter were to:

1. Confirm HCD-induced intestinal inflammation for adult zebrafish and mice.
2. Assess signal 1 of inflammasome activation during HCD-induced intestinal immune cell accumulation in zebrafish larvae.
3. Identify the cellular origin of HCD-induced inflammasome activation and investigate whether IL-1 β is involved in HCD-induced intestinal inflammation.
4. Investigate the relevance of mechanisms initiating acute HCD-induced intestinal inflammation for longer-term local and systemic pathologies.

3.3 Results

3.3.1 The effect of HCD on accumulation of myeloid cells in the intestine of adult zebrafish and mice

As demonstrated previously [267] and further confirmed in this study (see 3.3.2), 6 dpf-old zebrafish larvae fed an HCD develop an acute innate inflammatory response in the intestine within 24 hours. Notably, at that stage of development, the zebrafish only possesses innate immune function as full maturation of the adaptive immune system is not reached until 4-6 wpf [189]. To confirm the relevance of intestinal inflammation following HCD for fully immunocompetent zebrafish and higher organisms with a more complex immune system such as mammals, both adult zebrafish and mice were exposed to an HCD and investigated for intestinal inflammation.

Adult zebrafish

To investigate the effect of HCD on immune cell accumulation in the intestine, adult zebrafish were fed with a standard control diet (Hikari) supplemented (or not) with 8% cholesterol (HCD) prior to analysis by flow cytometry. This concentration of cholesterol was adopted from previous experiments in zebrafish larvae where the addition of cholesterol to a standard diet leads to an accumulation of myeloid cells in the intestine in a dose dependent manner [267]. Further, this concentration also induced atherosclerotic features of myeloid cell and lipid accumulation in the vasculature of larvae zebrafish when administered in a longer-term fashion [259] and is within the same range to that used in atherogenic diets in inbred mice [260]. To ensure sufficient ingestion of diets, zebrafish were starved for two days prior to exposure and their feeding confirmed by monitoring feeding behavior at the water surface after addition of food (Fig. 3.3A). An exposure time of 6 hours and the analysis time-point of 15 hours following feeding was also adopted from experiments in larvae, where significant accumulation of myeloid cells in larval intestine following HCD was detected from 12 hours post-feeding onwards and peaked at 18 hours [267].

To allow quantification of intestinal immune cells by flow cytometry, single cell suspension were prepared from intestines of adult transgenic zebrafish with fluorescently tagged immune cells. Fig. 3.3B represents a typical FSC-SSC (Forward Scatter-Side Scatter) flow cytometry profile of adult intestinal tissue where the forward scatter

correlates with the size of cells and the side scatter with their granularity. Fig. 3.3B also highlights the gating strategy that was carried out to exclude doublet events, i.e. FSC-Height (FSC-H) versus (vs.) FSC-Area (FSC-A).

The intestines of *Tg(mpx:GFP)* zebrafish expressing GFP under control of the *mpx* (myeloperoxidase) promoter were analysed to assess the effect of HCD on neutrophil accumulation. The gate for GFP⁺ cells in *Tg(mpx:GFP)* was assigned according to a control sample of WT intestinal cells that do not express GFP (Fig. 3.3C). Flow cytometry analysis of single cell suspensions prepared from the intestines of adult *Tg(mpx:GFP)* zebrafish after 15 hours following HCD for 6 hours (Fig. 3.3A) revealed a significant accumulation of live GFP⁺ neutrophils in HCD-fed fish (Fig. 3.3D-E).

Further co-labelling of single-cell suspensions with an L-Plastin antibody (rabbit anti zebrafish) following fixation was performed to assess the effect of HCD on leukocytes. To assign the gate for L-Plastin⁺ cells and to control for unspecific binding of the TRITC-labelled secondary (2nd) antibody (goat anti rabbit), staining only with the 2nd antibody in absence of the primary L-Plastin antibody was performed, and no nonspecific staining was observed (Fig. 3.3F). Analysis of intestinal cells after 15 hours following HCD for 6 hours demonstrated a significant increase in L-Plastin⁺ leukocytes present in the intestines following HCD (Fig. 3.3G-H). Together, these results indicate that HCD-induced intestinal inflammation is similar in zebrafish larvae and immunocompetent adult fish.

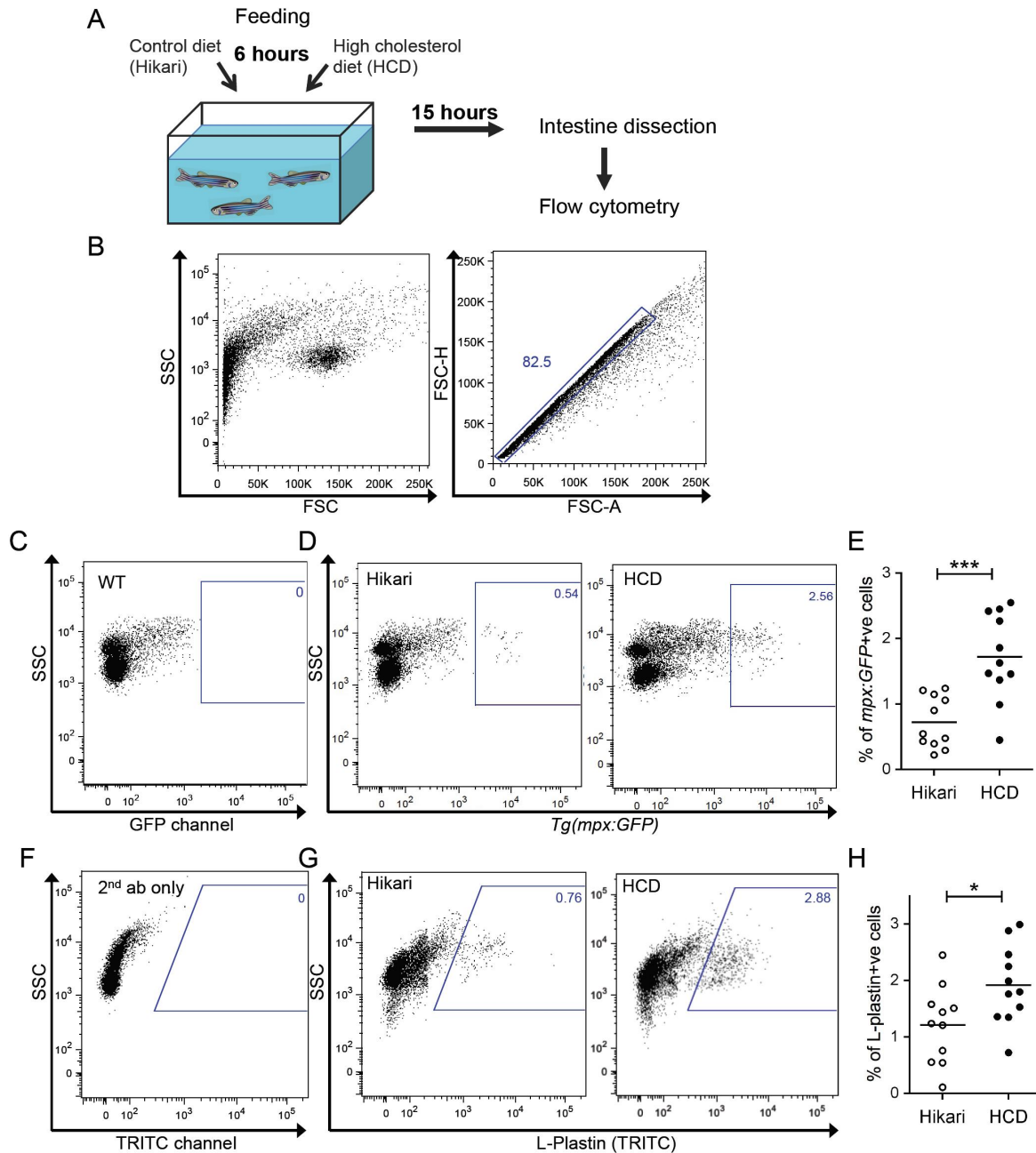


Fig. 3.3 Analysis of immune cell accumulation following acute HCD in adult zebrafish.

(A) Schematic representation of experimental procedure. Adult *Tg(mpx:GFP)* zebrafish were starved for 2 days before treatment with Hikari control diet or HCD for 6 hours. 15 hours after feeding intestinal cells were analysed by flow cytometry. (B) Representative flow cytometry plots of FSC-SSC profile of adult intestinal cells and gating strategy FSC-A vs. FSC-H to exclude doublets. (C) Flow cytometry plot of SSC vs. GFP channel of WT zebrafish intestinal cells. (D) GFP+ cells in the intestine of adult *Tg(mpx:GFP)*. (E) Quantification of % of GFP+. Each dot represents one individual fish pooled from three experiments (n=11). (F) Flow cytometry plot of SSC vs. TRITC channel of 2nd antibody (ab) control sample. (G) L-Plastin-labelled cells in the intestine of adult *Tg(mpx:GFP)*. (H) Quantification of % L-Plastin+ cells. Each dot represents one individual fish pooled from three experiments (n=11). * $p < 0.05$, *** $p < 0.001$, Student's t test.

Adult mice

To validate the results obtained in zebrafish in a mammalian system, the effect of an HCD on immune cell accumulation in mice was assessed. Oral gavage of cholesterol in a soluble form was chosen as mode of administration to allow standardisation of the amount of ingested cholesterol. A source of solubilised cholesterol is butter (210 mg / 100g = 0.21% of cholesterol). Butter gavage in Balb/C mice has been shown to induce TNF- α transcripts in lamina propria macrophages, however, a possible effect of butter gavage on immune cell accumulation was not investigated [278]. Hence, this experiment set out to assess the effect of an HCD in form of butter administered by gavage on immune cell accumulation in the intestine of mice. Balb/C mice were starved for 12 hours before feeding butter by oral gavage (Fig. 3.4A) and after 12 hours, the intestines were harvested. Since Fujiyama *et al.* detected the increase in TNF- α transcripts following butter gavage in lamina propria macrophages isolated from the ileum [278] and since N. Sangha detected the increase in myeloid cell accumulation following HCD in the mid- and anterior intestine of larval zebrafish [267], it was important to assess immune cell accumulation in the different intestinal sections following butter gavage. Therefore, during tissue harvest, the mouse intestines were split in three groups as illustrated in Fig. 3.4B: small intestine upper part containing the duodenum and the proximal jejunum, small intestine lower part containing the distal jejunum and the ileum and the colon. Dr L. Bugeon performed mouse gavage and intestine dissection and I extracted lamina propria lymphocytes and prepared single cell suspensions to assess the effect of butter gavage on the number of CD11b⁺ myeloid cells using flow cytometry analysis.

Fig. 3.4C represents a typical FSC-SSC flow cytometry profile and highlights the gating strategy that was carried out to exclude dead cells using DAPI and doublet events. Since the CD11b antibody is directly conjugated with FITC, an unstained sample was used to assign the gate for CD11b⁺ cells (Fig. 3.4D). Flow cytometry analysis of lamina propria lymphocytes prepared from intestines showed a significantly increased % of CD11b⁺ cells in the lower part of the small intestine following butter gavage (Fig. 3.4E&F) whereas no effect of butter gavage on the % of CD11b⁺ cells was recorded in the upper part of the small intestine (Fig. 3.4G) or the colon (Fig. 3.4H). These data suggest that HCD in the form of butter induces accumulation of CD11b⁺ myeloid cells in the small intestine.

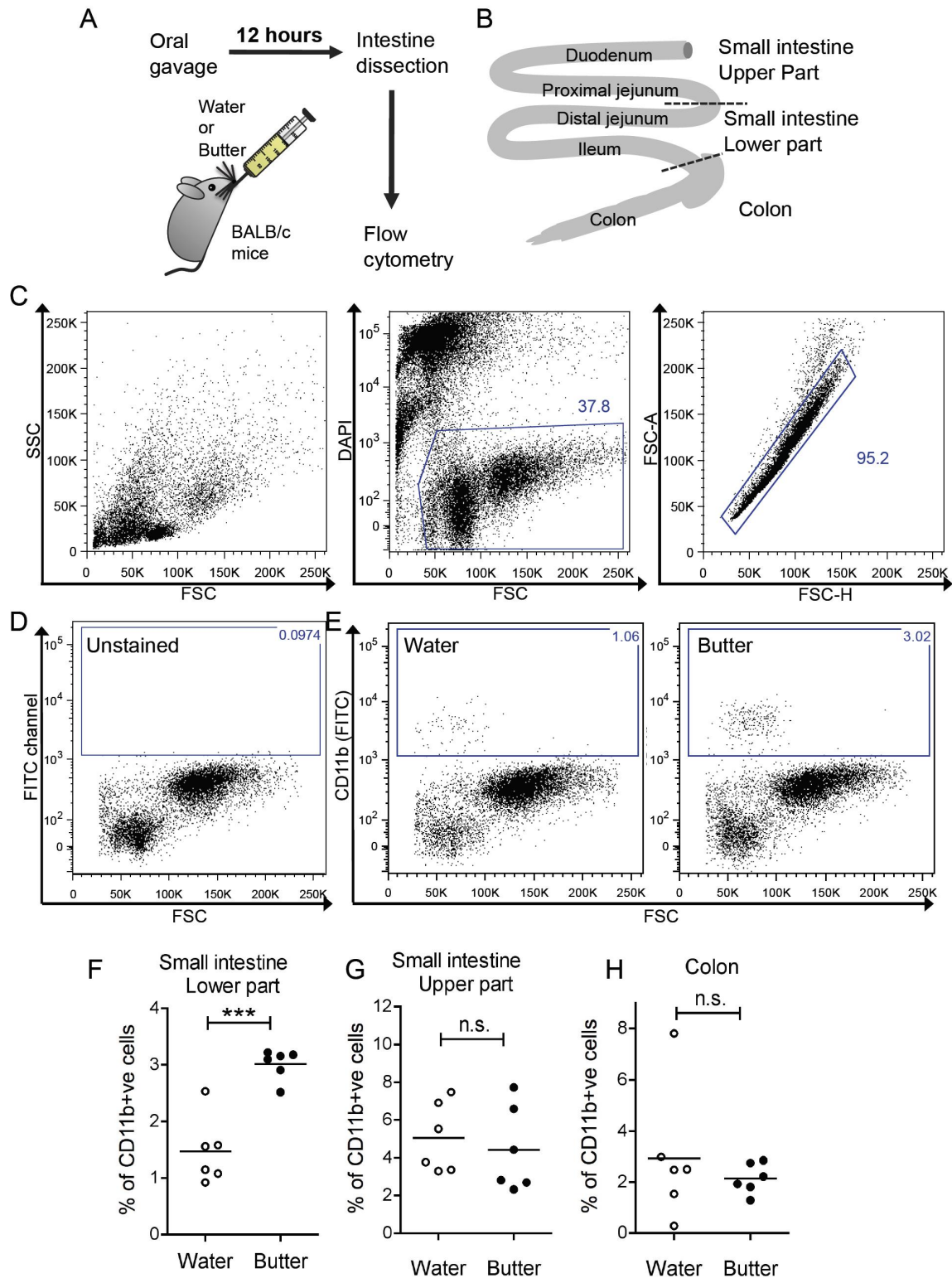


Fig. 3.4 Analysis of myeloid cell accumulation in intestine of Balb/C mice following butter gavage.

(A) Schematic representation of experimental procedure. Mice were starved for 12 hours before being treated with either 200 μ l of water or butter by oral gavage. 12 hours after gavage intestinal cells were analysed by flow cytometry. Mouse gavage and dissection of the intestine was performed by Dr L. Bugeon. (B) Schematic overview of mouse intestinal structure indicating the sections analysed by flow cytometry. (C-E) Representative flow cytometry plots of cells of the lower part of the small intestine. (C) FSC-SSC profile and gating strategy DAPI vs. FSC to exclude dead cells and FSC-H vs. FSC-A to exclude doublets. (D) FITC channel vs. FSC of unstained sample. (E) CD11b-labelled cells. (F-H) Quantification of % of CD11b+ cells in the lower part (F) and upper part (G) of the small intestine and the colon (H). Each dot represents one individual mouse pooled from two experiments (n=6). *** $p < 0.001$, Mann-Whitney U test.

However, in addition to cholesterol, butter is also high in saturated fatty acids, some of which have been shown to have pro-inflammatory properties [62]. To ascertain in the current experiments whether it was cholesterol or fatty acids mediating the inflammatory effects a direct comparison of these components was needed. To facilitate administration of cholesterol in a soluble form and since the uptake of cholesterol requires the presence of fatty acids [262], cholesterol had to be administered in the presence of oil. Gavage of 200 μ l corn oil with cholesterol at a concentration of 40 mg/mL was chosen, since successful uptake of cholesterol into intestinal epithelial cells of the small intestine has been previously demonstrated under these conditions [297]. At a usual daily amount of food intake of about 3.5 g in 8-week-old-mice [278], the amount of cholesterol (8 mg) administered by gavage corresponds to a day's feeding at 0.2% cholesterol, which equals the percentage used routinely in atherogenic diets in genetically modified, atherosclerosis-susceptible mice such as ApoE^{-/-} or LDLR^{-/-} mice [260]. To allow distinction between potential pro-inflammatory effects of cholesterol and fatty acids, in the next series of experiments Balb/C mice were gavaged with water and compared to mice gavaged with corn oil alone or with corn oil supplemented with cholesterol. Since the butter-gavage-induced accumulation of CD11b⁺ myeloid was only detected in the lower part of the small intestine (Fig. 3.4), only this section of the gut was analysed in the cholesterol gavage experiment.

Flow cytometry analysis on lamina propria lymphocytes prepared from the lower part of the small intestines showed a significantly increased % of CD11b⁺ (Fig. 3.5A) and CD11c⁺ (Fig. 3.5B) myeloid cells following cholesterol gavage when compared to gavage with water or corn oil alone. This confirmed that the accumulation of myeloid cells occurs in response to cholesterol rather than fatty acids alone, at least under these conditions.

Cholesterol-crystals added *in vitro* to (LPS)-primed human peripheral blood mononuclear cells and mouse macrophages leads to the release of IL-1 β and IL-18 dependent on NLRP3 inflammasome activation [61]. To quantify release of these mature cytokines, ELISA or immunoblotting is performed routinely [61]. However, since these techniques are not established for assessing proteins released by cells that are part of complex tissues such as the intestine *in vivo*, transcript analysis using qRT-PCR on whole tissue isolates of the small intestine was performed. A small, but significant increase in *Il1b* transcripts in cholesterol-treated mice compared to those treated with water or oil was observed (Fig. 3.5C), while no significant changes in the transcript levels of *Il18* were detected (Fig. 3.5D). These data show that cholesterol in its dietary form results in an increase of *Il1b* but

not *Il18* mRNA. Production of their mature forms would have to be confirmed by ELISA or immunoblotting using whole tissue-lysates.

Since NLRP3 transcripts are induced upon inflammasome trigger, at least *in vitro* [60], the transcript levels of *Nlrp3* mRNA as well as *Nlrc4* and *Nlrp6*, two other inflammasome components shown to be active in intestinal cells [51, 52] were assessed by qRT-PCR. Despite a slight increase following cholesterol gavage, no significant changes in *Nlrp3*, *Nlrc4* or *Nlrp6* transcripts were detected.

These results confirmed that the acute intestinal inflammation occurring in zebrafish larvae in response to both an HCD and an HFD also occurs in adult fish and mice. This confirms that HCD-induced intestinal inflammation is conserved in zebrafish and mice.

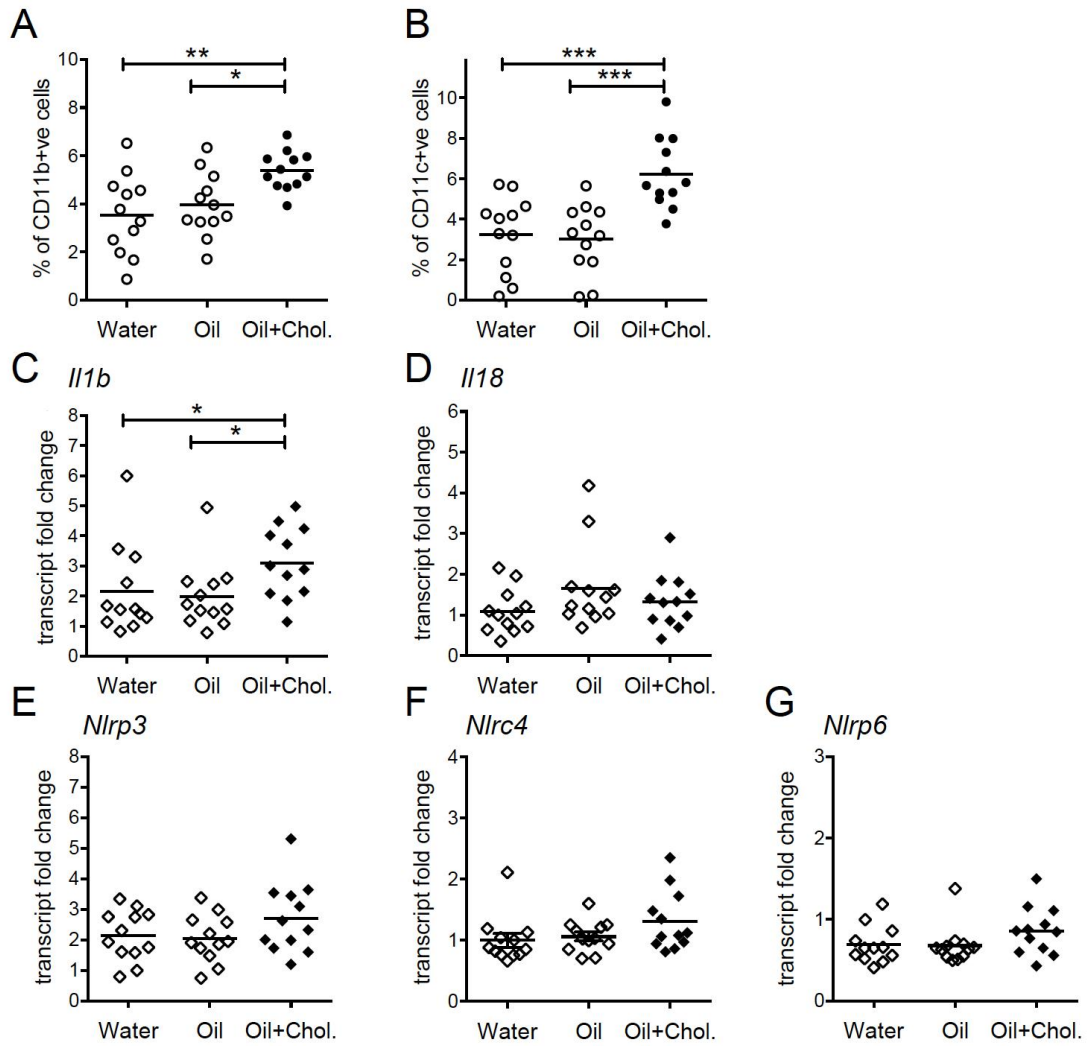


Fig. 3.5 Effect of cholesterol gavage on inflammation in small intestine of Balb/C mice.

Mice were starved for 12 hours before being treated with either 200 μ l of water or oil or oil + cholesterol (40 mg/mL) by oral gavage. 12 hours after gavage intestinal cells of small intestine were analysed by flow cytometry or qRT-PCR. Mouse gavage and dissection of the intestine was performed by Dr L. Bugeon. (A-B) Flow cytometry quantification of % of (A) CD11b+ and (B) CD11c+ in the lower part of the small intestine. Each dot represents one individual mouse pooled from four experiments (n=12). (C-G) qRT-PCR analysis of (C) *Il1b*, (D) *Il18*, (E) *Nlrp3*, (F) *Nlrc4* and (G) *Nlrp6* mRNA expression. Dot plot shows the relative expression values obtained for individual mice (n=12) which were normalised to 18S and expressed as fold change relative to one control sample. * $p < 0.05$, ** $p < 0.01$, *** $p < 0.001$. One-Way-Anova.

3.3.2 Signal 1 of HCD-induced inflammasome activation

Experimental set-up

For all acute feeding experiments designed to study the mechanisms of HCD-induced inflammation, previously established conditions were used [267]. In brief, since the completion of intestinal development and the onset of independent feeding in zebrafish larvae is achieved by about 5 dpf [226] zebrafish at an age of 6 dpf were chosen for acute feeding experiments to ensure full intestinal development and function across experimental groups. Zebrafish larvae were left unfed until the beginning of the experiment to ensure food uptake. To allow sufficient time for food ingestion, an exposure time to HCD of 6 hours was chosen. As a read-out of myeloid cell accumulation following HCD, the number of L-Plastin+ myeloid cells in the intestine was quantified at 18 hours post feeding, which represents the peak of L-Plastin+ myeloid cell accumulation [267]. Inhibitors were added 30 min before the feeding period and were present during the 6 hours feeding time (Fig. 3.6).

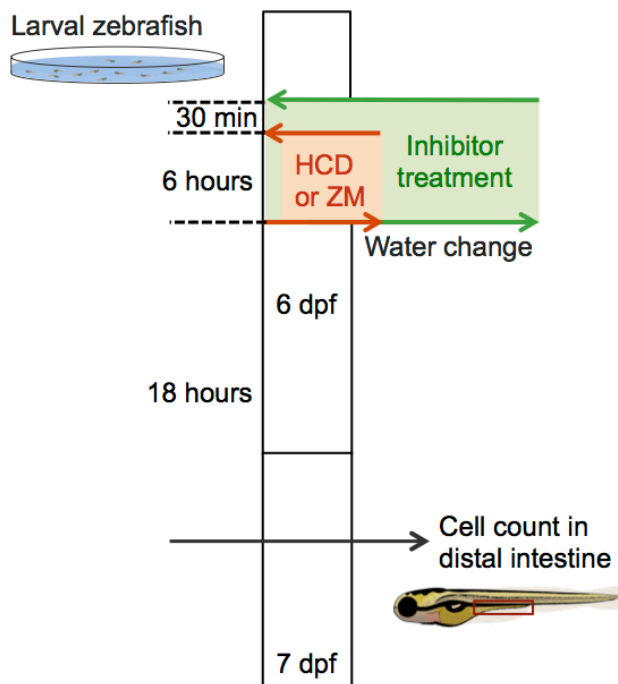


Fig. 3.6 Time-line of experimental procedure.

Zebrafish larvae were fed with either ZM control diet or HCD for 6 hours. Inhibitors were added 30 min before the feeding and were present during the 6-hour feeding period. Larvae were then transferred to fresh system water and the number of L-Plastin+ cells quantified after 18 hours. Experimental procedure adopted from N. Sangha [267].

NFkB activation during HCD-induced inflammation

Whilst N. Sangha demonstrated that signal 2 of HCD-induced intestinal inflammation in zebrafish larvae is provided by cholesterol binding/uptake via NPC1L1 involving lysosomal disruption and ROS [267] (Fig. 3.1C), the means by which signal 1 is delivered is unknown and was investigated in this study.

Firstly, it had to be established whether signal 1, *i.e.* NFkB activation [60], is required at all for HCD-induced intestinal inflammation. Kanther *et al.* demonstrated that treatment of *Tg(NFkB:EGFP)* zebrafish larvae with 200 nM of the inhibitor of NFkB activation (NAI) significantly reduced EGFP reporter activity, therefore sufficiently abrogating NFkB *in vivo* in larval zebrafish [222]. In this study larval zebrafish were pre-treated for 30 min with 200 nM of the inhibitor of NAI before exposure to HCD for 6 hours. However, while carrying out the experiments, the original dose of NAI used (200 nM) reduced fish survival in some instances and resulted in a visual reduction of larva activity (*i.e.* less active swimming behaviour). Therefore, experiments were repeated at a lower dose of NAI (150 nM) and this abrogated the accumulation of L-Plastin⁺ cells to the intestine following HCD (Fig. 3.7A).

Given the effect of the higher concentration of NAI on survival and activity of zebrafish larvae, it had to be ensured that the effect on myeloid cell accumulation was not simply due to the fact that larvae were less active and ingested less food. An assay was set up to assess food uptake, intestinal motility and transit in zebrafish larvae in which ZM and HCD were supplemented with nonmetabolisable yellow-green fluorescent polystyrene microspheres and fed to zebrafish larvae in the presence of 150 nM NAI [261]. To assess the amount of ingested food, zebrafish larvae were imaged after 2 hours of feeding since at that time-point the ingested food was still present in the anterior bulb (Fig. 3.7B). The area of the bulb filled with fluorescent microspheres-labelled food was quantified and used as measure of the amount of ingested food (Fig. 3.7B). Additionally, the percentage of fish that ingested food at 2 hours and 6 hours was recorded. As shown in Fig. 3.7C&D, there was no difference in the amount of food that had been ingested or the percentage of fish that had eaten by 2 or 6 hours when comparing DMSO-treated ZM or HCD fed fish and HCD-fed fish treated with 150 nM NAI. This result suggests that neither the type of food nor the NAI-treatment at a concentration of 150 nM alters food intake. Of note, larvae treated with 200 nM NAI showed significantly less ingested food at 2 hours of feeding (Fig. 3.7C). This result demonstrates that this new strategy to estimate food intake in larval zebrafish by computing the area of the fluorescence occupied by the intestine, as opposed

to quantifying the total amount of a tracer [262], is valid to detect differences in the amount eaten.

To assess the kinetics of food movement through the intestine and to allow comparison with published food transit rates following feeding [261] and microgavage [298], the transit zones and scoring system established by Field *et al.* [261] was adopted scoring the most anterior position of the food (Fig. 3.7E). As demonstrated in Fig. 3.7F&G, a great variability in intestinal speed amongst individual was observed. Whilst some larvae had already completely cleared microspheres from their anterior bulb by 6 hours, some had still full intestines (Fig. 3.7F). However, by 24 hours, most larvae had fully evacuated all of the microspheres and the remaining larvae exhibited beads only in the distal transit zones (Fig. 3.7G). These transit profiles correspond to those of previous studies indicating that the intestinal movement of larvae in our experiments is similar to that previously observed [261, 298]. Further, there was no difference in transit rates or amount of food ingested between DMSO and NAI-treated larvae. These data confirm that NAI-treatment at 150 nM does not affect the ability of larvae to ingest or to process food.

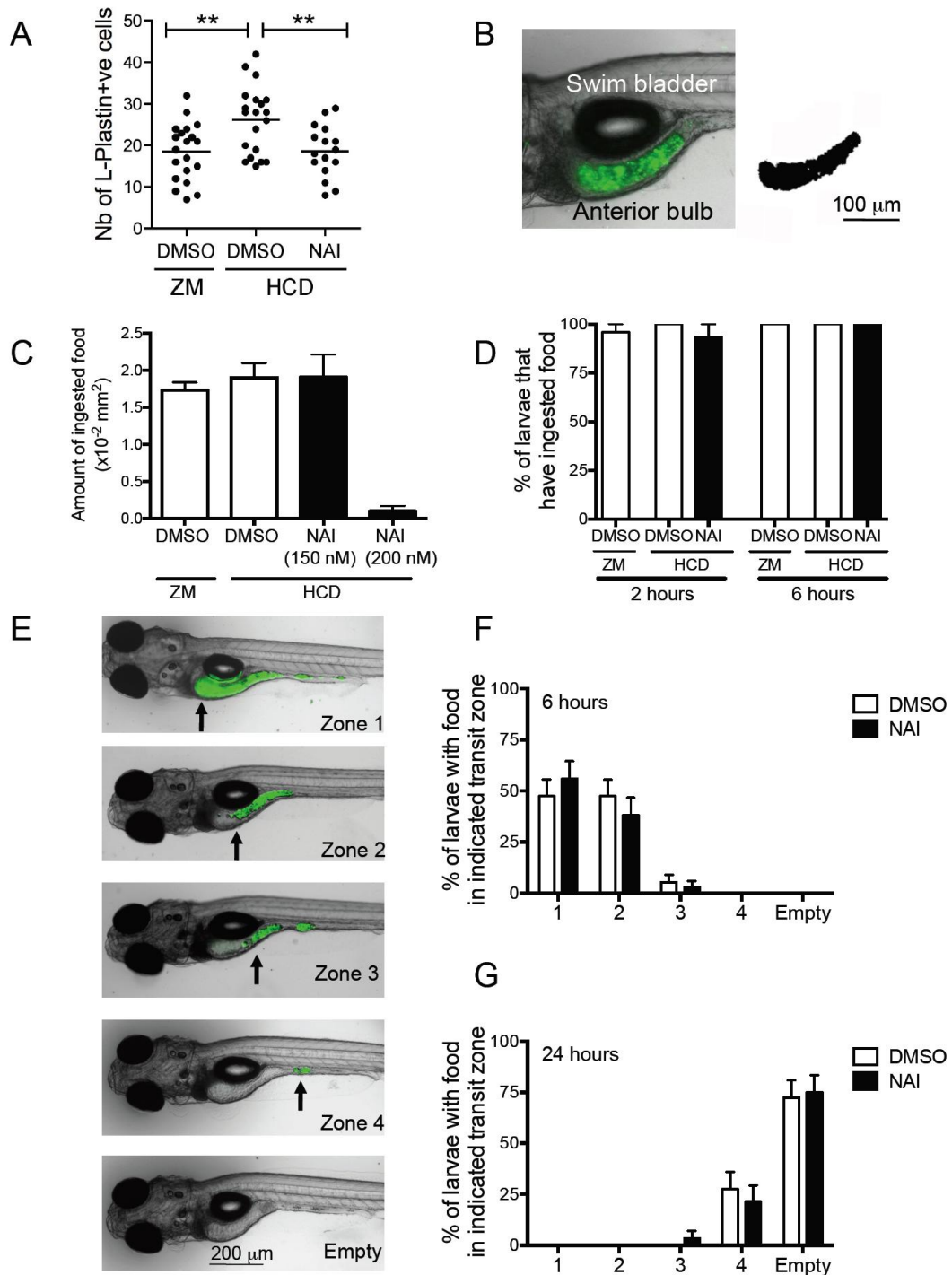


Fig. 3.7 Effect of NF κ B-inhibition on HCD-induced intestinal inflammation.

(A) Number of intestinal L-plastin+ve cells in NAI inhibitor (150 nM) treated larvae. Each dot represents one larva ($n \geq 21$) pooled from two experiments. (B) Representative fluorescent image of zebrafish larvae fed HCD supplemented with fluorescent microspheres for 2 hours. The amount of ingested food was assessed by quantifying the thresholded binary patterns of the area of the anterior bulb filled with fluorescent microspheres-labelled HCD (right inset). (C) Amount of ingested food at 2 hours. Larvae were treated with DMSO or NAI (150 nM or 200 nM) and fed ZM or HCD. (D) % of larvae that have ingested food by 2 hours and at the end of the 6 hour feeding period. Larvae were treated with DMSO or NAI (150 nM) and fed ZM or HCD. (E) Example of food transit through the intestine using HCD supplemented with fluorescent microspheres over time. Transit zones according to Field *et al.* [261] are indicated. Food transit was assessed by recording to most anterior position of labelled HCD using live stereomicroscopy. (F&G) Quantification of larvae with ingested HCD in intestinal transit zones at 6 hours (F) and 24 hours (G) during treatment with DMSO or NAI (150 nM). Data is pooled from two experiments ($n \geq 32$). Errors bars are SEM. ** $p < 0.01$, One-Way-Anova.

Since NF κ B activation, the central pathway of signal 1, was required for HCD-induced intestinal inflammation, three possible mechanisms of signal 1 provision, based on evidence from the literature, were hypothesised and investigated in this study (Fig. 3.2): (i) direct stimulation of NF κ B signalling following PRR receptor engagement of the commensal microbiota, (ii) indirect activation by HCD-induced alterations of the microbiome and (iii) direct PRR receptor engagement by cholesterol.

(i) Direct stimulation of NF κ B and PRR signalling by the commensal microbiota.

The concept of the microbiota delivering signal 1 constitutively in the steady state has arisen from experiments in mice in which treatment with antibiotics impaired the expression of pro-IL-1 β transcripts and reduced secretion of mature IL-1 β protein in the BAL upon influenza infection [299]. To assess the involvement of the microbiota in HCD-induced intestinal inflammation larvae were raised in germ-free (GF) conditions according to the protocol of Pham *et al.* [232]. Zebrafish eggs derived from natural breeding are fertilised externally and the resulting embryos develop in an axenic GF environment within their protective chorion until they hatch at 2-3 dpf. Despite a relatively high initial microbial burden due to exposure to microorganisms in the cloaca and in fecal matter at the bottom of the tanks, zebrafish chorions can easily be sterilised by treatment with bleach just after fertilisation. Pre and post hatching embryos are then raised in antibiotic-containing medium to ensure development under GF conditions. Throughout the experiments sterility of embryo media and dissociated larvae in sterile dH₂O were confirmed by spotting on tryptic soy agar plates and incubation under aerobic conditions. As demonstrated (Fig. 3.8A), bacterial growth was only detected in CONV conditions. To further confirm sterility, whole embryos were tested by qRT-PCR using broad-range universal primers targeting 16S ribosomal RNA (rRNA) gene to estimate total bacterial load [300]. 16S rRNA is comprised of highly conserved regions between different species allowing the estimation of relative abundance of bacteria. Even though the average Ct value obtained for GF larvae (Ct=34) was lower than the No Template Control (NTC, Ct=36), a statistically significant difference compared to conventionally (CONV) raised larvae (Ct=26) was detected (Fig. 3.8B).

To limit PRR stimuli during the subsequent feeding experiment by potential microbial contaminations of zebrafish diets, sterile ZM (sZM) and HCD (sHCD) were prepared by autoclaving. sHCD fed to CONV raised larvae was able to elicit an intestinal L-Plastin+ cell accumulation when compared to unfed or sZM-fed larvae (Fig. 3.8C). These data

suggest that the accumulation of myeloid cells occurs in response to cholesterol and that sterilisation, *i.e.* autoclaving, does not affect the ability of HCD to trigger the response in normal larvae. In contrast to CONV raised larvae, sHCD fed to GF raised larvae was unable to elicit L-Plastin cell accumulation in the intestine (Fig. 3.8C) suggesting that commensal bacteria are required for HCD-induced intestinal inflammation.

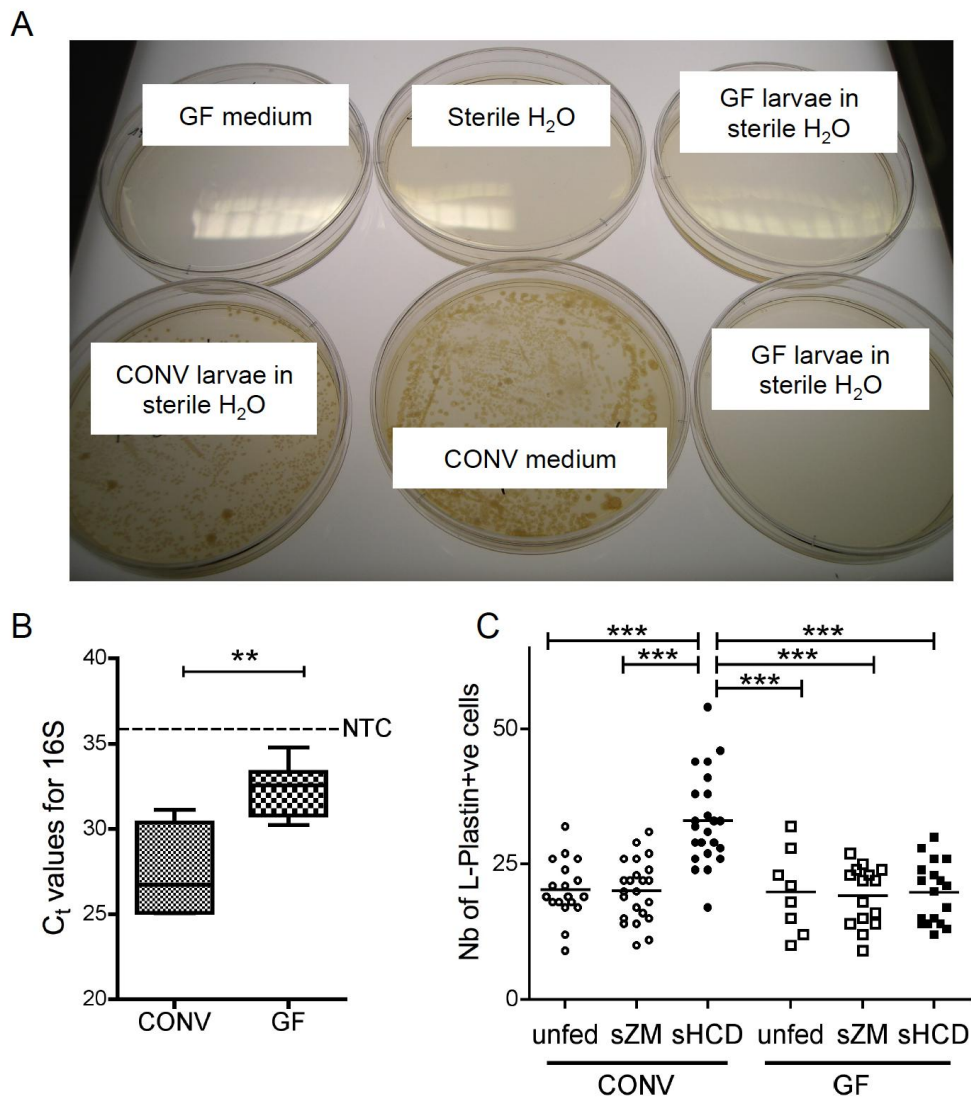


Fig. 3.8 HCD-induced intestinal inflammation is dependent on the microbiota.

(A) Representative picture of routine sterility test of GF samples using tryptic soy agar plates. (B) qRT-PCR analysis of C_t values of 16S ribosomal RNA genes in CONV and GF raised larvae. Box and whisker plot of $n=6$ larvae pooled from two experiments. Dashed line = NTC. (C) Number of intestinal L-Plastin+ cells in larvae reared in conventional or GF conditions and fed sterile ZM control, HCD or unfed for 6 hours. The number of L-Plastin+ cells was recorded at 18 hours after the removal of the diet. Each dot represents one larva ($n \geq 8$) pooled from two experiments. ** $p < 0.01$, *** $p < 0.001$, One-Way-Anova.

Studies in zebrafish larvae have shown that microbial colonisation contributes to intestinal development and function [231, 233]. GF larvae lack fully differentiated gut epithelium in terms of goblet and enteroendocrine cells and brush border intestinal alkaline phosphatase activity; the intestines of GF larvae undergo faster peristalsis and are unable to absorb protein macromolecules in the posterior portion [233]. Therefore, it had to be ruled out that neither food uptake/ transit, nor cholesterol-uptake into intestinal epithelial cells was affected in GF raised larvae as this could potentially explain why sHCD did not induce the accumulation of myeloid cells as seen in CONV larvae. Firstly, to assess food uptake and transit in GF larvae the same assays as described (Fig. 3.7B&E) was applied, except that in this case, sHCD instead of HCD was supplemented with fluorescent microspheres. As demonstrated (Fig. 3.9A&B), neither the amount of ingested sHCD at 2 hours of feeding, nor the percentage of fish that had taken up sHCD at 2 hours and 6 hours was affected in GF larvae when compared to CONV larvae. Even though the amount of ingested sHCD at 2 hours ($\approx 1.4 \times 10^{-2}$ mm² of intestinal area) in these conditions was slightly lower compared to HCD in DMSO and NAI treated fish ($\approx 1.9 \times 10^{-2}$ mm² of intestinal area, Fig. 3.7C) it was sufficient to induce myeloid cell accumulation in CONV raised fish (Fig. 3.8C). Analysis of intestinal transfer revealed no significant differences between CONV and GF raised fish (Fig. 3.9C&D). The same transit profiles as in previous experiments (Fig. 3.7F&G) and compared to the literature [261, 298] were observed.

Since Bates *et al.* demonstrated that the microbiota can influence intestinal motility [233], the peristalsis in GF larvae was examined and compared to CONV raised larvae. Due to the optical clarity of zebrafish larvae, intestinal motility is readily visible from 5 dpf onwards using videomicroscopy [233]. The number of larvae with intact peristalsis, *i.e.* regular patterns of spontaneous intestinal contractions and waves without disruption, was quantified at 18 hours following feeding at the peak of myeloid cell accumulation. No difference in the percentage of larvae with intact peristalsis ($\approx 80\%$) was observed between GF and CONV raised larvae (Fig. 3.9E). When analysing the average time between contractions (≈ 42 s), no difference was found between GF and CONV raised larvae (Fig. 3.9F) suggesting that the microbiota does not affect the peristalsis, at least under the conditions investigated. This was in contrast to observations by Bates *et al.* where GF larvae had faster contractions (≈ 40 s) compared to CONV larvae (≈ 49 s) [233]. However, the fact that in the study by Bates *et al.* zebrafish larvae were not fed before analysis of intestinal motility might explain the differences observed. Altogether, these data suggest that neither food uptake nor food transit is impaired in GF raised larvae.

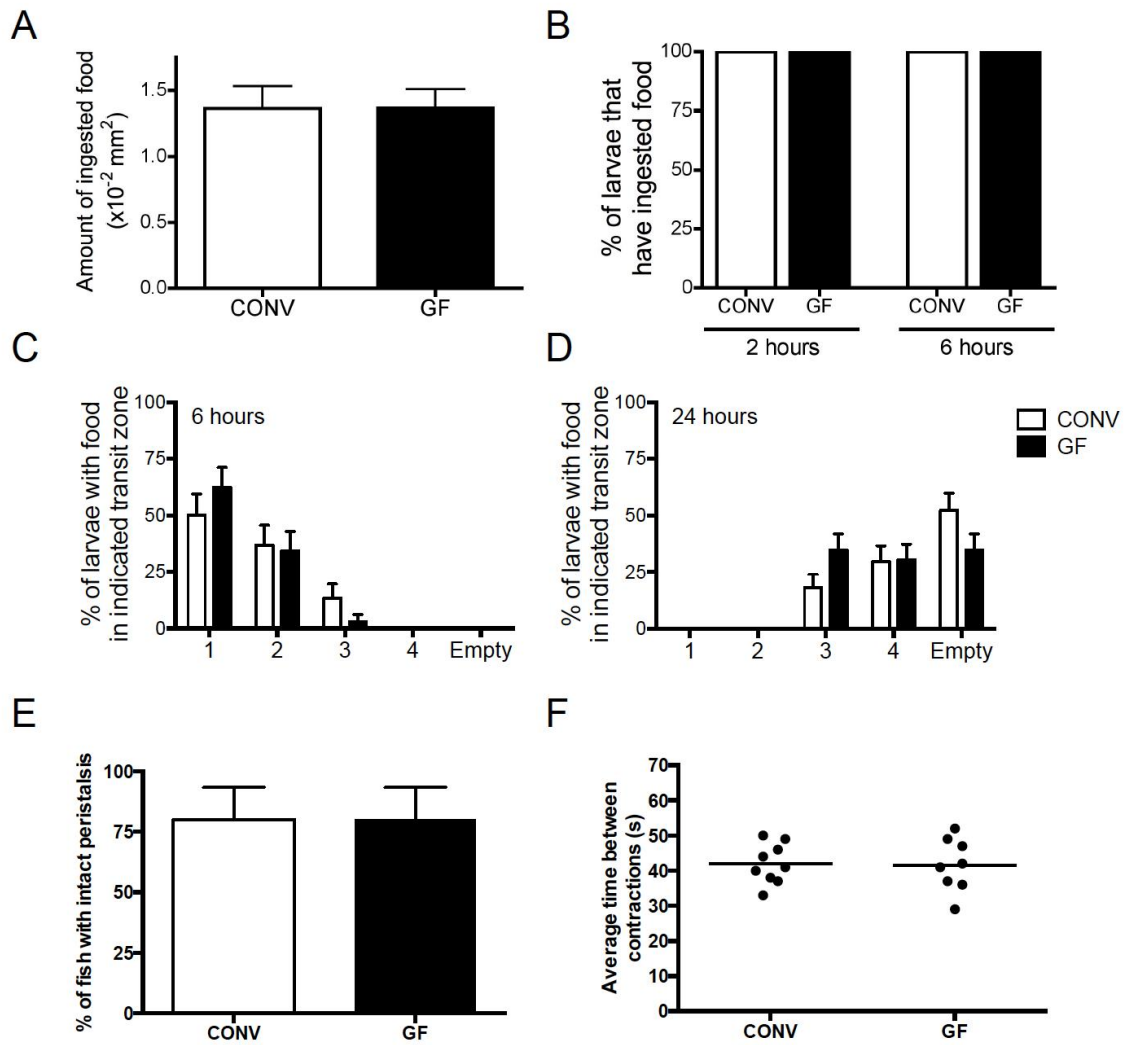


Fig. 3.9 Food uptake and transit of zebrafish raised under germ free conditions.

(A) Amount of ingested food at 2 hours in CONV or GF raised larvae. (B) % of larvae that have ingested food by 2 hours and at the end of the 6 hour feeding period. (C&D) Quantification of larvae with ingested HCD in intestinal transit zones described in Fig. 3.7E at 6 hours (C) and 24 hours (D). Data is pooled from two experiments ($n \geq 29$). (E&F) Quantification of zebrafish larvae with intact peristalsis (E) and average time between intestinal contractions (F) in CONV and GF raised larvae at 18 hours following 6 hours of sHCD. Data is pooled from two experiments ($n \geq 8$). Errors bars are SEM.

Since Semova *et al.* demonstrated that the uptake of fatty acids into intestinal epithelial cells is reduced in GF larvae [231], it was important to examine whether the same is true for cholesterol. The previously established assay of cholesterol uptake using fluorescently labeled BODIPY-cholesterol was adopted [262]. Uptake and metabolism of BODIPY-cholesterol in zebrafish larvae is similar to native cholesterol and allows its visualisation *in vivo* using confocal microscopy [262]. As shown in Fig. 3.10A, unfed larvae (GF or CONV) that ingested BODIPY-cholesterol for 6 hours did not exhibit cytoplasmic fluorescence and BODIPY fluorescence was only detectable in the intestinal lumen, confirming previous observations by Walters *et al.* that cholesterol is not taken up into epithelial cells in the absence of fatty acids [262]. Following feeding of sHCD for 6 hours, BODIPY-cholesterol was readily visible in the cytoplasm of intestinal epithelial cells (Fig. 3.10B) and quantification of cholesterol uptake revealed no differences between GF and CONV raised larvae (Fig. 3.10C). These results suggest that cholesterol-uptake by epithelial cells is not affected in GF raised fish.

Since neither food uptake and transit, nor uptake of cholesterol into epithelial cells was affected in germ-free conditions, it can be concluded that HCD-induced accumulation of myeloid cells requires the presence of the commensal microbiota.

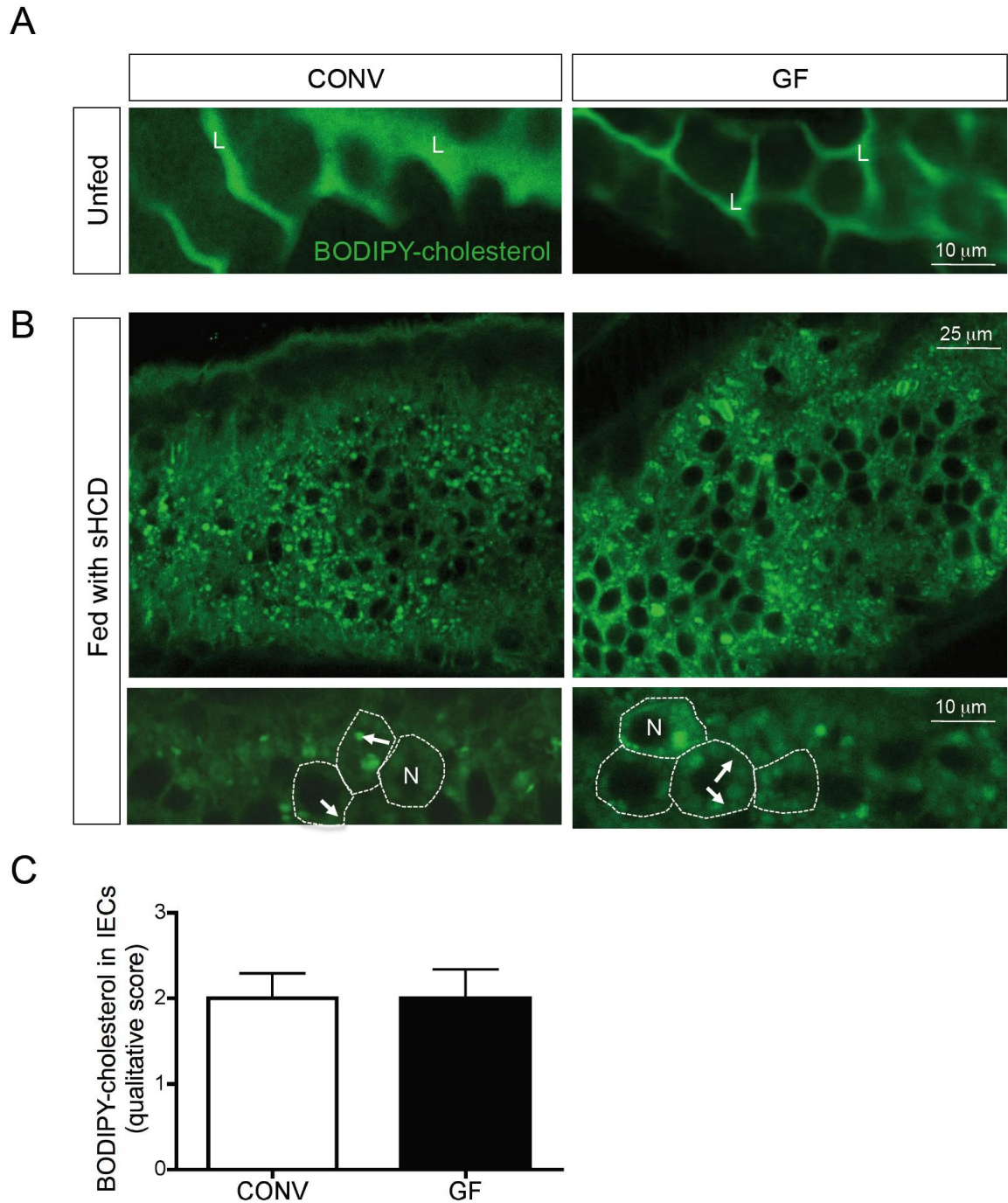


Fig. 3.10 Cholesterol uptake by intestinal epithelial cells of zebrafish raised under germ free conditions. (A&B) Representative confocal images (63x) of live IECs of larvae raised under conventional (left panels) or germ-free (right panels) conditions and left unfed (A) or fed sterile HCD (B) following treatment with BODIPY-cholesterol. L=lumen, N=nucleus. White arrows indicate BODIPY fluorescence in cytoplasm of IECs. Dashed white line outlines IECs. (C) Qualitative score of presence of BODIPY-cholesterol in cytoplasm of IECs. Presence of strong fluorescence intensity and an abundant signal was scored with 3 and the absence of a signal was scored with 0. Images were scored blindly. Bar chart shows mean+SEM, pooled from two independent experiments (n=9).

(ii) Indirect activation by HCD-induced alterations of the microbiome.

Since the microbiota was required for HCD-induced intestinal accumulation of myeloid cells, the next step was to assess whether this was due to cholesterol-mediated changes of the microbiota. To test whether HCD could alter the microbiome during the short duration of the current feeding experiments, the microbial load and composition was compared between control and HCD fed fish at 18 hours (for larvae) and 15 hours (for adults) following 6 hours of feeding. For analysis of microbial load in larvae, 20 intestines were pooled, whereas individual intestines were harvested from adult zebrafish. To quantify the microbial load, the same broad-range universal primers targeting 16S rRNA genes as above were used [300]. No difference in the ratio of 16S:18S rRNA following HCD was detected in either larvae (Fig. 3.11A) or adult zebrafish (Fig. 3.11B) suggesting that cholesterol does not affect the microbial load within 24 hours following feeding.

In addition to highly conserved areas allowing quantification of overall microbial abundance, the 16S rRNA gene also contains hypervariable regions for detection of species-specific sequences allowing bacterial identification. Hence, to assess the composition of the bacterial species present in the intestine of larvae following HCD, 16S rDNA amplicons were generated from cDNA of isolated RNA and sequenced using 454 pyrosequencing technology which is based on the sequencing by synthesis principle. For that 16S rRNA gene amplicons were generated and subsequently sequenced. The obtained sequences were subsequently aligned, sorted based on a predefined level of homology and classified according to taxonomic databases. The diversity and relative abundance of bacterial species distinguished by different operational taxonomic units (OTUs) obtained from ZM and HCD treated larval intestines were then compared and quantified. I provided the cDNA samples and Dr Julian Marchesi (CU, ICL) performed all other subsequent steps, such as sample preparation for sequencing and analysis (Appendix 1A). There was no statistical difference in the overall alpha levels of diversity between ZM or HCD fed groups (Appendix 1B). Further, the relative abundance of bacterial species was then calculated per sample and is presented in Appendix 1B. All samples were dominated by Proteobacterium phylum sequences and no statistically significant alterations in the relative abundance of specific bacterial taxa subsequent to HCD feeding in larvae in terms of total transcript expression were detected (Appendix 1C). These data suggest that HCD does not influence the microbial load or the community composition within the 24 hours of feeding experiments.

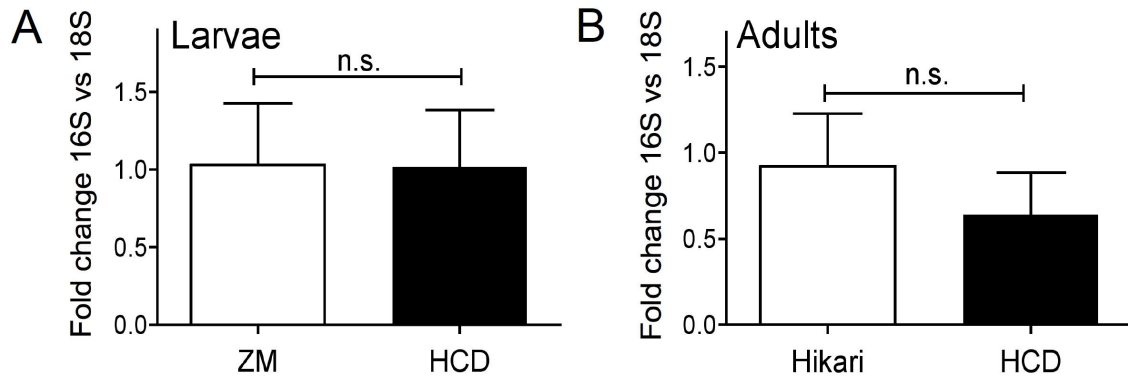


Fig. 3.11 Effect of HCD on the load of the commensal microbiota.

Microbiome analysis was performed at the peak of myeloid cell accumulation at 18 hours following ZM or HCD for 6 hours. **(A&B)** Fold change in bacterial load: ribosomal RNA 16S versus 18S in intestines from larvae (pool of 20 intestines) (A) or adult (individual) zebrafish (B) fed either ZM (A) or Hikari control (B) and HCD. Each bar represents $n \geq 6$, pooled from three experiments. Mann Whitney test.

(iii) Direct PRR receptor engagement by cholesterol.

Having established that cholesterol does not change the microbial load or composition within the short timeframe of these experiments, but that the microbiota is required for HCD-induced intestinal immune cell accumulation, the possibility of cholesterol directly activating PRR signalling and NF κ B leading to enhanced signal 1 activation could not be excluded. To test whether signal 1 during HCD-induced inflammasome activation is delivered or enhanced directly by HCD, *Tg(NF κ B:EGFP)* larvae were fed an HCD and the levels of EGFP expression assessed as a measure of NF κ B activation [222]. Due to the long half-life of EGFP of over 24 hours [301], analysis was performed at 18 hours following feeding for 6 hours.

As demonstrated previously [222] and confirmed here in Fig. 3.12, NF κ B was clearly activated in 7 dpf zebrafish larval guts, however, EGFP expression in the intestine was not different between unfed, ZM- and HCD-fed zebrafish larvae (Fig. 3.12A). Thorough quantification of EGFP expression in the larval intestine consequent to HCD by flow cytometry showed no detectable differences, either in the number of EGFP⁺ cells (Fig. 3.12B&C) or in the EGFP fluorescence intensity (Fig. 3.12C&D). These data suggest that neither potential microbial contaminations of the diet, the diet itself, nor cholesterol further activate NF κ B in the intestine of larval zebrafish, but that NF κ B is expressed in the intestines of zebrafish larvae in a steady state.

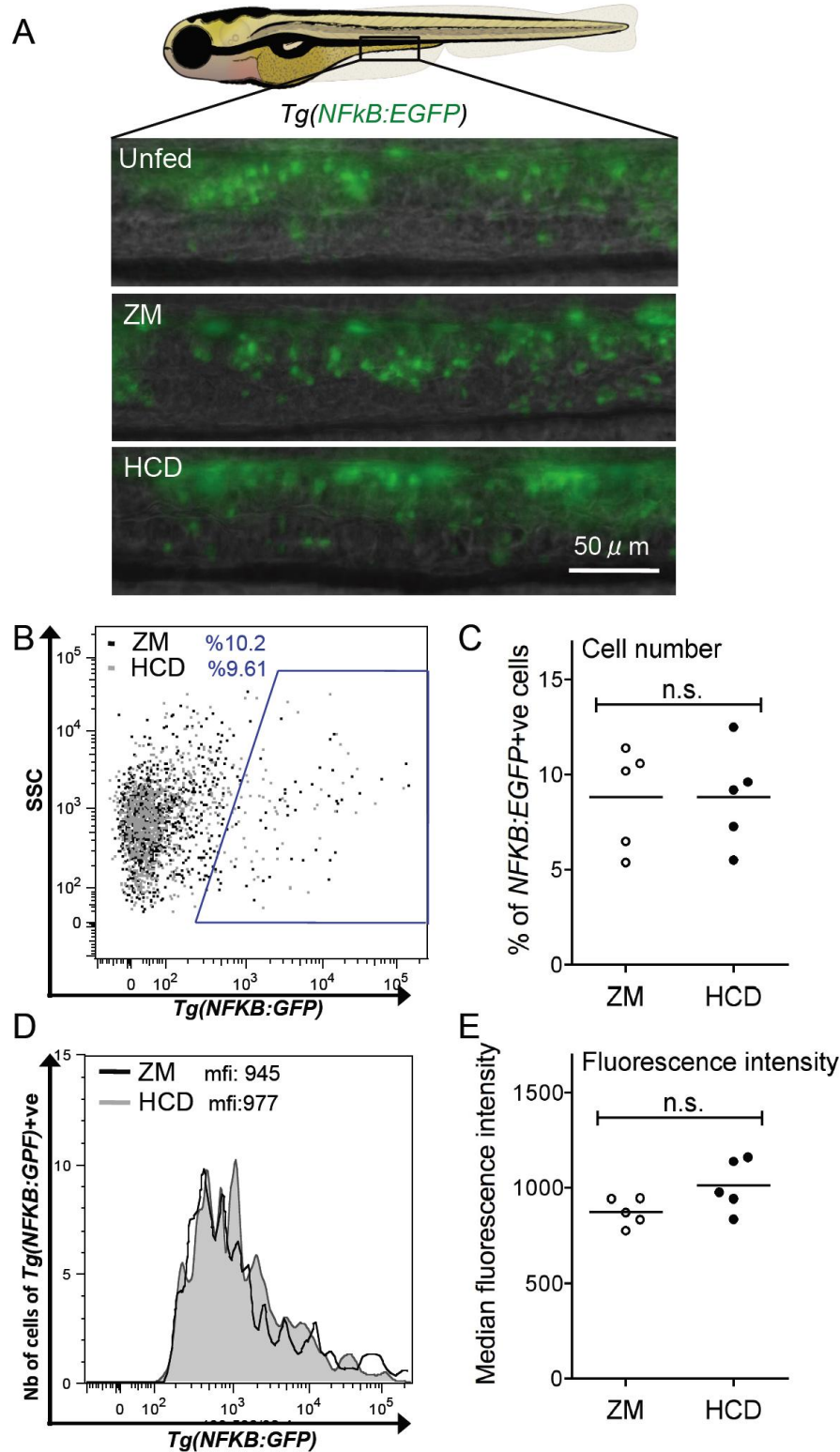


Fig. 3.12 Analysis of NFkB expression in the intestine of *Tg(NFkB:EGFP)* following HCD.

All analysis represented here was performed at 18 hours following 6 hours of feeding ZM or HCD. **(A)** Representative images of intestine of *Tg(NFkB:EGFP)* larvae at 7 dpf. **(B)** Representative flow cytometry dot plot showing overlay of intestinal cells of *Tg(NFkB:EGFP)* larvae fed ZM (black) or HCD (grey). **(C)** Percentage of intestinal EGFP+ cells quantified by flow cytometry. Each dot represents a pool of 3 larvae. Shown is one representative experiment of two. **(D)** Representative flow cytometry histogram showing overlay of EGFP+ cells in intestine of *Tg(NFkB:EGFP)* larvae fed ZM (black) or HCD (grey). **(E)** Median fluorescence intensity (mfi) of intestinal GFP+ cells quantified by flow cytometry. Each dot represents a pool of 3 larvae. Shown is one representative experiment of two.

Using double transgenic *Tg(NFkB:EGFP)xTg(ifabp:dsRed)*, Kanther *et al.* previously established that NFkB activation in the intestine occurs, at least in part, within intestinal epithelial cells (dsRed⁺ cells) [222]. Whether or not NFkB is also activated in myeloid cells is an important question, especially with regards to the cellular origin of inflammasome activation consequent to HCD. Analysis of larval intestines of double transgenic zebrafish larvae *Tg(NFkB:EGFP)xTg(fms:mCherry)*, in which macrophages are highlighted as mCherry⁺ cells (Fig. 3.13A), showed very few EGFP⁺/mCherry⁺ double positive cells detectable by fluorescence microscopy (Fig. 3.13B) and flow cytometry (Fig. 3.13C&D). Further, there was neither a statistically significant difference of EGFP⁺/mCherry⁺ double positive cells (Fig. 3.13B&D), nor a difference in the intensity of EGFP expression of mCherry⁺ macrophages between ZM and HCD fed larvae (Fig. 3.13E). These data suggest that the NFkB pathway is activate in non-haematopoietic intestinal cells as well as macrophages, however, NFkB is not further stimulated in either cell compartments following HCD.

Since the analysis of NFkB activation was performed after 18 hours following 6 hours of feeding, at the peak of myeloid cell accumulation, a significant increase in mCherry⁺ macrophages should be detectable. While the number and percentage of mCherry single positive macrophages was indeed significantly increased, there was no change in the percentage of EGFP⁺/mCherry⁺ double positive cells (Fig. 3.13B&D). This result suggests that the increase in mCherry single positive cells corresponds to the accumulation of macrophages following HCD but that these potentially ‘infiltrating’ cells do not exhibit NFkB activation (*i.e.* EGFP expression).

In conjunction with the observations from Kanther *et al.*, these data indicate that HCD-induced intestinal inflammation is dependent on NFkB activation and that signal 1 of inflammasome activation is not delivered by cholesterol itself or by HCD-mediated alterations of the microbiota, but rather by constitutive NFkB activation mediated by the commensal microbiota.

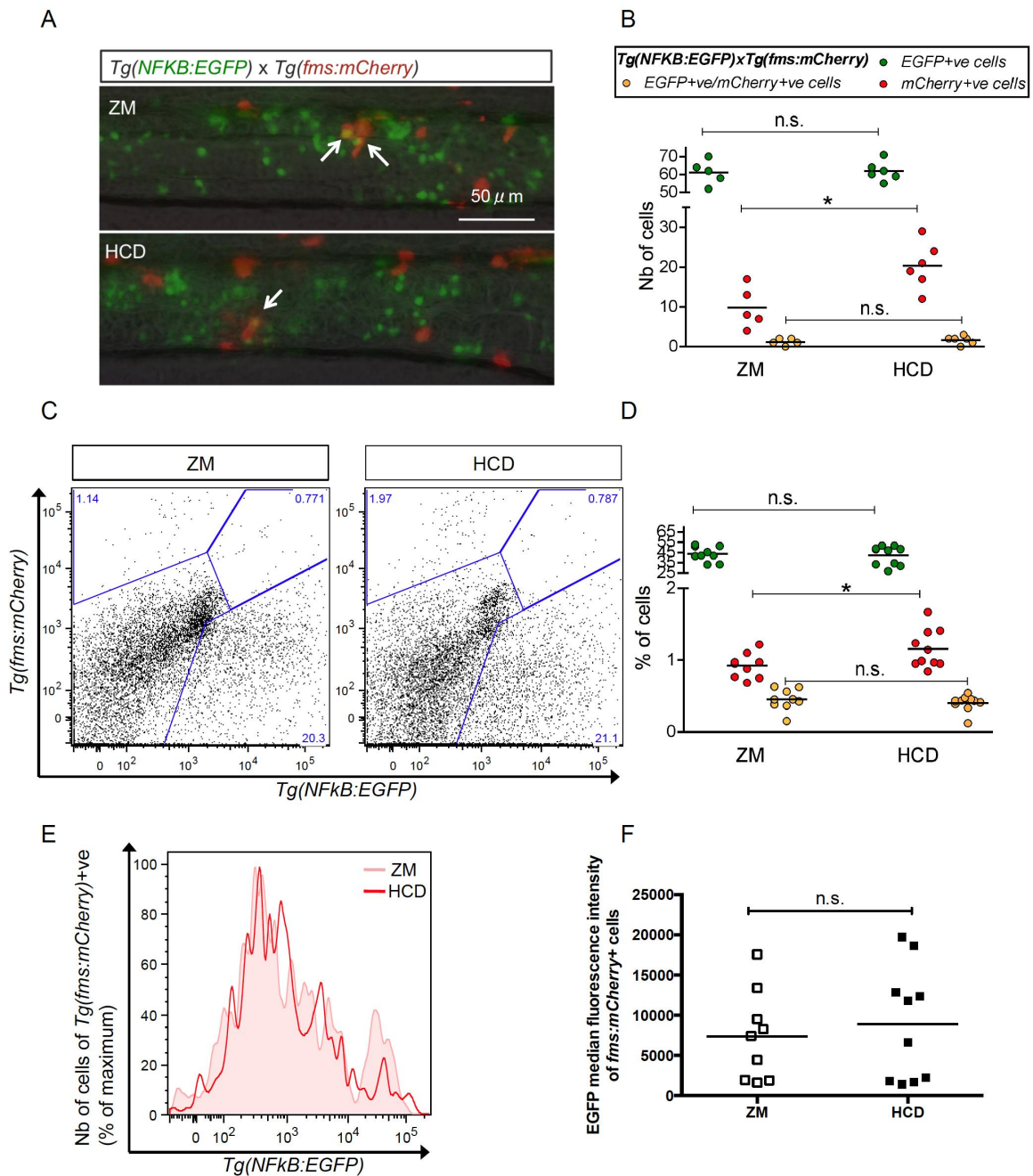


Fig. 3.13 Analysis of NFkB activation in the intestine of *Tg(NFkB:EGFP)xTg(fms:mCherry)* following HCD.

All analysis represented here was performed at 18 hours following 6 hours of feeding ZM or HCD. **(A)** Representative images of intestine of *Tg(NFkB:EGFP)xTg(fms:mCherry)* larvae at 7 dpf. Arrows indicate EGFP/mCherry double positive cells. **(B)** Number of GFP+ cells, mCherry+ and GFP+/mCherry+ cells in the intestine of *Tg(NFkB:EGFP)xTg(fms:mCherry)* larvae fed ZM or HCD analysed by ImageJ. Each dot represents one individual larva ($n \geq 5$) from one experiment. **(C)** Representative flow cytometry dot plots showing intestinal cells following doublet exclusion. **(D)** Percentage of GFP+ cells, mCherry+ and GFP+/mCherry+ cells analysed by ImageJ. Each dot represents a pool of 5 individual larva ($n \geq 9$, pooled from two experiments). **(E)** Representative flow cytometry histogram showing overlay of mCherry+ cells in intestine of larvae fed ZM (rose) or HCD (red). **(F)** EGFP median fluorescence intensity of mCherry+ cells. Each dot represents a pool of 5 individual larva ($n \geq 9$, pooled from two experiments). n.s.=non significant, * $p < 0.05$. Mann Whitney U test.

3.3.3 Examination of cellular origin of inflammasome activation consequent to HCD

As recently demonstrated, cholesterol activates the NLRP3 inflammasome in human and mouse macrophages [61]. We have shown that dietary cholesterol directly induces acute inflammasome-dependent intestinal inflammation in zebrafish larvae [267], while constitutive NF κ B expression provoked by commensals potentially delivers signal 1 of inflammasome activation, apparently, mainly in intestinal epithelial cells [222]. Intestinal epithelial cells (IECs) are the first cells that dietary components encounter in the intestine. Whilst inflammasomes are expressed in non-haematopoietic cells such as IECs [51, 174], it is unknown whether or not cholesterol can trigger its activation in those cells. The final step during inflammasome assembly and activation is cleavage of pro-IL1 β by activated caspase-1 [56].

This series of experiments set out to assess whether inflammasome activation upon HCD occurs in haematopoietic cells or in IECs. To localise inflammasome activation, caspase-1 activity was assayed using the caspase-1 specific fluorescent detection probe termed Fluorescent Labeled Inhibitor of Caspase Activity (FLICA). The caspase-1 specific FLICA FAM-YVAD-fmk is comprised of a fluorescent tag (FAM), the affinity peptide inhibitor sequence for activated caspase-1 (YVAD) and a fluoromethyl ketone (fmk) moiety facilitating irreversible binding [302]. FLICA has been successfully employed to detect activity of caspase-1 in plaques on frozen sections throughout the aortic root of *ApoE*^{-/-} mice fed an atherogenic, high-fat, high-cholesterol diet over a period of 12 weeks [288]. The zebrafish has two orthologues for caspase-1, namely caspase a and b, both of which possess the highly conserved catalytic domain [218] that FLICA is designed to bind. Previous attempts in the lab to localise caspase-1 activity using FLICA *in vivo* were unsuccessful due to insufficient cellular resolution and high levels of autofluorescence in the intestines of larval zebrafish [267]. To overcome that problem, FLICA-labelling was performed on single cell suspensions of adult zebrafish intestines and analysed by flow cytometry. Since there is no suitable control available (*e.g.* a FLICA compound with non-matching recognition side for caspase-1), gating for FLICA⁺ cells is carried out based on an unstained sample (Fig. 3.14A). However, this gating strategy does not allow control for non-specific binding of the FLICA substrate. Thus, only changes in the percentage of FLICA⁺ cells between treatments (*i.e.* diets), rather than absolute percentages of FLICA⁺ cells (based on an unstained sample), were considered as appropriate measure for caspase-1 activity.

Zebrafish were starved for two days and exposed to HCD for 6 hours (Fig. 3.14A). Immediately after exposure, single cell suspensions of dissected intestines were incubated with FLICA and subjected to flow cytometry analysis. A significant increase in FLICA+ cells was detected in intestinal cells of adult WT zebrafish consequent to HCD (Fig. 3.14B&C) indicating that dietary cholesterol induces inflammasome activation in intestinal cells.

To determine the cell type in which caspase-1 activation occurred, FLICA-incubated intestinal cells were fixed and co-stained with a cytokeratin antibody raised against mouse cytokeratin but which had been shown to detect cytokeratin in zebrafish epithelial cells [303]. To control for non-specific binding of the AF633-labelled 2nd antibody (goat anti mouse), staining only with the 2nd antibody in absence of the primary L-Plastin antibody was performed. No non-specific staining of the 2nd antibody was observed, when compared to an unstained sample and true cytokeratin+ cells were detected when staining with both antibodies (1st and 2nd) (Fig. 3.14D). A significant increase of FLICA+/cytokeratin+ cells was observed in intestines of HCD-fed fish (Fig. 3.14E&F) while FLICA+/cytokeratin- cells were unaffected (Fig. 3.14E&G) indicating that caspase-1 activation upon HCD occurs in IECs (cytokeratin+) but not in other intestinal cells (cytokeratin-).

Caspase-1 activity was also assessed in myeloid cells using FLICA-labelling was performed in *Tg(lyz:dsRed)* zebrafish (Fig. 3.14H). *Tg(lyz:dsRed)* express the dsRed fluorophore into adulthood which does not spectrally overlap with the FLICA substrate. No effect of HCD on FLICA+/dsRed+ cells was observed (Fig. 3.14I) indicating that caspase-1 is not activated in myeloid cells, or at least in neutrophils, following HCD. There was however a significant increase in FLICA+/dsRed- cells (Fig. 3.14J) demonstrating that caspase-1 is clearly activated in the non-neutrophil cell compartment of the intestine. Together, these data establish that caspase-1 activation upon HCD occurs in intestinal epithelial cells but not neutrophils.

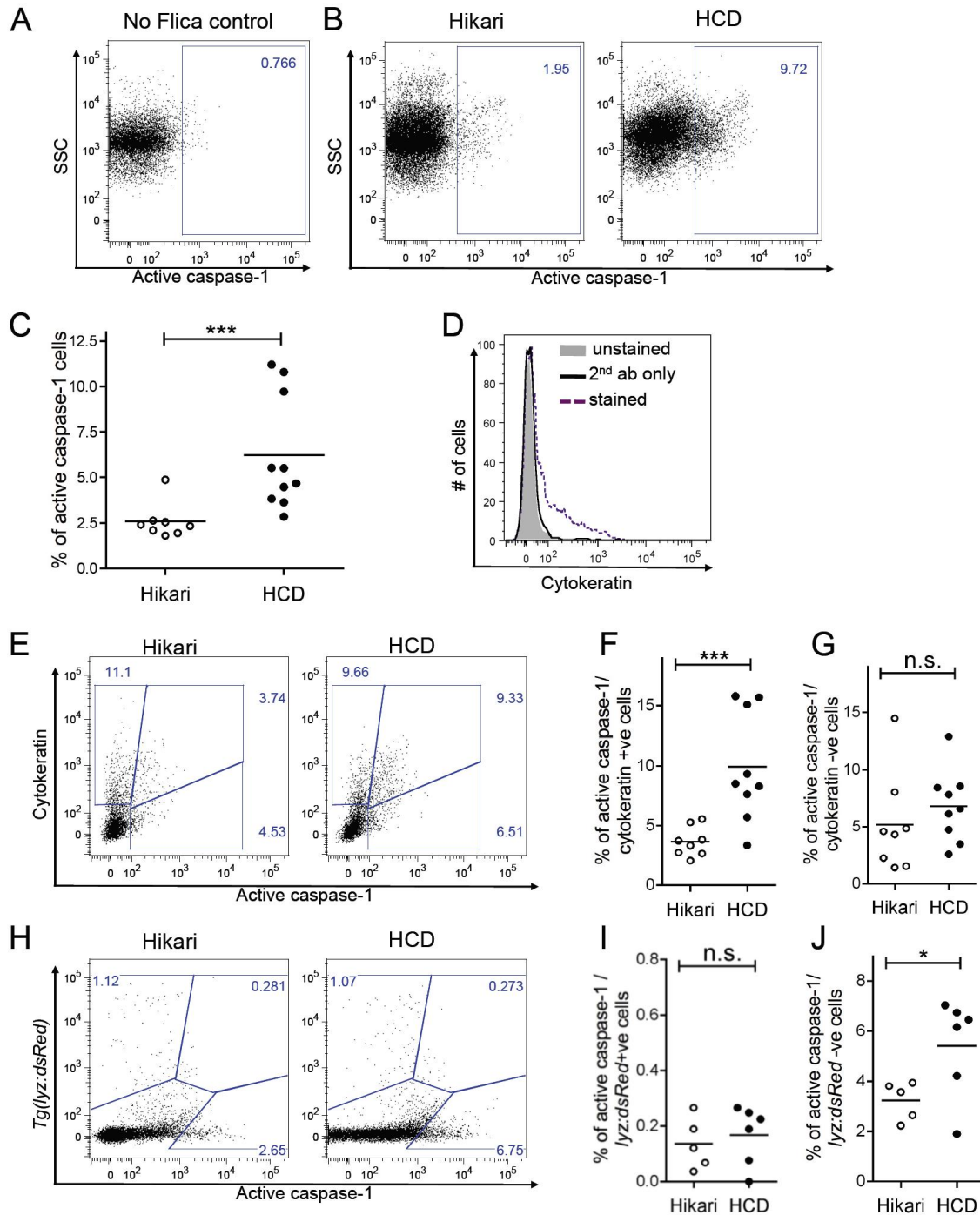


Fig. 3.14 Analysis of caspase-1 activity in intestinal cells following HCD.

(A) Flow cytometry plot of intestinal tissue from an adult zebrafish. (B&E&H) Representative flow cytometry plots of intestinal tissue from adult zebrafish fed Hikari control or HCD treated with the active caspase-1 FLICA substrate (B), or double stained for cytokeratin (D) or performed in *Tg(lyz:dsRed)* (H). (D) Flow cytometry histogram of overlay of unstained sample (grey), 2nd antibody (ab, black) and 1st+2nd antibody (purple). (C&F&G&I&J) Quantification of % of intestinal cells positively labeled for active caspase-1 (B), active caspase-1 and cytokeratin+ve (D), active caspase-1 and cytokeratin-ve (E), active caspase-1 and dsRed+ve (G) and active caspase-1 and dsRed-ve (H). Each dot represents one adult (n≥5) pooled from two or more experiments. Two-tailed t-test. * p < 0.05, *** p < 0.001.

Having established that caspase-1 activity is detectable in cytokeratin-expressing IECs and therefore inflammasome activation upon HCD potentially occurs in these cells, the ability of morpholino oligonucleotides (MOs) to knock down components of the inflammasome complex in IECs was investigated. One component of the inflammasome that is highly and ubiquitously expressed in E-cadherin⁺ IECs in mouse is ASC, while only very few ASC-expressing cells are found within the lamina propria [53]. N. Sangha previously demonstrated that using both splice-blocking and translational-blocking MOs targeting ASC inhibit HCD-induced intestinal myeloid cell accumulation in zebrafish larvae in a concentration-dependent manner [267]. MOs are routinely injected in single cell staged embryos and their effect can be evaluated up to 5 dpf [182]. However, the intestinal epithelium has a high turnover rate which could lead to decreasing MO knock-down efficiency at the time of the feeding experiment (6-7 dpf), hence, a novel delivery method was devised by simply treating larvae with MO added to the water [267]. However, neither the uptake of MO by intestinal cells, nor the ability of MO to knock down ASC in intestinal cells, was proven previously [267]. This study set out to identify the cell type within the zebrafish larval intestine that takes up the ASC MO as an indirect means to localise the cellular origin of inflammasome activation following HCD.

According to previously established protocols [267], 6 dpf larvae were treated 24 hours prior to and during the 6 hours HCD feeding period before analysis of MO-uptake (Fig. 3.15A). As detected by confocal microscopy and shown in Fig. 3.15B&C, larvae treated with a FITC tagged ASC splice-blocking MO (ASC FITC MO) exhibited green fluorescence of the FITC molecule in the entire gastrointestinal tract when compared to larvae that were left untreated. Imaging at higher magnification revealed that the FITC fluorophore was detected in intestinal cells (Fig. 3.15D). In comparison to fluorescent cholesterol in IECs, which only localises in the cytoplasm of IECs (Fig. 3.10B) [262], FITC fluorescence appeared to be in both the cytoplasm and the nucleus of IECs. The nuclear localisation of this ASC splice-blocking MO is consistent with the fact that this type of MO exerts its function in the nucleus during pre-mRNA splicing, however, the exact localisation of the ASC FITC MO within IECs would have to be confirmed by co-labelling using a nuclear dye, such as DAPI or DRAQ5.

The FITC fluorescence was exclusively detected within intestinal cells of the mid intestine (Fig. 3.15C&E), a region that is comprised of specialised enterocytes that utilise macropinocytosis to internalise luminal contents and may play a role in mucosal immunity in fish [225]. This region can be visualised by histochemical detection of ingested and

pinocytosed HRP [225]. Zebrafish larvae were treated ASC FITC MO (Fig. 3.15A), imaged by confocal microscopy and subsequently treated with HRP according to the protocol established by Wallace *et al.* [225]. As shown in Fig. 3.15E, the ASC FITC MO was detected in the same region as HRP suggesting that the MO is taken up via pinocytosis by specialised enterocytes of the mid intestine.

Even though it cannot be confirmed that the FITC fluorophore is still attached to the MO at this stage, these data suggest that the ASC FITC MO localises within intestinal cells.

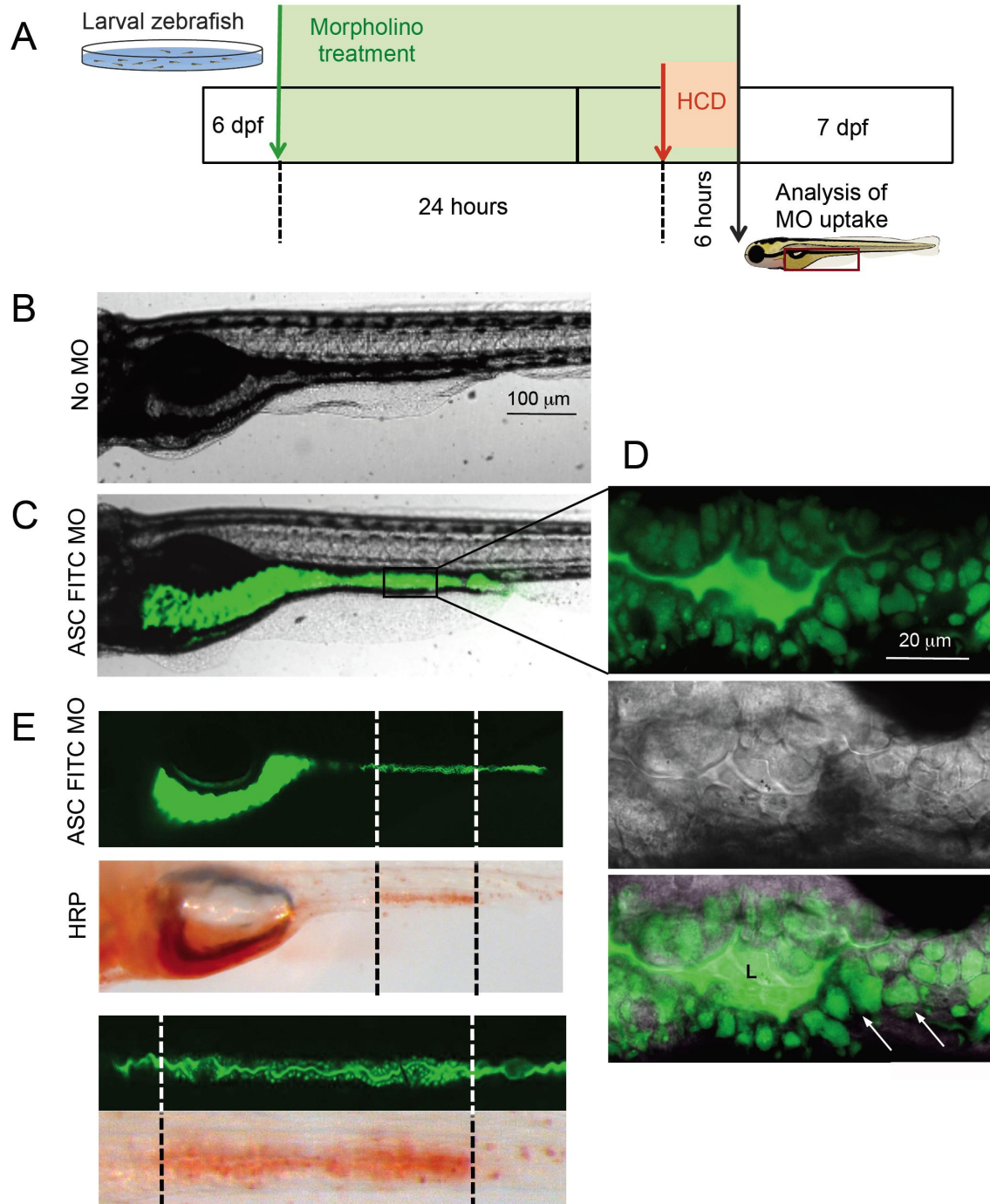


Fig. 3.15 Confocal analysis of MO uptake into intestinal cells.

(A) Time-line of experimental procedure. Zebrafish larvae (6 dpf) were pre-treated with 20 μ M FITC-tagged ASC splice-blocking morpholino (ASC FITC MO) for 24 hours and analysed following an HCD for 6 hours in the presence of the MO. (B&C) Representative fluorescent images of larvae treated with 20 μ M ASC FITC MO (C) or left untreated (B) for 24 hours and analysed following HCD for 6 hours. Representative of $n=15$. (D) Insets highlight green fluorescence of ASC FITC MO in intestinal lumen (L) and in epithelial cells (white arrow). Top panel shows the fluorescent image, middle panel the brightfield channel and bottom channel the overlay. (E) Representative fluorescent images of larvae treated with 20 μ M ASC (top panel), which were subsequently treated with 10 mg/mL HRP for 2 hours. HRP was detected histochemically (bottom panel) and found localised in the same region as the MO (indicated by the black and white dotted lines). Insets show enlarged images of the region containing specialised enterocytes that have taken up the ASC FITC MO and the HRP. Representative images of $n=7$.

To assess whether the MO efficiently targets the gene of interest and to address the possibility that the fluorescence detected in intestinal cells might simply be due to uptake of free FITC, the ability of the ASC FITC MO to reduce ASC (*pycard*) transcripts in cells positive for FITC fluorescence was assessed. For this following the protocol described in Fig. 3.15A larvae, were treated with either the FITC tagged splice blocking MO or a FITC tagged ASC specific control (mismatch) MO, both at the concentration of 20 μ M previously shown to be successful in abrogating myeloid cell accumulation consequent to HCD in previous experiments [267]. 50-100 larval intestines were then dissected and pooled for FACS of FITC⁺ cells. The gating strategy is presented in Fig. 3.16A-C. Following debris exclusion based on forward scatter (FSC) (Fig. 3.16A) and dead cell exclusion using DAPI (Fig. 3.16B), cells were plotted using a FITC/PE-two-colour dot plot (Fig. 3.16C). Overcompensation of the FITC fluorescence results in the true FITC positive population moving downwards to the x-axis, while the autofluorescent cell population remains in a diagonal line (Fig. 3.16C). This gating method allowed separation of the true FITC population from the autofluorescent population. FITC⁺ cells were sorted and subjected to qRT-PCR analysis of ASC (*pycard*) mRNA expression. A significant decrease in ASC transcripts could be detected in FITC⁺ intestinal cells of larvae treated with the ASC splice-blocking MO (Fig. 3.16D).

These data suggest that the FITC fluorophore either might still be attached to the MO when entering intestinal cells or might be taken up in a similar way as the MO allowing localisation of ASC FITC MO in intestinal cells and sorting of those cells. Nevertheless, these data confirm previous results by N. Sangha that HCD-induced immune cell accumulation depends on ASC in intestinal cells. Further, the fact that the ASC FITC MO is exclusively taken up by specialised enterocytes in the mid intestine confirms the previously suggested relevance of these cells in intestinal immune responses [225].

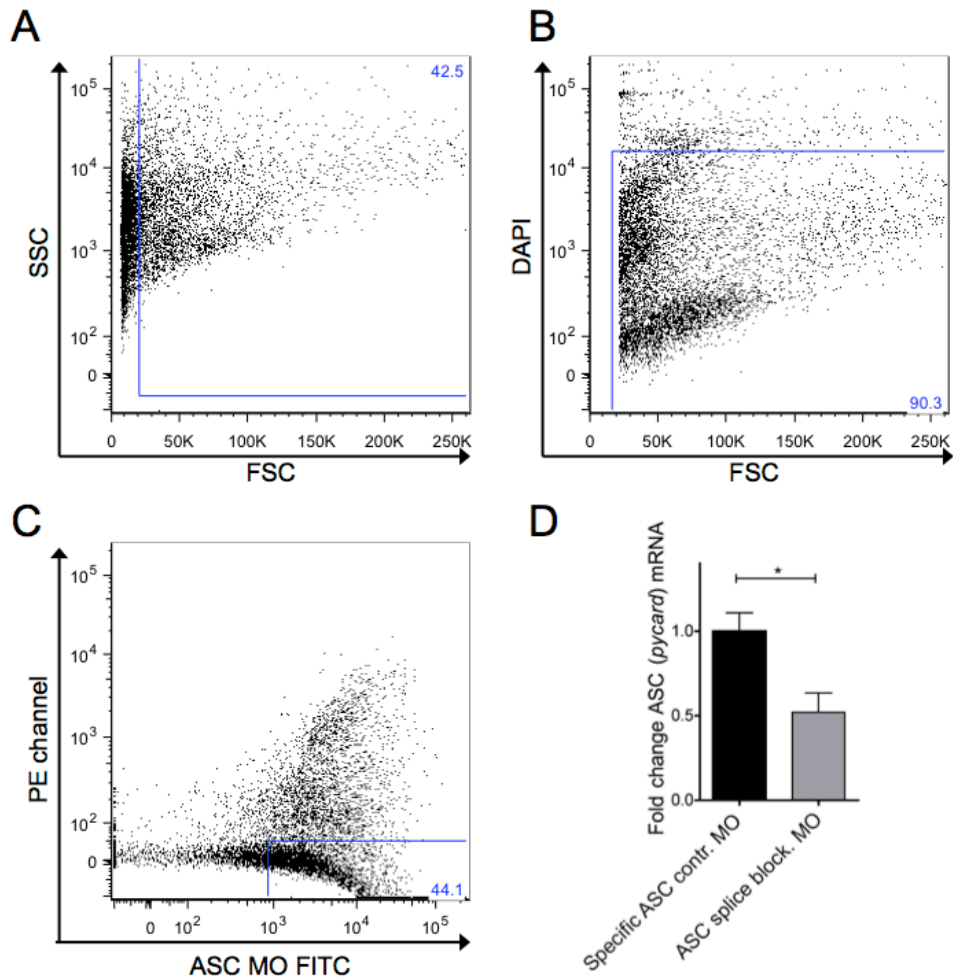


Fig. 3.16 Analysis of ASC transcripts in intestinal cells following treatment with ASC MO.

WT zebrafish larvae (6 dpf) were pre-treated with 20 μM of FITC-tagged ASC splice-blocking morpholino or FITC tagged specific ASC control MO for 24 hours and exposed to HCD for 6 hours. Intestines were dissected and single cell suspensions prepared for FACS sorting and subsequent qRT-PCR analysis. (A-C) Representative FACS gating strategy to sort true FITC+ cells. (A) Dot plot depicts FSC vs. SSC profile showing debris exclusion. (B) FSC vs. DAPI dot plot gated on live cells (DAPI-ve cells). (C) Dot plot showing overcompensated FITC vs. PE channel gated on true FITC+ cells. (D) qRT-PCR analysis of FITC+ sorted intestinal cells of zebrafish larvae treated with either 20 μM of FITC ASC-specific control MO or FITC ASC splice blocking MO (pool of n=50-100 larval intestines/sample). Relative expression values were normalised to 18S and expressed as fold change relative to the control sample. Data are mean + SEM of triplicates and representative of two experiments. Mann Whitney test. * p < 0.05.

Having established that the uptake of MO by intestinal cells can be assessed by flow cytometry, further analysis was performed in order to identify the cell type that initiates intestinal immune cell accumulation following HCD. Zebrafish larvae were treated with 20 μ M of the FITC tagged splice-blocking MO or left untreated and the dissected intestinal cells fixed and co-labelled with a cytokeratin antibody. Flow cytometry analysis revealed an increase in FITC fluorescence in cytokeratin+ epithelial cells in intestinal cells from larvae treated with the ASC FITC MO when compared to untreated larvae (Fig. 3.17A&B) indicating that the MO is taken up by about 50% of the IECs. In contrast, further analysis in *Tg(lyz:dsRed)* and *Tg(fms:mCherry)* larvae showed no increase in FITC fluorescence in dsRed+ neutrophils (Fig. 3.17C&D) or mCherry+ macrophages (Fig. 3.17E&F) from larvae treated with the ASC FITC MO when compared to untreated larvae. These results indicate that the ASC FITC MO is taken up by IECs, but not by myeloid cells.

Together with the fact that FLICA (caspase-1 activity) is also detected in cytokeratin+ IECs, but not dsRED+ neutrophils in *Tg(lyz:dsRed)* fish, these data indicate that cholesterol activates the inflammasome in IECs, which leads to subsequent immune cell accumulation.

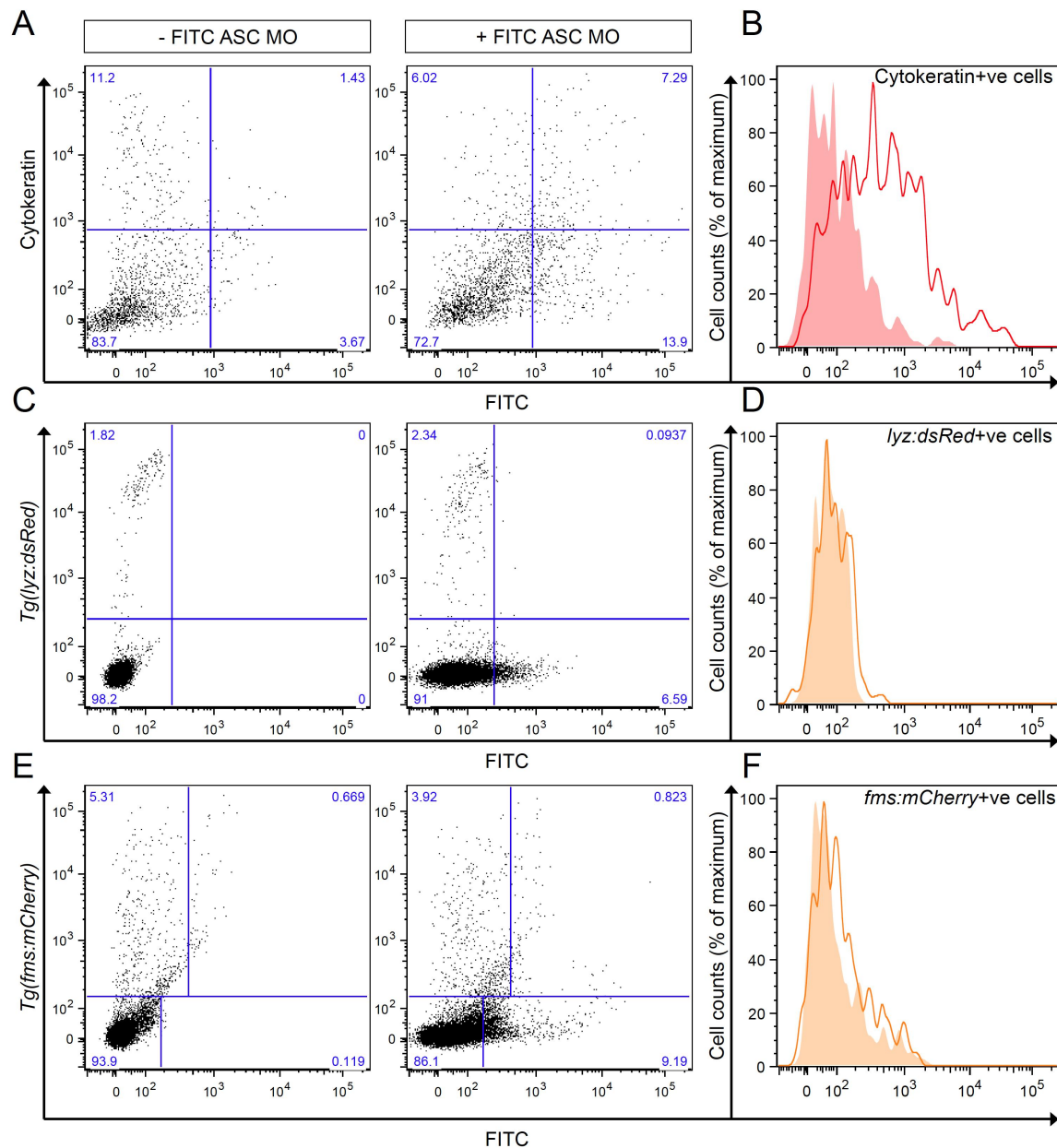


Fig. 3.17 Flow cytometry analysis of MO uptake into intestinal cells.

WT, *Tg(lyz:dsRed)* or *Tg(fms:mCherry)* zebrafish larvae (6 dpf) were pre-treated with 20 μ M of FITC-tagged ASC splice-blocking morpholino or left untreated for 24 hours and exposed to HCD for 6 hours. Intestines were dissected and single cell suspensions prepared for flow cytometry analysis directly or fixed and co-stained with a cytokeratin antibody. Dead cell and doublet exclusion was performed as illustrated in **Fig. 3.16A&B** and that the 2nd antibody does not bind unspecifically was confirmed. (**A&C&E**) Representative dot plots showing untreated (left panels) and FITC ASC MO treated (right panels) intestinal cells of WT larvae co-stained with cytokeratin (**A**) or intestinal cells of *Tg(lyz:dsRed)* (**C**) and *Tg(fms:mCherry)* (**E**). (**B&D&F**) Histograms depict FITC fluorescence in intestinal cells of larvae treated with FITC ASC MO (solid line) or untreated (filled histogram) and double-stained for cytokeratin (**B**), gated on dsRed+ cells in *Tg(lyz:dsRed)* (**D**) or mCherry+ cells in *Tg(fms:mCherry)* (**F**). Pool of $n \geq 10$ larval intestines, representative of at least two experiments.

A further proof-of-principle experiment was performed to test for efficient protein knock down. Since an antibody for ASC was not commercially available, a GFP MO (not tagged with FITC) was used to target EGFP in *Tg(ubi:EGFP)* fish (Fig. 3.18A). This work was done in collaboration with Nagisa Yoshida (ICL) as part of her Master's project. Nagisa found that due to the long half-life of EGFP of over 24 hours [301], larvae had to be treated for 48 hours with 20 μ M of control and GFP MO (Fig. 3.18B) to detect a significant decrease in EGFP fluorescence intensity using fluorescence microscopy and image analysis. I performed flow cytometry analysis of dissected intestinal cells as an additional method to quantify EGFP fluorescence. Flow cytometry analysis revealed a significant decrease in EGFP fluorescence intensity in intestinal cells of fish treated with the GFP MO (Fig. 3.18C). Together, the successful decrease of ASC transcripts following treatment with and ASC MO and the decrease of EGFP fluorescence intensity in *Tg(ubi:EGFP)* following treatment with an EGFP MO confirms the feasibility of this novel MO delivery method to target genes in intestinal cells within the mid intestine, or at least ASC and EGFP.

Therefore, this MO delivery method was chosen in an attempt to identify the inflammatory mediator that triggers myeloid cell accumulation following inflammasome activation in IECs. Cholesterol gavage in mice slightly increased *Il1b* transcript levels (Fig. 3.5C) suggesting this cytokine as a potential inflammatory mediator of HCD-induced intestinal inflammation. Thus far, N. Sangha did not detect any change in *il1b* transcript levels using qRT-PCR of zebrafish dissected intestinal cells following HCD [267]. However, given the fact that only a small percentage of intestinal cells take up the MO, small changes in *il1b* transcripts could be masked when whole intestinal samples are analysed.

Larval zebrafish were treated as before (Fig. 3.15A) with a previously published IL-1 β MO [294], which abrogated accumulation of L-Plastin⁺ cells following HCD. These data suggest that IL-1 β is, at least in part, involved in HCD-induced intestinal inflammation.

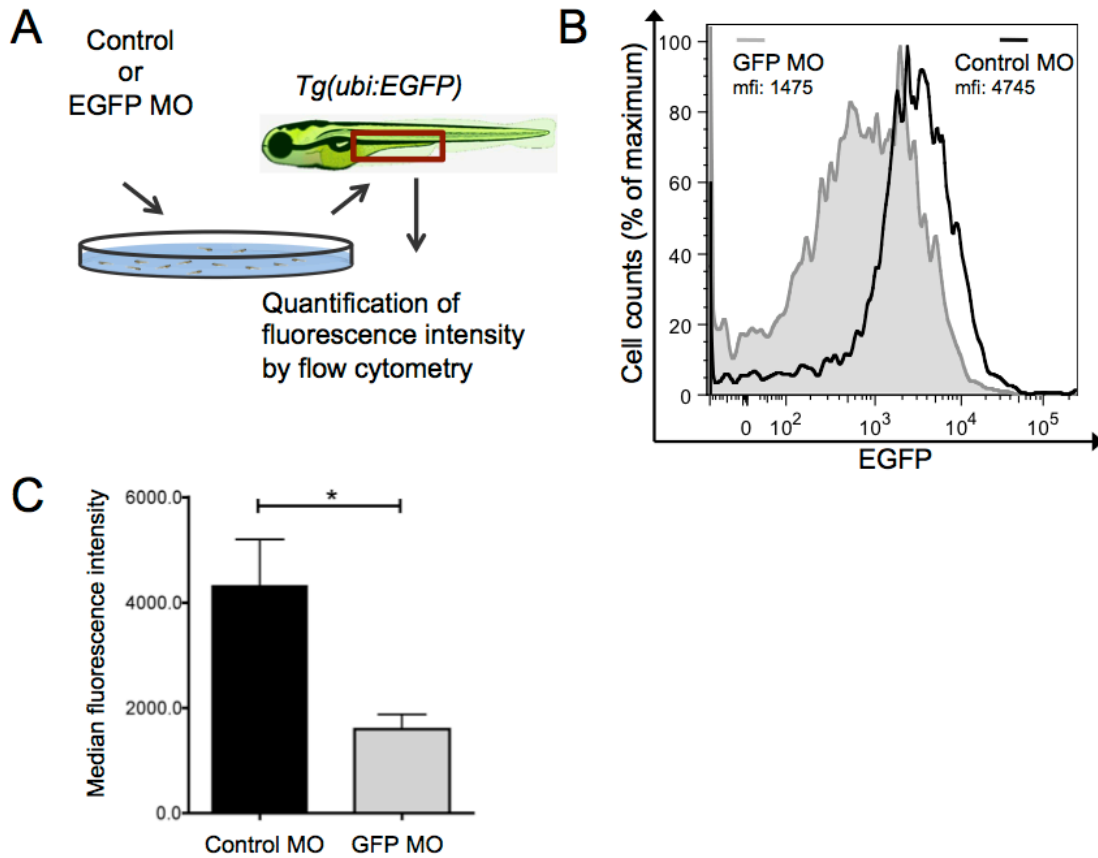


Fig. 3.18 Effect of GFP MO treatment on EGFP fluorescence intensity in intestinal cells of *Tg(ubi:EGFP)*

(A) Illustration of experimental procedure. *Tg(ubi:EGFP)* zebrafish larvae (6 dpf) were treated with 20 μ M EGFP MO or control MO for 48 hours and analysed by flow cytometry. (B) Representative flow cytometry histograms of intestinal cells pooled from 5 larvae. (C) Median fluorescence intensity of cell suspension isolated from the intestine of 8 dpf *Tg(ubi:EGFP)* zebrafish larvae and analysed by flow cytometry. $n \geq 31$, pooled from four experiments * $p < 0.05$. Error bars represent SEM.

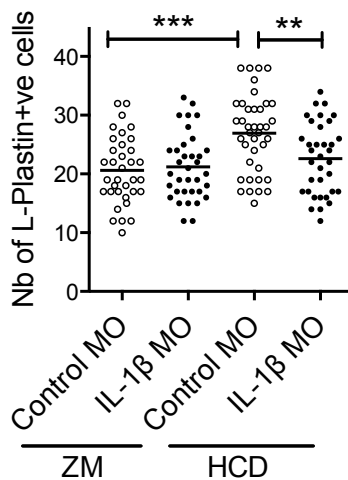


Fig. 3.19 Effect of IL-1 β MO treatment on HCD-induced myeloid cell accumulation

Number of intestinal L-Plastin+ cells in zebrafish larvae that were treated with 20 μ M IL-1 β or control MO for 24 hours and fed with either ZM control diet or HCD for 6 hours according to the protocol illustrated in Fig. 3.15A. The number of L-Plastin+ cells was recorded at 18 hours after the removal of the diet. Each dot represents one larva ($n \geq 35$) pooled from two experiments. One-Way-Anova. ** $p < 0.01$, *** $p < 0.001$

3.3.4 Analysis of pathologies following extended HCD

Prolonged exposure to diets rich in saturated fatty acids and cholesterol have been associated with chronic local auto-inflammatory diseases such as inflammatory bowel disease, or systemic conditions such as obesity, atherosclerosis and metabolic syndrome [159]. Stoletov *et al.* have demonstrated that feeding zebrafish larvae an HCD for 10 days results in vascular lipid accumulation accompanied by vascular inflammation [259] suggesting relevance of the zebrafish model in studying systemic conditions associated with prolonged ingestion of diets rich in cholesterol. However, the local effects of an extended HCD on the intestine have not been studied yet and were therefore analysed here by feeding larvae an HCD for 10 days (6-15 dpf, Fig. 3.20A).

Since chronic inflammation is the hallmark of intestinal conditions such as IBD, larvae were first investigated for myeloid cell accumulation following HCD for 10 days. A sustained accumulation of L-Plastin⁺ cells was found in the intestines of HCD-fed fish (Fig. 3.20B-D).

Recent evidence in mice demonstrated that intestinal inflammation following prolonged ingestion of a HFD is indirectly induced by diet-mediated changes of the microbiota [158, 159]. In contrast, here the possibility of a direct effect of cholesterol in mediating local inflammation following extended HCD was investigated using ezetimibe, the inhibitor of cholesterol uptake/binding [259, 280, 284, 297]. A concentration of 25 μM of ezetimibe was chosen since this concentration has previously been shown to be successful in abrogating myeloid cell accumulation following acute HCD [267]. Continuous treatment with ezetimibe during exposure to HCD for 10 days abrogated sustained L-Plastin cell accumulation when compared to DMSO treated controls (Fig. 3.20D) suggesting that inflammation following extended HCD is directly mediated by cholesterol. Since acute HCD results in inflammasome activation, its role during sustained myeloid cell accumulation following extended HCD was investigated. Unfortunately, the previously used caspase-1&5 inhibitor N-Acetyl-WEHD-al, which abrogated myeloid cell accumulation following acute HCD [267], was discontinued and could therefore not be used for this purpose. Thus, the cathepsin B inhibitor (Ca-074-Me) which is also able to inhibit L-Plastin accumulation following acute HCD [267] was used. Continuous treatment with 10 μM of Ca-074-Me during 10 days of exposure to HCD abrogated sustained L-Plastin cell accumulation when compared to DMSO treated controls (Fig. 3.20E)

suggesting that inflammation following extended HCD is dependent on cathepsin B and therefore potentially inflammasome activation by cholesterol.

Patients suffering from functional gastrointestinal disorders often experience motility disturbance without an identified origin [131]. Due to the availability of transparent mutants, such as *Tra*^{-/-}/*Nac*^{-/-}, which allow *in vivo* imaging up to later stages of development, the zebrafish offers a valuable tool to assess intestinal motility. Intestinal contractions and waves were observed and imaged by microscopy and the length of peristaltic waves was quantified in *Tra*^{-/-}/*Nac*^{-/-} fish following extended HCD. Analysis of the intestinal motility revealed a marked increase of fish with impaired peristalsis as demonstrated by a reduced average length of peristaltic waves following extended HCD when compared to extended ZM (Fig. 3.21A-B). To assess the role of cholesterol binding/uptake as well as inflammasome activation in this condition, larvae were again continuously treated with ezetimibe (Fig. 3.21C) and Ca-Me-074 (Fig. 3.21D), both of which restored HCD-induced intestinal motility impairments to the levels of extended ZM. These data suggest cholesterol binding to NPC1L1 and cholesterol-induced inflammasome activation plays a role in motility disturbances in the intestine following extended HCD.

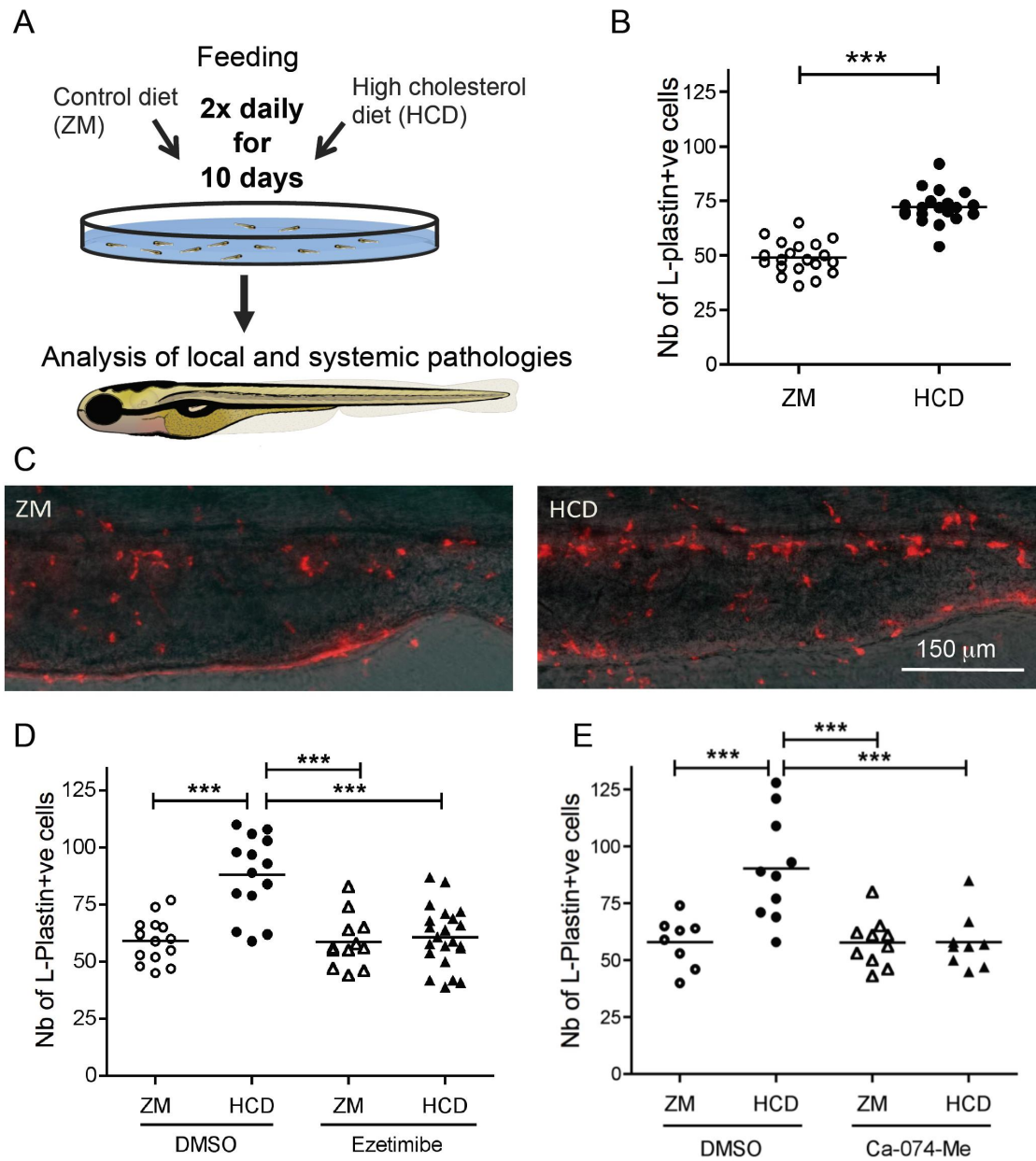


Fig. 3.20 Analysis of intestinal L-Plastin cell accumulation following extended feeding.

(A) Schematic representation of experimental procedure of extended feeding experiments of larval zebrafish. (B&C) Quantification (B) and representative images (C) of intestinal L-Plastin+ cells of 15 dpf *Tra*^{-/-}/*Nac*^{-/-} larvae fed ZM control or HCD for 10 days. Each dot represents one larva (n=20), one representative experiment of four. (D&E) Intestinal L-Plastin+ cells of ezetimibe (25 μ M, D) and cathepsin inhibitor (Ca-074-Me, 10 μ M, E) treated larvae. Each dot represents one larva (n \geq 8). One experiment representative of two is shown. *** p < 0.001. Student's t test (B) and One-Way-Anova (D&E). The number of L-Plastin+ve cells (B) was quantified by Nagisa Yoshida (ICL).

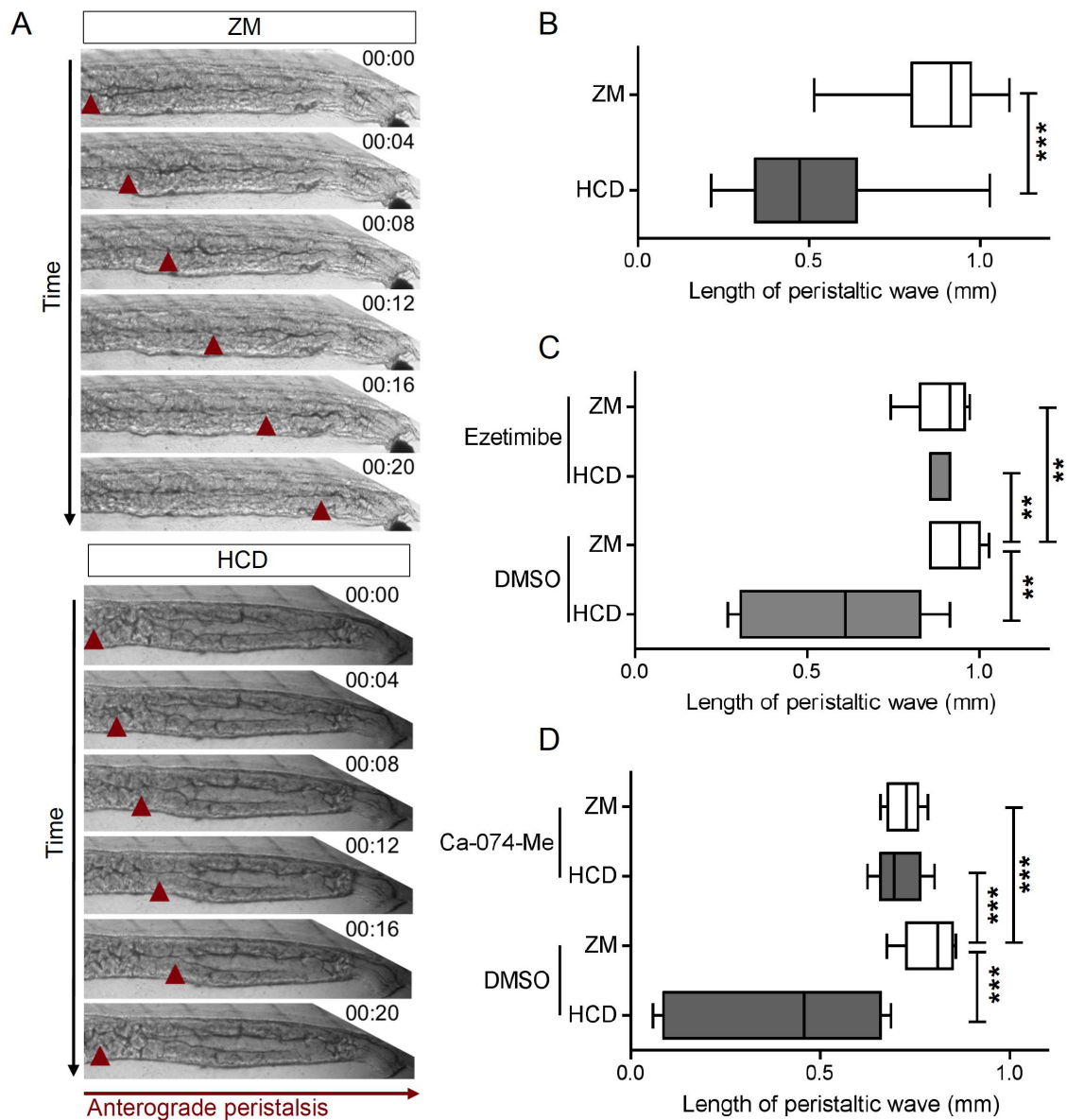


Fig. 3.21 Analysis of intestinal motility following extended HCD.

All results are obtained from 15 dpf *Tra⁺/Nac⁻* larvae fed ZM control or HCD for 10 days according to **Fig. 3.20A**. **(A)** Representative images of anterograde peristalsis with contractions (red arrowhead) over time (20 s) of the distal intestine of larvae fed ZM control and HCD. **(B)** Average length of peristaltic wave of anterograde peristalsis of the distal intestine of larvae fed ZM control and HCD ($n=18$). One representative experiment of three. **(C&D)** Average length of peristaltic wave of ezetimibe (25 μ M, C) and cathepsin inhibitor (Ca-074-Me, 10 μ M, D) treated larvae. Each dot represents one larva ($n\geq 10$). One experiment representative of two is shown. ** $p < 0.01$, *** $p < 0.001$. Mann-Whitney U test (B) and One-Way-Anova (C&D).

Intestinal inflammation has been associated with impairment of gastrointestinal motility, even though the mechanisms are not fully characterised. For instance, patients recovering from abdominal surgery often experience postoperative paralytic ileus [132, 133, 304] and inflammatory intestinal disorders are accompanied by functional intestinal impairment [131].

To test for a possible correlation between inflammation and impairment of intestinal motility, L-Plastin+ cells and peristaltic waves were quantified individually in HCD-fed larvae. HCD-fed larvae with intact peristalsis exhibited significantly less L-Plastin+ cells in their intestine as compared to larvae with impaired peristalsis (Fig. 3.22A) while a direct correlation between the severity of impairment in peristalsis and the degree of inflammation was observed (Fig. 3.22B). These data support the notion of previously suggested inflammation-induced functional impairments of the intestine and further suggest the contribution of dietary components, in this case cholesterol, to these conditions.

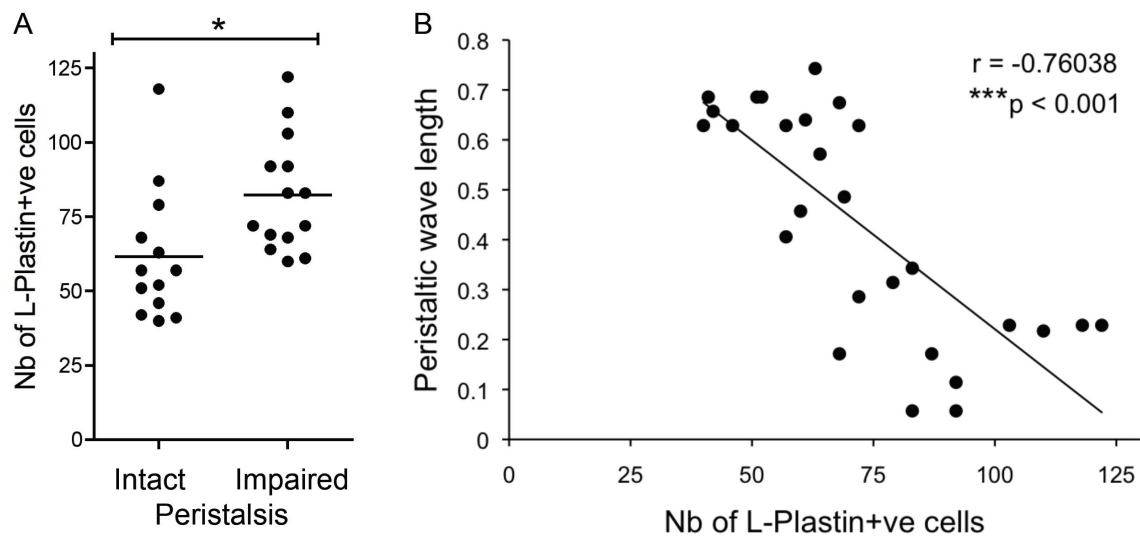


Fig. 3.22 Severity of impairments in peristalsis following extended HCD correlates with degree of inflammation.

(A) Quantification of intestinal L-Plastin+ cells of 15 dpf *Tra*^{-/-}/*Nac*^{-/-} larvae fed HCD for 10 days. Larvae were grouped according their peristalsis: intact or impaired. Each dot represents one larva ($n \geq 13$) and the results are pooled from two experiments. * $p < 0.01$. Student's t test. **(B)** Correlation of peristaltic wave length with number of L-Plastin+ cells in intestine of 15 dpf *Tra*^{-/-}/*Nac*^{-/-} larvae fed HCD for 10 days. The correlation coefficient is: -0.76, which is statistically significant at the 0.001 (***) two-tailed level.

Apart from persistent intestinal inflammation and impaired intestinal function, chronic inflammatory conditions of the intestine such as IBD are marked by intestinal epithelial damage and altered goblet cell physiology leading to a compromised mucus layer [2]. To examine the effect of extended HCD on intestinal architecture, histological analysis was performed. For this, sections were taken through various areas of the mid intestine of ZM and HCD-treated larvae (Fig. 3.23A). Fig. 3.23B represents area 1 of the mid intestine of ZM control and HCD-fed larvae showing small structural changes observed following HCD, which were a slight increase in goblet cells and a slight reduction in projections and crypts. However, thorough analysis and quantification of these two characteristics throughout the length of the mid intestine (area 1, 2 and 3) revealed that, apart from a slight but significant decrease in the number of crypts in area 1 following HCD, no changes in the numbers of goblet cells or crypts were detected (Fig. 3.23C&D). Together, these data suggest that 10-day extended HCD does not lead to any gross morphological changes of the gastrointestinal tract.

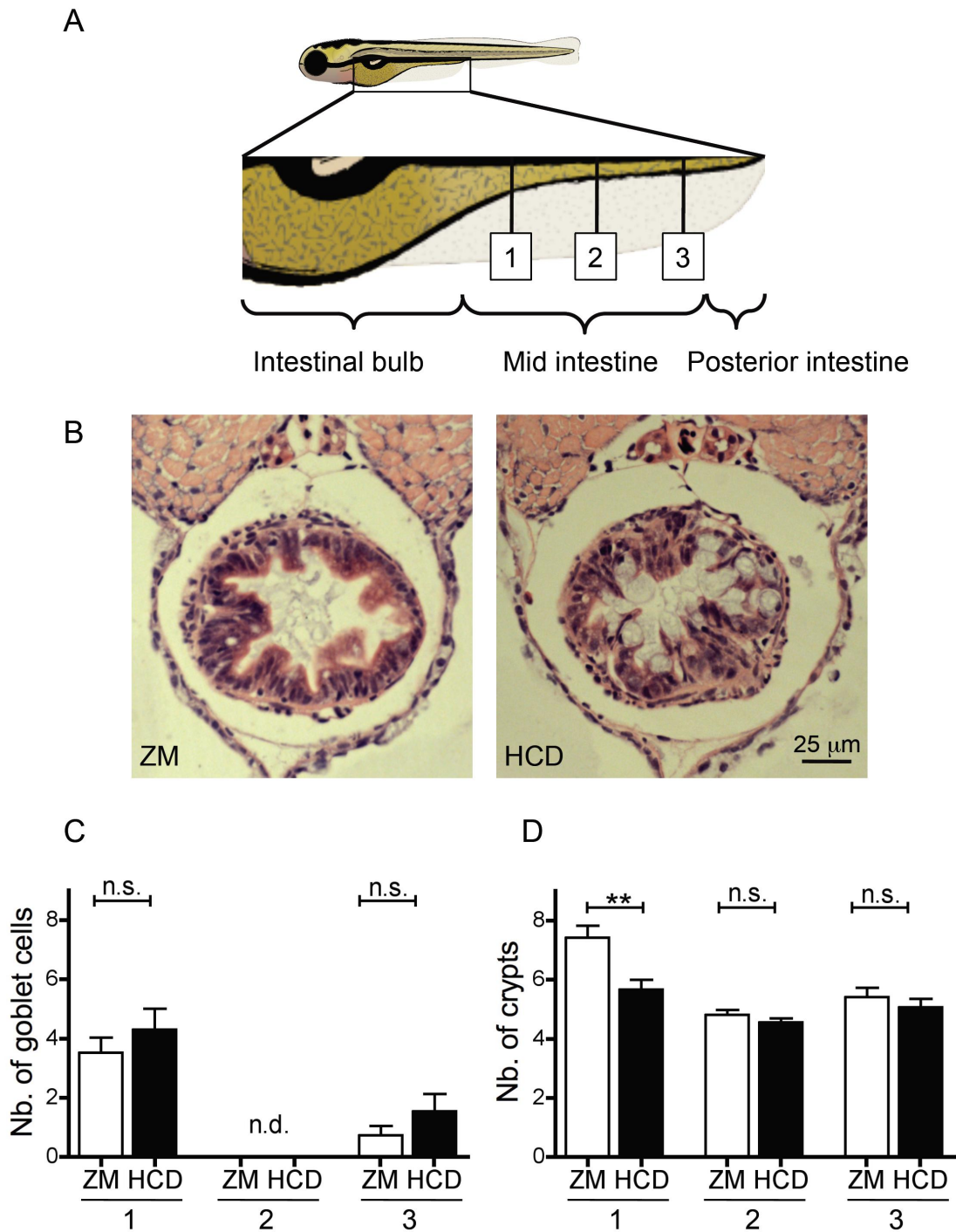


Fig. 3.23 Slight changes in intestinal architecture following extended HCD feeding.

All results are obtained from 15 dpf *Tra^{-/-}/Nac^{-/-}* larvae fed ZM control or HCD for 10 days according to Fig. 3.20A. (A) Schematic overview of zebrafish larval intestine indicating the areas of the mid intestine that were examined by histology. Segments of the anterior, mid and posterior intestine were classified according to Wallace *et al.* [225]. (B) Representative images of paraffin transverse sections stained with H&E of the posterior intestine of area 1. (C&D) Quantification of the number of goblet cells (C) and the number of crypts (D) of indicated areas of posterior intestine. The total number of cells or crypts was quantified per section. Bar charts are mean + SEM of $n \geq 15$ larvae. ** $p < 0.01$. Student's t test comparing ZM and HCD for each area.

Whilst performing histological analysis of the architecture of the gastrointestinal tract, it was observed that larvae fed HCD for 10 days showed evidence of hepatic steatosis (Fig. 3.24A). Thorough histological analysis of H&E stained transverse histological sections revealed that 56% of HCD-fed fish showed a vacuolation phenotype, which was found in significantly less ZM-fed fish (Fig. 3.24B). To confirm this phenotype, lipid accumulation was assessed using Oil-Red-O (Fig. 3.24C) which revealed a significant increase in larvae with Oil-Red-O staining in the liver following extended HCD (Fig. 3.24D). These results indicate that extended HCD induces hepatic steatosis in zebrafish larvae and together with previously reported atherosclerotic features [259], suggests the relevance of the zebrafish model for studying systemic conditions associated with prolonged ingestion of cholesterol-enriched diets.

To assess the importance of intestinal cholesterol binding/uptake in the development of this condition, larvae were continuously treated with ezetimibe during extended HCD, which significantly abolished HCD-induced Oil-Red-O staining in the liver and also slightly decreased the liver Oil-Red-O staining in ZM treated larvae (Fig. 3.24E). This result suggest that cholesterol binding/uptake in the intestine directly contributes to this condition.

In contrast, continuous treatment with the cathepsin B inhibitor Ca-074-Me following extended HCD did not affect liver Oil-Red-O staining (Fig. 3.24F). However, a slight increase in liver Oil-Red-O staining in Ca-074-Me-treated ZM-fed larvae was observed. This observation suggests that lipid accumulation following extended HCD is not dependent on cathepsin B.

Altogether, these results indicate that extended HCD induces systemic pathologies analogous to these seen in mammals fed high fat diets and that local pathologies such as sustained myeloid cell accumulation and incomplete peristalsis are dependent on cholesterol binding/uptake and inflammasome activation even over this extended period.

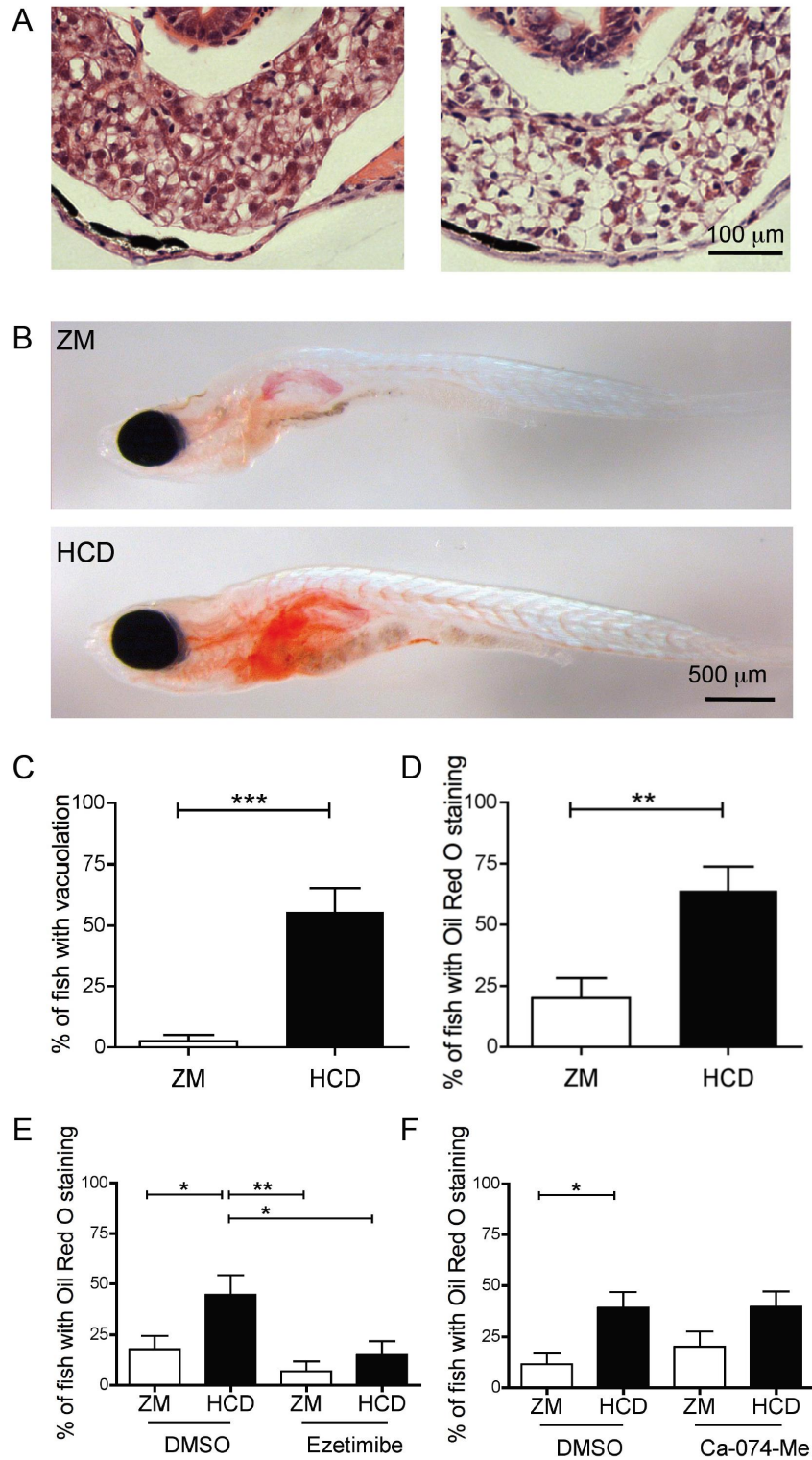


Fig. 3.24 Steatosis in liver following extended HCD.

All results are obtained from 15 dpf *Tra^{-/-}/Nac^{-/-}* larvae fed ZM control or HCD for 10 days according to **Fig. 3.20A**. **(A)** Representative images of paraffin transverse sections stained with H&E of the liver of 15 dpf *Tra^{-/-}/Nac^{-/-}* larvae fed ZM control or HCD for 10 days. **(B)** Representative image of whole-mount Oil Red O stained 15 dpf larvae fed ZM control or HCD for 10 days. **(C)** Percentage of fish showing vacuolation in the liver. $n \geq 34$, pooled from two experimental replicates. **(D)** Percentage of fish showing Oil Red O staining in the liver. $n = 25$, pooled from two experimental replicates. **(E&F)** Percentage of fish showing Oil Red O staining in the liver following treatment with ezetimibe (25 μ M, E) and cathepsin B inhibitor (Ca-074-Me, 10 μ M, F). $n \geq 20$, pooled from two experimental replicates. * $p < 0.05$ ** $p < 0.01$ *** $p < 0.001$. Mann-Whitney U test. Error bars represent SEM.

3.4 Summary

3.3.1 Dietary cholesterol-induced myeloid cell accumulation in the intestine is conserved between zebrafish and mice, since acute exposure to HCD leads to accumulation of myeloid cells in the intestine of adult zebrafish and an accumulation of myeloid cells and an increase in *Il1b* transcripts in the lower part of the small intestine of Balb/C mice.

3.3.2. HCD-induced immune cell accumulation in zebrafish larvae is dependent on NFkB activation and the microbiota, while acute HCD-exposure does not alter the load or composition of the microbiota and does not further activate NFkB in the intestine. Together, these data suggest that signal 1 of HCD-induced inflammasome activation is delivered by constitutive NFkB activation by the commensal microbiota.

3.3.3. Acute HCD-exposure leads to caspase-1 activation in IECs. Further, treatment of zebrafish larvae with an ASC FITC MO in the water results in the uptake of the MO by IECs where it induces a detectable decrease of ASC (*pycard*) transcripts. Together, these data indicate that cholesterol elicits ASC-dependent inflammasome activation in IECs. Further, HCD-induced intestinal inflammation is, at least in part, dependent on IL-1 β .

3.3.4. Extended HCD-exposure, still consequent to cholesterol binding and inflammasome-induced inflammation, induces sustained intestinal inflammation that correlates with impairments in intestinal motility. Hepatic steatosis following extended HCD is dependent cholesterol binding.

3.5 Discussion

3.5.1 Conservation of HCD-induced acute inflammation between zebrafish and mice and its relevance to humans

The data presented here and in the PhD thesis of N. Sangha [267] provide, to our knowledge, the first evidence that a single short exposure to an HCD results in acute inflammatory response in the intestine. Of note, zebrafish larvae at the developmental stage used for the experiments exhibit firstly, an innate only and therefore not fully functional immune system and secondly, a potentially ‘pre-mature’ microbiota that has colonised the intestine only 3 days before the experiment. Thus, in the present study, previous observations of an HCD-induced accumulation of inflammatory leukocytes in the intestines of zebrafish larvae [267] were confirmed for fully immunocompetent zebrafish adults and mice with an ‘established’ microbiota. Butter gavage-induced accumulation of myeloid cells in mice was observed in the lower part of the small intestine (the distal jejunum and the ileum). Likewise, as previously established by N.Sangha [267], the accumulation of myeloid cells in the zebrafish larval intestine following HCD occurs in the mid- and distal intestine, the respective teleost counterparts to the mammalian jejunum and ileum [225, 226]. This was confirmed for adult zebrafish where an increase of myeloid cells was detected in the lower part of the small intestine indicating the conservation of the location of acute inflammation following HCD. It cannot however be excluded that acute inflammation in zebrafish adults might also occur in other intestinal sections as the upper part of the small intestine or the colon were not analysed. The magnitude of accumulation of myeloid cells in the intestine showed the same two-fold increase for mice, zebrafish larvae and adults, indicating that not only the location but also the magnitude of inflammation was conserved. While NPC1L1 localisation in the zebrafish intestine has not yet been described in the literature, uptake of BODIPY-cholesterol by IECs was detected in the anterior- and mid intestine, the counterparts to the mammalian upper part of the small intestine (duodenum and the proximal jejunum). Thus, the location of cholesterol absorption in the intestine also seems conserved between species.

Duewell *et al.* first described the ability of cholesterol crystals to induce inflammasome activation in atherosclerotic plaques in murine macrophages [61]. Our data extends the knowledge of the proinflammatory properties of cholesterol to include the effects of dietary cholesterol in the intestine, *i.e.* its physiological route of entry. Additionally, we

show in zebrafish that dietary cholesterol-induced intestinal inflammation is also dependent on inflammasome-activation (further discussion see below). Together with the described similarities in intestinal structure, microbiota and the intestinal immune system, it could be hypothesised that not only the location and magnitude of immune cell accumulation following HCD, but also the mechanism of inflammasome activation by cholesterol induced intestinal inflammation is evolutionarily conserved between zebrafish and mice. However, whether these findings translate to humans in the context of a high-cholesterol meal remains unknown.

Egg, a cholesterol rich food, contains only 0.3% cholesterol. Hence, the amount of cholesterol ingested by zebrafish larvae (4 - 8 %) in this study and used in atherogenic diets in inbred mice (1 – 3 % [260]) represents a rather ‘excessive’ dose compared to that usually ingested in humans. It should be borne in mind that the HCD used in our study, which is a control diet enriched only with cholesterol, does not however reflect a cholesterol-rich meal/diet for humans. Cholesterol-rich meals often also contain a high level of saturated fatty acids which also exhibit potent pro-inflammatory effects [62, 274, 275]. Using the same model of intestinal inflammation in zebrafish larvae, N. Sangha demonstrated that a HFD enriched with saturated fatty acids (such as palmitic acid) induces the accumulation of leukocytes to the intestine in the same manner as an HCD, whereas an unsaturated fatty acid-enriched diet (such as oleic or linoleic acid) did not [267]. With regards to any suggested potential synergistic effect on inflammation, a high-cholesterol, high-fat diet (delivered as clotted cream which contains 0.17% of cholesterol [267]) induced accumulation of immune cell recruitment in the same magnitude as induced by individual cholesterol- or palmitic acid-enriched diets. Likewise, the butter gavage in mouse (containing a total of 0.4 mg cholesterol) induces the same inflammatory response as the oil + cholesterol gavage (containing a total of 8 mg cholesterol). As there is more total fat in the oil + cholesterol gavage compared to the butter this suggests that it may induce a more prominent inflammatory response. The similarity in severity of inflammation between the two diets, despite the higher fat content in oil + cholesterol, may be explained by differences in composition of fatty acids. Corn oil contains only 15% of saturated fatty acids and more unsaturated fatty acids (55%) compared to butter, which contains a high amount of saturated fatty acids (63%) and only few unsaturated fatty acids (4%). With regards to previously demonstrated pro-and anti-inflammatory properties of these different fatty acids [275-277], it can be hypothesised that not only the content of cholesterol and fatty acids, but potentially also the type of fatty acid has an effect on the

outcome of inflammatory responses in the intestine. Further, Walters *et al.* demonstrated that fatty acids facilitate uptake of cholesterol by enterocytes by inducing relocation of NPC1L1 from the a resident perinuclear position to the apical brush border membrane of enterocytes [262]. Thus, it could be suggested that the more fatty acids present (potentially of a particular type), the more cholesterol is absorbed and the more inflammation induced. Once in the enterocyte, cholesterol is re-esterified by acyl CoA cholesterol acyltransferase before it is packaged into chylomicrons and excreted from the basal domain into the mesenteric lymph [282]. Fatty acids have been shown to directly increase chylomicron formation [305]. However, the potential of fatty acids to increase the rate of cholesterol processing has not yet been studied. In contrast, mobilisation of NPC1L1 away from the brush border has been proposed as a protective mechanism of enterocytes to prevent excessive levels of cholesterol uptake [306]. Excess dietary cholesterol present in enterocytes has been suggested to be excreted back into the intestinal lumen via ATP-binding cassette hemi-transporter G5 and 8 [282, 307]. Of note, most of these findings were obtained from cultured cells *in vitro* and it is not clear if they capture physiologic responses of the highly specialised environment of the intestine. In conclusion, how dietary cholesterol in conjunction with different types of fatty acids induces intestinal inflammatory responses should be explored further in a live whole animal model. The relevance of our findings in the context of pathologies associated with long-term ingestion of cholesterol are discussed below.

3.5.2 Constitutive NFκB activation delivers signal 1 of HCD-induced inflammasome activation in the intestine of larval zebrafish

Successful inflammasome assembly *in vitro* requires two distinct signals: priming (signal 1) and activation (signal 2) of the inflammasome complex [60]. Priming *in vitro* is achieved by stimulation with LPS, however, since previously inflammasome activation by cholesterol crystals *in vivo* has been suggested for ‘sterile’ inflammatory set-ups, alternative mechanisms for delivering signal 1 have been proposed: phagocytosis of cholesterol crystals by macrophages or CD36-mediated intralysosomal conversion of oxLDL into cholesterol crystals [61, 287, 288]. The results of this study together with previous results by N. Sangha [267] confirm the requirement of two distinct signals for cholesterol-mediated inflammasome activation *in vivo* in the intestine of larval zebrafish. In fact, here we hypothesise that dietary cholesterol is able to activate the inflammasome in the ‘non-sterile’, microbial-rich environment of the intestine by two unrelated signals,

NFκB activation by the microbiota and cholesterol binding/uptake via NPC1L1 [267] (see further discussion below). Signal 2 in cholesterol crystal mediated inflammasome activation is explained by induction of lysosomal damage [61]. N. Sangha demonstrated that HCD-induced intestinal inflammation is dependent on ROS and cathepsin B and therefore potentially lysosomal destabilisation [267]. Atherosclerotic lesions have been detected *in vivo* as early as 2 weeks following an atherogenic diet [61]. In contrast, *in vitro* formation of cholesterol crystals in macrophages following exposure to oxLDL has been reported as early as 1 hour after exposure [61]. Thus, even though cholesterol crystal formation has so far only been described for macrophages, there is a possibility that NPC1L1-mediated binding/endocytosis of dietary cholesterol leads to the formation of cholesterol crystals and lysosomal destabilisation (signal 2) in IECs. Whilst potential intralysosomal cholesterol crystal formation following cholesterol uptake into IECs awaits further study, the discussion below will support the hypothesis that cholesterol-induced inflammasome activation requires two independent signals.

Signal 1 of HCD intestinal inflammation was dissected using various approaches. Firstly, the involvement of NFκB signalling was confirmed using a pharmacological inhibitor of NFκB activation. Secondly, as previous studies suggested that the microbiota is able to provide signal 1 [299] and that colonisation of germ-free intestines in mice and zebrafish results in NFκB activation [222, 289], the potential of the microbiota to deliver signal 1 was tested in GF larvae. The microbiota was clearly important for HCD-induced intestinal inflammation, since, in contrast to CONV raised larvae, GF larvae did not recapitulate myeloid cell accumulation following HCD. However, whether cholesterol mediated changes of the microbiota, which potentially indirectly activate NFκB, or whether cholesterol further activated NFκB in presence of the microbiota could not have been ruled out at that stage and was therefore assessed.

It is widely recognised that long-term dietary intake shapes the structure and the activity of microbial communities in the intestine [271, 272]; however, how rapidly the intestinal microbiota is able to respond to dietary changes was unclear for a long time. Recent efforts in understanding short-term kinetics established that diet-induced changes to gut-associated microbial communities of both mice and humans can occur within a single day [290, 291]. These data are in contrast to observations in this study, where no changes of the microbiome were detected in larval zebrafish intestines within 24 hours of feeding an HCD. While this study assesses the microbiome following a cholesterol-enriched diet, which is fundamentally composed of the same macronutrients (fats, proteins and carbohydrates),

studies in both mice and humans established microbial responses after dramatic macronutrient changes, *i.e.* from a low-fat, plant polysaccharide-rich diet to a high-fat, high-sugar diet in mice (40% fat, 40% sugar [290]; and in humans following a diet composed entirely of animal products or an entirely plant-based diet [291]. Hence, it can be suggested that small changes in diet, such as the addition of cholesterol, do not affect the microbiome following a short-term exposure, at least in zebrafish larvae, although it remains unknown whether or not this is the case for adult zebrafish or mammals. For zebrafish larvae, this hypothesis can be supported with previous microbiota composition studies performed by Semova *et al.* [231]. Semova *et al.* demonstrated that there were no differences in the microbial composition when comparing larvae fed on a control diet or a low-calorie diet for 1 day [231]. However, they also demonstrated that feeding was important for the establishment of diversity of bacterial communities in the zebrafish gut as *Firmicutes* were enriched in fed but not in starved larvae [231].

Of note however, one major difference of using zebrafish larvae at the onset of independent feeding (around 5-6 dpf) compared to studies performed in mammals, is that their intestines have not previously been exposed to food. Thus, their commensal communities might not be enriched for one particular diet-dependent phyla yet, but rather predominantly influenced by the surrounding environment, *i.e.* the water. Consistent with that notion, Semova *et al.* detected a similar enrichment for *Proteobacteria* and *Firmicutes* in intestines of zebrafish larvae that were raised in water supplemented with food from 3 dpf onwards, whereas starved larvae and water samples exhibited predominantly *Proteobacteria* while *Firmicutes* were completely absent [231]. In the present study, *Proteobacteria* are the dominant phylum and no sequences were detected for *Firmicutes* after 1 day of feeding suggesting that the present microbiota resembles that of the starved larvae of Semova *et al.* where diet-dependent phyla such as *Firmicutes* are still absent. This is consistent with findings in mice where starvation for 24 hours results in a marked decrease of *Firmicutes* [308] and humans where changing the diet of obese people to low-fat, low-carbohydrates contents decreases the abundance of *Firmicutes* [309]. However, there is also a possibility that the presence or absence of *Firmicutes* could simply be explained by the different diets used (here: ZM diet and Semova *et al.*: Zeigler diet) or by differences in aquarium water specific microbiota. Nevertheless, in this study, a diet-enriched in cholesterol is not able to change the type or load of microbiota within 24 hours. Together with the fact that caspase-1 activity can be detected from as early as 6 hours, it can be suggested that the pro-inflammatory effect of HCD in the intestine is not mediated

via alterations of the microbiome. However, even though 16S rDNA-based high-throughput sequencing analysis did not detect any changes in bacterial diversity and composition following HCD, changes in the specific metabolic activity of bacteria cannot be excluded. For example, Devkota *et al.* demonstrated that dietary fat mediates the generation of taurocholic acid from host hepatic bile acid, which as a consequence increases the availability of organic sulphur and promotes growth of the sulphite-reducing pathobiont, *Bilophila wadsworthia* that emerges under pathological intestinal inflammatory conditions [158]. Thus, potential microbial metabolism of cholesterol-derived compounds produced by the hosts (bile acids and steroids) cannot be excluded and need further investigation using mass spectrometry. Nevertheless, since HCD-induced intestinal inflammation is directly dependent on cholesterol uptake/binding via NPC1L1, the pro-inflammatory effect is mediated via cholesterol rather than the microbiota.

To assess the possibility that cholesterol might directly contribute to signal 1 was analysed by measuring EGFP expression in *Tg(NFkB:EGFP)* zebrafish larvae. Recent reports demonstrated that this approach allows quantification of NFkB activation in epithelial cells in several different anatomical sites in zebrafish larvae, including the intestine following microbial colonisation [222] or after treatment with NSAID glafenine [255], in epidermal epithelial cells following a tail-injury [294] and in epithelial cells lining the swimbladder following infection with *Candida albicans* [219]. In this study, no change in intestinal EGFP expression following HCD was detected suggesting that cholesterol does not directly induce further NFkB activation. However, in contrast to the more dramatic NFkB stimuli described above, there is a possibility that cholesterol only slightly enhances NFkB activation, which might not be detectable by measuring the level of GFP expression. This notion is supported by the result that oil + cholesterol gavage in mice slightly, but not significantly, increased Nlrp3 mRNA expression, which has been shown to be upregulated *in vitro* following delivery of signal 1 [60]. Thus, whether cholesterol contributes to inflammasome priming is not established, but, as demonstrated in germ-free larvae, HCD alone is not able to induce inflammation and therefore signal 1.

Together, it can be hypothesised that in the microorganism-rich environment of the intestine, constitutive NFkB activation in IECs contributes to immune homeostasis but by constantly providing signal 1 delivers the priming signal that allows IECs to be able to react quickly to potential insults from dietary antigens.

3.5.3 HCD induces inflammasome activation in intestinal epithelial cells

To investigate which cellular compartment initiated the acute inflammatory response against HCD, intestinal cells of zebrafish adults were stained for active caspase-1, which is activated during successful inflammasome assembly [56]. Further, co-labelling of cells expressing active caspase-1 with a cytokeratin antibody, localised inflammasome activation following HCD within IECs. In mammals, cholesterol crystals have been shown to act via the NLRP3 inflammasome leading to the activation of caspase I in macrophages [61]. Although the functional significance of inflammasomes and the Nod-like receptor family has not been widely studied in zebrafish, members of the mammalian NLR family (NOD1, NOD2 and NOD3) as well as a subfamily resembling the mammalian NALPs are abundant [213, 214] and the NLR molecules are conserved across bony fish [215]. In addition, caspase-1 orthologues have been described in zebrafish [310] and caspase-1 like activity resulting in IL-1 β processing has been demonstrated in adult zebrafish leukocytes [218]. Hence, it is likely that the role of inflammasomes in immune activation is conserved across vertebrate phylogeny [214] and that cholesterol exposure could result in inflammasome activation involving caspase I activity (caspase a or caspase b) as shown in this study in intestinal epithelial cells of zebrafish adults.

Two distinct signals are required for successful inflammasome assembly [56]. Therefore, both signal 1 and signal 2 would have to be provided to the same cell within the epithelial layer for inflammasome activation to occur. Consistent with this hypothesis, using the double transgenic line *Tg(NFkB:EGFP)xTg(ifabp:dsRed)* Kanther *et al.* demonstrated that NFkB activation (signal 1) in the intestine upon microbial colonisation occurs in dsRed+ IECs [222]. In the present study, analysis of larval intestines of *Tg(NFkB:EGFP)xTg(fms:mCherry)* showed a high number of EGFP+/mCherry- single positive non-haematopoietic cells but only very few EGFP+/mCherry+ double positive haematopoietic cells confirming observations by Kanther *et al.* that NFkB in the intestine is mainly activated in IECs [222]. The fact that NPC1L1 (potentially mediating signal 2 via cholesterol binding/uptake) is expressed at the apical domain of intestinal enterocytes [284] further suggests inflammasome activation by dietary cholesterol directly in the enterocyte-subpopulation of IECs. This is in line with observations by Kanther *et al.* where EGFP reporter activity of *Tg(NFkB:EGFP)* was detected in cells stained for the brush border marker 4E8 but not for the secretory cell marker 2F11 revealing that NFkB activation upon colonisation with commensals occurs at least in part in absorptive enterocytes [222]. Furthermore, Song-Zhao *et al.* discovered that IECs in mice express

high levels of ASC [53]. Using a novel MO-mediated knock-down approach, N. Sangha showed that HCD-induced intestinal inflammation is dependent on ASC [267]. The present study demonstrated MO localisation and a decrease in ASC (*pycard*) transcripts in IECs and therefore confirms the notion of HCD-induced inflammasome activation in IECs.

Of note, although NPC1L1 is predominantly expressed in IECs, macrophages also exhibit expression of NPC1L1, albeit at much lower levels [286]. Further, albeit at much lower numbers compared to IECs, results in this study show that there are some NFkB activated macrophages (EGFP⁺/mCherry⁺ cells) in the intestine in *Tg(NFkB:EGFP)x Tg(fms:mCherry)*. Thus, although it seems unlikely, there is a possibility that myeloid cells are able to contribute to cholesterol-induced inflammasome activation. However, no evidence for inflammasome activation following HCD in myeloid cells was found, as firstly, HCD does not increase caspase-1 activity in myeloid cells investigated and secondly, using a novel delivery method for MO, the ASC FITC MO that abrogates HCD-intestinal inflammation cannot be detected in myeloid cells. Together, our results confirm inflammasome-activation as a mechanism for cholesterol-induced intestinal inflammation in zebrafish larvae and adults [267] and demonstrate that inflammasome-activation occurs in IECs.

Our data adds to the recently emerging functions of inflammasome activation in IECs [52, 53, 58], even though the exact NLR gene that is involved in HCD-induced intestinal inflammation in zebrafish is yet to be defined. Six genes in the NLR-B subfamily of NLR genes that correspond to mammalian NALPs have been identified in zebrafish so far [215], however, their direct orthologs remain to be determined. Our novel model of MO delivery might offer the possibility to further characterise the role of individual members of this gene family in the intestine by selectively targeting their expression in IECs. Further, the mechanism linking inflammasome activation and myeloid cell accumulation is yet to be defined. Although IL-1 β has been shown to be important for HCD-induced myeloid cell accumulation in the zebrafish intestine, whether cholesterol-induced activation of caspase-1 induces proteolytically cleavage of IL-1 β or whether cholesterol induces caspase-1 dependent cell death (pyroptosis) upon which IL-1 β is released remains to be investigated. An established assay testing for a key events occurring during cell death, *e.g.* terminal deoxynucleotidyl transferase mediated dUTP nick-end labelling (TUNEL) assay, could be used to test this hypothesis in the zebrafish intestine following HCD.

3.5.4 Relevance of HCD-induced inflammation for chronic auto-inflammatory pathologies

The intestinal mucosa faces the challenging task of maintaining innate immune homeostasis in an environment rich in dietary antigens and microbes. An orchestrated interplay between intestinal haematopoietic cells and the microbiota has long thought to be crucial in maintaining intestinal immune homeostasis, while non-haematopoietic IECs were considered innocent bystanders simply forming a physical barrier [56]. Only recently has it been established that, in addition to haematopoietic cells, IECs themselves are equipped with danger-signal detecting inflammasome sensors [51, 56], but their precise role in human intestinal inflammatory diseases such as IBD still remains to be fully elucidated. So far conflicting observations have been made regarding the roles of the inflammasomes in the DSS chemical-induced model of inflammation. In different studies, mice deficient for the inflammasome components caspase-1 (*Casp1*^{-/-}) and Nlrp3 (*Nlrp3*^{-/-}) exhibited either increased and decreased severity of intestinal DSS-induced pathology (reviewed in Strowig *et al.* [174]). While in those studies the cellular location of inflammasome activation is not clear (*i.e.* intestinal haematopoietic or epithelial cells), a study using Nlrp6 deficient mice (*Nlrp6*^{-/-}), where Nlrp6 expression is restricted to IECs, demonstrated increased disease severity following DSS exposure [51]. Thus, this discrepancy in disease outcomes not only highlights the complexity of the role of inflammasomes in intestinal immunity, but also suggests opposing inflammasome functions (*i.e.* beneficial versus detrimental) within different intestinal cell types (*i.e.* haematopoietic cells versus IECs) and emphasises the need for novel tools to investigate the cell-type specific role of inflammasomes in intestinal inflammatory pathologies. Whilst conditional knock-out animals still await development, recent studies have used bone-marrow chimeras to shed light on the role of inflammasome components in the non-haematopoietic cell compartment of the intestine. For example, innate immune recognition by Nlrc4 or Nlrp3 within IECs directly confers protection against the enteric pathogens *Citrobacter rodentium* [52, 53] and Nlrp12 deficiency in non-haematopoietic intestinal cells results in increased DSS-induced intestinal pathology [58].

Our results demonstrate that dietary components such as cholesterol can also be detected by inflammasomes in IECs and induce accumulation of myeloid cells. This appears to be in contrast to the above-described roles of inflammasomes during microbial sensing [52, 53]. However, the exact inflammasome mediating the pro-inflammatory effect upon cholesterol in zebrafish is not known and might therefore be a different one compared to

those studied in mice. Further, it is perhaps not surprising that mice in which inflammasome components are completely knocked-out lack their protection against invading pathogens following dramatic epithelial damage upon DSS or infection with enteric pathogens. In contrast, our novel MO delivery approach only temporarily inhibits inflammasome machinery and might therefore facilitate the dissection of the role of inflammasome for detection of dietary components in intestinal cells, a task that might be independent or in addition to those from protection from pathogens.

Interestingly, the magnitude of intestinal myeloid cell accumulation following HCD was increased by the same two-fold range as that observed following DSS in zebrafish larvae [251]. In contrast to pro-inflammatory cytokine production following DSS in zebrafish, so far no cytokines have been detected by qRT-PCR in intestinal tissues of zebrafish following acute or extended HCD [267]. The absence of detectable cytokines may suggest that the inflammation induced by exposure to HCD is only mild compared to severe intestinal epithelial damage following DSS or TNBS treatments. Indeed, no gross changes in intestinal architecture were detected in acute and extended HCD exposed zebrafish. Nevertheless, extended HCD induced functional defects in the intestine with sustained accumulation of myeloid cells that correlated with impaired intestinal motility, both of which are characteristics of inflammatory pathologies of the intestine [131]. Although further investigations are needed to assess whether our zebrafish model of intestinal inflammation induced by acute or extended exposure to cholesterol resembles human intestinal inflammatory conditions, it may offer a more physiologically relevant model for studying aspects of intestinal inflammation. Irrespective of this, the fact that pathologies following extended HCD in zebrafish are dependent on cholesterol binding/uptake and inflammation (or at least cathepsin B) suggests that inflammatory responses in the intestine induced by cholesterol and potentially other dietary components may contribute to intestinal inflammatory disorders.

Of note, although our results are consistent the notion that inflammation plays a role in functional intestinal disorders [132, 133, 304], the exact functions of different intestinal cells during these conditions is far less defined. Some studies have implicated mast cells in the pathogenesis of functional intestinal disorders [90]. However, recent evidence suggests that crosstalk between intestinal macrophages and cells of the enteric nervous system could regulate gastrointestinal motility [311]. Here, the zebrafish system will offer a valuable tool to further dissect the role of mucosal mast cells, macrophages and enteric neurons during intestinal motility *in vivo*. Whilst a transgenic zebrafish line labelling mast cells still

awaits development [188] (S. Renshaw, University of Sheffield, UK, *personal communication*), *in situ* hybridisation for the zebrafish mast cell marker gene *carboxypeptidase A5 (cpa5)*, immunohistochemistry or histochemical staining could be performed [200] to reveal the resolution of mast cells during HCD-induced functional intestinal impairment. Transgenic lines visualising cells of the enteric nervous system have been identified from the zTrap database [312], characterised and are readily available (Tiffany Heanue, National Institute for Medical Research, UK, *personal communication*) and could be employed in conjunction with macrophage reporter systems to perform *in vivo* imaging.

Metabolic and immune systems represent highly integrated and functionally interdependent pathways that are fundamental for survival and homeostasis and their deregulation can lead to severe metabolic disorders [313]. Prolonged exposure to diets rich in fat and cholesterol is associated with chronic systemic disease including obesity, cardiovascular and gastrointestinal diseases that are all increasingly global health issues [140]. Beyond functional impairment in the intestine, zebrafish exposed to extended HCD showed lipid accumulation and vacuolation in the liver, the first manifestations of non-alcoholic fatty liver disease [314]. Together with previous findings by Stoletov *et al.* who demonstrated vascular lipid accumulation accompanied by vascular inflammation [259], suggests the relevance of the HCD-zebrafish model in the study of systemic pathologies. The fact that cholesterol uptake/binding is important for the liver pathologies observed following extended HCD not only support previous studies showing that cholesterol absorption from the gut is important for this condition [314], but also is consistent with the notion of diet-induced systemic pathologies. However, the underlying mechanisms still remain to be defined. Interestingly, inhibition of inflammation using the cathepsin B inhibitor during an extended HCD had no effect on lipid accumulation in the liver, while slightly exacerbating lipid accumulation in control fed larvae. This is in concordance with previous observations in *Caspase1^{-/-}*, *Asc^{-/-}* and *Nlrp3^{-/-}* mice which showed increased severity of liver disease compared to WT animals when fed a non-alcoholic fatty liver disease-inducing diet [268]. Due to the lack of inflammasome components, these mice fail to respond to opportunistic pathogenic microbiota. This compromises intestinal barrier integrity and results in epithelial translocation of bacterial PAMPs that are consequently transported from the intestine to the liver via the portal circulation where they initiate inflammation [268]. Whether hepatic lipid accumulation in the zebrafish following

extended HCD feeding is accompanied by or a consequence of hepatic inflammation remains to be investigated. Since cholesterol is first encountered, absorbed and metabolised by the intestinal mucosa and elicits an inflammatory response in intestinal epithelial cells which is involved in long-term local pathologies, it is of importance to further investigate the impact of this local inflammation on systemic conditions. For instance, whether extended HCD feeding compromises the intestinal barrier function could be assessed *in vivo* in zebrafish larvae, for instance by microgavage of a fluorescent dextran [298]. Recent evidence has emerged suggesting that intestinal inflammation precedes and therefore is associated with diet-induced systemic conditions [159] and further, that cholesterol absorption from the gut has been shown to play a role in most of these conditions [315]. However, its relevance for systemic inflammation in metabolically relevant tissues is controversial [315] and will remain subject of future investigations. The developed zebrafish model of HCD-induced intestinal inflammation might offer a valuable tool to investigate the mechanisms how diet-associated systemic inflammatory conditions are triggered.

3.6 Conclusion

Together with previous findings by N. Sangha [267] we established a zebrafish model that reveals a novel route by which ingested cholesterol can initiate intestinal inflammation through inflammasome activation in intestinal epithelial cells. Our data provide *in vivo* evidence for nutrient induced acute intestinal inflammation, previously suggested by *in vitro* studies [273, 274] and demonstrate how dietary choices can directly perturb intestinal immune homeostasis. This model offers the potential not only to study the influence of other dietary components on gastrointestinal mucosal inflammation but also to contribute to defining new therapeutic targets which could be used in preventing chronic auto-inflammatory responses that represent a major health problem worldwide.

Chapter 4

Inflammation and tissue remodelling of zebrafish gills upon exposure to irritants and/or cryoinjury

Chapter 4 | Inflammation and tissue remodelling of zebrafish gills upon exposure to irritants and/or cryoinjury

This chapter presents the work on the zebrafish gill to ascertain its value as a model for the study of acute and chronic mucosal lung inflammation and tissue remodelling. This part of my thesis resulted from a collaboration with the part-sponsor of my PhD project, the pharmaceutical company Boehringer Ingelheim, whose interest is to develop a treatment for human lung fibrosis. Due to the lack of clinically relevant animal models for this condition (see background below), Boehringer Ingelheim were interested in exploring the relevance of zebrafish gills to study mechanisms of fibrosis. As described in the introduction (1.4.4), zebrafish gills have not been used to model human inflammatory lung diseases so far [256]. Therefore, this project set out to assess whether exposure to irritants associated with human pulmonary fibrosis would induce an inflammatory response in zebrafish gills and whether persistent inflammation would consequently induce scarring. Understanding the mechanisms of fibrosis and scarless healing/ regeneration of wounds after injury is a much sought after goal and has the potential to lead to the development of novel therapeutic strategies.

4.1 Introduction

Pulmonary fibrosis

Pulmonary fibrosis (scarring of the lung) is a serious condition which is characterised by alveolar epithelial cell injury and hyperplasia, accumulation of inflammatory cells and fibroblasts, deposition of excess fibrous connective tissue and progressive scar formation resulting in impaired efficiency of gas exchange and pulmonary function [46]. Fibrosis is a physiological response resulting in a reparative or reactive process in an organ or tissue during which excess fibrous connective tissue is formed. Under normal conditions, tightly regulated interplay between constituents of the ECM and different components/ processes of the immune system result in the correct repair of tissue after damage [46, 47]. During that process, epithelial and endothelial cells trigger a clotting cascade, which allows the entry of inflammatory cells into the tissue out of blood vessels by increasing vessel wall permeability. Pro-inflammatory cytokines released by recruited inflammatory cells (firstly

neutrophils, followed by macrophages) trigger the subsequent recruitment and activation of fibroblasts. Activated fibroblasts, termed myofibroblasts, release components of the ECM and collagen required for wound repair [45]. If the initial response does not resolve but becomes chronic, inflammation and repair processes occur simultaneously leading to persistent tissue remodelling responses and fibrosis. Therefore, although initially beneficial, the wound-healing process can become pathological and can result in the formation of a permanent scar. Scar formation is the result of fibrosis obliterating the architecture, organisation and sometimes function of the underlying organ or tissue [112]. The key cellular driver of fibrosis is the collagen-producing myofibroblast (α -SMA+) that can be activated by a wide array of signals, including paracrine factors secreted from epithelial cells, activated lymphocytes and macrophages and autocrine signals derived from myofibroblasts [45, 47, 146]. Key cytokines secreted during wound healing processes are TGF- β , IL-13 and Platelet-derived growth factor (PDGF), which maintain macrophage and myofibroblast activation and therefore drive fibrosis. Fibrosis is strongly linked to T_h2 responses and key cytokines such as IL-4 and IL-13 can stimulate collagen and fibronectin synthesis by myofibroblasts [45]. Indeed, the induction of anti-fibrotic T_h1 responses through the production of IFN- γ has been suggested as potential therapeutic treatment [47]. M2 macrophages have controversial roles during wound healing and fibrosis. Whilst initially M2 responses were considered as detrimental drivers of fibrosis that promote ECM production and drive T_h2 responses, recent evidence suggest that their presence during fibrotic processes might be required for the resolution of fibrosis and the initiation of fibrosis-suppressing T_{reg} cells through the release of IL-10 [47]. Macrophages also produce matrix metalloproteinases (MMPs), which are extracellular zinc endopeptidases known for their activity as physiological mediators of collagen turnover and ECM remodelling. MMPs and their specific tissue inhibitors of metalloproteinases (TIMPs) form a stoichiometric 1:1 complex under homeostatic conditions that becomes unbalanced during pathological conditions. Fibrosis occurs as a result of a net increase in collagen that exceeds the rate at which it is degraded by MMPs. Therefore, stimulation of macrophages to produce MMPs that could directly degrade interstitial collagen might promote resolution of fibrosis. However, patients experiencing an exacerbation of COPD, asthma and pulmonary fibrosis are characterised by increased expression of MMP-9 and experimental animal models of fibrosis report conflicting results about the role of this metalloproteinase during fibrosis [316]. The possibility that MMPs might have distinct roles during specific

disease stages awaits further study. The diagram below illustrates the current understanding of the process of pulmonary fibrosis (Fig. 4.1).

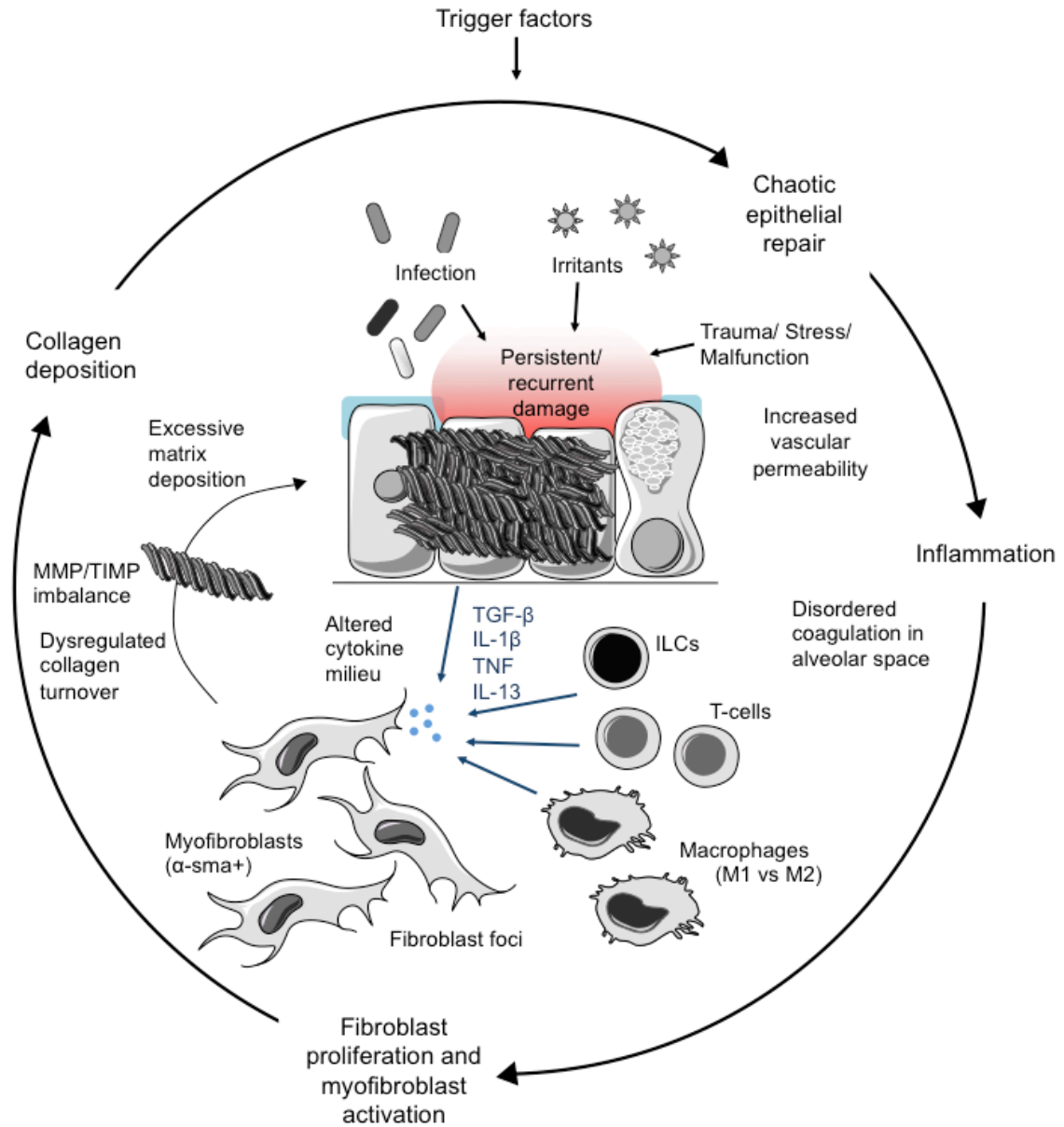


Fig. 4.1 Schematic representation of lung fibrosis.

Trigger factors that initiate fibrosis in the lung are often unknown. However, a wide variety of stimuli are associated with this disease. Epithelial injury leads to the activation of immune cells, which together with epithelial cells activate myofibroblasts through the release of pro-fibrotic cytokines and growth factors. Activated myofibroblasts secrete ECM proteins that are deposited. If the stimulus is persistent and/ or recurrent the initial inflammation does not resolve but turns chronic and the continuous collagen deposition through myofibroblasts progressively impairs organ function. During fibrosis this cycle becomes self-perpetuating. Adapted from Dancer *et al.* [316] and Friedman *et al.* [146]

Regeneration versus fibrosis in vertebrates

In mammals, embryonic and fetal wounds heal rapidly and efficiently and without scar formation, whereas tissue repair in adults leads to irreversible scar formation often associated with functional impairment of underlying tissue. Differences in the inflammatory response following injury in embryos versus adults have been associated with the different wound-healing outcomes [317, 318]. For example, compared to adults, embryonic wounds are characterised by fewer inflammatory leukocytes, which are less differentiated and less persistent, and by reduced numbers of cytokines and growth factors associated with fibrosis, such as TGF- β [317-320]. Thus, the causative relationship between inflammation and fibrosis has been a focus of scientific interest over many years, although conflicting evidence suggests both beneficial and detrimental effects of inflammatory cells during fibrotic repair responses [321, 322]. For example, skin-wounding experiments in the absence of all leukocyte populations in PU.1 knock-out mice showed enhanced re-epithelialisation and reduced scar formation compared to WT littermates suggesting a detrimental effect of leukocytes during wound-healing [323]. Knockdown of the inflammation-dependent downstream effector protein osteopontin results in accelerated healing and reduced scarring in mice [324]. Over-expression of the regulatory and anti-inflammatory cytokine IL-10 in adult wounds reduced scarring in adult mice [325], while in contrast, the absence of IL-10 in *Il10*^{-/-} mice demonstrates scar formation into fetal wounds which healed without a scar in WT littermates [326]. Further, introduction of bacteria in fetal wounds leads to adult-like wound-healing response with scar formation [327]. These data suggest not only a detrimental effect of inflammation during repair processes but also highlights the potentially damaging influence of bacterial infections during wound healing responses. However, a robust inflammatory response is essential during the wound-healing responses to fight invading pathogens and clear dying cells and debris [321].

Macrophage ablation in adult salamanders inhibits limb regeneration and induces fibrosis. This suggests a critical role for macrophages in successful wound repair [328]. Consistently, macrophage ablation in adult zebrafish inhibits tail regeneration [329]. While in both studies macrophages were essential for regeneration during the inflammatory phase and blastema formation, their presence during the tissue-remodelling phase was dispensable [328, 329]. However, macrophage depletion during tissue-remodelling phase delayed regeneration and affected neovascularisation in salamander [328] and fin patterning in zebrafish [329]. Further, a temporal depletion study of macrophages in the

liver of mice showed that their absence in the inflammatory phase during wound healing reduced the occurrence of fibrosis, whereas their depletion during the remodelling phase had no effect [330]. These studies highlight the complexity of the precise role of an inflammatory response during successful wound-healing/regeneration processes with regards to scarring and fibrosis. Nevertheless, fibrosis is considered as an “out-of-control” inflammatory disorder where persistent tissue injury and persistent inflammation induce an unstoppable healing response together with excessive scar formation. Common factors identified in animal models of pulmonary fibrosis and in patient samples are: elevated levels of pro-fibrotic markers (TGF- β , collagen type I and III) and pro-inflammatory cytokines (IL-1 β and TNF- α). Recent studies using animal models of fibrosis indicated that stimulation of the NLRP3 inflammasome pathway of the innate immune system, with tissue irritants, can lead to acute lung injury [63, 64]. Involvement of inflammasome mediated signalling in pulmonary fibrosis is supported by the recent demonstration that caspase-1 activity is increased in the lungs of patients chronically exposed to cigarette smoke and patients with COPD [331]. Despite the fact that animal models of fibrosis have been instrumental in understanding different aspects of the disease pathology of fibrosis, none of them are able to fully recapitulate interstitial pulmonary fibrosis with all its features, especially in respect of the progressive and irreversible nature of the condition. This might explain why, so far, no drug has been successfully applied in the clinic, and pulmonary fibrosis is still not curable [146]. But the question remains - what is a good animal model for fibrosis?

Here, the zebrafish gill was investigated for its potential to serve as a model for understanding fundamental mechanisms of pulmonary fibrosis. A type of mucosal injury had to be chosen that would allow the study of wound healing processes as well as the involvement of inflammation.

Choosing a model to induce fibrosis in zebrafish gills

Several mouse models have been developed to study the pathological process of fibrotic responses in lungs, including exposure to bleomycin, silica, asbestos, FITC and irradiation or lung tissue-specific expression of transgenes [180].

The bleomycin-induced model of pulmonary fibrosis is the most widely used and well-characterised. The extensive use of bleomycin in animal models is because it is commonly used as chemotherapeutic in humans and may cause lung fibrosis at high concentrations [181]. Bleomycin is an antibiotic and it is believed that it induces fibrosis by forming a

pseudoenzyme through the chelation of metal ions. These, in the presence of oxygen, produce ROS leading to the recruitment of inflammatory cells and fibroblasts, pulmonary toxicity and fibrosis [332]. The level of tissue-specific expression of bleomycin hydrolase, the bleomycin-inactivating enzyme, in the lungs determines the pro-fibrotic effects of this drug in patients [180, 181], as well as in different mouse strains making Balb/c mice less susceptible to bleomycin-induced fibrosis than C57Bl/6 mice [333]. Although one orthologue of bleomycin hydrolase has been identified in zebrafish, its tissue-specific expression has not yet been characterised in the literature. The weakness of the bleomycin model is that it is partially reversible and clinically not relevant as in most cases in humans lung fibrosis are not caused by bleomycin [181]. Thus, the mechanism by which fibrosis develops in humans might be different to the one studied in the bleomycin model. This might also explain why none of the drugs effective in the bleomycin model have proven beneficial in clinical trials. Therefore, the use of the bleomycin model in translational fibrosis research is questionable.

To develop a more relevant model of fibrosis, which recapitulates the human pathologic process, it is pertinent to apply risk factors associated with fibrosis and assess their ability to induce similar pathologies. These fibrosis-associated risk factors, identified by epidemiological studies, include exposure to persistent lung-tissue irritants such as asbestos, silica and cigarette smoke [147]. Heavy, often occupational, exposure to crystalline silica (part of sand or quartz) or asbestos is common in the history of patients diagnosed with silicosis or asbestosis respectively. Both are serious, irreversible and progressive forms of pulmonary fibrosis with no effective treatment nor a complete understanding of the pathogenesis [334]. Upon inhalation, crystalline silica, namely silicon dioxide, is deposited deep in the small airways of the lung where it cannot be cleared by the mucociliary apparatus. There, silica is engulfed by resident alveolar macrophages leading to the production of pro-inflammatory cytokines, pro-fibrotic factors and pro-apoptotic signals. Apoptotic cells and their subsequent ingestion by macrophages is thought to initiate a cycle of persistent inflammation, eventually leading to fibrosis [145]. Silicosis in mice or other rodents induces persistent pulmonary fibrosis, making it more relevant than the bleomycin model. However, in this model fibrosis takes time to develop and it is therefore not ideal for high-throughput drug screening [145, 180].

Accordingly, in the current study exposure to silica and cigarette smoke, both risk factors associated with fibrosis [147, 335], were chosen and their potential to induce fibrosis in

zebrafish gills investigated. In view of the differences in scarring between embryos and adults, adult zebrafish were chosen for the study.

Regeneration versus fibrosis in zebrafish

In contrast to mammals, teleosts have a marked capacity to regenerate tissue without irreversible scarring, even into adulthood [336]. Hence, there is increased interest in using the zebrafish caudal fin injury or cryoinjury of the zebrafish heart as models in which the mechanisms of vertebrate tissue regeneration can be explored [337, 338]. Although adult zebrafish display a great ability to regenerate organs and complex tissues following injury, the healing process does not always occur in a scarless fashion [337]. There are two reports in the literature of a collagen-rich scar in adult WT zebrafish. The first reports a laser-inflicted wound of the zebrafish skin [339]; the second a cryocauterisation induced localised injury of the heart [337, 338, 340]. However, in both cases, the scar is only transient and slowly regresses over time demonstrating not only the remarkable capacity to regenerate lost tissue but also the ability to completely eliminate and resolve deposited scar tissue, replacing it with functional tissue. In comparison to tissue resection of the zebrafish heart which heals without scarring [338, 341], cryoinjury-induced transient scar formation is a result of extensive apoptosis and death of damaged cells and exuberant inflammation [337, 338, 340]. As in these models the intensity of the scar seems to correlate with the degree of inflammatory response, the link between inflammation and scarring suggested for mammals also seems to be the case for zebrafish. Yet in contrast to mammals, adult zebrafish seemingly have a mechanism in place to avoid fibrosis and to resolve scarring, suggesting a potentially different inflammatory response compared to mammals. Whether immune-cell rich mucosal organs such as the zebrafish gills regenerate severely wounded-tissue at all or in presence together with transient scar is not known. This project investigated whether apoptotic/necrotic lesions caused by cryoinjury of the zebrafish gills would regenerate or fibrose.

Transcriptome profiling of zebrafish gill injury

Understanding the mechanisms of fibrosis and scarless healing/ regeneration of wounds after injury is a much sought after goal and has the potential to lead to the development of novel therapeutic strategies. Therefore, the final aim of this PhD project was to identify and characterise the established models of mucosal gill injury and/ or fibrosis using transcriptome profiling. RNA-seq was chosen as the method of transcriptome profiling for several reasons. Firstly, it is the method of choice for discovery-based experiments. In

comparison to a microarray-approach that is restricted to the reference material available at the time of the array production, RNA-seq results can be updated as new sequence information becomes available. Secondly, RNA-seq detects more differentially expressed genes than microarrays at a larger range of expression levels, especially genes expressed at low levels [342]. Thirdly, RNA-seq can reveal sequence variation such single-nucleotide polymorphisms (SNPs) and splice-variants [342]. Therefore, RNA-seq is indeed an appropriate tool to assess transcript dynamics to allow identification of genes and pathways involved in repair and/ or fibrosis. However, it is important to note that transcriptome analysis it is also limited, it does not take into account any regulation of gene expression or any post-translational modifications resulting in the fact that transcript levels do not always accurately represent protein expression. Therefore results of RNA-seq analysis will have to be validated.

4.2 Aims

Although zebrafish possess great regenerative abilities, it was hypothesised that zebrafish gills could develop fibrosis upon exposure to irritants and/ or tissue injury and that a model could be established to study the mechanisms of mucosal inflammation in the lung.

More specifically, the aims of this chapter were to:

1. Investigate the acute inflammatory response in zebrafish gills following exposure to irritants (silica particles and cigarette smoke)
2. Examine the inflammatory and tissue-remodelling responses following chronic exposure to these irritants
3. Assess the inflammatory and tissue-remodelling responses following physical gill tissue injury (cryoinjury) alone or in combination with exposure to silica particles
4. Perform transcriptome profiling using RNA-seq analysis of fibrotic tissue to identify and characterise pathways involved in fibrosis and/ or repair

4.3 Results

4.3.1 Acute exposure to silica and smoke

Experimental set-up

In order to investigate the effects of silica particles and cigarette smoke in the gills, adult zebrafish were exposed to silica particles dispersed in system water or to cigarette smoke infused in system water (Fig. 4.2A) while control fish were exposed to system water only. As the aim was to provoke scarring and to study the mechanisms involved in fibrosis, silica particles and smoke extracts were first tested for their ability to provide sufficient inflammatory stimuli before chronic exposure to these irritants was performed. Following exposure for the indicated time-points, zebrafish gills were dissected and their inflammatory status analysed (Fig. 4.2B). Transgenic zebrafish expressing fluorescent proteins under the control of specific immune cell markers allow quantification of immune cells in the dissected gill tissue by flow cytometry. However, the only transgenic lines available in the Dallman lab that express fluorescent proteins into adulthood were *Tg(mpx:GFP)*, labelling neutrophils (GFP^{high}) and potentially macrophages (GFP^{low}), at least in embryos [191, 343], and *Tg(lyz:dsRed)*, marking neutrophils in embryos [192, 208] but potentially labelling a more macrophage-like cell population in adults [339]. Therefore, only the presence of innate immune cells was quantified when setting up different models of mucosal gill inflammation. In addition, qRT-PCR for transcripts of immune cell marker genes and/or pro-inflammatory cytokines was performed on dissected gill tissues following exposure (Fig. 4.2B). Adaptive immune responses were studied as part of the RNA-seq analysis (4.3.4).

As shown in Fig. 4.3, myeloid cells (dsRed⁺ cells) and neutrophils (GFP⁺ cells) are readily detectable in gills of transgenic zebrafish adults *Tg(lyz:dsRed)* and *Tg(mpx:GFP)* using fluorescence microscopy. The presence of lymphocytes (macrophages, DCs or B cells) located at the bottom of each filament based on MHC class II immunohistochemistry has previously been described for salmonids [242]. As shown Fig. 4.3, both dsRed⁺ and GFP⁺ myeloid cell populations were also found at the bottom of each filament, while additionally the majority of GFP⁺ in *Tg(mpx:GFP)*, and especially the dsRed⁺ cells in *Tg(lyz:dsRed)* seem to be located at the bottom of each lamella. Only very few myeloid cells were detected within the lamellar epithelium Fig. 4.3.

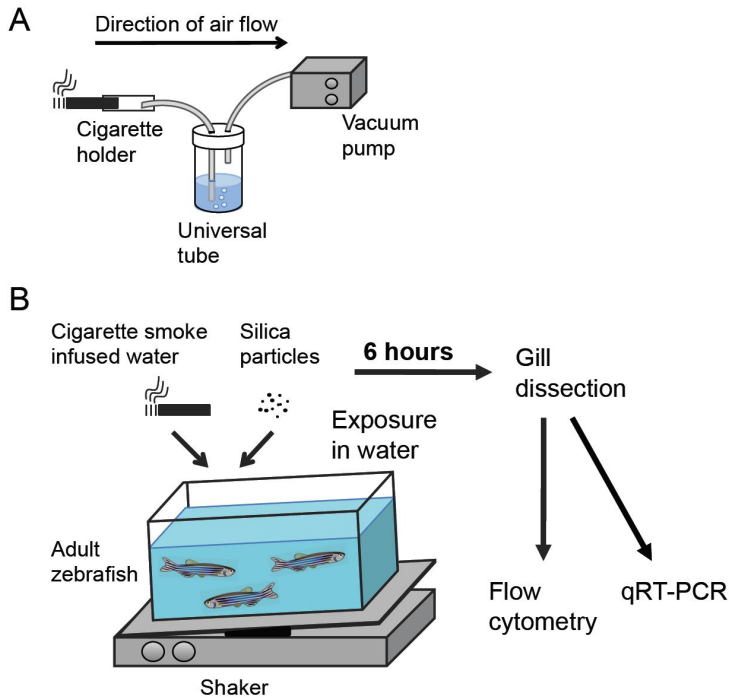


Fig. 4.2 Schematic representation of experimental procedure.

(A) Experimental set-up of preparation of cigarette smoke infused water. One standard reference research cigarette 3R4F was bubbled through 5 ml of system water contained in a Universal container using an electrical vacuum pump to standardise the pressure. (B) Adult zebrafish were exposed to cigarette smoke-infused system water or to silica particles dispersed in system water at indicated concentrations for 6 hours. Following treatment, gill tissue was dissected and analysed by flow cytometry, and qRT-PCR.

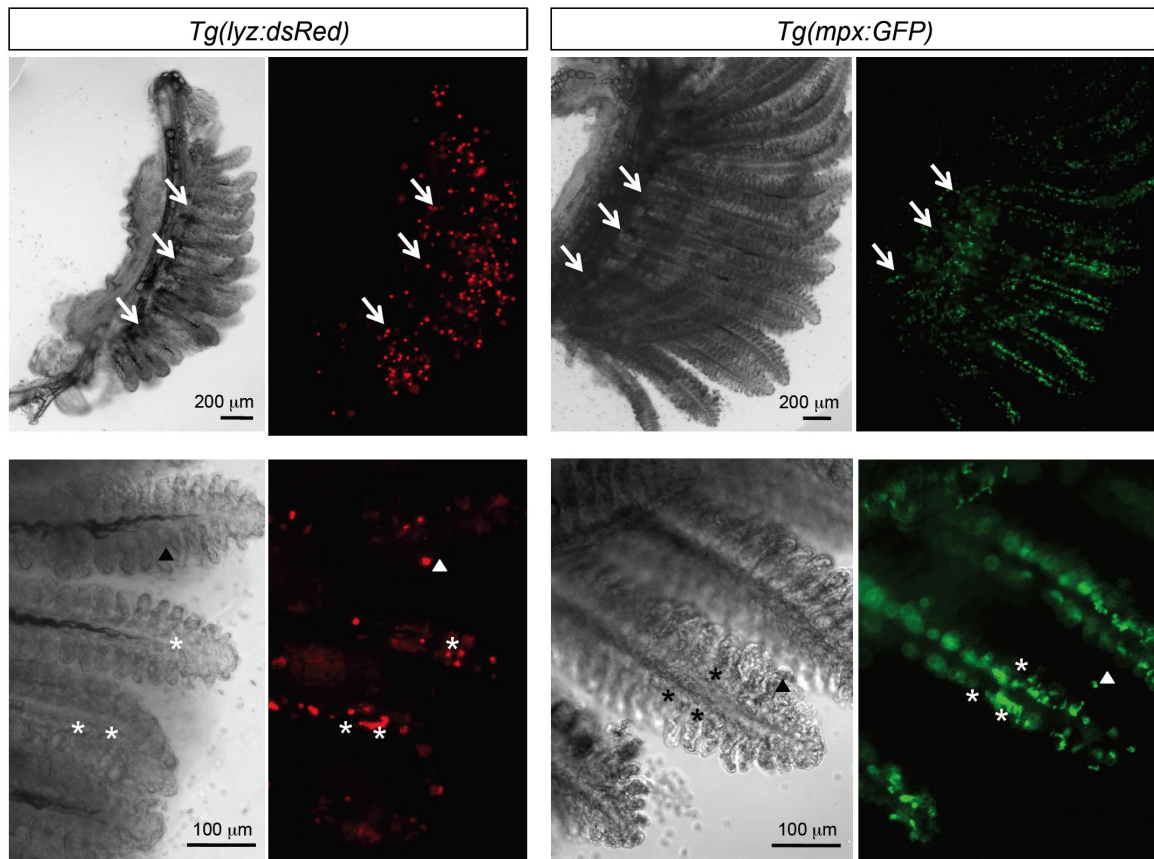


Fig. 4.3 Localisation of immune cells in zebrafish gill tissue.

Whole gill tissues from adult transgenic zebrafish *Tg(lyz:dsRed)* and *Tg(mpx:GFP)* were dissected and imaged live using fluorescence microscopy. Images are representative of $n=5$. Arrows indicate cells located at the bottom of the filaments, asterisks highlight cells at the bottom of lamellae and arrow heads indicate cells located within the lamellar epithelium. The two brightfield images of the *Tg(lyz:dsRed)* are the same as in Fig. 1.8.

The effect of acute silica exposure on local immune responses

In mouse models of silicosis a wide concentration range of silica and different means of exposure are used to induce lung inflammation and fibrosis. When mice are exposed to silica by inhalation over longer periods of time (*i.e.* several days/weeks) to mimic occupational silica exposure in humans, a concentration of silica of 250 mg/m³ (= 0.25 µg/ml) is given [344]. However, when only a single dose of silica is administered via intranasal or orotracheal instillation in mice, a dose of 0.2-1 mg is used [63, 65]. A dose of 0.5 mg/ml silica is used for *in vitro* cell experiments with an exposure time of 6 hours [64, 65]. Since the initial aim was to test whether acute silica exposure would induce an inflammatory response in the gill tissue of zebrafish, the silica concentration previously used in the cell culture system was used. Zebrafish were exposed to 0.5 mg/ml of silica dispersed in system water for 6 hours and immune cell accumulation assessed by flow cytometry in gills of transgenic zebrafish.

Adult transgenic zebrafish *Tg(lyz:dsRed)* immersed in water containing silica showed an increase in the number of dsRed⁺ myeloid cells in their gills as analysed by flow cytometry, peaking at 6 hours of exposure (Fig. 4.4B). A similar significant increase in the number of GFP⁺ neutrophils was observed using flow cytometry analysis of gill tissues from *Tg(mpx:GFP)* after 6 hours of exposure to silica (Fig. 4.4C). Gill tissue from WT zebrafish served as a negative control to assign the gates for dsRed⁺ and GFP⁺ cells, as previously performed for flow cytometry of intestinal cells (Fig. 3.3C). Analysis of the transcripts of the neutrophil specific gene *mpx* by qRT-PCR revealed a similar transient increase (Fig. 4.4D), which suggests that the level of *mpx* transcripts correlates with the number of neutrophils present in the gill. To assess whether silica would initiate an inflammatory response in larval zebrafish, parallel experiments were performed in 15 dpf *Tg(mpx:GFP)*, the age from which zebrafish larvae start to depend fully on their gills to provide their oxygen requirements [236]. Again, silica exposure resulted in a significant increase in the number of neutrophils (GFP⁺ cells) after 6 hours exposure to silica (Fig. 4.4E&F). Taken together, these data suggest that exposure to silica elicits transient neutrophilia in the gills of zebrafish at early and later developmental stages.

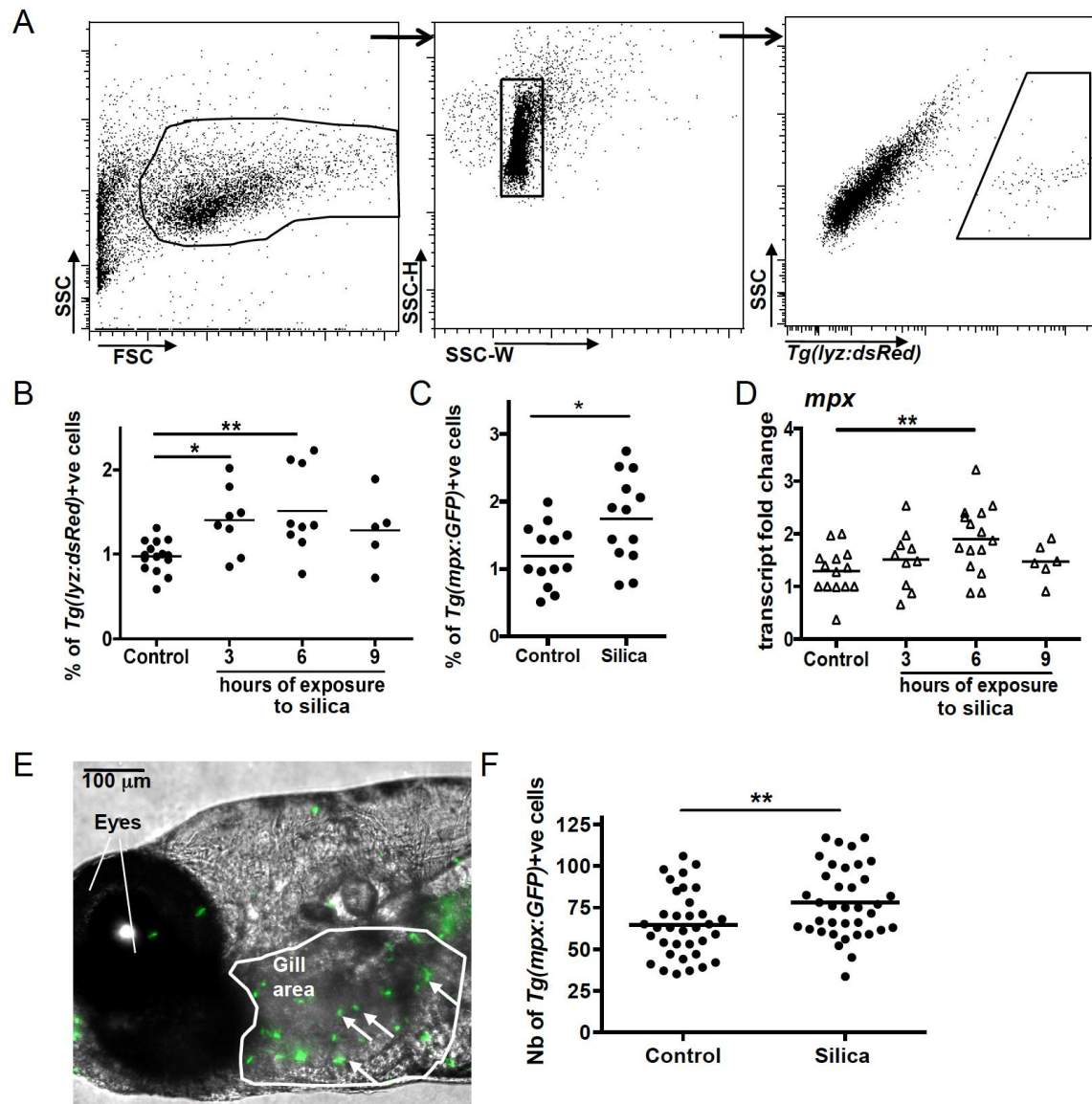


Fig. 4.4 Analysis of immune cell accumulation following acute silica exposure.

(A) Flow cytometry analysis on dissected and enzymatically digested gill tissue of adult *Tg(lyz:dsRed)* transgenic zebrafish. Dot plots represents the gating strategy of debris and doublet exclusion and gating for dsRed+ cells. (B) Flow cytometry quantification of % of adult *Tg(lyz:dsRed)*+ cells in zebrafish gills after silica exposure. Each single dot represents the % of dsRed+ cells obtained for one individual ($n \geq 5$). Three experimental replicates were performed and data were pooled (each experiment following the same trend). The mean is shown. Kruskal Wallis test. (C) Flow cytometry quantification of % of adult *Tg(mpx:GFP)*+ cells in zebrafish gills after 6 hours of silica exposure. Each single dot represents the % of GFP+ cells obtained for one individual ($n=13$). Two experimental replicates were performed and data were pooled (each experiment following the same trend). The mean is shown. Two-tailed t-test. (D) Dissected gill tissues were subjected to qRT-PCR analysis for *mpx* transcript levels. Dot plot shows the relative transcript values obtained for individual fish ($n \geq 6$) which were normalised to 18S and expressed as fold change relative to one control sample. Three experimental replicates were performed and data were pooled (each experiment following the same trend). The mean is shown. One-way Anova. (E) Representative merged fluorescent and bright field image of a 15 dpf *Tg(mpx:GFP)* transgenic larvae head (anterior to the left and posterior to the right). Z-plane images taken every 10 μ m through the gill area of fish heads using a wide-field microscope were merged and the number of GFP+ cells counted. The white outline depicts gill area selected for counting of GFP+ cells (white arrows). Scale bar: 100 μ m. (F) Quantification of GFP+ cells in 15 dpf old larvae after 6 hours exposure to silica. Each point represents an individual larva. Two-tailed t-test. * $p < 0.05$, ** $p < 0.01$. Experiments in (E) and (F) were performed with Rachel Vaux (ICL).

Inhalation of silica can lead to acute lung inflammation characterised predominantly by IL-1 β pro-inflammatory cytokine release [63-65]. Thus, *illb* transcripts were assessed by qRT-PCR on dissected gill tissue following exposure to silica over time. An increase in *illb* transcripts was detected which peaked at 3 hours of exposure and returned back to base-line levels by 9 hours (Fig. 4.5A). Transcripts of *tnfa* also were assessed but found to be unchanged during 9 hours of exposure to silica with Ct values fluctuating around the detection limit (Cycle threshold, Ct = 35). As discussed before, although analysis of *illb* transcripts by qRT-PCR does not confirm the release of mature IL-1 β , it gives an indication of cytokine production. Together with the increase in neutrophils, which are recruited upon IL-1 β cytokine release [73], collectively, these data suggest that silica-exposure might induce IL-1 β expression in the gills of zebrafish.

Since previous studies have demonstrated the essential role of the NLRP3 inflammasome in silicosis in mammals [63-65], the potential involvement of the inflammasome pathway in inflammatory responses in zebrafish gills induced by silica was evaluated. Inflammasome activation results in increased caspase I-activity, which was analysed here, using the caspase I-specific fluorescent FLICATM probe. As demonstrated before for dissociated gut tissue following exposure to HCD, when bound to active caspase I, the fluorescence of the probe can be detected by flow cytometry analysis, which was performed on single cell suspensions of dissociated adult gill tissue (Fig. 4.5B). A significant increase in FLICA⁺ cells was observed in adult gill tissue after 6 hours of silica exposure (Fig. 4.5B).

Additionally, binding of FLICA to active caspase-1 was assessed *in vivo* by FLIM. This work was done in collaboration with Natalie Andrews (ICL), a PhD student in the Dallman lab, who is working on evaluating FLIM readouts *in vivo* in zebrafish using optical projection tomography [345]. FLIM measures the decay in fluorescence over time after fluorophore excitation allowing intensity-independent read-out [346]. Therefore, FLIM can overcome common problems such as high autofluorescence that can interfere with the actual fluorescent signal. Due to size limitations (for technical reasons) of the specimens that could be imaged at the time these experiments were performed, young zebrafish had to be used. To meet the size requirements but ensuring that zebrafish had switched their route oxygen uptake from the skin to the gills [236], 19 dpf larval zebrafish were used (Fig. 4.5C). Following 6 hours of exposure to silica a significant increase in FLICA-specific fluorescence life-time was detected when compared to unexposed larvae (Fig. 4.5C).

Of note however, as shown in Fig. 4.5C, the fluorescence life-time did not only appear to be increased in the gill area, but also overall in the epidermis of zebrafish larvae. At this stage of development, zebrafish do not possess scales that protect the zebrafish from exposure to silica. The epidermis covering the organism at that developmental stage is only bilayered, consisting of a basal layer and a periderm, which is interconnected by tight junctions [347]. There is a possibility which is consistent with the data presented that silica exposure would not only affect the gills tissue but also the immature epidermis where it could potentially elicit inflammasome activation.

As discussed in the first results chapter, inflammasome activation requires priming of cells (signal 1), which involves NFkB activation. The zebrafish intestine exhibits a high number of cells that are NFkB activated at steady state. To examine NFkB activation in the adult zebrafish gill, flow cytometry analysis of dissected and dissociated gill tissue of *Tg(NFkB:EGFP)* was performed. Gill tissue from a WT zebrafish was used to gate for GFP+ cells. Additionally, the whole kidney marrow (WKM), that is the haematopoietic organ of the zebrafish equivalent to the mammalian bone marrow, was analysed by flow cytometry. As shown in Appendix 2 a higher number of EGFP+ cells were detected in the gills compared to the WKM of *Tg(NFkB:EGFP)*. These data suggest that the gills, similar to the intestine, exhibit cells that are NFkB activated at steady state; however, whether silica further activates NFkB should be addressed in future experiments.

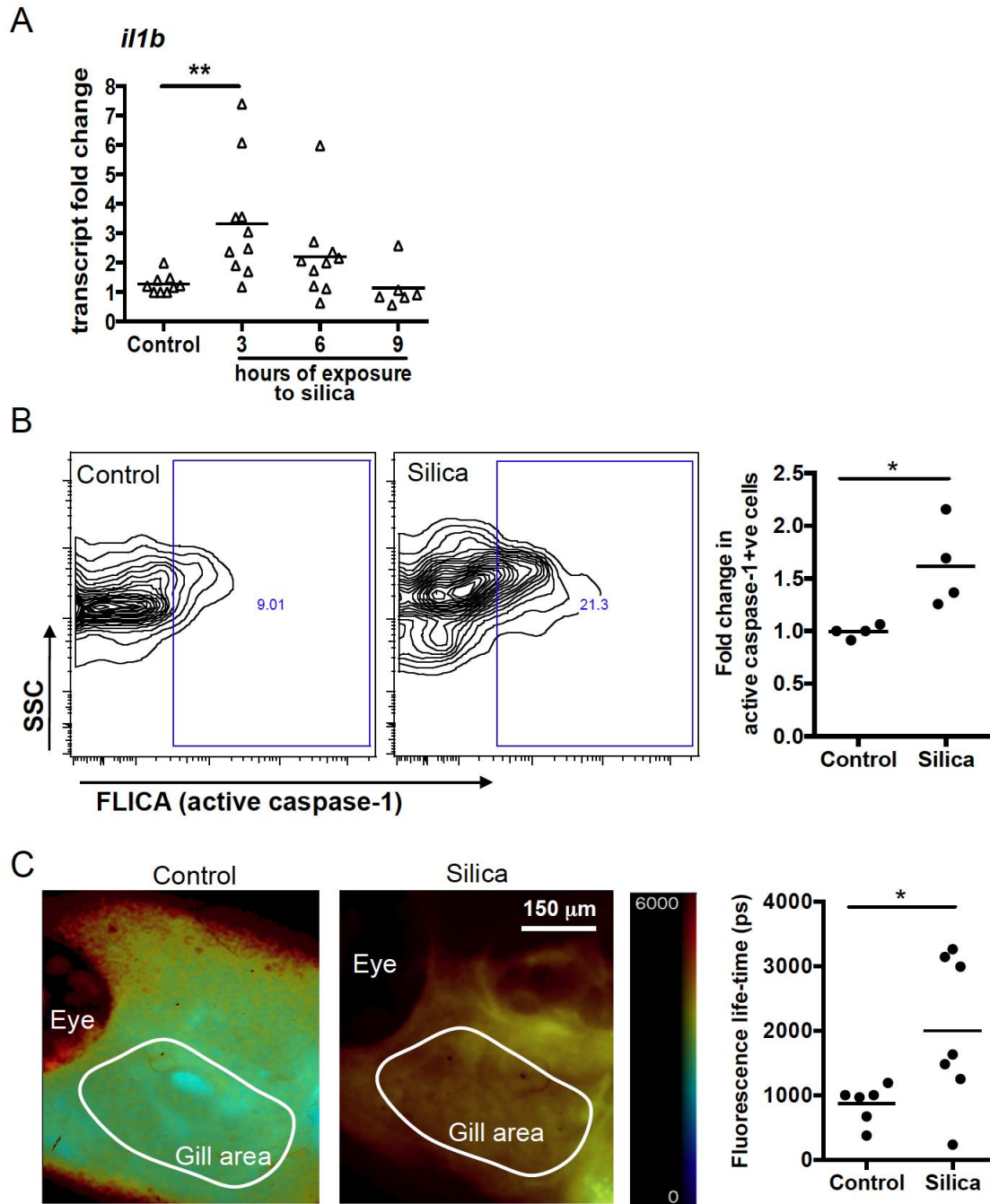


Fig. 4.5 Analysis of inflammatory status following acute silica exposure.

(A) Dissected gill tissues were subjected to qRT-PCR analysis for *il1b* mRNA expression. Dot plots show relative expression values obtained for individual fish ($n \geq 6$) which were normalised to 18S and expressed as fold change relative to one control sample. Three experimental replicates were performed and data were pooled (each experiment following the same trend). The mean is shown. Kruskal Wallis test. (B) Representative flow cytometry analysis of silica-exposed gills following incubation with caspase I-specific FLICA probe. Flow cytometry quantification of active caspase-1 (FLICA+) cells. Each single dot shows the fold change of FLICA+ cells relative to one control sample obtained for one individual ($n=4$). Two experiments were performed and the data were pooled. Mann-Whitney test. (C) After exposure to silica for 6 hours, 19 dpf fish were anaesthetised incubated with an active caspase-1 specific probe and imaged using FLIM. Images obtained were merged with fluorescence intensity images, analysed for fluorescence life-time in the gill area (scale bar shown on the right in pico seconds, ps) and summarised in dot plots. All pictures show left lateral views of the larval zebrafish head, anterior to the top left. The eye and the gill area are indicated. Imaging and data analysis was performed by Natalie Andrews (ICL). Data for individual larva are shown. Results are pooled from two experiments. Mann-Whitney test. * $p < 0.05$, ** $p < 0.01$.

The effect of acute smoke exposure on local immune cell accumulation

Cigarette smoke exposure in the lungs of mammals provokes an acute inflammatory response leading to high levels of pro-inflammatory cytokines such as TNF- α , IL-6 and IL-1 β by activation of the TLR pathway [348]. In order to test whether cigarette smoke infused water has a similar effect in gills, juvenile and adult zebrafish were exposed to smoke and their survival as well as inflammatory response (*i.e.* recruitment of immune cells and cytokine release) investigated. Fish tolerated a concentration of 1×10^{-3} c/mL in system water over 24 hours whereas higher concentrations were toxic leading rapidly to death (Fig. 4.6A). Consequently, all following experiments were performed at a concentration of 1×10^{-3} c/mL of smoke.

In contrast to silica exposure, cigarette smoke leads to a slight decrease in the number of neutrophils (GFP⁺ cells) present in the gills of *Tg(mpx:GFP)* after 6 hours of exposure as assessed by flow cytometry (Fig. 4.6B). A time-course analysis of *mpx* transcripts as well as the leukocyte marker *l-plastin* (*lcp1*) transcripts by qRT-PCR (Fig. 4.6C) confirmed the decrease, which persisted over time, failed to return to baseline level within 24 hours of exposure (Fig. 4.6C) and was significant at 6 hours exposure (Fig. 4.6D). These data suggest that exposure to cigarette smoke at sub-lethal concentrations induces a reduction of neutrophils and, potentially, all leukocytes.

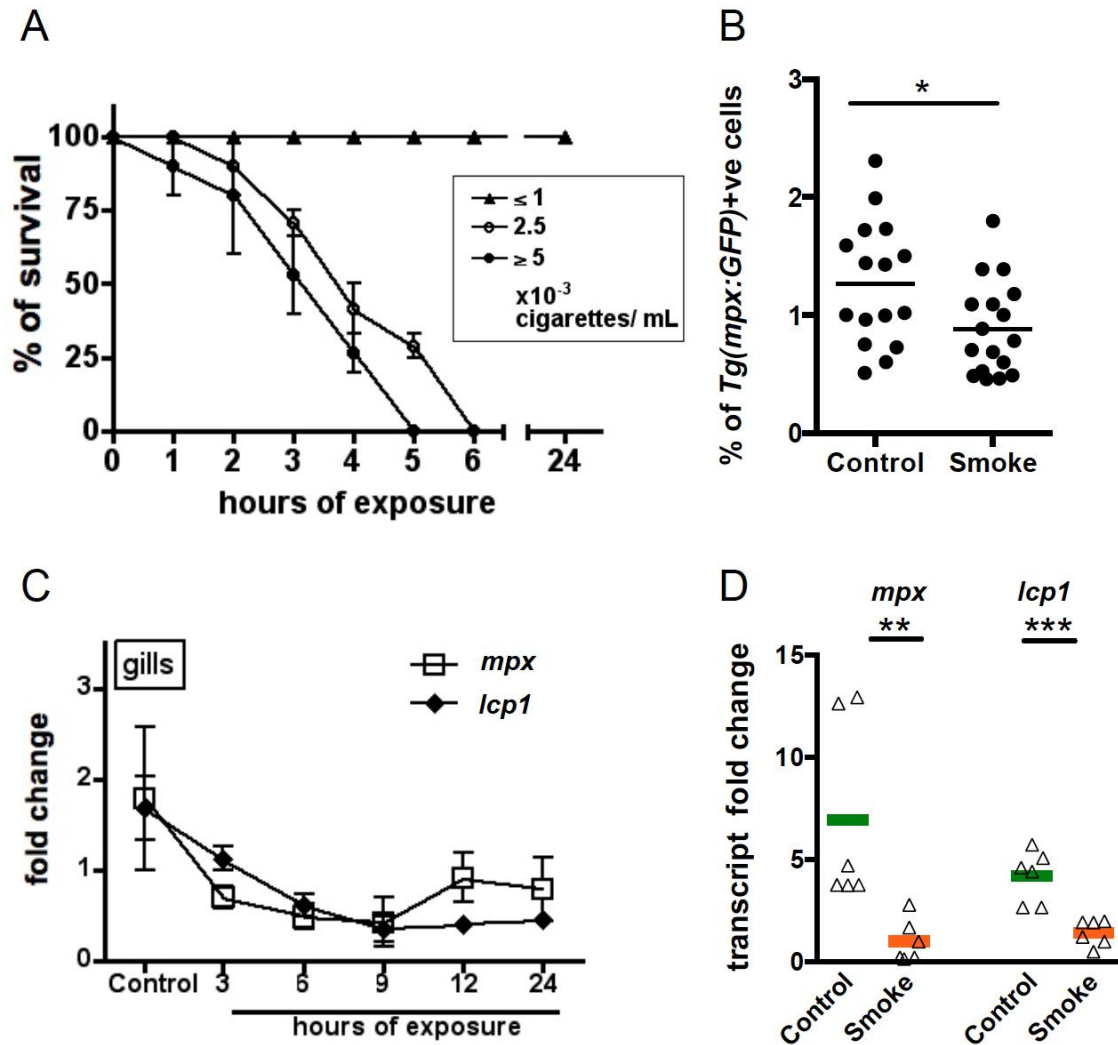


Fig. 4.6 Analysis of immune cells accumulation following acute smoke exposure.

(A) Zebrafish juveniles and adults were exposed to smoke and their survival (%) monitored over 6 or 24 hours. The median \pm SEM is shown for each concentration ($n \geq 5$). (B) Flow cytometry quantification of % of GFP⁺ cells in Tg(*mpx*:GFP) zebrafish gills after 6 hours of smoke exposure. Each single dot represents % of GFP⁺ cells obtained for one individual ($n \geq 16$). Two experimental replicates were performed and data were pooled (each experiment following the same trend). The mean is shown. Two-tailed t-test. (C) Dissected gill tissues were subjected to qRT-PCR analysis at indicated time-points of exposure and analysed for *mpx* and *lcp1* mRNA expression. Mean \pm SEM of relative expression values obtained for individual fish ($n=3$) are shown which were normalised to 18S and expressed as fold change relative to one control sample. (D) qRT-PCR analysis of *mpx* and *lcp1* after 6 hours of smoke exposure. Dot plots show relative expression values obtained for individual fish ($n \geq 6$) which were normalised to 18S and expressed as fold change relative to one smoke-exposed sample. Three experimental replicates were performed and data were pooled (each experiment following the same trend). The mean for each group is shown as coloured bar: control (green) and smoke (orange). Mann Whitney test. * $p < 0.05$, ** $p < 0.01$, *** $p < 0.001$

The effect of acute smoke exposure on cytokine production

Despite the significant decrease in neutrophils as well as *mpx* and *lcp1* transcripts, qRT-PCR analysis from the same samples of the time-course experiment showed an increase in the levels of *tnfa* and *illb* transcripts, peaking at 9 hours of exposure followed by a complete return to baseline expression levels present in control fish by as soon as 24 hours (Fig. 4.7A). Further qRT-PCR analysis at 6 hours of exposure revealed a significant increase in *tnfa* and *illb* transcripts, confirming the observations of the time-course analysis, and also showed an increase in *m17* (*il6*-like) transcripts (Fig. 4.7B). No change in *il8* transcripts was detected (Fig. 4.7B). Together, these data suggest that smoke-exposure may lead to an increase of pro-inflammatory cytokines TNF- α and IL-1 β in zebrafish gills.

To investigate whether or not the spontaneous decrease of *tnfa* and *illb* transcripts after 24 hours is due to a decrease in stimulus potency (*e.g.* by evaporation or degradation) fish were exposed to smoke that was previously left for 24 hours in system water after preparation. In addition, to assess whether smoke-infused water could be frozen in big batches to avoid potential discrepancies between batches of smoke preparations, freshly prepared smoke was frozen for 24 hours before exposure of zebrafish. No difference in *tnfa* transcripts in gills from fish exposed to fresh, 24 hour old or frozen smoke could be detected, however, less *illb* transcripts were found in fish exposed to 24 hour old as well as frozen smoke when compared to freshly prepared smoke (Fig. 4.7C). These results suggest that cigarette smoke extracts responsible for an increase in *tnfa* transcripts are not degraded over time and that the decrease of *tnfa* transcripts after 24 hours of exposure does not correlate with a decrease in stimulus potency. The opposite could be argued in the case of *illb* transcripts, as 24 hour old or frozen smoke is unable to cause the same increase expression as freshly prepared smoke. Altogether, the observations suggest that zebrafish are able to resolve the cigarette smoke induced acute inflammatory response in the gills within 24 hours and that only freshly prepared smoke extracts are able to cause an acute inflammatory response that is comparable amongst different experiments. Hence, freshly prepared cigarette smoke was used for all further experiments.

A short smoke exposure (1 hour) was performed in order to mimic human smoking behaviour and that of smoking models in mouse and compared to a longer 6 hours exposure. Only when used at a concentration of 5×10^{-3} c/mL could the 1-hour exposure reproduce the same increase in *tnfa* transcripts as that obtained following a 6-hour exposure at 1×10^{-3} c/mL (Fig. 4.7D). However, CSW at 5×10^{-3} c/mL resulted in variable

survival of fish (Fig. 4.6A) and was therefore not suitable for further long-term exposure experiments.

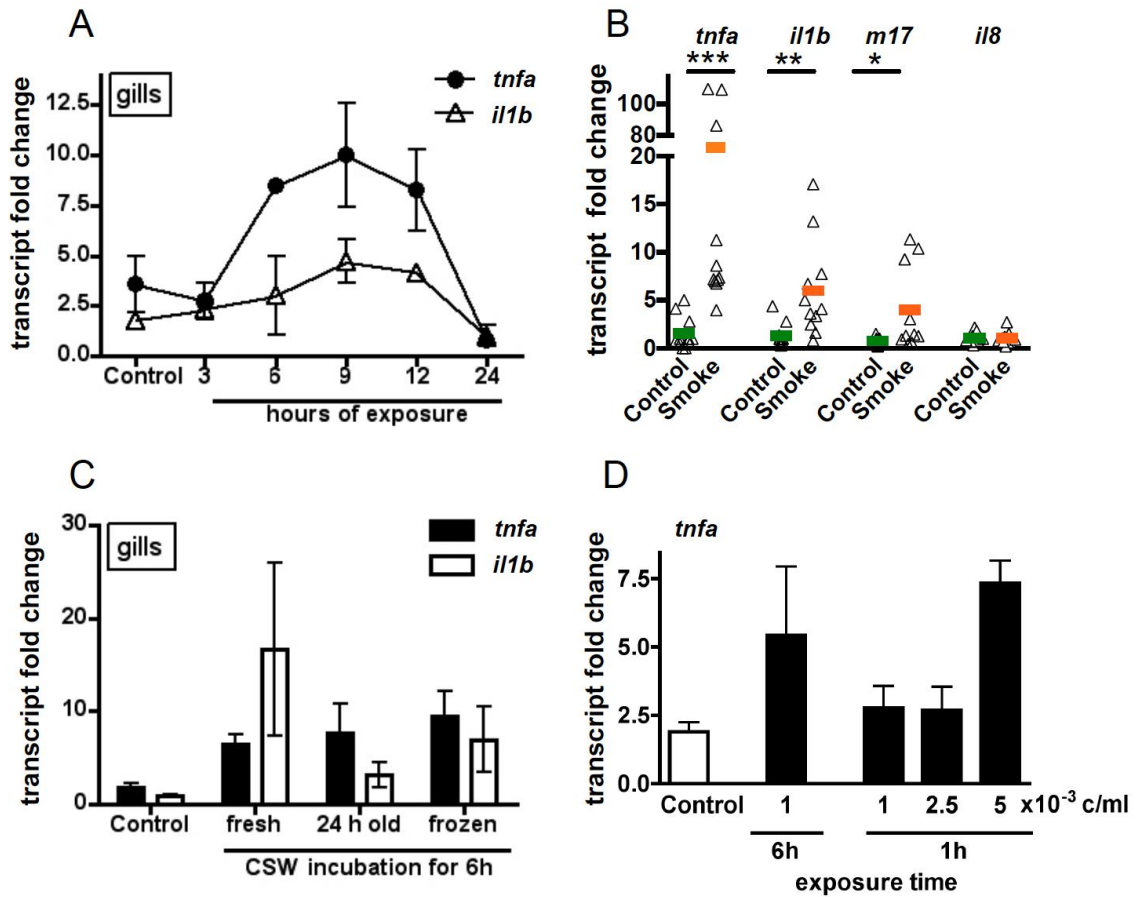


Fig. 4.7 Pro-inflammatory cytokine expression following acute smoke exposure.

In all experiments fish were either exposed to system water containing cigarette smoke extracts at 1×10^{-3} c/mL or to system water only (control) for 6 hours or as otherwise indicated. **(A)** Dissected gill tissues were subjected to qRT-PCR analysis at indicated time-points of exposure and analysed for *tnfa* and *il1b* mRNA expression. Mean \pm SEM of relative expression values obtained for individual fish ($n=3$) are shown which were normalised to 18S and expressed as fold change relative to one control sample. **(B)** qRT-PCR analysis of *tnfa*, *il1b*, *il6*-like (*m17*) and *il8* mRNA after 6 hours of smoke exposure. Dot plots show relative expression values obtained for individual fish ($n \geq 6$) which were normalised to 18S and expressed as fold change relative to one control sample. Three experimental replicates were performed and data were pooled (each experiment following the same trend). The mean for each group is shown as coloured bar: control (green) and smoke (orange). Mann Whitney test. **(C&D)** qRT-PCR analysis of *il1b* (C) and *tnfa* transcripts (C&D). Mean \pm SEM of relative expression values obtained for individual fish ($n \geq 6$) are shown which were normalised to 18S and expressed as fold change relative to one control sample for each gene analysed. * $p < 0.05$, ** $p < 0.01$, *** $p < 0.001$.

The effect of combined silica and smoke on local immune cell accumulation and cytokine production

The data so far indicate that acute exposure to silica or smoke for 6 hours resulted in different types of inflammatory responses in the gills of zebrafish. To potentially maximise the chances of inducing scarring following repeated long-term exposure to these irritants, a combined exposure of silica+smoke was investigated for its ability to act synergistically or additively on the induction of inflammatory responses in zebrafish gills.

Flow cytometry analysis of GFP+ neutrophils in gills of *Tg(mpx:GFP)* zebrafish following 6 hours exposure to silica, smoke or silica + smoke (Fig. 4.8A) showed a decrease following combined exposure at the same magnitude compared to that induced by smoke only (Fig. 4.8A). Further, the previously demonstrated silica-induced increase (Fig. 4.4C) and the smoke-induced decrease of neutrophils (Fig. 4.6) were confirmed (Fig. 4.8A). The trend towards a decrease in neutrophils following combined exposure was reflected in the levels of *mpx* transcripts (Fig. 4.8B), which again confirmed previous results obtained for single exposure to either silica (Fig. 4.4D) or smoke (Fig. 4.6C&D). Analysis of *lcp1* transcripts potentially highlighting the presence of leukocytes followed the same pattern: increase following silica-exposure and decrease following smoke and silica + smoke exposure (Fig. 4.8C). Further, combined treatment of silica + smoke increased transcript levels of pro-inflammatory cytokines *tnfa* and *illb*, which were significantly higher when fish were exposed to silica combined with smoke compared to fish exposed to smoke only (Fig. 4.8D). Altogether, these data confirm the opposing effects of silica and smoke exposure on the accumulation of leukocytes and indicate that when combining treatments, the effect of smoke is predominant.

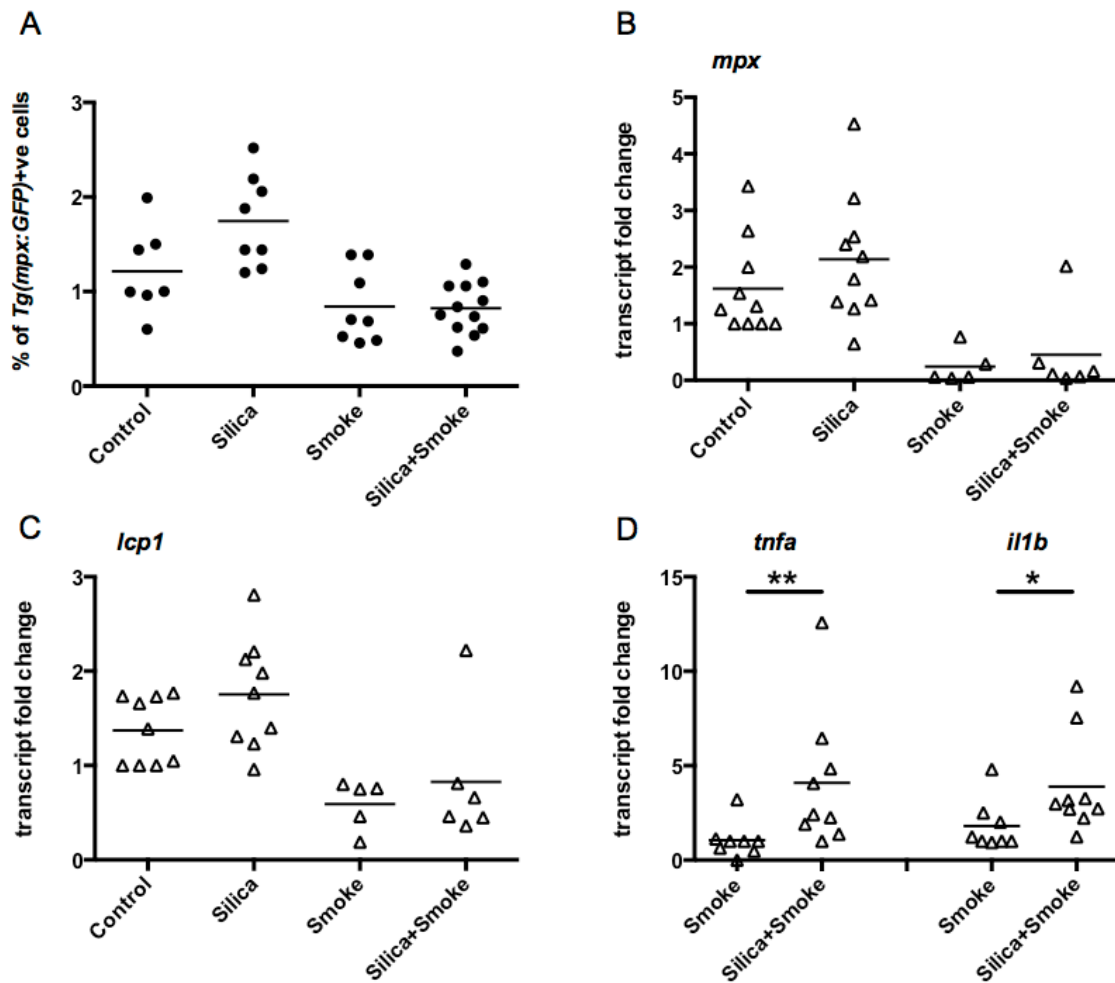


Fig. 4.8 Analysis of inflammatory status following combined treatment of silica + smoke.

(A) Flow cytometry quantification of % of GFP⁺ cells in *Tg(mpx:GFP)* zebrafish gills after 6 hours of exposure to silica, smoke or silica+smoke. Each single dot represents % of GFP⁺ cells obtained for one individual ($n \geq 7$). Two experimental replicates were performed and data were pooled (each experiment following the same trend). The mean is shown. (B-D) Dissected gill tissues were subjected to qRT-PCR analysis for analysis of (B) *mpx*, (C) *lcp1*, (D) *tnfa* and *il1b* mRNA expression following 6 hours of exposure to silica, smoke or silica+smoke. At least two experimental replicates were performed and data were pooled (each experiment following the same trend). Data are relative expression values obtained for individual fish (B&C, $n \geq 5$ and D, $n \geq 8$) which were normalised to 18S and expressed as fold change relative to (B&C) one control sample or one (D) smoke sample, respectively. (A-C) Kruskal Wallis test. Non-significant. (D) Two-tailed t-test. * $p < 0.05$, ** $p < 0.01$.

4.3.2 Long-term exposure to silica and/ or smoke

Inflammatory status of gills following long-term exposure to smoke or silica

Since acute exposure of zebrafish gills to silica and cigarette smoke resulted in similar inflammatory responses to those seen in mammalian lungs exposed to similar insults [63-65, 334, 348], it was reasoned that long-term exposure to these irritants, associated with lung fibrosis in humans, may give similar fibrotic responses in zebrafish gills. In order to study the effects of long-term silica and smoke treatment on the gill tissue, zebrafish were repeatedly exposed for 6 hours a day, 3 days a week, for 6 weeks (Fig. 4.9A). After 6 weeks, half the group of exposed fish was harvested and the percentage of immune cells in the gills quantified. In addition, the gill tissue of individual fish was histologically examined and the levels of pro-fibrotic marker transcripts analysed using qRT-PCR. The other half of the group of treated fish was left to recover, *i.e.* in system water only, for 4 weeks. All experiments were performed in *Tg(mpx:GFP)* zebrafish, so that the percentage of neutrophils (GFP^{high}) as well as macrophages (GFP^{low}) could be quantified by flow cytometry (Fig. 4.9B). No change in the percentage of either cell type was observed after 6 weeks of exposure (Fig. 4.9C&D). Further, qRT-PCR analysis of pro-inflammatory cytokines showed that there was no significant change in *tnfa* and *illb* transcript levels following 6 weeks of exposure to silica, smoke or silica + smoke, however a slight decreasing trend was observed in all treatment groups when compared to the untreated control group (Fig. 4.9E&F). Together, these data suggest that long-term exposure to smoke or silica, at least in the conditions assessed in this study, does not induce chronic inflammation.

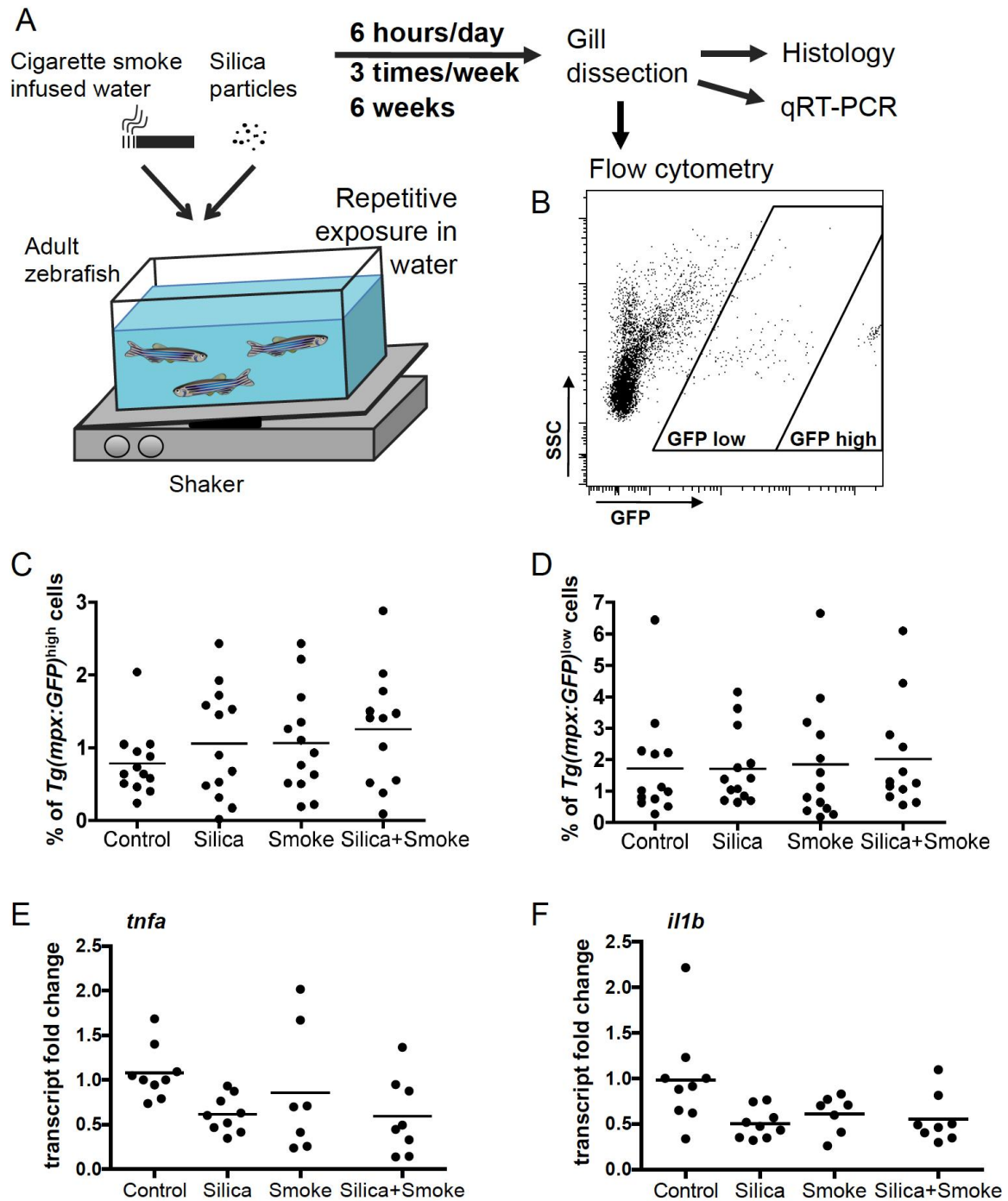


Fig. 4.9 Analysis of immune cell accumulation following long-term exposure to silica and/ or smoke.

(A) Schematic representation of experimental procedure. Adult zebrafish were exposed to 0.75×10^{-3} c/mL of cigarette smoke-infused system water only, 0.5 mg/L of silica only or both for six hours a day, three days a week, for six weeks. Following treatment, gill tissue was dissected and analysed by flow cytometry, qRT-PCR and histology. (B) Flow cytometry analysis of dissected and enzymatically digested gill tissue of *Tg(mpx:GFP)* transgenic zebrafish. Dot plot represents usual gating for GFP^{low} (macrophages) and GFP^{high} cells (neutrophils) after debris and doublet exclusion. (C&D) Flow cytometry quantification of % of (C) GFP^{high} and (D) GFP^{low} in *Tg(mpx:GFP)* zebrafish gills after silica, cigarette and combined silica+smoke exposure. Each single dot represents the % of $GFP^{\text{high/low}}$ cells obtained for one individual ($n \geq 12$). Three experimental replicates were performed and data were pooled. (E&F) qRT-PCR analysis of (E) *tnfa* and (F) *il1b* transcript levels following 6 hours of exposure to silica, smoke or silica + smoke. Data are relative expression values obtained for individual fish ($n \geq 7$) which were normalised to 18S and expressed as fold change relative to one control sample. The mean is shown. There was no statistical differences between the treatment groups. Kruskal Wallis test.

Histological analysis of gill tissue following long-term exposure to smoke and/ or silica

Next, histological analysis was performed which revealed dramatic but different morphological changes in gills after exposure to silica and/ or smoke for 6 weeks. Silica-exposure induced epithelial changes (Fig. 4.10A) when compared to control (Fig. 4.10B). These epithelial changes appeared to be epithelial cell hyperplasia and/or epithelial cell damage, however, without further high-resolution analysis using, for example, electron microscopy, no further characterisation of silica-induced tissue damage can be made. In contrast to the slight changes observed following silica exposure, more dramatic changes were observed when fish were exposed to cigarette smoke \pm silica, where gills displayed lamellar fusion (Fig. 4.10C&D) together with the presence of mucus cells as confirmed by Alcian blue/PAS staining for the smoke-treated gills (Fig. 4.10E). Fish exposed to silica + smoke consistently appeared to show less lamellar fusion and a lower number of mucus cells, although this was not statistically significant (Fig. 4.10F). These data indicate that chronic treatment with silica, smoke or both induces gill tissue remodelling.

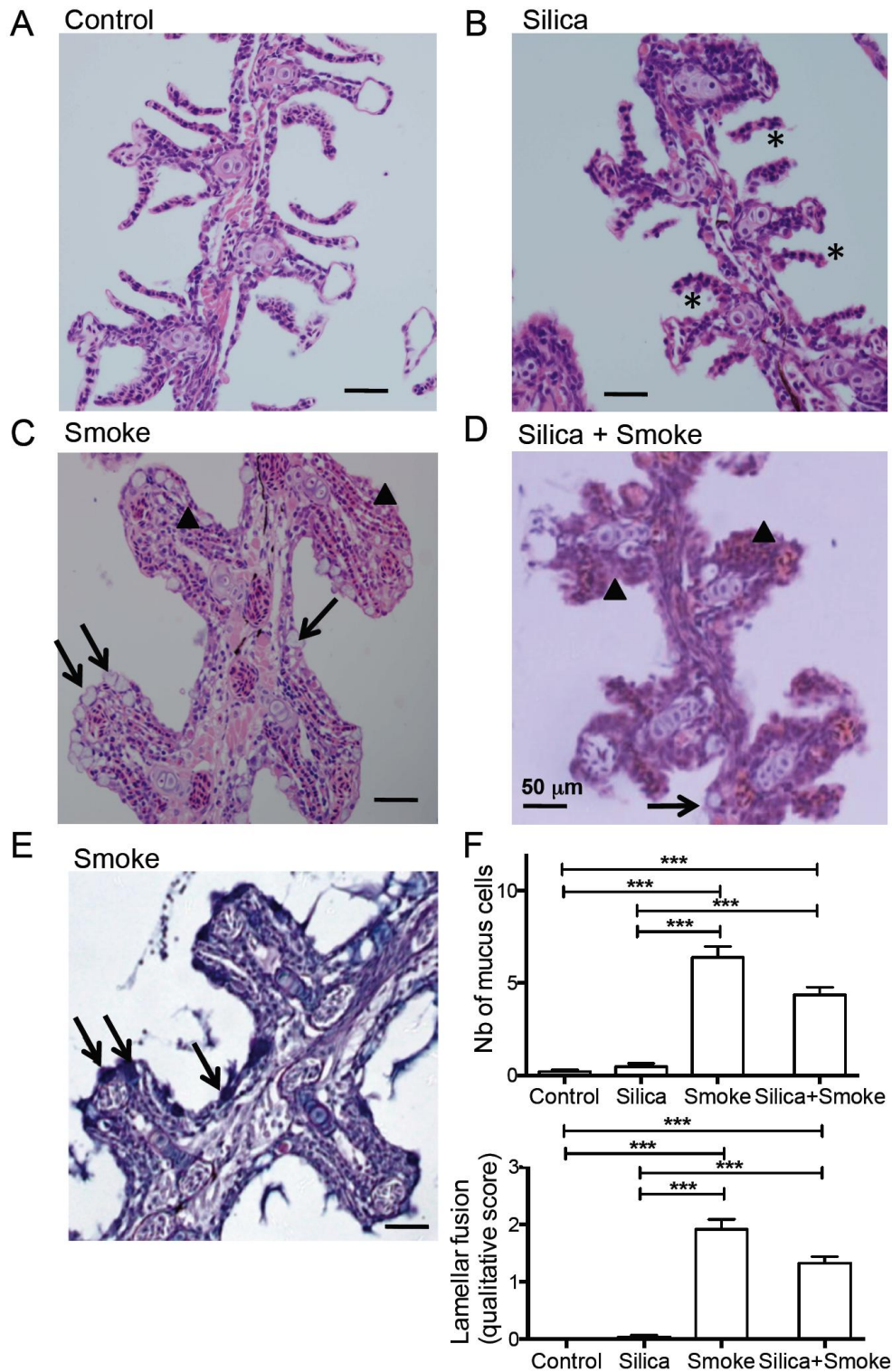


Fig. 4.10 Histological analysis of gill tissue after long-term exposure to silica and/ or cigarette smoke. (A-E) Coronal sections of FFPE zebrafish heads stained with H&E (A-D) and Alcian blue/PAS (E) showing the gills. Fish were exposed to 0.5 mg/L silica or 0.75×10^{-3} c/mL smoke extracts for six hours a day, three days a week, for six weeks. Asterisks indicate epithelial changes in silica-exposed fish (B), triangles indicate lamellar fusion (C&D) and arrows indicate mucus cells (C&D) observed in smoke and silica + smoke exposed fish. Representative images of three experiments are shown. (F) Quantification of the number of mucus cells (top panel) and the degree of lamellar fusion (bottom panel) of the gill tissue within the area of a filament. Qualitative score of lamellar fusion ranging from 0 to 3: severe lamellar fusion affecting all lamella as indicated in (C) was scored with 3 and the absence of lamellar fusion was scored with 0. Images were scored blindly. Bar charts are mean + SEM of $n \geq 18$ gill. Data is pooled from three experiments. Kruskal Wallis test. *** $p < 0.001$.

The effect of long-term smoke or silica exposure on collagen synthesis and deposition

The hallmark of scarring and fibrosis is the deposition of ECM proteins, with collagen type 1 being the main collagen type found in mammals and zebrafish [112, 320, 339, 349]. The level of *coll1a1* transcripts was analysed by qRT-PCR in zebrafish gills exposed to silica or smoke or both for 6 weeks. As demonstrated in Fig. 4.11A, silica exposure for 6 weeks leads to an increase in *coll1a1* transcripts which was small whilst non-statistically significant consistent between more than three experiments. No change in *coll1a1* transcripts was found in gills of fish exposed to smoke only or following the combined silica + smoke treatment (Fig. 4.11A), suggesting that long-term smoke and silica treatments provoke opposing responses in fish gills. This is consistent with observations made before with regards to the presence of neutrophils following combined treatment (Fig. 4.6B) and the fact that fewer mucus cells and less lamellar fusion was observed upon combined treatment when compared to smoke only treated fish (Fig. 4.10F). In order to confirm the increase in *coll1a1* transcripts in silica-exposed fish at the protein level, histological analysis was performed to identify the presence of collagen protein by the collagen-specific PSR stain under polarised light. As shown in Fig. 4.11B&C, collagenous structures were readily detectable by the PSR, however, no differences between fish exposed to silica compared with control were observed. No change in PSR stain was detected in smoke and smoke + silica exposed fish gills when compared to control (Fig. 4.11D&E). In addition to PSR, trichrome staining was performed, but no differences between silica- or smoke-exposed fish could be observed (Appendix 3). Analysis of fish that were left to recover in system water for 4 weeks following exposure to silica, smoke and silica + smoke, showed completely restored gill architecture with no epithelial damage, nor lamellar fusion remaining (Appendix 4).

Altogether the results indicate that long-term exposure to silica slightly increases the expression of pro-fibrotic marker gene collagen type 1 at the transcript level, but collagen deposition at the protein level is undetectable. These data suggest the increase in collagen transcript levels does not lead to an increase at the protein level detectable by the methods used. Together, these results indicate that zebrafish have mechanisms in place to avoid collagen deposition and fibrosis.

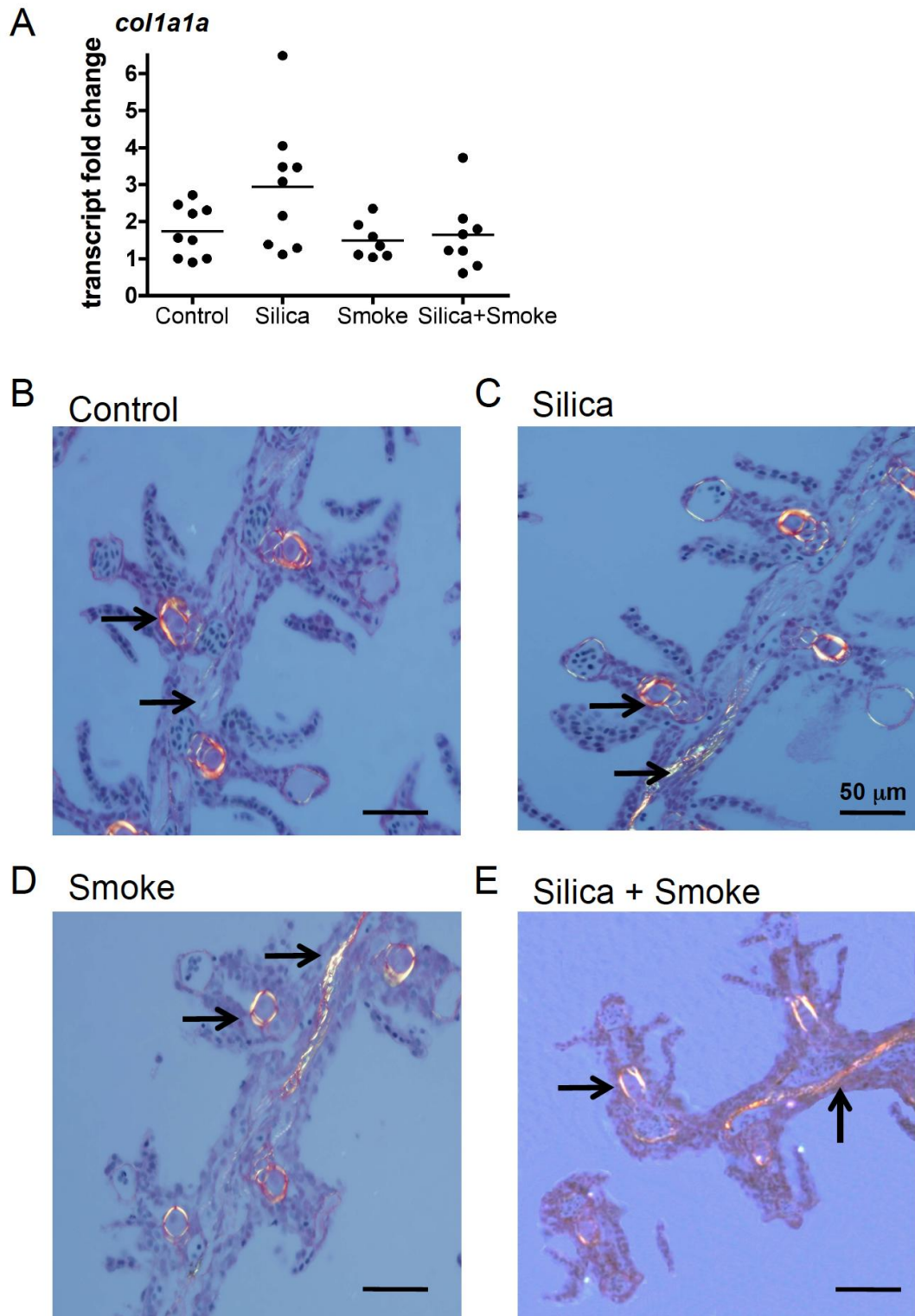


Fig. 4.11 Analysis of collagen deposition following long-term exposure to silica.

Fish were exposed to 0.5 mg/L silica and/ or 0.75×10^{-3} c/mL smoke extracts for six hours a day, three days a week, for six weeks. **(A)** Dissected gill tissues were subjected to qRT-PCR analysis and expression of *colla1a* analysed. Dot plots shows relative expression values obtained for individual fish ($n \geq 6$) which were normalised to 18S and expressed as fold change relative to one control sample. Two experimental replicates were performed and data were pooled (each experiment following the same trend). The mean is shown. One-way Anova. Non-significant. **(B-E)** Coronal sections of FFPE zebrafish heads stained with PSR showing the gills. Images show representative gill tissues of fish left untreated (control, B) or exposed to silica (C), smoke (D) or silica + smoke (E). Arrows indicate collagenous structures. Representative images of three experiments are shown.

4.3.3 Cryoinjury of zebrafish gills

The effect of local cryoinjury on acute inflammation

Despite local acute inflammatory responses following short-term exposure to irritants, long-term treatment did not induce collagen deposition, thus, an alternative mode of local gill tissue injury that could induce scarring was performed. Necrotic lesions in adult zebrafish, induced either by laser-induced wounding of the zebrafish skin [339] or by cryoinjury inflicted damage to the heart of zebrafish [337, 338] have been reported to result in transient collagen-rich fibrotic scars. We hypothesised that local cryoinjury-induced necrotic wounds might induce scarring in the gills. In order to investigate this hypothesis, I designed a cryoprobe, which I applied under anesthesia unilaterally directly onto the gill tissue (Fig. 4.12), the idea being that the other uninjured gill side would be sufficient to perform oxygen uptake required for the fish survival and well-being. Indeed, this procedure did not lead to any mortality when performed on healthy adults and zebrafish showed no abnormal breathing behaviour following cryoinjury, *e.g.* gasping for air at the water surface. Zebrafish were harvested at various time-points post-injury in order to monitor the induced damage (by histological analysis), the inflammatory response (using flow cytometry and qRT-PCR) as well as the regenerative capacity of the gill tissue.

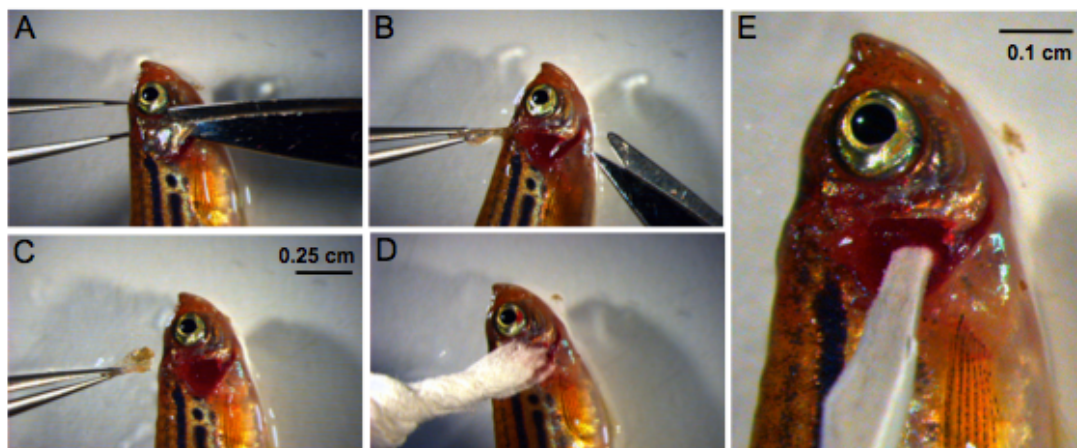


Fig. 4.12 Detailed description of gill cryoinjury in an adult zebrafish.

All pictures show right lateral views of the upper half of the adult zebrafish body, anterior to the top. An anaesthetised adult zebrafish is placed on its left lateral side in a petri dish under a dissection microscope. **(A)** Generation of incision using scissors at bottom of operculum. **(B-C)** Gill operculum is removed using forceps. **(D)** The gill tissue is dried with a tissue wipe. **(E)** Cryoinjury of the gill tissue. The cryoprobe is placed in liquid nitrogen for a few seconds and subsequently applied for 10 seconds on the gill tissue before the fish is then returned into the water.

At day 1 post cryoinjury, the number of GFP⁺ neutrophils and dsRed⁺ myeloid cells present in the gill tissue was significantly increased as visualised by fluorescence microscopy in *Tg(mpx:GFP)xTra^{-/-}/Nac^{-/-}* (Fig. 4.13A&E) and as quantified by flow cytometry in *Tg(lyz:dsRed)* (Fig. 4.13D), respectively. With time after injury, the number of myeloid cells in the gill tissue decreased and returned back to baseline level by around 14 dpi, when compared to the myeloid cell level in the uninjured side (Fig. 4.13D&E). At the same time, the area of damaged tissue, identifiable as white tissue without visible blood vessels, decreased over time (Fig. 4.13E).

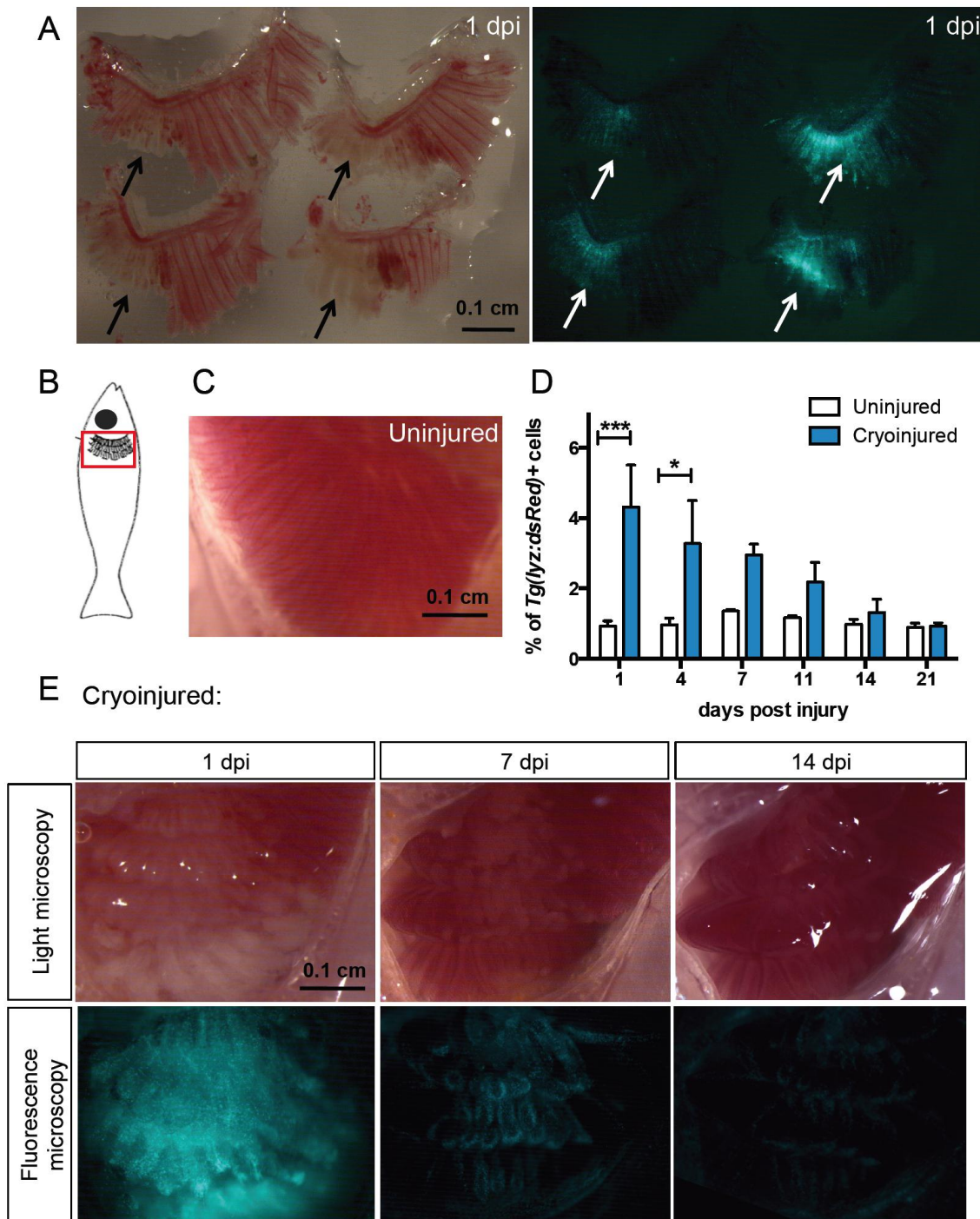


Fig. 4.13 Inflammatory response after gill cryoinjury in an adult zebrafish.

(A) Pictures show four dissected gill arches of an adult zebrafish *Tg(mpx:GFP)xTra^{-/-}/Nac^{-/-}* after cryoinjury. Arrows indicate the damaged area (left panel) and the infiltration of neutrophils (GFP+ cells, right panel) at 1 dpi. (B) Schematic overview of adult zebrafish with red rectangle depicting the gill area to demonstrate the orientation of the following images during live imaging of gill area after cryoinjury. (C) Gill tissue of the uninjured side. (D) Flow cytometry quantification of % of dsRed+ cells in *Tg(lyz:dsRed)* in zebrafish gill at various time-points after cryoinjury. Bar chart shows the % of dsRed+ cells for each individual fish (n≥3). Result are pooled from two experiments and the mean + SEM is shown. Two-way Anova. ***p<0.001, *p<0.05 (E) Cryoinjured area of the same fish at 1 dpi (left), 7 dpi (middle) and 14 dpi (right). Corresponding fluorescent images showing neutrophils in cryoinjured area at 1 dpi (left), 7 dpi (middle) and 14 dpi (right). All pictures in (C, E) show right lateral views of the gill area, anterior to the top.

The effect of local cryoinjury on tissue scarring

To monitor the wound healing process and assess potential scarring, histological analysis was performed at successive intervals after the injury. At 4 dpi the cryoinjured gill tissue was found to be severely damaged showing lamellar fusion and a high number of mucus cells (Fig. 4.14A&B). By 7 and 14 dpi, the mucus cells had disappeared but lamellar fusion persisted (Fig. 4.14B). At 21 dpi single lamellae could be detected amongst areas of ongoing wound healing. 7, 14 and 21 dpi collagen-rich structures were detected using PSR staining. In order to assess the dynamics of collagen synthesis, qRT-PCR analysis of *coll1a1a* mRNA was performed at successive intervals after the injury. *Coll1a1a* (Fig. 4.14C) transcripts were increased at 7 dpi, returning to base-line level by 21 dpi. By 6 wpi (=42 dpi) neither lamellar fusion, nor PSR staining different from the uninjured side was detected (Fig. 4.14D). These data suggest that the increase in *coll1a1a* transcript levels reflect the temporal dynamics of collagen production during the wound-healing processes following cryoinjury. Together, these results show that cryoinjury performed on the gill tissue of adult zebrafish induces a wound that heals completely over time in presence of a transient collagen-rich scar which resolves and does not lead to permanent fibrosis.

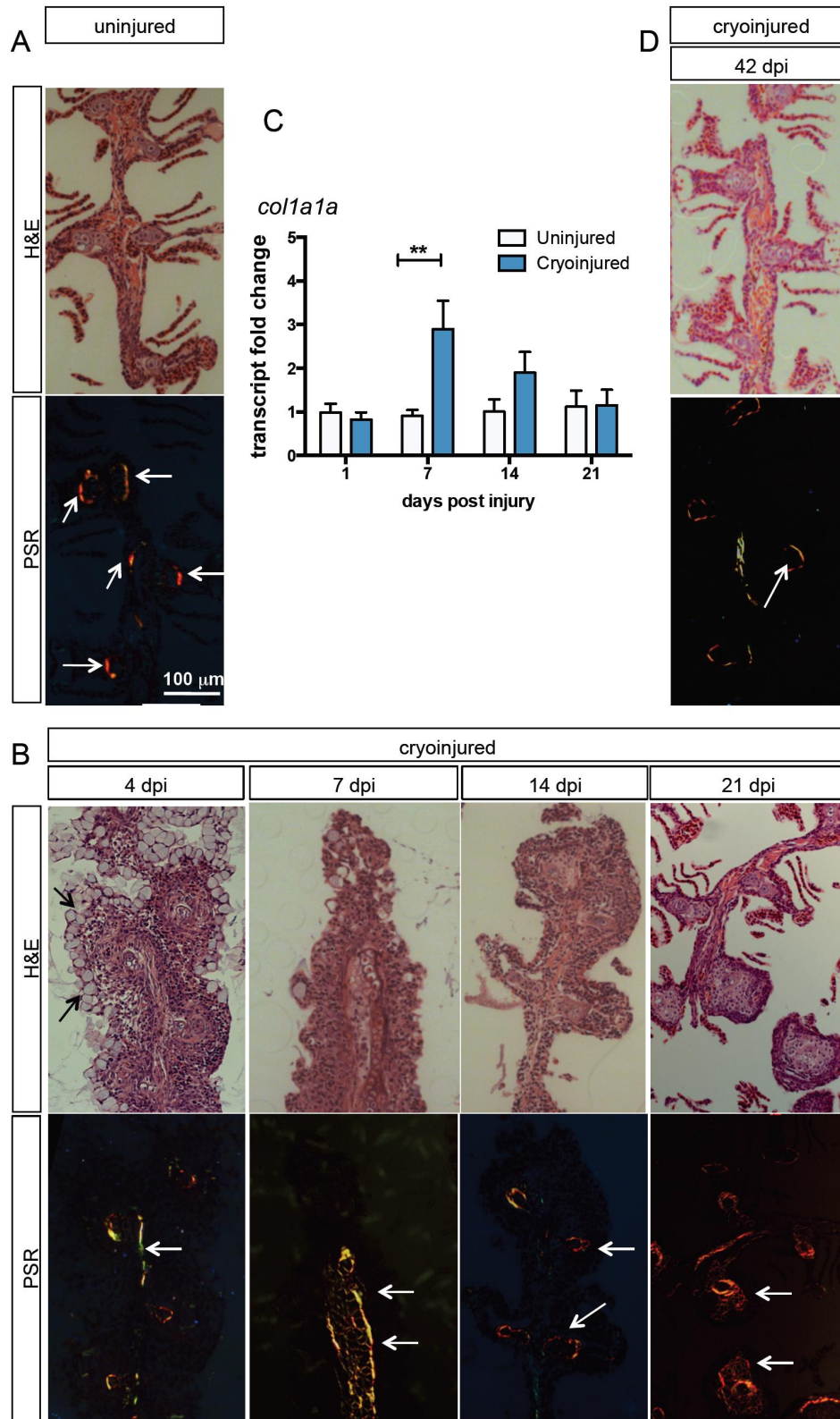


Fig. 4.14 Histological analysis of zebrafish gill tissue after cryoinjury.

(A&B&D) Coronal sections of FFPE zebrafish heads stained with H&E (top panels) and PSR (bottom panels) showing the gills at indicated time-points post cryoinjury. Black arrows indicate mucus cells. White arrows indicate collagenous structures. Representative of three experiments. (C) qRT-PCR analysis of *coll1a1a* transcript. Bar graph shows relative expression values of *coll1a1a* mRNA obtained for individual fish ($n \geq 6$) which were normalised to 18S and expressed as fold change of the cryoinjured side relative to the uninjured side for each individual fish. Three experimental replicates were performed and data were pooled (each experiment following the same trend). The mean is shown + SEM. One-way Anova. ** $p < 0.01$.

Analysis of the inflammatory and wound healing response after cryoinjury followed by continuous exposure to silica

Having established a model of wound healing in zebrafish gills induced by cryoinjury and demonstrated that long-term treatment with silica results in epithelial damage/changes and a slight increase in expression of pro-fibrotic markers at the transcriptional level, it was reasoned that silica treatment after injury may potentially de-regulate the process of wound healing and induce a fibrotic response. In order to investigate the effect of silica exposure on wound healing, zebrafish were continuously exposed to silica after a single injury performed with a cryoprobe (Fig. 4.15A). As demonstrated before (Fig. 4.13E), by 2 wpi, the cryoinjured gill tissue is almost visually indistinguishable from the uninjured area (Fig. 4.15B). In contrast, the cryodamaged area in silica-exposed fish persisted at 2 wpi (Fig. 4.15B). To allow monitoring of wound-healing processes over time in the same fish, I devised a classification system simply scoring the presence or absence of an injured area readily visible by short inspection of fish gills using a dissection microscope. About 40% of the fish at 2 wpi and about 25% of the fish at 4 wpi still exhibited visible tissue damage following cryoinjury (Fig. 4.15C). Silica treatment significantly delayed the wound-healing process, as the damage following cryoinjury was still visible in about 75% of the fish at 2 wpi and about 60% of the fish at 4 wpi still (Fig. 4.15C). However, by 5-6 wpi there was no statistically significant difference in the proportion of fish with damaged gill tissue between treatment groups (Fig. 4.15C) and by 10-20 wpi all fish had healed completely. This was confirmed by histological analysis, where no tissue damage (*i.e.* lamellar fusion) or excess collagen (*i.e.* PSR stain) were detected in fish gills analysed at 10 wpi and 20 wpi.

Concurrent with the persistent visible tissue-damage following silica-treatment, the number of neutrophils (GFP+) in the wounded area of silica-exposed *Tg(mpx:GFP)* fish visible by fluorescence microscopy (Fig. 4.15B) remained high at 2 wpi when compared to cryoinjured only fish. Subsequent analysis by flow cytometry at 2 wpi confirmed these findings and revealed that the number of neutrophils (GFP^{high} cells) was comparable in between cryoinjured and uninjured gill tissue but increased in the cryoinjured + silica treated fish (Fig. 4.15D, left panel). A similar increase was observed in the silica-treated gill tissue. However, by around 3 wpi the number of neutrophils in gills of the cryoinjured + silica treated fish returned to baseline levels (Fig. 4.15D). The same persistent accumulation of cells at 2 wpi was observed for macrophages (GFP^{low} cells) in cryoinjury

+ silica treated gills when compared to cryoinjury only, and those again returned to baseline-levels by 3 wpi (Fig. 4.15D, right panel). These data suggest that silica-treatment following cryoinjury of gill tissue might delay the resolution of inflammation.

Together, these data indicate that silica treatment following cryoinjury delays wound healing processes, however, zebrafish are able to overcome the challenge of an additional insult of silica and are able to heal wounded gills without any long-term deposition of collagen or fibrosis.

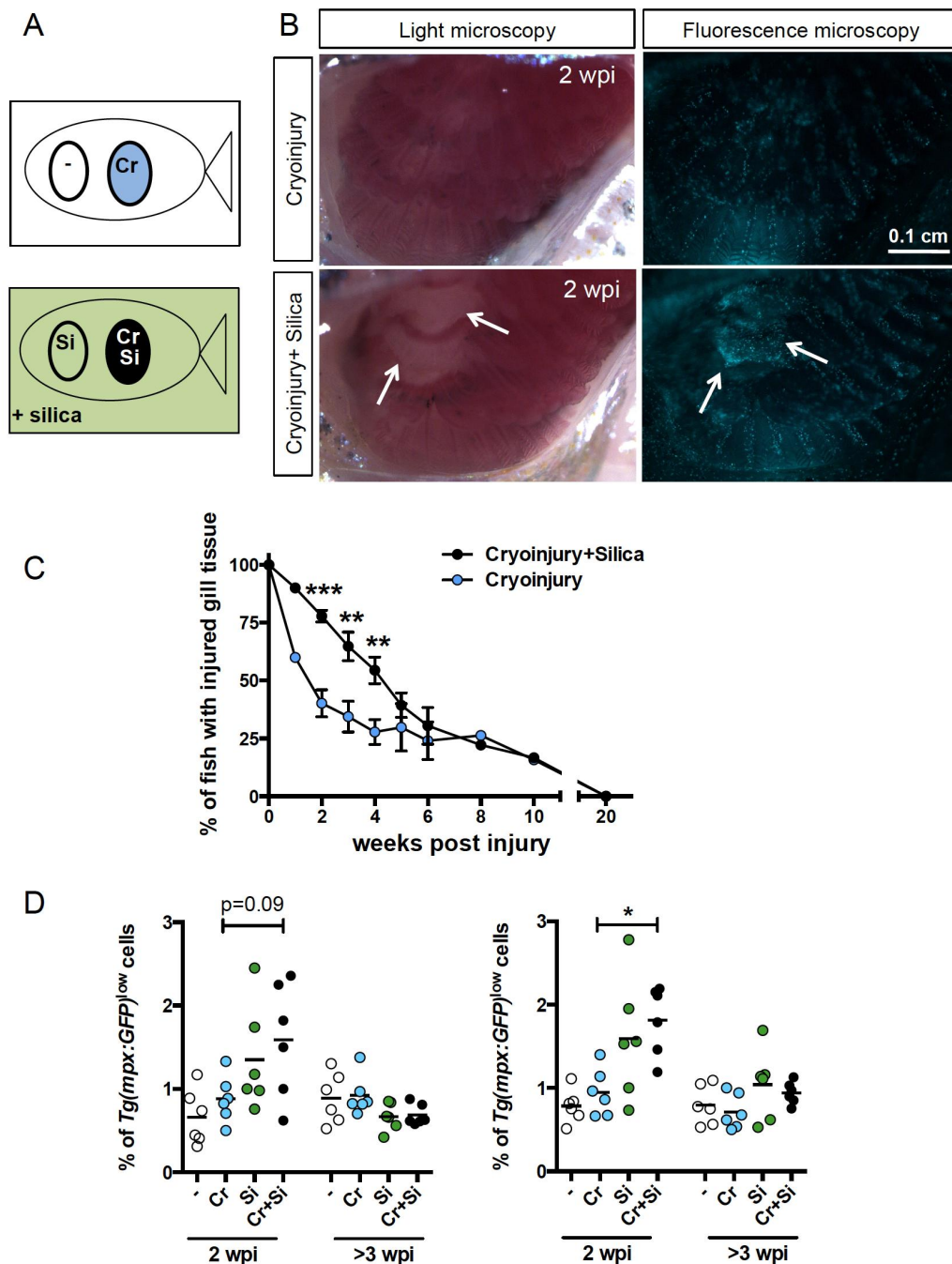


Fig. 4.15 Inflammatory and wound-healing response after cryoinjury followed by continuous exposure to silica.

(A) Schematic illustrating the four different treatment groups and the corresponding colour code: uninjured and untreated gill side = control (white), cryoinjured and untreated gill side = cryoinjury (blue), uninjured and silica treated gill side = silica (green), cryoinjured and silica treated gill side = cryoinjury + silica (black). (B) Bright-field (left panels) and fluorescent images (right panels) of gill tissue of cryoinjured side (top panels) and cryoinjured+silica-treated side (bottom panels) at 2 wpi of *Tg(mpx:GFP)*. All pictures show right lateral views of the gill area, anterior to the top. Arrows indicate persistent injured area and accumulation of GFP+ neutrophils. (C) Scoring of % of fish with visible injured gill tissue identifiable using live imaging of the gills at indicated time-points following cryoinjury ± silica. Mean±SEM. Results shown are pooled from more than three experiments (n≥6). Two-way Anova. (D) Flow cytometry quantification of % of neutrophils (GFP^{high}, left graph) and macrophages (GFP^{low}, right graph) in *Tg(mpx:GFP)* at 2 wpi and > 3 wpi (=pooled data from 22 dpi and 27 dpi) after cryoinjury ± silica. Dots show the % of cells for each individual fish (n=6). Results are pooled from two experiments, each showing the same trend. Kruskal Wallis test. *p<0.05, **p<0.01.

4.3.4 Transcriptome profiling using RNA-seq analysis

RNA-seq analysis at 2 weeks post injury

Despite a transient collagen-rich scar, neither cryoinjury alone nor cryoinjury followed by continuous exposure to silica resulted in persistent fibrosis of the mucosal gill tissue in zebrafish. Having identified a delay in the inflammatory response as possible cause of a delay in wound healing, this project set out to perform transcriptome profiling to explore whether the zebrafish gill models of mucosal injury developed above offer the possibility of studying mechanisms of wound-healing versus fibrosis and facilitating a comparative analysis with mammals in a system of fibrosis. RNA-seq using the Illumina sequencing by synthesis technique was readily available at Boehringer Ingelheim.

Since there was no experience in the lab with transcriptome profiling of any zebrafish tissue, a pilot experiment at a single time-point following cryoinjury was performed. Since the most significant difference in phenotype between cryoinjury only and cryoinjury + silica was found at 2 wpi (Fig. 4.15C), this time-point was chosen for RNA-seq analysis. To minimise variability between samples within one treatment, a sample number of n=10 per treatment group was chosen. Thus, 20 fish were cryoinjured following which 10 were continuously treated with silica and the other 10 left untreated (Fig. 4.16A). After 2 wpi, prior to dissection, the gill tissues were scored for the presence and absence of visible gill tissue damage (Fig. 4.16B) according to the previously used scoring system above (Fig. 4.15C). 80% of the cryoinjury + silica treated fish showed visible gill tissue damage at 2 wpi in comparison to only about 35% of cryoinjury untreated fish (Fig. 4.16B) confirming previous results (Fig. 4.15C). To quantify gill damage more accurately, a detailed scoring method was carried out post mortem during tissue dissection. This qualitative scoring system confirmed the results of the basic scoring system showing a significant higher degree of damage in cryoinjury + silica treated fish when compared to cryoinjury only (Fig. 4.16C). Of note, tissue of the uninjured untreated and the uninjured silica treated side were also harvested but not scored as no injury was performed and no tissue damage was detectable using simple stereomicroscopy.

Prior to shipping of samples to Boehringer Ingelheim for further processing, the extracted RNA of all 40 samples was subjected to RNA quality control using Agilent Bioanalyser. Fig. 4.16D shows a representative electropherogram of RNA samples analysed. The Agilent Bioanalyser performs traditional gel electrophoresis on a chip format and detects the two distinct 18S and 28S ribosomal RNA fragments in eukaryotic samples while the

incorporated software calculates an RNA integrity number (RIN) to allow estimation of RNA quality/purity/integrity. The RIN takes possible degradation products into account (detectable between the marker and the 18S rRNA peak) and is given in a score ranging from 1 to 10, with 10 being the most intact. All samples analysed exhibited good RIN scores (ranging from 8-10) and were therefore shipped to Boehringer for RNA-seq processing (Fig. 4.16A).

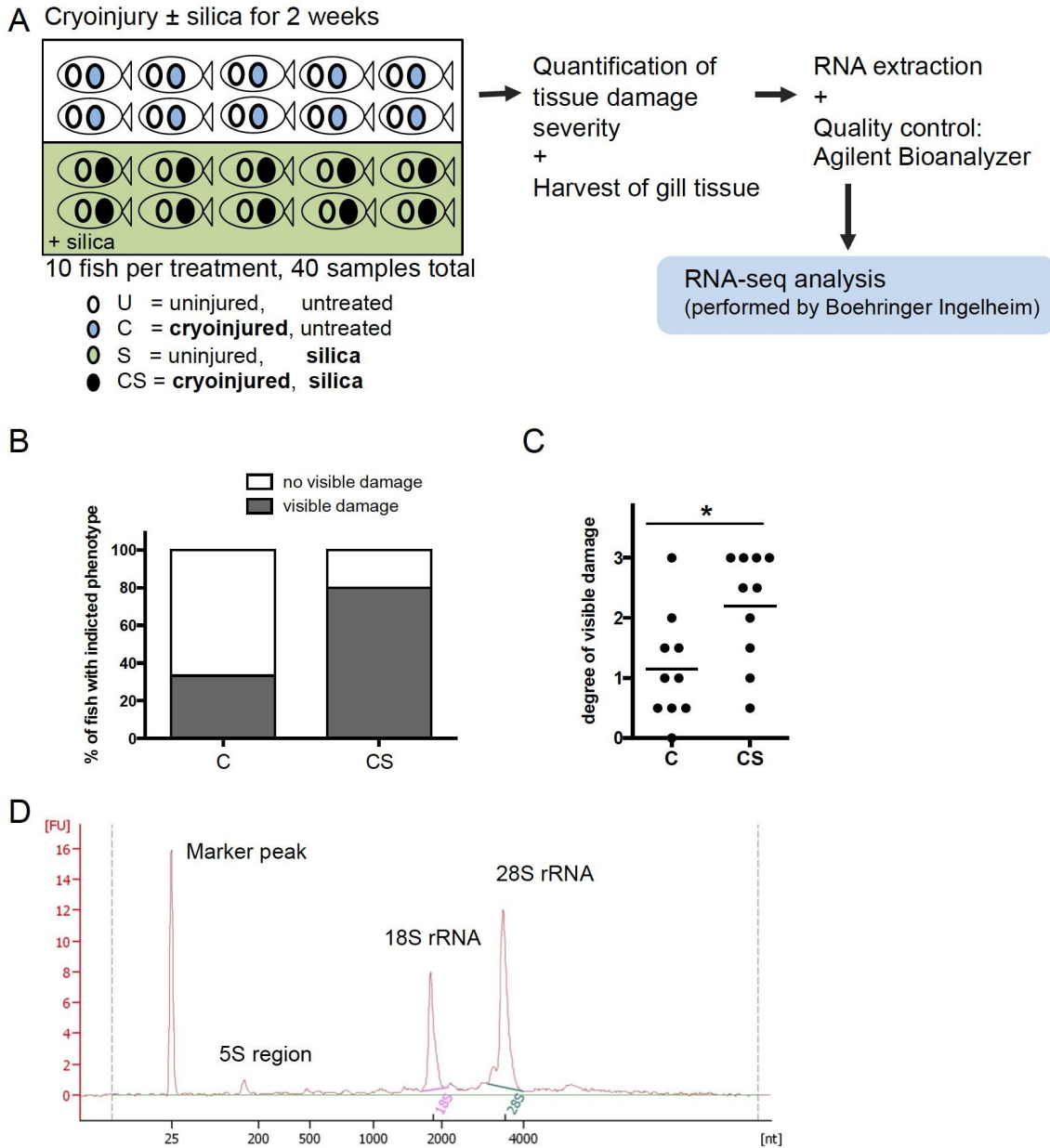


Fig. 4.16 Sample preparation for RNA-seq analysis.

(A) Experimental set up and workflow of sample preparation for subsequent RNA-seq analysis. 20 fish were cryoinjured followed by continuous exposure to silica (10 fish) or not (10 fish). After 2 wpi, fish gill tissues were harvested and their damage scored (see B-D). RNA was extracted from harvested gill tissues and subjected to quality control using Agilent Bioanalyzer. (B) Quantification of fish with visible gill tissue damage. (C) Qualitative score of gill tissue damage assigned during dissection with 3=large area of damage, 0=absence of damage. (D) Representative electropherogram of an RNA sample obtained from Agilent Bioanalyser analysis. Two-tailed t-test. * $p < 0.05$

At Boehringer Ingelheim, the RNA was fragmented and adaptors were ligated to both ends of each fragment to facilitate amplification and sequencing (Fig. 4.17A). Following sequencing, the raw data was provided to Geraint Barton (ICL) who performed the data analysis (Fig. 4.17B). In brief, the unaligned reads were aligned to the zebrafish reference genome from Ensembl (Zv9) and the counts for each gene were obtained using the R package edgeR. Before performing analysis of differentially expressed genes, Geraint carried out principal component analysis (PCA) to detect possible outliers.

Fig. 4.17C shows the PCA plot for all samples, where each dot represents one sample and its position in the PCA is determined following correlation of the average and the variation of the p-values of genes between samples. Therefore, samples exhibiting similar gene expression levels cluster together, while genes with different gene expression patterns are positioned apart. As demonstrated in Fig. 4.17C, sample 6C was detected as a technical outlier since its overall gene expression levels did not correlate with the other samples analysed and thus, was discarded from further analysis. Following PCA, Geraint performed pairwise comparisons between treatment groups to determine the p-value and the *fdr*. For gene expression studies involving microarrays or RNA-seq, it is common practice to select differentially expressed genes based on *fdr* rather than p-value. The *fdr* estimates the expected proportion of incorrectly rejected null hypotheses and therefore controls for false discoveries and minimises false positives. Thus, I carried out the following selection strategy to identify differentially expressed genes. Firstly, a *fdr* cut-off of 0.01 was applied. Secondly, all genes with counts below 50 across treatment groups were excluded since these genes exhibit negligible expression levels. Thirdly, all genes with a coefficient of variance (CofV) greater than 1.5 were removed, as the CofV indicates the variance between different replicates within one treatment group and a high CofV is a result of outliers (Fig. 4.17D).

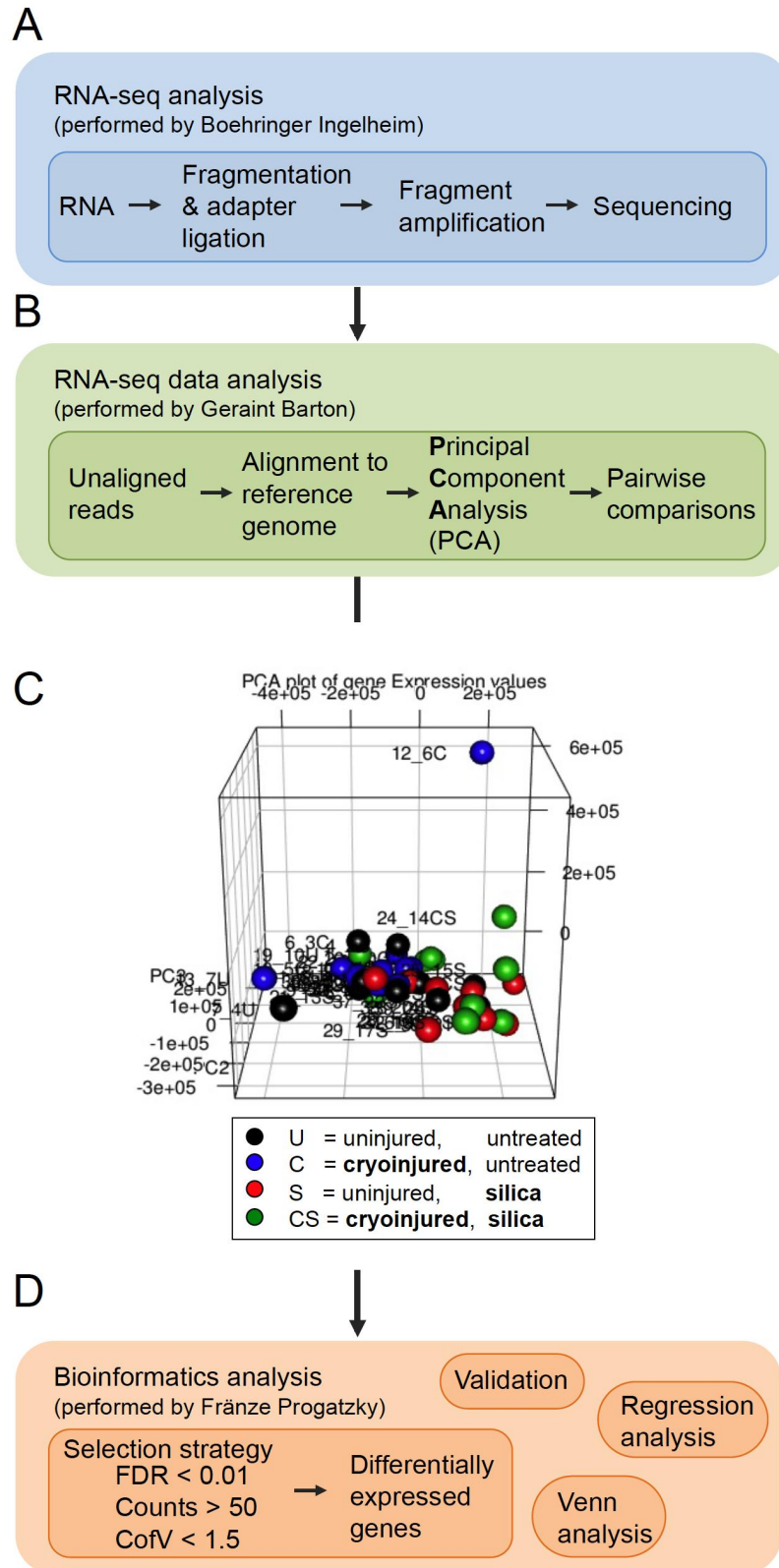


Fig. 4.17 Workflow of RNA-seq analysis and Principal Component Analysis of samples.

(A) RNA-seq analysis of RNA samples was performed at Boehringer Ingelheim. (B) Geraint Barton processed the raw data, *i.e.* the unaligned reads, by alignment to the Zv9 zebrafish reference genome following which PCA was performed and all genes between treatment groups were pairwise compared. (C) PCA of all samples. (D) Selection strategy for determination of differentially expressed genes and summary of subsequent bioinformatics analysis.

This selection strategy resulted in a number of differentially expressed genes as summarised in Fig. 4.18A. There were more differentially expressed genes following silica only treatment (443 genes) compared to the cryoinjury treatment (232), despite the fact that silica treatment does not lead to any visible tissue injury compared to the dramatic tissue damage inflicted by cryoinjury. While cryoinjury primarily resulted in increased transcripts (227 genes with increased transcript levels compared to only 5 genes with decreased transcript levels), silica-treatment predominantly induced decreased transcript levels (87 genes with increased transcript levels compared to only 356 genes with decreased transcript levels) when compared to the uninjured untreated samples. The combined treatment cryoinjury + silica treatment resulted in the highest number of differentially expressed genes (1549 genes), with about the same number of genes showing increased and decreased transcript levels, (891 vs. 658 genes respectively) in comparison to the uninjured untreated samples.

Venn analysis of the genes with significantly increased and decreased transcripts was performed to assess whether common genes are differentially expressed following different treatments. Apart from two genes (*uroplakin 3b* and *cathepsin La*), there was no overlap in those genes with increased transcript levels following either silica-or cryoinjury treatment (Fig. 4.18B). The same was observed for genes that exhibited decreased transcripts following either treatment (Fig. 4.18C). Further, there were no common genes between those showing increased transcripts following cryoinjury and those showing decreased transcripts following silica treatment (Fig. 4.18D), apart from one not yet annotated gene (*ARHGAP32_2 of 2*). Together, these results suggest that both treatments provoke completely different responses at 2 wpi.

When comparing genes with increased and decreased transcripts following cryoinjury with those following cryoinjury + silica treatment it was noted that almost all genes with transcripts significantly changed by cryoinjury treatment overlapped with those following combined treatment (Fig. 4.18B&C). This was in contrast to silica treatment where only about 30% of genes with increased and about 50% of genes with decreased transcripts were in common with the combined treatment cryoinjury + silica (Fig. 4.18B&C).

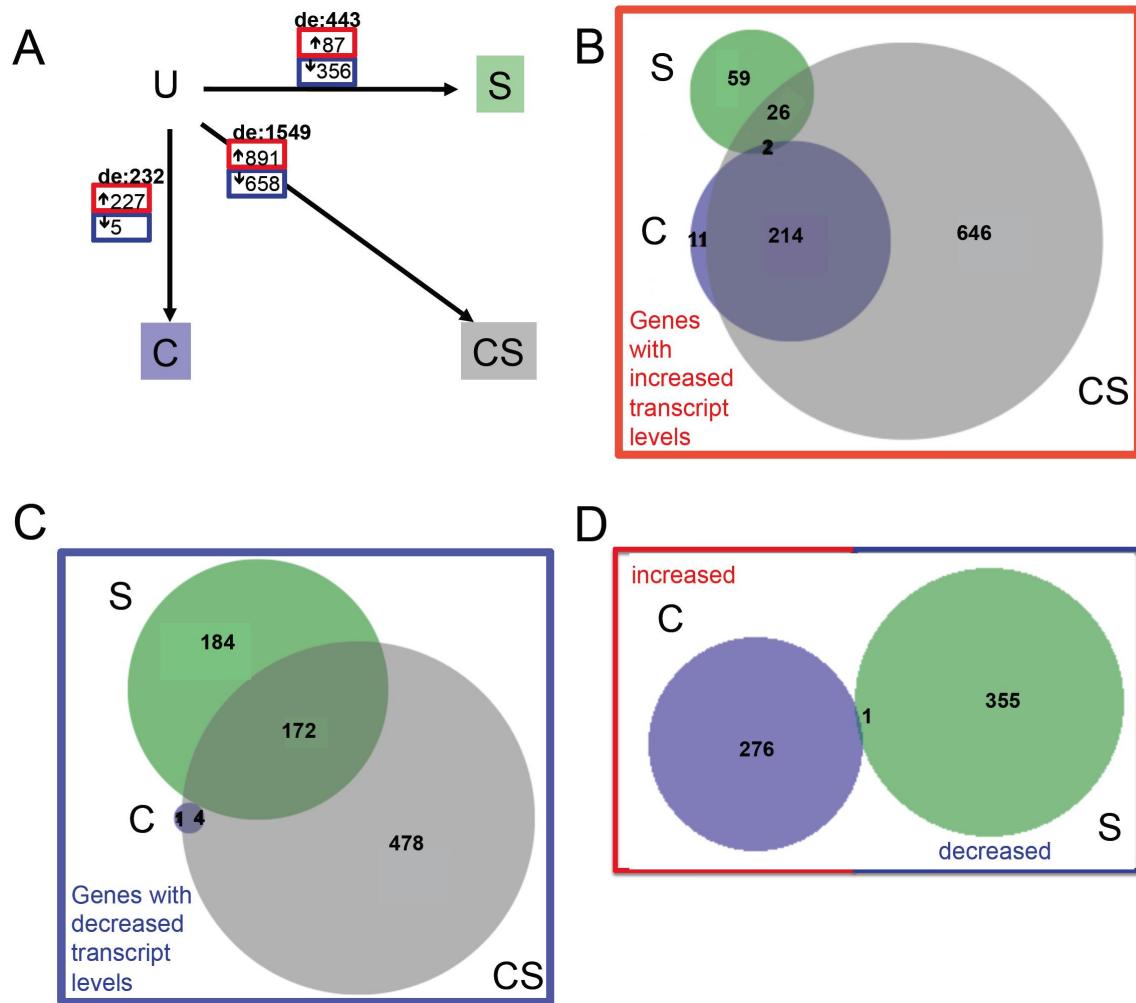


Fig. 4.18 Venn analysis of differentially expressed genes.

Samples of zebrafish gill tissue were analysed at 2 wpi following cryoinjury ± silica by RNA-seq analysis. U = uninjured, untreated; C = cryoinjured, untreated (blue); S = uninjured, silica (green); CS = cryoinjured, silica (grey). **(A)** Differentially expressed genes (de) between indicated treatment groups. Red boxes highlight genes with increased transcript levels and blueboxes genes with decreased transcript levels. **(B-D)** Area-proportional Venn diagrams (using the BioVenn online tool [350]) of the genes with increased transcript levels (B) and decreased transcript levels (C) following silica-treatment (green), cryoinjury (blue) and the combination of cryoinjury + silica (grey). In (D) genes with increased transcripts following cryoinjury (blue) are compared to those showing decreased transcript levels following silica treatment (green).

Next, it was important to assess whether the gene expression values obtained from RNA-seq analysis reflected those obtained by qRT-PCR. To determine the correlation between these two techniques a regression analysis was performed. *Collala* was chosen as gene of interest to carry out this correlation, as a significant increase in *collala* transcripts was previously detected by qRT-PCR analysis at 14 dpi (Fig. 4.14B).

Firstly, the levels of *collala* transcripts were compared using both techniques. Since the temporal expression profile of *collala* mRNA following cryoinjury seemingly correlated with the kinetics of the wound-healing process (Fig. 4.14A&B) and since silica treatment following cryoinjury significantly delayed this wound-healing process (Fig. 4.15B&C), higher *collala* transcripts in cryoinjury + silica treated samples compared to cryoinjury only were anticipated. Indeed, both RNA-seq and qRT-PCR analysis revealed a significant increase in *collala* transcripts following cryoinjury and a more significant increase following cryoinjury + silica treatment (Fig. 4.19A&B). No change in *collala* transcript levels was detected between uninjured untreated and silica treated gills (Fig. 4.19A&B). Of note, both means of analysis showed the same variability of expression values between individuals of the same treatment group.

Secondly, regression analysis was performed to correlate the expression values for each sample obtained by the two different techniques. As shown in Fig. 4.19C, there was a statistically significant correlation between *collala* mRNA expression values obtained from RNA-seq with those from qRT-PCR analysis. Although this direct comparison was only performed for one gene, these data suggest RNA-seq analysis as a valid method to explore gene expression in zebrafish gill tissues. Further, these data confirm the notion that *collala* transcript levels correlate with the degree of injury, therefore reflecting persistence in tissue-injury and the delay in wound-healing in silica exposed fish following cryoinjury.

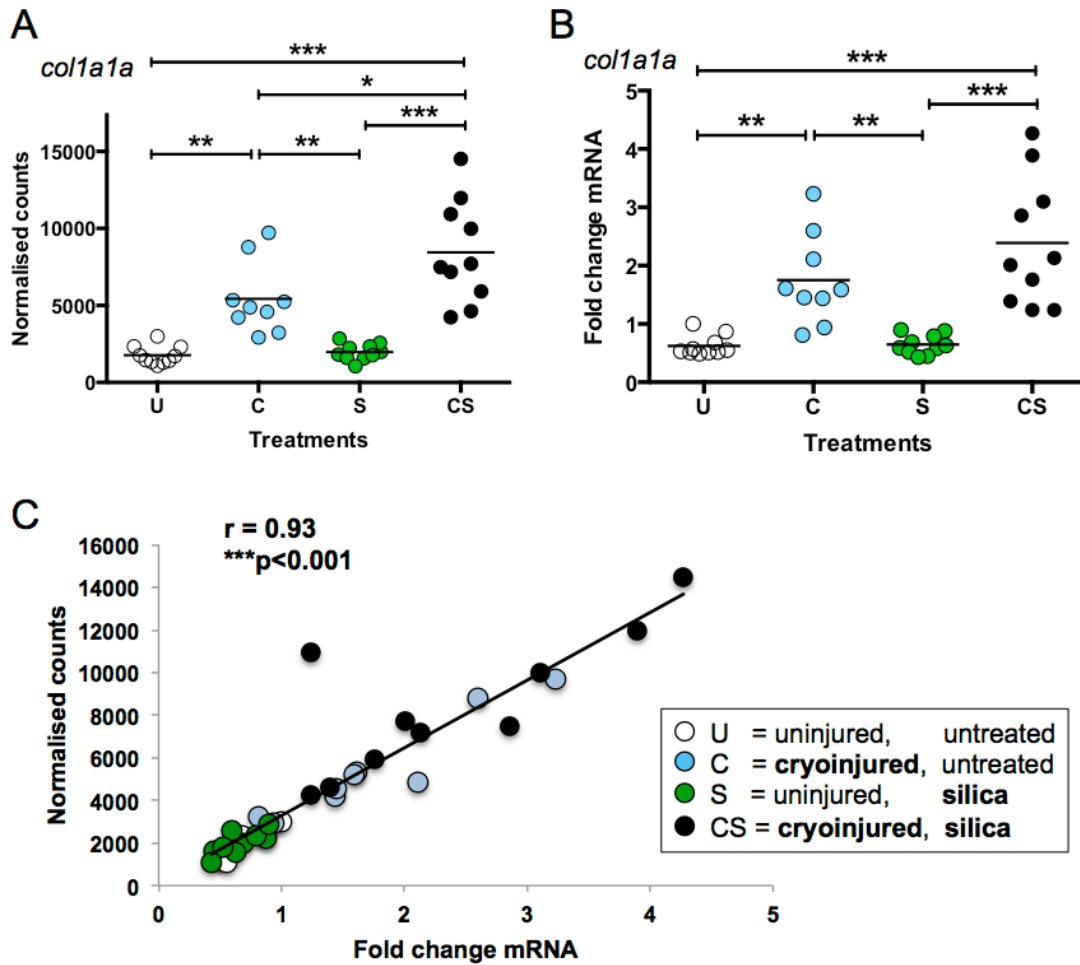


Fig. 4.19 Validation and correlation of *coll1a1* mRNA expression values between RNA-seq and qRT-PCR.

Samples of zebrafish gill tissue were analysed at 2 wpi following cryoinjury \pm silica. U = uninjured, untreated; C = cryoinjured, untreated; S = uninjured, silica; CS = cryoinjured, silica. **(A)** Normalised counts for *coll1a1* mRNA obtained by RNA-seq. **(B)** Relative expression values for *coll1a1* mRNA obtained by qRT-PCR analysis following normalisation to 18S. Data are expressed as fold change relative to one control sample (U). * $p < 0.05$, ** $p < 0.01$, *** $p < 0.001$. One-way Anova. **(C)** Regression analysis of *coll1a1* expression values obtained from normalised counts from RNA-seq with relative expression values from qRT-PCR analysis. The correlation coefficient is: 0.93, which is statistically significant at the 0.001 (***) two-tailed level. Each dot represents data obtained for one sample from one individual fish.

Having established that the expression values obtained by RNA-seq correlate well with those obtained by qRT-PCR, the identified differently expressed genes were characterised to assess whether their expression was consistent with expected physiological responses.

Transcript levels of genes significantly induced by silica exposure were ranging from a 1.5 fold to a 16 fold increase. Amongst those genes with most significantly increased transcripts following silica exposure, a high number of genes with catalytic activities were noted. These were for example *trypsin* (*try*, 8 fold) and *amylase* (*amy2a*, 14 fold) as shown in Fig. 4.20A, and others such as *elastase* genes (*ela3l*, 11 fold; *ela2*, 10 fold; *ela2l*, 9 fold), *carboxyl ester lipase 1* (*cel.1*, 15 fold), *carboxypeptidase A4* (*cpa4*, 13 fold), *carboxypeptidase B1* (*cpb1*, 12 fold). Genes that showed decreased transcripts following silica exposure were ranging from a 1.5 fold to a 50 fold decrease, however, all genes with the largest fold decrease are not yet annotated. Amongst those already annotated genes with decreased transcript levels, a number of immune cell related genes were noted. These were for example *il10* (2 fold) and *lck* (2 fold) as shown in Fig. 4.20B. These data suggest that silica induces the expression of genes with catalytic activity and down-regulates the expression of certain genes associated with immune responses.

Transcript levels of genes significantly induced by cryoinjury were ranging from a 1.5 fold to a 20 fold increase. Amongst those genes with most significantly increased transcripts following cryoinjury, a high number of genes involved in tissue remodelling during wound healing and fibrotic processes were noted. These were for example *osteopontin* (*spp1*, 13 fold), *periostin b* (*postnb*, 9 fold), *colla2* (3 fold), *fibronectin a* (*fn1a*, 2 fold) and *matrix metalloproteinase 9* (*mmp9*, 6 fold) (Fig. 4.20C). Of note, the blastema marker gene *muscle segment homeobox B* (*msxb*, 8 fold) was amongst the genes with the most significantly increased transcripts (Fig. 4.20C). Further, as shown in Fig. 4.20C, the mean expression value of these genes were slightly higher in cryoinjury + silica treated fish compared to cryoinjury only treated. These data suggest that the cryoinjury induces gill tissue remodelling responses at 2 wpi are exacerbated by silica treatment.

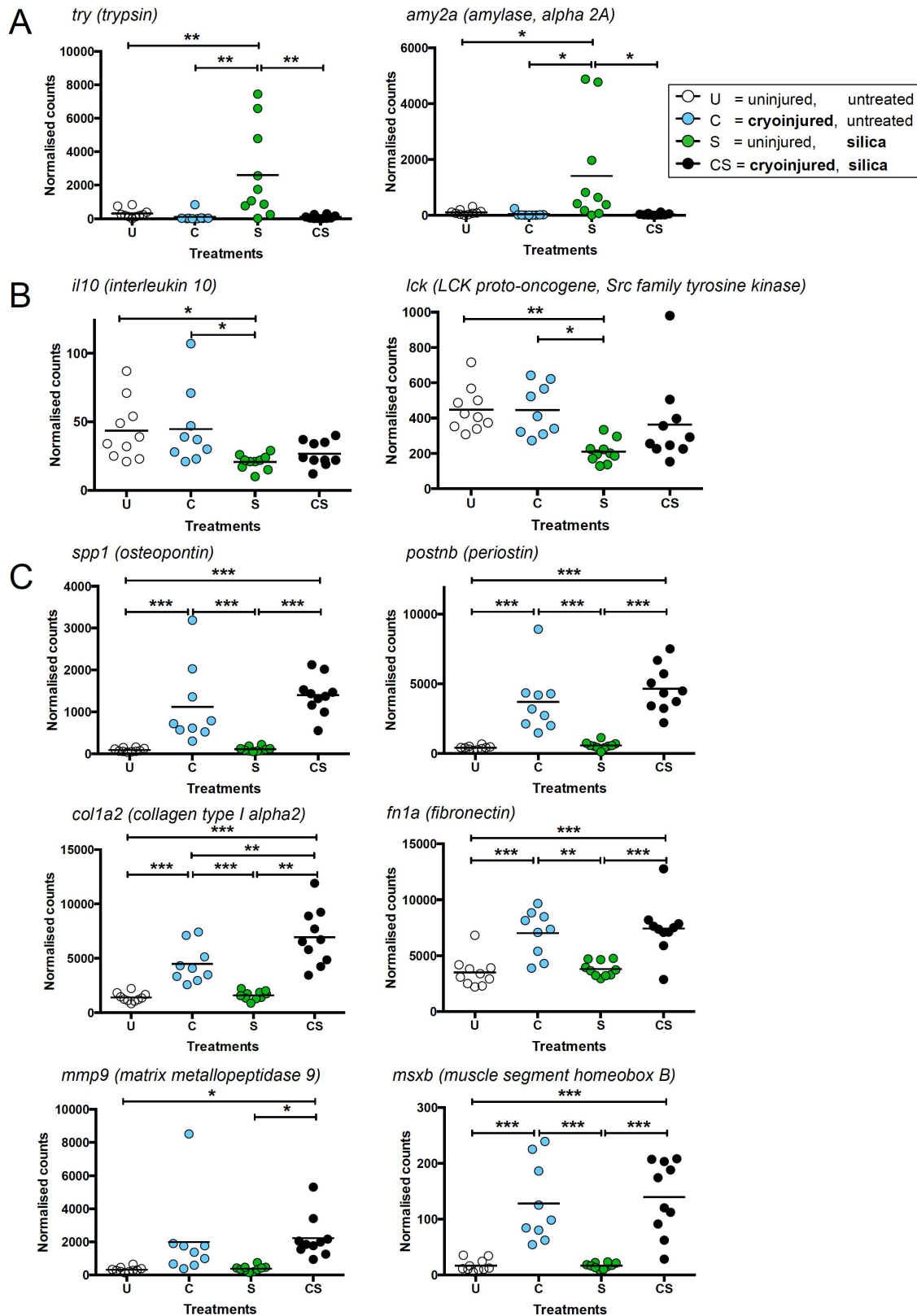


Fig. 4.20 Examples of most significantly differentially expressed genes following silica and cryoinjury. Samples of zebrafish gill tissue were analysed at 2 wpi following cryoinjury \pm silica. U = uninjured, untreated; C = cryoinjured, untreated; S = uninjured, silica; CS = cryoinjured, silica. Relative counts obtained by RNA-seq analysis are shown. (A&B) Example genes with significantly increased (A) and decreased (B) transcript levels following silica treatment. (C) Example genes with significantly increased transcript levels following cryoinjury and cryoinjury + silica treatment. One-way Anova. * $p < 0.05$, ** $p < 0.01$, *** $p < 0.001$

To further investigate the relationship between the visible severity of tissue damage and the transcript levels of genes associated with gill tissue remodelling a regression analysis was performed. For each individual sample the mRNA expression value for each individual gene obtained from RNA-seq analysis was correlated to its corresponding qualitative score of gill tissue damage recorded during tissue harvest (Fig. 4.16C). This analysis was performed on all cryoinjury \pm silica treated samples. All genes were analysed, irrespective of whether they were previously identified as differentially expressed or not, and for each gene the correlation coefficient was calculated. As summarised in Fig. 4.21A&B, correlation analysis between transcript levels and damage of cryoinjured \pm silica treated gill tissue samples revealed positively and negatively correlated genes at different significance levels. Overall, there were more positively correlated than negatively correlated genes (Fig. 4.21). A high number of genes associated with tissue remodelling were highly positively correlated. Fig. 4.21C&E show examples of the most significantly positively correlated genes *spp1* (correlation coefficient $r=0.61$) and *coll1a1* ($r=0.6$). The fact that *coll1a1* was amongst these positively correlated genes confirmed its previously suggested use as an indicator for visible tissue-damage/wound-healing. Others genes that were noted amongst those highly positively correlated were *vimentin* (*vim*, $r=0.5$), *tenascin c* (*tnc*, $r=0.5$), *postnb* ($r=0.56$), *fn1a*, ($r=0.49$) and *platelet derived growth factor b* (*pdgfb*, $r=0.5$). Together, these data confirm that cryoinjury \pm silica induces a gill tissue remodelling response.

In contrast, no tissue-remodelling associated genes were amongst the negatively correlated genes but rather some genes associated with the immune system, such as *ccr6b* (Fig. 4.21D) and the *LYN proto-oncogene*, *Src family tyrosine kinase* (*lyn*, Fig. 4.21F). These data suggest again that silica might decrease certain immune responses.

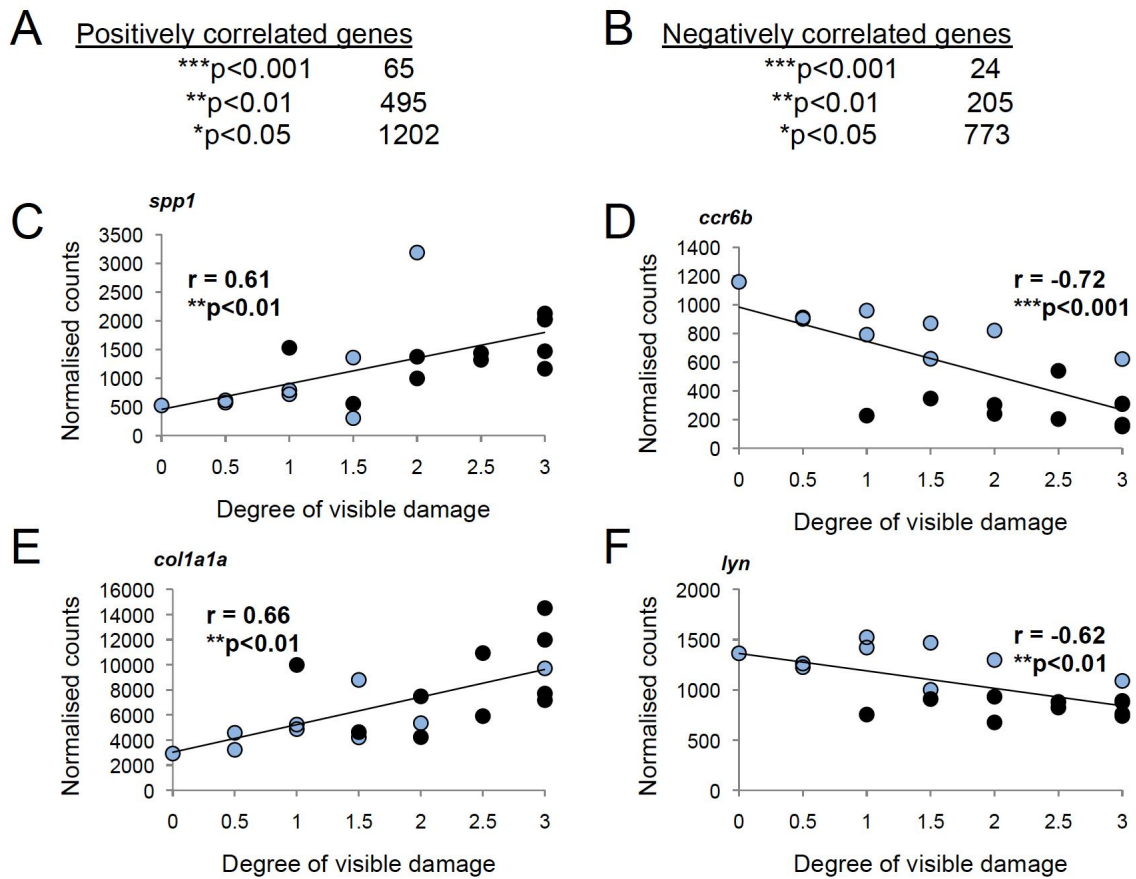


Fig. 4.21 Regression analysis between gene expression and gill tissue-damage.

(A&B) Normalised counts obtained from RNA-seq analysis were correlated with the scores reflecting the degree of visible damage of samples of cryoinjury (blue) and cryoinjury + silica (black) treated gill tissues. The correlation coefficient was calculated for each gene and the number of positively (A) and negatively (B) correlated genes recorded according to the following levels of significance ***p<0.001 ($r \geq \pm 0.69$), **p<0.01 ($r \geq \pm 0.57$), *p<0.05 ($r \geq \pm 0.46$). (C-F) Example for positively regulated genes (C&E), *spp1* (C) and *colla1a* (E), as well as negatively regulated genes (D&F), *ccr6b* (D) and *lyn* (F).

Overall, this preliminary experiment using RNA-seq to analyse transcript levels of treated zebrafish gill tissue samples following cryoinjury \pm silica demonstrated low variability between samples within one treatment group and indicated that the RNA-seq data is robust as it accurately reflects transcript levels obtained by qRT-PCR. Further, this RNA-seq data set confirmed the expression patterns of many genes known to be involved in tissue remodelling responses of wound-healing and/or fibrotic processes in mammals. Despite a clear correlation between tissue damage and the transcript levels of genes associated with these mammalian tissue-remodelling responses, zebrafish heal without fibrosis. Therefore, to gain a better understanding of the molecular mechanisms of these different injuries, a time-series experiment was set-up. A time-course analysis will take into account the temporal aspect of transcript levels and would allow comparison with datasets available at Boehringer Ingelheim and in the literature from models of lung injury or tissue samples of patients.

Preliminary RNA-seq time-course analysis

To allow direct comparison with datasets available at Boehringer Ingelheim from mouse models of lung injury (*i.e.* bleomycin-induced lung fibrosis and TGF- β overexpression), the same time-points of 3 dpi, 7 dpi, 14 dpi and 28 dpi were chosen. Since the preliminary RNA-seq analysis at 14 dpi established that samples within the same treatment group exhibit low variability in expression values, this time only 5 samples instead of 10 were chosen for the subsequent analysis. 40 fish were cryoinjured following which 20 were continuously treated with silica and the other 10 left untreated. At indicated time-points the gill tissues were harvested, scored for presence and absence of visible gill tissue damage and a qualitative damage score was given. The temporal profile of gill tissue damage following cryoinjury was the same as in previous experiments and the two scoring systems correlated, showing the biggest difference in damage at 14 dpi (Fig. 4.22A&B). These data suggest that the experiment was repeatable and suitable for further analysis. The samples were processed as described above and transferred to Boehringer Ingelheim for transcriptome profiling using RNA-seq. Geraint Barton (ICL) again performed the subsequent data analysis and I set out to assess whether the data would be suitable for comparative analysis.

Firstly, it was important to validate the expression values from RNA-seq analysis. For that, *coll1a1a* was again chosen as reference gene to carry out the correlation between the two methods of transcriptome analysis. Both RNA-seq and qRT-PCR analysis revealed a

significant increase in *collala* transcript levels following cryoinjury \pm silica (Fig. 4.22C&D). As expected, the increase in *collala* transcripts persisted in the cryoinjury + silica treated samples as compared to cryoinjury only treated fish (Fig. 4.22C&D). No change in *collala* mRNA levels was detected between uninjured untreated and silica treated gills over the time-frame analysed (Fig. 4.22C&D). Of note, both means of analysis showed again the same low variability of gene expression level between samples of the same treatment group.

Secondly, regression analysis was performed to correlate the expression values for each sample obtained by the two different techniques. As shown in Fig. 4.22E, there was a statistically significant correlation between *collala* mRNA expression values obtained from RNA-seq with those from qRT-PCR analysis. These data confirm RNA-seq as a robust and quantitative method to analyse gene-expression analysis in adult gill tissue.

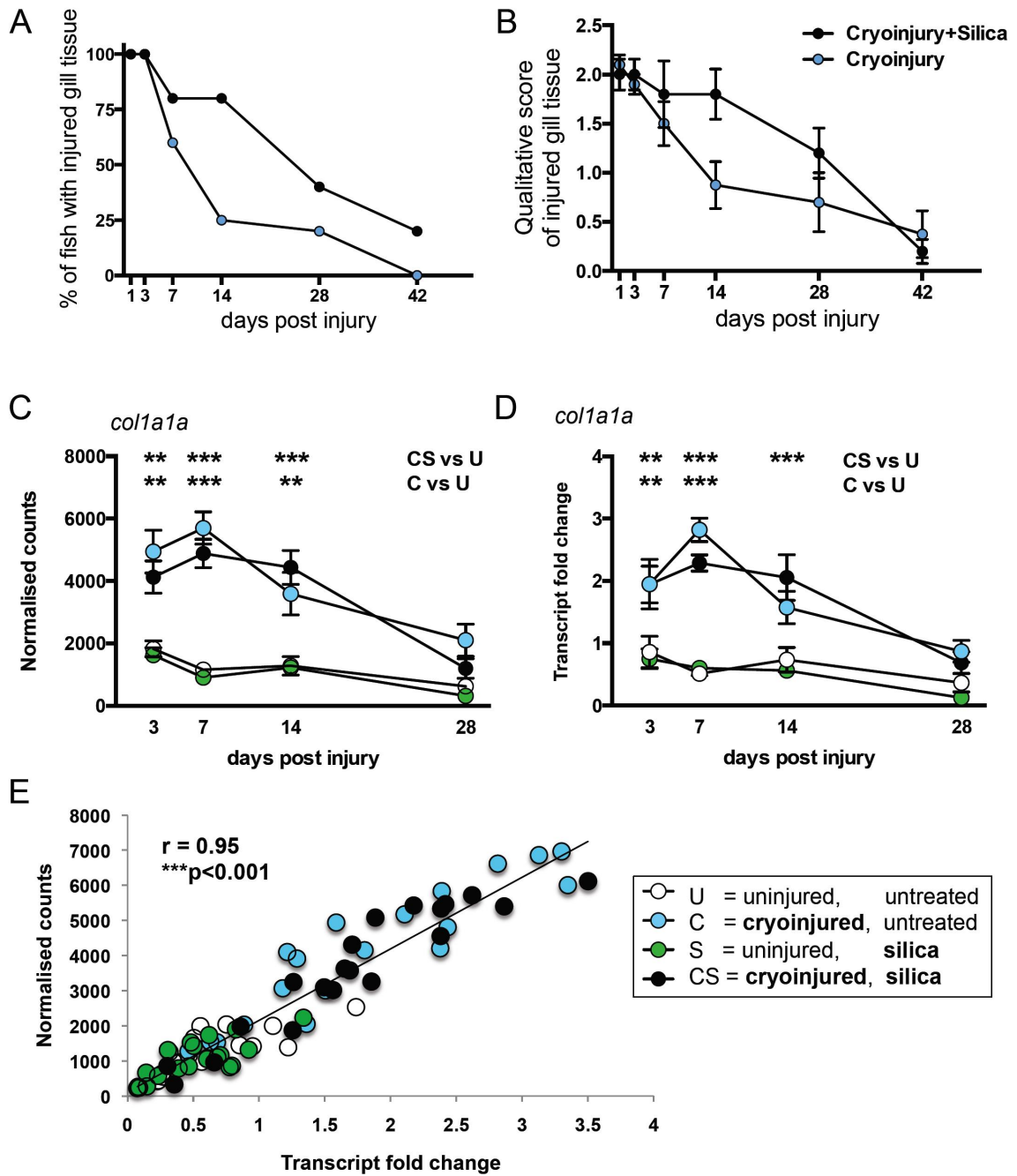


Fig. 4.22 Quantification of gill tissue damage and validation of *coll1a1* mRNA expression values.

Samples of zebrafish gill tissue were analysed at indicated time-points following cryoinjury±silica. U = uninjured, untreated; C = cryoinjured, untreated; S = uninjured, silica; CS = cryoinjured, silica. **(A)** Quantification of fish with visible gill tissue damage. **(B)** Qualitative score of gill tissue damage assigned during dissection with 3=large area of damage, 0=absence of damage. **(C)** Normalised counts for *coll1a1* mRNA obtained by RNA-seq. **(D)** Relative expression values for *coll1a1* mRNA obtained by qRT-PCR analysis following normalisation to 18S. Data are expressed as fold change relative to one control sample (U). * $p < 0.05$, ** $p < 0.01$, *** $p < 0.001$. Two-way Anova. **(E)** Regression analysis of *coll1a1* expression values obtained from normalised counts from RNA-seq with relative expression values from qRT-PCR analysis. The correlation coefficient is: 0.95, which is statistically significant at the 0.001 (***) two-tailed level. Each dot represents data obtained for one treatment group (=mean of $n=5 \pm \text{SEM}$, A-D) or data for one sample from one individual fish (E).

Next it was important to assess whether the same differentially expressed genes were identified at 14 dpi of the RNA-seq time-course analysis compared to the preliminary experiment. The same strategy was applied ($\text{fdr} < 0.01$, $\text{counts} > 50$, $\text{CofV} < 1.5$) to select differentially expressed genes between the different treatment groups of samples harvested at the 14 dpi time-point. Subsequently, Venn analysis was performed to determine the degree of overlap of genes with significantly increased and decreased transcript levels following cryoinjury \pm silica between the two experiments.

Fig. 4.23A shows that three times more genes (264 vs. 87 genes) were found to exhibit significantly increased transcript levels following silica treatment at 14 dpi during the time-course experiment when compared to the preliminary experiment and of those only 19 genes overlapped ($\approx 21\%$ of the preliminary experiment). Similar number of genes were identified with significantly decreased transcript levels (245 vs. 356) at 14 dpi following silica treatment between the two experiments while only 39 genes ($\approx 11\%$ of preliminary experiment) were in common (Fig. 4.23B). Fig. 4.23C shows that less than half the number of genes (102 vs. 227 genes) were found to exhibit significantly increased transcript levels following cryoinjury at 14 dpi during the time-course experiment when compared to the preliminary experiment and of those 73 genes ($\approx 32\%$ of the preliminary experiment) overlapped. There were no genes with significantly decreased transcript levels at 14 dpi following cryoinjury of the time-course experiment (Fig. 4.23D). Further, a similar number of genes with increased (710 vs. 891, overlapping 292, 32% of the preliminary experiment) and decreased (654 vs. 658, overlapping 198, 30% of the preliminary experiment) transcript levels following cryoinjury + silica were identified in the two experiments (Fig. 4.23E&F).

These data show that overall degree of overlap of differentially expressed genes between experiments was low. However, there was more overlap of significantly differentially expressed genes between the two experiments of fish receiving a cryoinjury compared to the silica treated fish suggesting that in particular the silica-treatment has induced different responses in the two experiments.

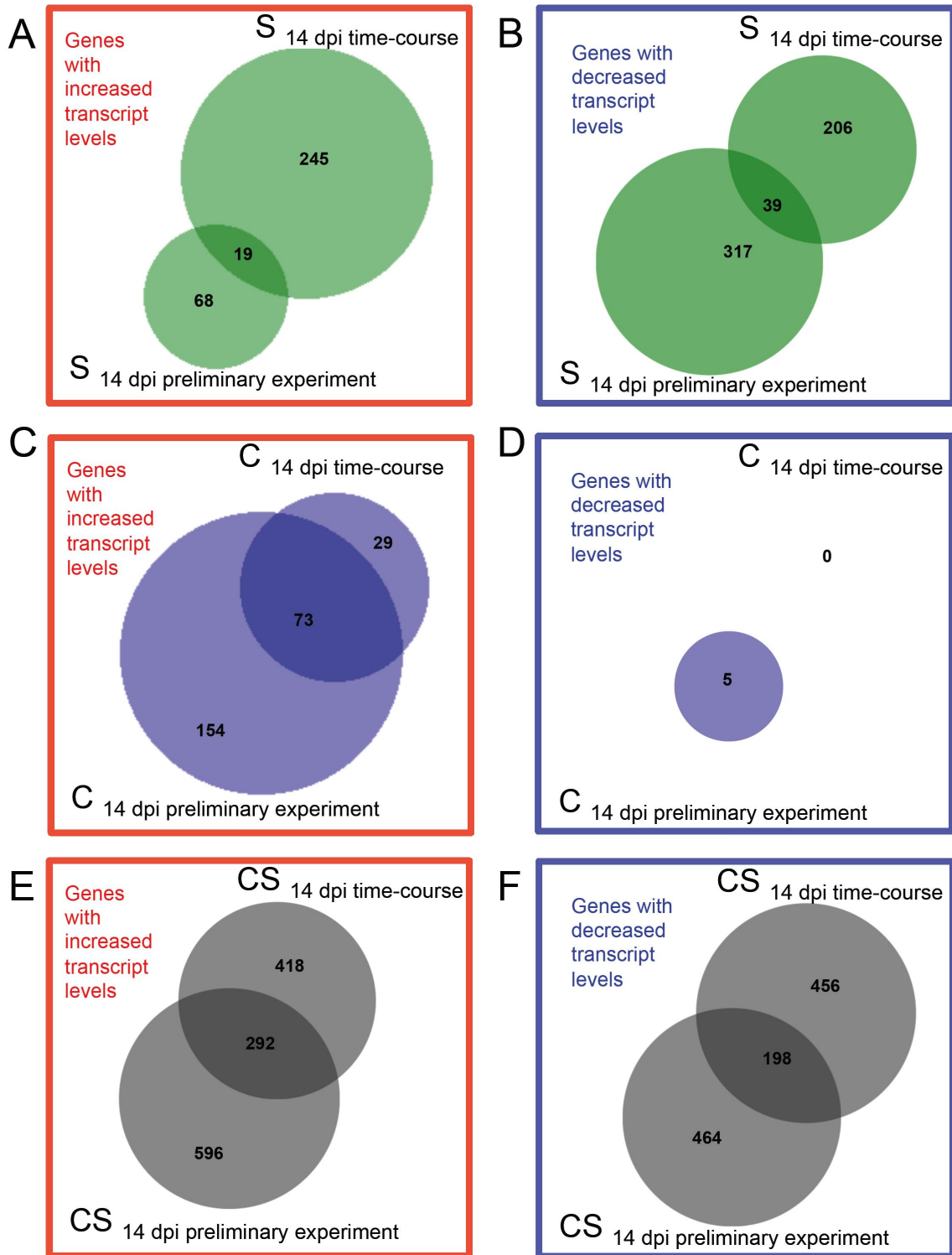


Fig. 4.23 Venn analysis of differentially expressed genes between experiments.

Venn diagrams of differentially expressed genes of zebrafish gill tissue samples at 2 wpi following cryoinjury \pm silica analysed by RNA-seq in the preliminary experiment or as part of the time-course experiment. Differentially expressed genes were determined relative to the uninjured, untreated gill tissue samples. Area-proportional Venn diagrams (using the BioVenn online tool [350]) of the genes (A) with increased transcript levels and (B) decreased transcript levels of S = uninjured, silica (green) treated fish. (C) Genes with increased transcript levels and (D) decreased transcript levels of C = cryoinjured, untreated (blue) fish. (E) Genes with increased transcript levels and (F) decreased transcript levels of CS = cryoinjured, silica (grey).

Next, the temporal expression profiles of the significantly differentially expressed genes identified during the preliminary RNA-seq analysis at 14 dpi (Fig. 4.20) were analysed.

First, genes that previously exhibited increased transcript levels following silica treatment were compared. None of the previously identified genes with catalytic properties (*try* and *amy2a*, *ela3l*, *ela2*, *ela2l*, *cel.1*, *cpa4* and *cpb1*) were found to be significantly different between treatment groups at any time point analysed. *Try* and *amy2a* are shown as examples (Fig. 4.24A). These data suggest that the silica treatment might not have evoked the same responses as in the previous experiment. However, those genes that showed significantly decreased transcript levels following silica treatment, were also decreased in the kinetic analysis. For example, *ill10* transcripts were significantly lower in silica and cryoinjury + silica treated fish at 14 and 28 dpi (Fig. 4.24B). *Lck* transcripts were also significantly lower at 14 dpi in silica treated samples when compared to control, although this decrease in expression did not persist over time (Fig. 4.24B).

Second, the temporal expression profiles of those genes with increased transcript levels following cryoinjury were analysed. As shown in Fig. 4.24C, genes associated with tissue remodelling (*spp1*, *postnb*, *colla2*, *fn1a* and *mmp9*) and blastema formation (*msxb*) showed significantly higher transcripts following cryoinjury and cryoinjury + silica over time when compared to control. Whilst *postnb*, *colla2*, *fn1a* and *msxb* showed almost identical temporal expression pattern for cryoinjury and cryoinjury + silica treated groups, *spp1* and *mmp9* showed temporal differences in expression following cryoinjury and cryoinjury + silica treatments. Further, there were different temporal mRNA expression pattern for different genes. For example, whilst *postnb* transcript levels peaked at early time-points following cryoinjury (*i.e.* around 3 dpi or even earlier), *msxb* and *colla2* peaked at 7 dpi and *spp1* peaked at 14 dpi. These data not only confirm the previous results obtained from the first RNA-seq analysis, but also suggest that the different temporal patterns of transcript levels of these genes correlate with different physiological responses and different stages of wound-healing following cryoinjury. As before, there was a low variability between samples of the same treatment group. This RNA-seq analysis of gill tissue samples following cryoinjury will be suitable for comparative studies with datasets available at Boehringer Ingelheim from models of lung injury.

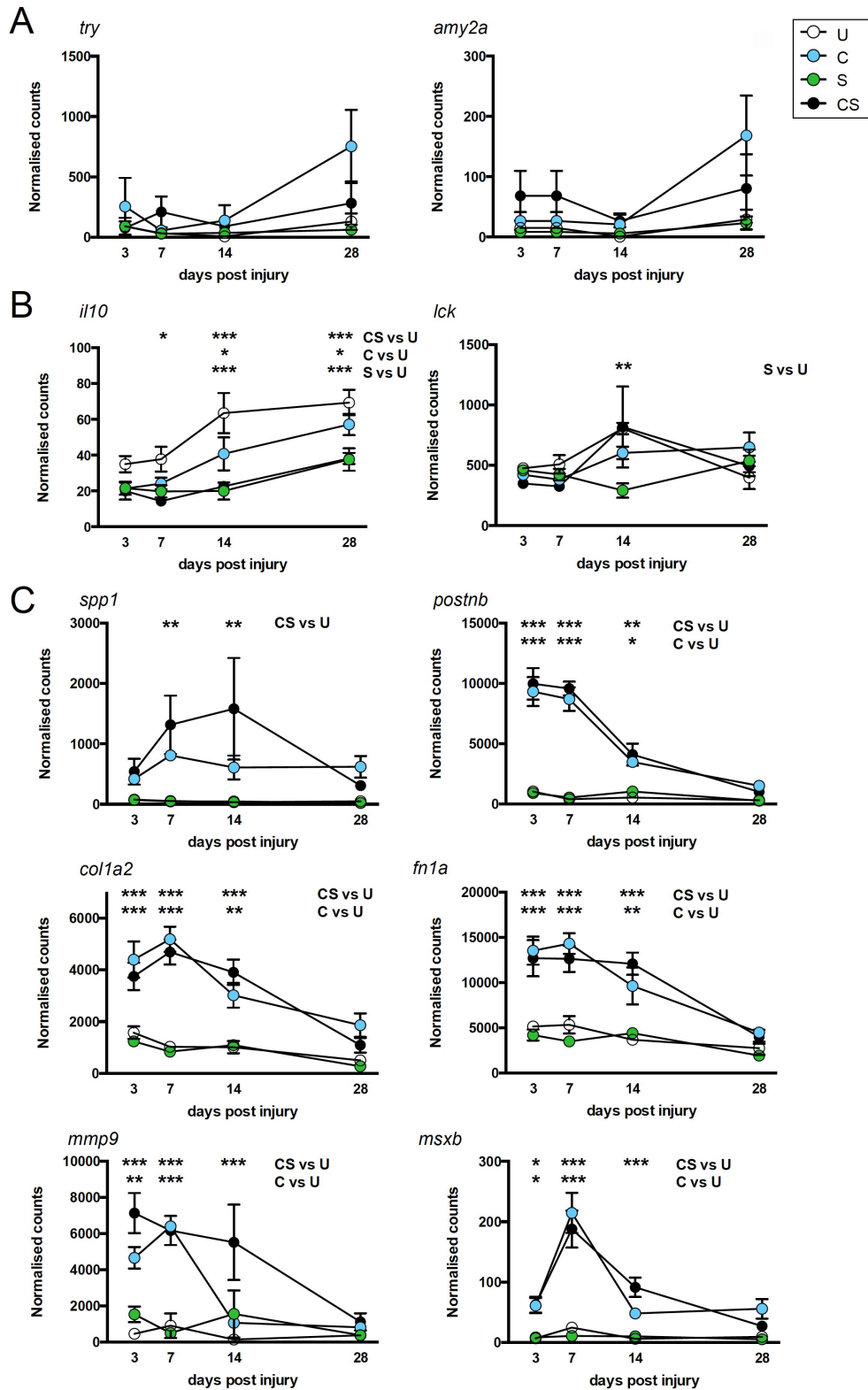


Fig. 4.24 Temporal profiles of example genes following silica and cryoinjury.

Samples of zebrafish gill tissue analysed at 2 wpi following cryoinjury \pm silica. U = uninjured, untreated; C = cryoinjured, untreated; S = uninjured, silica; CS = cryoinjured, silica. Relative counts obtained by RNA-seq analysis. (A&B) Previously identified example genes with significantly increased (A) and decreased (B) transcript levels following silica treatment (Fig. 4.20). (C) Example genes with significantly increased transcript levels following cryoinjury and cryoinjury + silica treatment. Statistical significant differences are indicated for the silica treated samples (S), the cryoinjury treated samples (C) and the cryoinjury + silica treated samples (CS) compared to the untreated uninjured group (U). Error bars = SEM. Two-way Anova. * $p < 0.05$, ** $p < 0.01$, *** $p < 0.001$

Lastly, it was important to assess whether known processes involved in wound healing in mammalian lungs also occur in zebrafish. Genes known to be involved in the inflammatory phase of the wound healing process were investigated. There was no statistically significant change in the transcript levels of the following selected inflammatory cell marker genes upon cryoinjury \pm silica within the time-frame analysed by RNA-Seq: *mpx* (neutrophils, Fig. 4.25A), *lyz* (myeloid cells, Fig. 4.25B), *lcp1* (leukocytes, Fig. 4.25C), *rag2* (lymphocytes, Fig. 4.25D) and *cd4* (T cells, Fig. 4.25E) and *lck* (T cells, Fig. 4.24B). The transcripts of *mpegl* (macrophages Fig. 4.25F) were also unchanged over time in cryoinjury \pm silica treated fish relative to the control samples, but significantly lower at 14 dpi in the silica only treated fish, similar to that seen for the temporal expression profile of *lck* (T cells, Fig. 4.24B). Only *csflra* (*fms*, macrophages, Fig. 4.25G) showed a significant increase in transcripts upon cryoinjury \pm silica which returned back to baseline levels in cryoinjured fish by 14 dpi and remained high in cryoinjury + silica treated fish at 14 dpi (Fig. 4.25A). Transcripts of pro-inflammatory cytokines such as *illb* (Fig. 4.25H), *tnfa* (Fig. 4.25I) and *tnfb* (Fig. 4.25J) were unchanged following cryoinjury \pm silica over the time-course analysed. Since the first time-point during this RNA-seq analysis is at 3 dpi, there is a possibility that acute inflammatory responses following cryoinjury \pm silica do not occur in the time-frame of the present analysis.

Genes known to be involved in new tissue formation and remodelling were analysed. Wound repair processes are characterised by new blood vessel formation to restore the damaged underlying tissue structure and to aid formation of a granulation tissue [351]. A key inducer of neovascularisation following wounding is the vascular endothelial growth factor A (*vegfaa* in zebrafish) [351]. Transcript levels of *vegfaa* were decreased following cryoinjury \pm silica compared to the uninjured \pm silica samples suggesting that the tissue damage by cryoinjury might have severely damaged the lamellar respiratory capillary system. Over the time-course of the RNA-seq analysis *vegfaa* transcripts increased and returned back to baseline levels of the control samples by 14 dpi following cryoinjury and by 28 dpi following cryoinjury + silica treatment (Fig. 4.26A). These results suggest that delayed angiogenesis following injury might play a role in the delayed wound healing observed in cryoinjury + silica treated fish.

A key mediator of myofibroblast activation during wound healing and fibrosis is TGF- β [320]. *Tgfb2* transcripts were significantly induced by cryoinjury, while *tgfb1a*, *tgfb1b* and *tgfb3* expression was unchanged over the time-course analysed (Fig. 4.26B-E). In addition to TGF- β signalling, fibroblast growth factor (Fgf) and Wnt/ β -catenin signalling are key

pathways that interactively regulate epithelial-mesenchymal interactions in the lung during developmental and repair processes [117]. Fgfs are a protein family that signal through high-affinity transmembrane tyrosine kinase receptors (Fgfr) [352]. Fgf signalling through Fgf10 regulates epithelial cell proliferation during lung development [353] and has also been implicated in lung repair process following injury [117]. Here, *fgf10a* transcripts were significantly increased in zebrafish gills following cryoinjury (Fig. 4.26F). *Fgf10* is a direct target of the Wnt/ β -catenin signalling [117]. Wnt proteins comprise several family members of secreted cysteine rich ligands that interact with a co-receptor complex formed of several Frizzled family members and the low-density lipoprotein receptor-related proteins 5/6. While Wnts can signal through several pathways, the canonical β -catenin pathway is best understood [354]. Wnt/ β -catenin signalling plays critical roles during developmental and repair processes of the lung and also regulates airway progenitors [117]. In contrast, β -catenin and other pathway components are detected in the alveolar epithelium around fibroblast foci in patients suffering from pulmonary fibrosis [355] suggesting that aberrant Wnt/ β -catenin signalling can have detrimental outcomes. Cryoinjury \pm silica significantly induced transcripts of β -catenin (*ctnnb1* in zebrafish). Together, these data suggest that TGF- β , Wnt/ β -catenin and Fgf signalling pathways play a role in wound-healing processes in zebrafish gills (Fig. 4.26G).

Reparative responses in the lung involve the contribution of progenitor cells termed basal cells [117]. Basal cells are characterised by their expression of the transformation-related protein 63 (*tp63* in zebrafish), keratin 5 (*krt5* in zebrafish) and *Krt14* [356]. While *Krt14* is not expressed in zebrafish (Zebrafish Model Organism Database, ZFIN), *tp63* and *krt5* transcript levels were significantly induced upon cryoinjury \pm silica (Fig. 4.26H&I). Although it is yet to be established whether similar progenitor cells to basal cells are found in the zebrafish gill epithelium, these data suggest that cells with stem cell potential might be involved in the regeneration of the gill tissue following cryoinjury.

Despite the fact that this analysis is selective and remains to be performed systematically in the future, the preliminary transcriptome data obtained by RNA-seq indicate that key mechanisms and pathways involved in wound healing in mammals also play a role in these processes in zebrafish. Further, this work lays the groundwork for future comparative analysis of wound healing mechanisms in different species, which might help to understand why repair processes in humans result in a permanent scar.

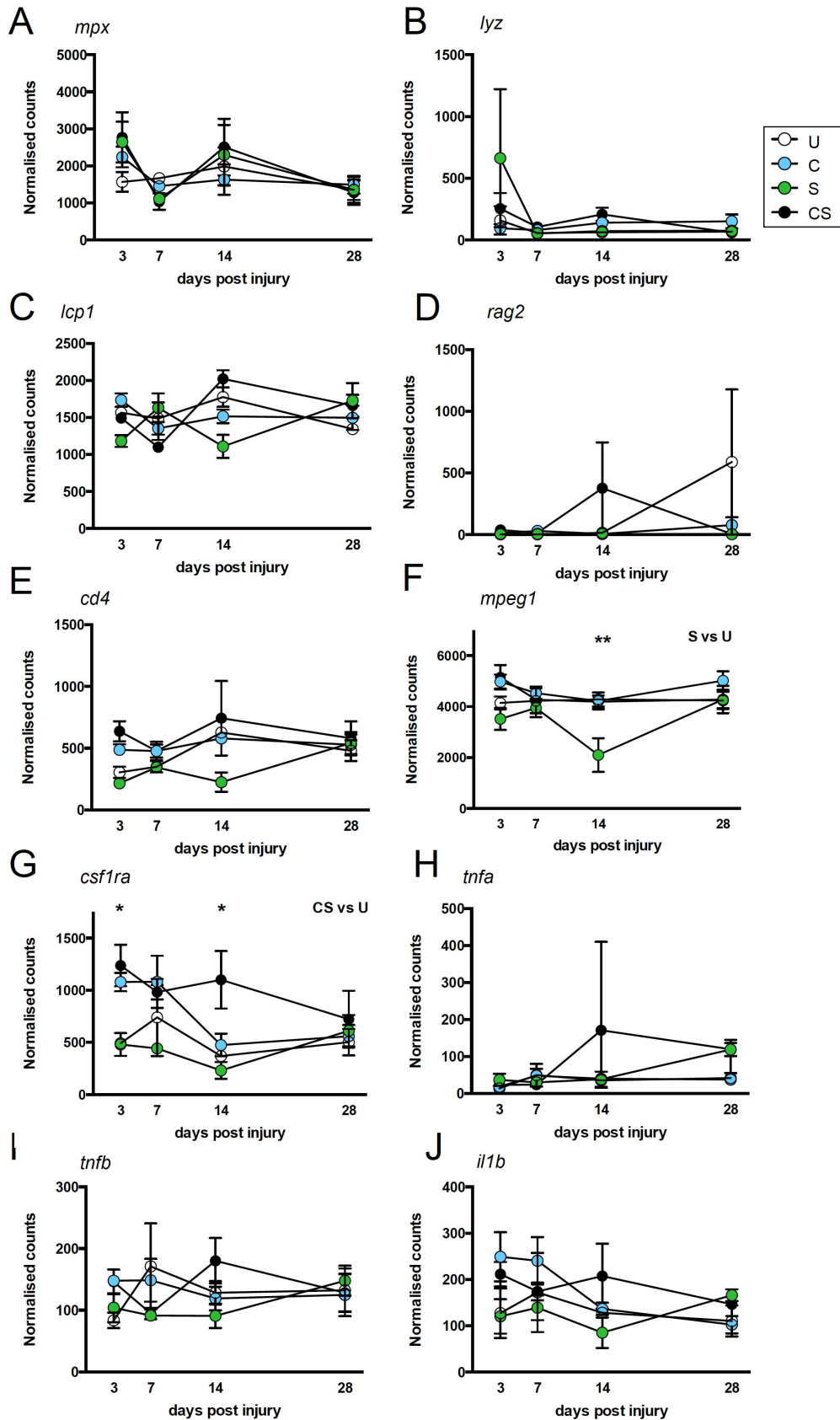


Fig. 4.25 Temporal profiles of example genes involved in inflammatory processes following injury. (A-J) Samples of zebrafish gill tissue were analysed at 2 wpi following cryoinjury ± silica. U = uninjured, untreated; C = cryoinjured, untreated; S = uninjured, silica; CS = cryoinjured, silica. Relative counts obtained by RNA-seq analysis are shown. Statistical significant differences are indicated only for silica treated samples (S), the cryoinjury treated samples (C) and the cryoinjury + silica treated samples (CS) compared to the untreated uninjured group (U). Error bars = SEM. Two-way Anova. * $p < 0.05$, ** $p < 0.01$, *** $p < 0.001$

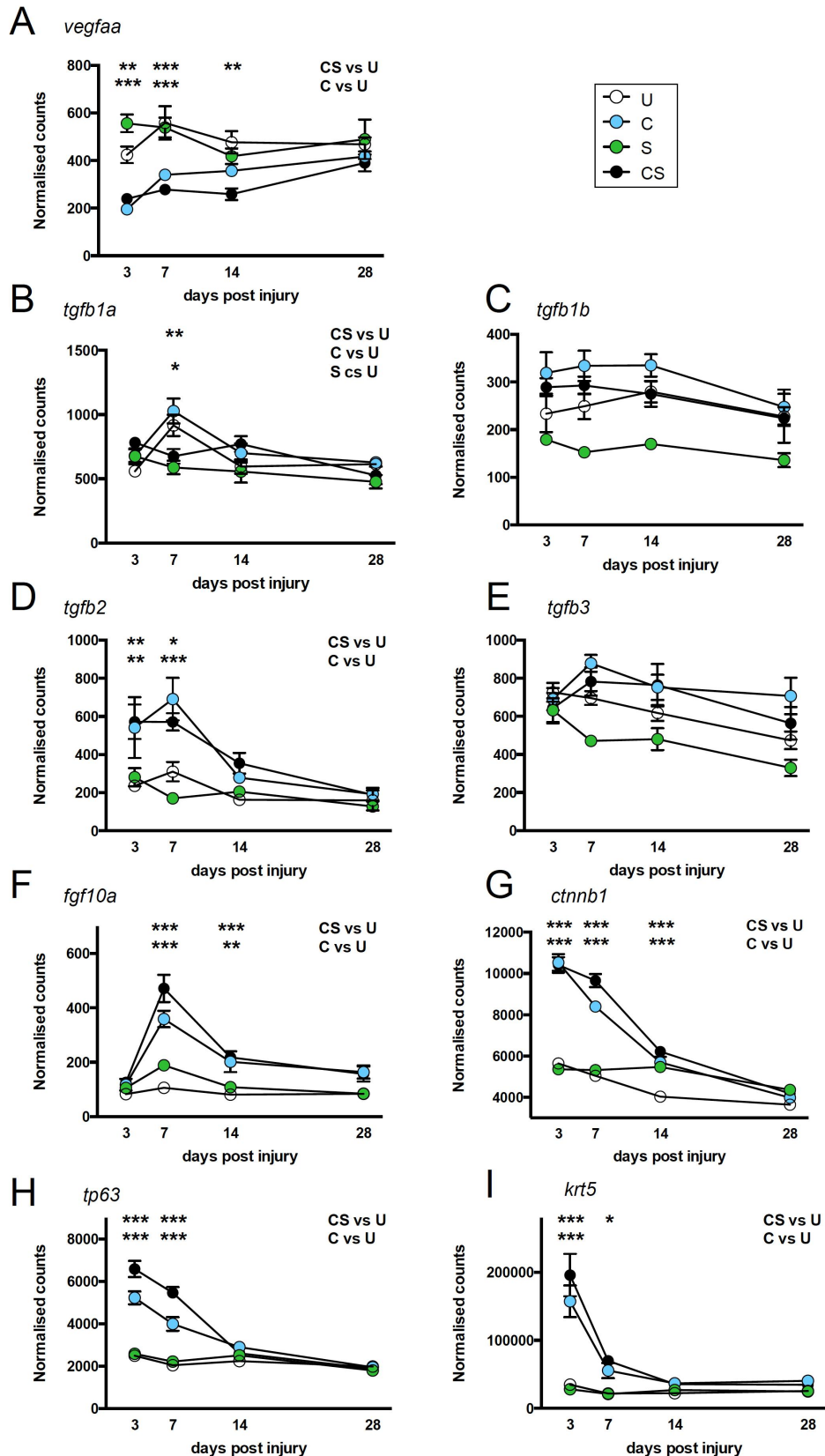


Fig. 4.26 Temporal profiles of example genes involved in lung repair processes.

(A-I) Samples of zebrafish gill tissue were analysed at 2 wpi following cryoinjury \pm silica. U = uninjured, untreated; C = cryoinjured, untreated; S = uninjured, silica; CS = cryoinjured, silica. Relative counts obtained by RNA-seq analysis are shown. Of note, the scale of the graph in (G) was adjusted to visualise the error bars. Statistical significant differences are indicated only for silica treated samples (S), the cryoinjury treated samples (C) and the cryoinjury + silica treated samples (CS) compared to the untreated uninjured group (U). Error bars = SEM. Two-way Anova. * $p < 0.05$, ** $p < 0.01$, *** $p < 0.001$

4.4 Summary

4.3.1. Acute exposure to silica induces transient neutrophilia, an increase in *illb* transcripts and caspase-1 activation in adult gill tissue. Acute exposure to smoke extracts results in a decrease in the numbers of myeloid cells and an increase in transcripts of the pro-inflammatory cytokines *illb* and *tnfa* in adult gill tissue. Together, these data suggest that both stimuli provoke acute inflammatory responses similar to those seen in mammalian lungs. Acute exposure to combined silica + smoke leads to a decrease in myeloid cells such as that seen following exposure to smoke only and a further increase in transcripts of pro-inflammatory cytokines *tnfa* and *illb*, significantly higher than following smoke only exposure.

4.3.2. Long-term exposure to silica, smoke and combined silica + smoke does not lead to chronic inflammation but induces gill tissue remodelling. However, neither treatment leads to collagen deposition at the protein level and fibrosis despite an increase in *coll1a1* transcripts transcript following silica exposure.

4.3.3. A single tissue wounding by cryoinjury induces an accumulation of myeloid cells and collagen-rich scars in zebrafish gills that repair over time. Continuous exposure to silica following cryoinjury appears to delay resolution of inflammation and wound-healing processes but does not induce fibrosis.

4.3.4. RNA-seq analysis of zebrafish gill tissues following injury was established as robust tool to perform large-scale transcript profiling. Preliminary analysis of the temporal expression profiles of selected transcripts revealed that mechanisms and signalling pathways known to be involved in mammalian reparative processes upon injury are partly conserved in zebrafish. The present dataset will facilitate comparative studies with mammalian wound healing processes in the future to study mechanism that lead to successful repair in zebrafish while similar injury results in detrimental fibrosis in humans.

4.5 Discussion

4.5.1 Conserved pathways of immune activation upon silica and smoke exposure

Acute exposure to silica particles

Lungs respond to inhalation of silica with an acute inflammatory response marked by neutrophil influx and release of IL-1 β by resident immune cells [65, 145]. Similarly, zebrafish exposed to silica rapidly mount an inflammatory response in their gills and exhibit increased neutrophil numbers and *il1b* transcripts suggesting that silica induces a pro-inflammatory response in the gills of zebrafish similar to that seen in mammalian lungs. In contrast to mice where increased neutrophil numbers can still be detected in the BAL by 18 hours following orotracheal silica instillation [65], in zebrafish neutrophilia appears to be transient as the number of neutrophils as well as *mpx* mRNA return to the same level as those of unexposed fish gills by 9 hours of treatment. The kinetics of neutrophil accumulation following silica is similar to that observed following tail transection through the zebrafish tail fin epithelium, where the peak in neutrophil recruitment is observed between 4-8 hpi [190]. Neutrophil accumulation following tail injury begins to resolve at 24 hpi and is fully resolved by 48 hpi [190]. A laser-inflicted wound of the adult zebrafish skin leads to neutrophil recruitment peaking at 18 hpi and resolving at 4 dpi [339]. Similarly, a cryoinjury induced neutrophil accumulation in the gill resolves around 7 dpi. These data are consistent with silica exposure causing only a mild irritation/ injury of the gill tissue.

Human peripheral blood mononucleated cells and mouse bone-marrow derived macrophages treated with silica secrete IL-1 β in an NLRP3-inflammasome-dependent way [63-65]. Pro-IL-1 β is not constitutively expressed in macrophages or monocytes, at least *in vitro*, and needs to be transcriptionally induced prior to treatment with silica. As for cholesterol-induced inflammasome activation and IL-1 β release [61], the delivery of the priming signal 1 is achieved through the pre-treatment of cells with the TLR stimuli LPS [63, 65]. Here, exposure to silica induces an increase in *il1b* transcripts and increases caspase-1 activity in adult zebrafish gills. Further, increased caspase-1 activity was observed in the larval gill area, which might potentially represent inflammasome activation in the epidermis of larval fish (19 dpf). Human, keratinocytes express AIM2

inflammasome components and cytosolic DNA can activate caspase-1 in psoriatic lesions [357]. Thus, although the exact inflammasome has not been identified here, there is a possibility that silica activates an inflammasome complex in zebrafish larval epidermis. Together, although the release of mature IL-1 β is yet to be confirmed, these data indicate that silica induces inflammasome activation *in vivo* in zebrafish gills without deliberate addition of a priming signal. As the gills are constantly exposed to the microbial-rich ambient water, there is a possibility that waterborne bacteria (*e.g.* paramecium etc.) constitutively provide signal 1 of inflammasome activation. Consistent with that notion, a high number of EGFP⁺ cells were detected in the gill tissue of untreated *Tg(NFkB:EGFP)* zebrafish, thus providing the pre-requisite signal 1 of inflammasome activation. Similarly, lungs are populated with an airway microbiota [32], which means that the resident bacteria could play a role in priming alveolar cells in human. In support of this hypothesis, Ichinohe *et al.* showed that antibiotic treatment in mice impaired pro-IL-1 β transcripts in lung tissue [299], although it is not clear which microbiota (*i.e.* from the intestine or from the lung) is responsible for delivering this priming signal.

The ability of macrophages to engulf silica particles and to induce inflammasome-dependent IL-1 β release has been demonstrated *ex vivo* in cells isolated from *Asc^{-/-}*, *Caspase1^{-/-}* and *Nlrp3^{-/-}* mice compared to WT littermates [63, 64], and it therefore has been suggested that silica induces inflammasome activation in alveolar macrophages. However, ASC is also constitutively expressed in human bronchial epithelial cells [358] and in mouse airway epithelial cells [57]. In addition, Influenza A infection leads to an increase in Nlrp3 transcription in these cells [57]. Further, infection of both the primary human airway epithelial cell line (HAE) and the human nasal airway epithelial cell line (JME) with Influenza A results in the release of IL-1 β [57]. Although alveolar macrophages have been suggested as main drivers of silica-induced inflammatory responses, there is a possibility silica particles could induce inflammasome activation in epithelial cells. Similarly, as in zebrafish the respiratory epithelium is the first barrier that encounters silica, it could be hypothesised that silica induces inflammasome activation and an increase in *il1b* transcripts in the gill epithelium. Consistent with this notion and consistent with NFkB activation in intestinal epithelial cells, the number of EGFP⁺ cells in untreated gills of *Tg(NFkB:EGFP)* was about 10 fold higher than the number of neutrophils and myeloid cells (GFP⁺ cells in *Tg(mpx:GFP)* and dsRed⁺ cells in *Tg(lyz:dsRed)* respectively). These observations suggest that the epithelial cells are the

source of constitutive NF κ B activation in mucosal tissues, such as the gills and the intestine. However, at least for the gills, the cellular localisation of NF κ B activation still needs to be confirmed. For that, the same approach as for intestinal cells could be carried out, *i.e.* co-labelling of dissected gill tissues with the cytokeratin antibody. Further, *Tg(NF κ B:EGFP)* crossed with *Tg(lyz:dsRed)* would allow quantification of NF κ B activation in myeloid cells. These approaches could be combined with the FLICA staining to determine the cellular origin of caspase-1 activity following silica.

Acute exposure to smoke extracts

Cigarette smoke extracts consists of a complex mixture of about 4,000 different compounds. Cigarette smoke exposure provokes an acute inflammatory response in mammalian lungs that is dependent on the MyD88 signalling pathway (TLR4/MyD88 and IL-1R1/MyD88) leading to high levels of pro-inflammatory cytokines such as TNF- α , IL-1 β and IL-6 [348]. This is consistent with cigarette smoke-exposed zebrafish gills which showed an increase in *tnfa*, *il1b* and *il6 (m17)* transcripts. These data suggest that smoke exposure leads to activation of similar inflammatory pathways as in mouse, although future experiments will have to be carried out to confirm the involvement of Myd88 and NF κ B in cigarette smoke-induced inflammation in zebrafish gills. For that, the *Tg(NF κ B:EGFP)* reporter line of NF κ B activation as well as the pharmacological inhibitor of NF κ B transcriptional activation NAI could be used [222].

Recently the activation of inflammasomes has been shown to be important for smoke-induced COPD in mice and humans [296]. The induction of caspase-1 activity in zebrafish gills following exposure to smoke could be assessed using FLICA.

Cigarette smoke exposure induces neutrophil accumulation in the bronchoalveolar space and pulmonary parenchyma of mice [348]. In contrast, zebrafish gills show a decrease in the number and transcripts of neutrophils and leukocytes. There is a possibility that smoke is toxic and induces leukocyte apoptosis or death. This idea is supported by recent findings suggesting that smoke exposure can induce the inflammatory form of cell death termed pyroptosis, which is caspase 1-dependent [296]. Various established assays testing for key events occurring during apoptosis and/ or cell death, *e.g.* TUNEL assay, Annexin V, mitochondrial membrane potential) could be used to test this hypothesis in zebrafish gills. This analysis could be performed in fluorescently labelled transgenic lines labelling different immune cells to gain cellular resolution of smoke-induced responses.

The fact that smoke exposure leads to an increase in pro-inflammatory cytokines but a decrease in the number of leukocytes raises the question of the cellular origin of these inflammatory mediators. As mentioned above, the respiratory epithelium has been shown capable of producing inflammatory cytokines and the immune signalling machinery within the epithelium contributes to inflammatory responses in the respiratory tract [57]. As in zebrafish the epithelium is likely to be the first cell type that encounters waterborne irritants, there is a potential that the respiratory epithelium contributes to the inflammatory mediators induced by cigarette smoke. Interestingly, combined silica + smoke treatment exacerbated pro-inflammatory cytokine expression while leukocyte numbers were again decreased. Together, these data indicate that an acute exposure for 6 hours to silica particles and/ or cigarette smoke results in different types of inflammatory responses in the gills of zebrafish similar to those seen in mammalian lungs.

4.5.2 Chronic exposure to irritants leads to tissue remodelling but no scarring

Persistent exposure to tissue irritants is implicated in chronic inflammation and the pathogenesis of pulmonary lung fibrosis [46, 145, 334]. The role of pro-inflammatory cytokines IL-1 β and TNF- α both in the onset and during the development of pulmonary fibrosis has been widely demonstrated [46]. In particular the role of IL-1 β in the pathogenesis of fibrosis seems to be two-fold. Firstly, it is a potent pro-inflammatory cytokine that attracts ROS-producing neutrophils, which in turn further damage the epithelium [46] and secondly, IL-1 β stimulates fibroblast proliferation and activation through promoting TGF- β production [46]. Humans with polymorphisms in the IL1Ra allele are more susceptible to silica-induced lung fibrosis [359]. The fact that *Il1b*^{-/-}, *Asc*^{-/-} and *Nlrp3*^{-/-} mice are more resistant to developing fibrosis demonstrates that the NLRP3 inflammasome and IL-1 β are essential for silica-induced fibrosis to occur [63, 344]. Further, a persistent accumulation of neutrophils is a hallmark of lung fibrosis. For instance, high numbers of neutrophils in BAL samples from IPF patients correlate with the rate of early mortality [360].

Given that acute exposure to silica and smoke and the combination of both provoked different acute inflammatory responses, all of which have been implicated with the pathogenesis of fibrosis in humans [147], zebrafish were treated chronically with these different stimuli. In contrast to humans, long-term exposure to treatments either individually or combined did not lead to fibrosis in zebrafish gills and no collagen

deposition could be detected. Long-term exposure of zebrafish gills to cigarette infused water resulted in gill tissue remodelling marked by mucus cell increase, tissue swelling and lamellar fusion, but key indicators of fibrotic events were absent. Indeed, it is well established that the latter processes occur as protective mechanisms of fish gills to reduce their vulnerable surface area and to increase the diffusion distance for toxic compounds [234]. These data are consistent with the hypothesis raised above that exposure to cigarette smoke is toxic to zebrafish gills. Fish showing lamellar fusion after 6 weeks had fully recovered by 4 weeks after the last cigarette smoke-exposure demonstrating again the great ability of fish to regenerate following tissue-damage. Long-term exposure of zebrafish to silica particles resulted in gill epithelial damage with slight increase of the pro-fibrotic marker *coll1a1* transcripts; however, no signs of excess collagen deposition could be detected at any time analysed. These data suggest that silica treatment initiates minor fibrotic responses at the mRNA level, but that these are somehow reversed / inhibited so that no collagen can be detected at the protein level. Proteases, especially MMPs, cleave assembled ECM proteins, such as collagen [146] and it would therefore be of interest to examine long-term silica-exposed fish gills for mechanisms limiting collagen deposition. Zebrafish treated with the combination of silica and smoke did not show an increase of collagen at the transcript level (as detected after silica only exposure). These results suggest that long-term smoke and silica treatments provoke opposing responses in fish gills. It would be interesting to understand which signalling pathways are activated by cigarette smoke and to investigate their relationship to fibrotic diseases.

Despite a pronounced acute inflammatory response following silica and/ or smoke exposure, chronic inflammation following long-term exposure was absent. This is in contrast to mammals, where exposure to these particular irritants has been implicated in chronic inflammatory conditions [147] and is used to induce COPD and fibrosis in mouse models [296, 344]. However, adaptive immune responses are yet to be characterised in these models of long-term exposure to irritants. This could be done in transgenic zebrafish lines available, such as *Tg(lck:EGFP)* [196], *Tg(rag2:EGFP)* [197] or *Tg(IgM1:EGFP)* [198], or using qRT-PCR analysis of adaptive immune cell marker transcripts or cytokines associated with adaptive immune responses. Adaptive immune responses could be involved in mediating gill tissue remodelling following chronic exposure to silica and/ or smoke. However, it seems unlikely that long-term exposure to irritants induces adaptive immune responses since transcripts of adaptive immune cell marker genes (*rag2* and *cd4*) analysed by RNA-seq were unchanged over the time-course analysed and *lck* transcripts

were decreased at 2 wpi in silica treated-fish compared to control gills. Together, these data suggest that zebrafish gills have mechanisms in place to avoid detrimental chronic inflammatory processes following exposure to irritants. Further, these yet unknown mechanisms that drive resolution of inflammation might also be responsible for preventing zebrafish gills from detrimental fibrosis.

4.5.3 Zebrafish heal without scarring following cryoinjury and/ or exposure to silica

In contrast to humans, zebrafish have a great capacity to heal wounds of complex organs such as the heart without leaving a scar [337, 338]. In this study, we performed cryoinjury on the adult gill tissue and monitored the wound healing process. Consistent with mammalian wounds, zebrafish respond to injury with an inflammatory response and the consequent tissue-remodelling phase, which results in a transient collagen rich scar [351]. In contrast to the healing process in mammals, zebrafish gills are not only able to resolve the scar but also to regenerate the architecture of the damaged tissue. These findings are consistent with wound healing studies performed on other complex tissues of the zebrafish where their great regenerative potential has been demonstrated. For instance, laser-inflicted wounding of zebrafish skin [339] and cryoinjury of the zebrafish heart lead to a transient collagen rich scar that is eliminated during the wound healing process [337-339].

These models of scarless healing after heart or tail injury have recently been exploited to explore pathways involved in regeneration [361-364]. Using genetic or pharmacological perturbations to interfere with their normal program of regeneration prevents the transient scar from resolving. However, the main aim of this study was to investigate whether fibrosis in zebrafish mucosal gill tissue can occur under physiological conditions without genetic or pharmacological perturbations. If zebrafish had developed fibrosis, potential anti-fibrotic drugs (provided by Boehringer Ingelheim) interfering with this process could have been tested in this model. Therefore, it was decided not to interfere with known processes of regeneration to induce scarring but rather mimic persistent tissue injury leading to fibrosis in mammals. Despite the fact that continuous exposure to silica significantly delayed the resolution of the wound healing process, zebrafish gills healed completely following cryoinjury without a permanent scar. A persistent presence of neutrophils and macrophages in cryoinjured + silica treated fish was observed during the tissue remodelling phase suggesting a role for these cells in the observed delay of healing. Fibrosis occurs when the repair process fails to terminate and the consequent ongoing wound healing process is driven by chronic inflammation [320]. This study provides

evidence that adult zebrafish gills do not develop either fibrosis or chronic inflammation following exposure to irritants and or tissue injury and apparently then zebrafish have mechanisms in place that promote resolution of inflammation thereby facilitating successful wound healing process in the absence of a non-removable scar. Indeed, these observations are consistent with injury studies performed in adult zebrafish brain demonstrating that leukocytes rapidly invade the wounded area following traumatic brain injury, but the initial inflammatory response resolves much faster than in mammals [365, 366]. Collectively, these data highlight potential differences between mammals and zebrafish in the regulation of the inflammatory response following injury. RNA-seq analysis was consequently carried out to gain further insights in the different wound healing programs in zebrafish compared to mammals and the role of inflammation.

4.5.4 Preliminary RNA-seq analysis reveals conserved mechanism of wound-healing between mammals and zebrafish

Most studies to understand wound healing in humans have been performed on the skin, which is easily accessible. Remarkably, the basic phases of wound healing upon injury are similar for all mammalian organ systems [351]. These major steps of wound healing, which include blood clotting, inflammation, new tissue formation, angiogenesis and tissue maturation, also occur in the zebrafish skin following laser injury [339]. However, whilst these repair mechanisms in mammals almost always lead to scarring, cutaneous wound healing in zebrafish occurs without a permanent scar [339]. Here, the results demonstrate that the major steps of wound healing also occur in the zebrafish gill following cryoinjury, while no permanent scar persists.

Inflammation

The coagulation, clotting and inflammatory responses upon wounding are rapidly induced to limit blood and fluid loss and protect the organism from invading pathogens [351]. These processes occur immediately after tissue damage and last only a few minutes/hours and days, respectively [351]. The RNA-seq analysis in this study performed at 3, 7, 14 and 28 dpi will not therefore address the early events following cryoinjury. Indeed, the temporal expression profiles of selected key inflammatory cell marker transcripts for innate and adaptive immune cells and pro-inflammatory cytokines are unchanged following cryoinjury ± silica within the time-frame analysed by RNA-Seq. These results were surprising in view of the presence of myeloid cells detectable by flow cytometry

analysis of gill tissues of *Tg(mpx:GFP)* at 2 wpi following cryoinjury. The *Tg(mpx:GFP)* has been generated using a bacterial artificial chromosome construct that has the GFP with more than 130 kb *mpx* upstream sequence [191]. Therefore it seems unlikely that the GFP transgene is under a different regulation as the *mpx* gene. Indeed, in experiments of acute exposure of zebrafish gills to silica the number of GFP+ cells correlated with the transcript levels of GFP suggesting that the GFP transgene expression is driven by the same regulatory elements as the *mpx* gene. Although unlikely, there is a possibility that there are negative regulatory elements that inhibit *mpx* mRNA expression under certain circumstances which are outside the promoter region used for the generation of the transgenic line. There is also a possibility that in these exact experiments the accumulation of myeloid cells following cryoinjury was less prominent and therefore not detectable any more during the time-frame analysed by RNA-seq. Indeed, although no statistically significant changes were detected over the time-frame analysed, *mpx* transcripts were higher at 3 dpi in cryoinjury ± silica treated fish when compared those left untreated.

Analysis showed the marker gene *csflra* (*fms*, macrophages) to have significantly increased transcript levels over time. This increase in *csflra* transcripts was significantly sustained at 14 dpi in fish that were treated with silica following cryoinjury potentially reflecting a delay in resolution of inflammation or a potential beneficial role of macrophages in wound healing. The causative relationship between inflammation and fibrosis has been a focus of scientific interest over many years [322]. In particular, the different macrophage subtypes (M1) and (M2) play critical roles during wound-healing and restoration of tissue-homeostasis following injury, but their detrimental role during excessive tissue repair and scarring has been suggested [46]. To date, the observation of functionally different macrophage subtypes in zebrafish has been elusive. However, specific markers for M1 (*e.g.* TNF- α and Nitric oxide synthase) and M2 (*e.g.* Arginase-I and Mannose receptor) macrophages are present in the zebrafish genome and some of them (*tnfa* and *arginase-I*) are expressed by L-Plastin+ leukocytes in zebrafish larvae [208]. Thus, the zebrafish might offer the potential of studying the influence of different macrophage subtypes to limit fibrosis. Further, ablation experiments could be carried out using transgenic zebrafish expressing a nitroreductase fusion protein that can metabolise the pro-drug metronidazole into a cytotoxic substance inducing cell death in transgene expressing cells. This approach has recently been applied to study the roles of macrophages and neutrophils during different stages of fin regeneration following

resection [329].

Interestingly, osteopontin has been associated with fibrosis in mammals, as it is up-regulated in association with the wound inflammatory response [367] and osteopontin knock-down leads to reduced scarring during repair processes [324]. Osteopontin transcript levels are induced in zebrafish gills throughout the wound-healing process despite the fact that zebrafish heal without a scar. There might be mechanisms in place that prevent detrimental effects of osteopontin during the wound-healing process. Together, these data support the hypothesis above that zebrafish have mechanisms in place to drive resolution of inflammation despite severe tissue damage or persistent exposure to irritants. Further analysis at earlier time-points following wounding will have to be carried out to characterise the inflammatory mediators and exact cell types involved in cryoinjury-mediated tissue damage.

New tissue formation and remodelling

As the RNA-seq analysis was performed at time-points that cover the later stages of wound healing including new tissue formation and tissue remodelling, genes known to be involved in these processes in mammals were anticipated to be involved. The main collagen types deposited following injury are collagen type I and type III [320, 351]. Consistently, transcripts of several collagen type I genes were induced following cryoinjury (e.g. *coll1a1*, *coll1a2*) as revealed by RNA-seq analysis which corresponded to detectable collagen deposition by histological analysis and PSR staining. Of note, zebrafish do not produce collagen type III (ZFIN) suggesting that there are differences in the composition of scar tissue between zebrafish and mammals, which might contribute to differences in the outcome of wound healing. Consistent with wound healing in mammals, zebrafish and salamander [320, 328, 361], fibronectin is induced in the zebrafish gills during the repair process. Both collagen type I and fibronectin are part of the ECM [320] and RNA-seq analysis revealed that *coll1a1* and *fn1a* mRNA show the same temporal expression profile. Zebrafish respond to cryoinjury with high levels of *mmp9* transcripts peaking at 7 dpi and returning back to baseline levels of uninjured fish by 14 dpi. Silica treatment prolongs this increase in *mmp9* transcripts resulting in a persistent significant difference between uninjured and cryoinjured zebrafish at 14 dpi. Prolonged MMP9 expression has been associated with fibrosis [316]. However, MMP9 is also expressed during repair processes of the lung [316]. Zebrafish apparently then respond to gill tissue injury in a similar fashion to mammalian lungs with an increase in *mmp9* transcripts

suggesting that this expression may restore the balance between ECM synthesis and catabolism preventing scarring. Cryoinjury also induced transcript levels of periostin, which significantly correlated with the severity of tissue damage. In the past periostin expression in the lung has been correlated with asthma, but more recently, periostin has been shown to promote lung fibrosis through myofibroblast proliferation and ECM deposition and therefore predicts disease progression in patients with IPF [368]. In zebrafish wound-healing/ regeneration studies [339, 349], *colla2* and *periostin* are routinely used as marker genes for fibroblasts. It follows that collagen production during gill tissue repair is carried out by fibroblasts/ myofibroblasts. However, as RNA-seq analysis revealed that these genes show different temporal expression profiles following cryoinjury, it can be suggested that fibroblasts change expression of these genes as they mature during wound healing or it is also possible that different fibroblast populations are involved in the repair processes (*i.e.* different types that co-exist in the gill tissue and/ or are recruited to the injury site). Indeed, it is possible that there are different fibroblast populations in different parts of the gills, *i.e.* the lamellae and the filaments. As different gill compartments become injured it is possible that these different temporal expression profiles mirror different responses in different compartments of the gill. *In situ* hybridisation of *colla2* and *postnb* could be performed to answer this question and to provide a spatial resolution of their expression.

Signalling pathways during wound healing

The key mediator of mammalian fibrosis is TGF- β [320]. In the current experiments cryoinjury induced changes the transcript levels of *tgfb2* in zebrafish gills during the time frame analysed. This result is in contrast to cryoinjury performed on the zbrafish heart tissue where the induction of all three *tgfb* genes is detected at 4 dpi using *in situ* hybridisation [361]. TGF- β is post-translationally activated through proteolytic cleavage of the latent TGF- β binding proteins, which explains why TGF- β gene expression often does not correlate with the presence of active TGF- β [320]. Therefore, to thoroughly characterise the involvement of the signalling pathway TGF- β isoform specific antibodies should be used.

Key signalling pathways involved in repair processes in the lung such as the Fgf and the Wnt/ β -catenin signalling pathways also seem to play a role in gill regeneration in zebrafish following cryoinjury. However, despite the fact that core components of these pathways are highly conserved during evolution, species-specific differences of these

signalling pathways are likely and might explain differences in regeneration versus fibrosis. Indeed, while these signalling pathways are critical during development of the mammalian lung [117], aberrant signalling in Wnt/ β -catenin pathway is implicated in fibrosis [355]. Similarly, interference with these pathways in zebrafish can lead to fibrosis. For instance, the importance of Fgf1 in regeneration after tail fin injury and heart cryoinjury in zebrafish [361-363] has been demonstrated by inhibition of Fgf1 using a chemical inhibitor (SU5402) [369]. This was confirmed by inhibiting *fgfr1* using a heat inducible dominant negative Fgfr1 transgenic zebrafish *Tg(hsp70l:dn-fgfr1)*, thereby blocking regeneration [362, 363]. A role for TGF- β /Activin signalling during fin and heart regeneration after wounding has been demonstrated using a chemical inhibitor (SB431542) [361, 364]. Interestingly, despite the fact that both pathways are essential for regeneration, only inhibition of *fgfr1* resulted in a persistent collagen rich scar whereas interference with the TGF- β /Activin signalling pathway resulted in the failure to deposit a collagenous matrix [361]. Similar approaches could be used to characterise the involvement of signalling pathways in wound healing processes in zebrafish gills.

Neovascularisation

As cryoinjury \pm silica induces expression of *vegfaa*, it can be suggested that angiogenesis occurs upon injury of adult gills. To confirm this idea, future work could make use of the transgenic zebrafish line *Tg(fli1:EGFP)* [370] in which the endothelium is fluorescently labeled, to visualise angiogenesis upon cryoinjury *ex vivo* using histological analysis or *in vivo* using fluorescence microscopy.

Stem cells and blastema

Wound repair of complete organ systems in amphibians occurs through the formation of a blastema, which is a mass of undifferentiated cells capable of regeneration and differentiation into multiple cell types [351]. The zebrafish tail also regenerates through formation of a blastema [369], while zebrafish heart regeneration has been explained through cell division from differentiated and undifferentiated progenitor or stem cells [349]. How the zebrafish gill regenerates following severe tissue damage is unknown. As cryoinjury induced a significant increase in the expression of the blastema marker gene *msxb* [369] and genes that mark airway progenitor cells in mammals (*tp63* and *krt5*) [117], regeneration of gill tissue following cryoinjury can be explained through both blastema formation and differentiation of progenitor populations. Indeed, little is known about the

exact cellular and molecular mechanisms of regeneration [351] and it is likely that both processes contribute to gill tissue regeneration. Understanding the responses that occur during the regeneration of complicated structure in zebrafish may provide novel insights which could be applied to promote tissue and organ regeneration in humans.

Collectively, these data suggest that key stages and mechanisms of wound healing are conserved between mammals and zebrafish. Further, the preliminary RNA-seq results confirm overall similarities to wound-healing processes in mammalian lungs and highlight the relevance of the models of gill tissue injury established in this project for comparative analysis with mammalian wound healing. Thus, these models offer the potential for identification of signalling pathways and mechanisms that lead to successful wound healing in zebrafish.

Drawbacks of RNA-seq analysis

Despite the fact that the RNA-seq data seems robust, there are also a few unexpected results that were noted and a few choices of the experimental set-up that might hamper future analysis.

Firstly, the fact that silica treatment significantly induced expression of genes associated with catalytic activities in the preliminary RNA-seq analysis at 2 wpi but not in the time course experiment is still puzzling. Similarly, there was a surprisingly low degree of overlap of significantly differentially expressed genes between the RNA-seq time-course analysis at 2 wpi compared to the preliminary experiment. One could argue that the effect of silica in the time-series was not as pronounced as in the preliminary experiment. However, phenotypic analysis of the gill tissue that was treated with a combination of cryoinjury + silica show similar results as those previously observed and these samples exhibited similar gene expression at 2 wpi. Together these results indicate that it is important to perform independent experimental repeats to reliably draw any conclusions from the results obtained. Therefore the time-course experiment should be repeated and samples analysed either by RNA-seq or by qRT-PCR of selected genes.

Secondly, one pitfall of the current RNA-seq analysis is the fact that no time-point zero was included, *i.e.* fish that were completely uninjured. This is of particular importance as it was also noted that a number of genes significantly changed over time in the control group that was left untreated and uninjured on one gill side. This change in expression could be explained by the fact that the samples were harvested several days and weeks apart and

might reflect ongoing developmental changes. However, it seems unlikely that genes dramatically change expression at steady state in adult zebrafish. There are genes that exhibit circadian rhythmicity of expression which might explain the different temporal expression patterns observed, but all samples were harvested at the same time during the day to minimise these effects. As the untreated uninjured samples originated from a fish that received a cryoinjury on the other gill side, there is a possibility that the unilateral injury induce systemic responses or specific processes in the uninjured gill tissue. Despite the fact that the fish showed no abnormal breathing behaviour following cryoinjury, it is possible that unilateral cryoinjury would alter gene expression of the uninjured gill side to some extent, as the uninjured gill side had to fulfill all the oxygen requirement. Further, it is also possible that the compromised gill epithelial barrier following cryoinjury is more prone to infections which could result in systemic inflammation. The reason for the experimental design chosen was to avoid variability between samples by having a control tissue of the same individual that would allow correlation of gene expression between treated and untreated for each individual fish. However, since there was low variability in gene expression of samples within one treatment group, this experimental set up might not be necessary and in future fish could be treated separately. In fact, it would be interesting to assess in detail which genes change expression in the untreated samples over time to clarify whether these changes are induced by the injury on the other side or not. This analysis might challenge other gene profiling studies where a single time-point zero is routinely used as control and calibrator.

Future direction

The results discussed above are preliminary and further systematic analysis is required to determine pathways involved in gill repair processes and their relevance to mammals in an unbiased manner. Thus far only simple statistical procedures were used to determine the significance of over- or under-expressed genes and their fold change compared to the uninjured untreated samples. These techniques are useful to identify differentially expressed genes at particular time-points but do not take into account the temporal aspect of gene expression. Therefore, several steps are planned for the future analysis of this RNA-seq time-series dataset. Firstly, clustering will be performed to reveal particular patterns of expression. This analysis will aid the unbiased identification of early and late responsive gene targets. It is possible that those genes driving resolution of inflammation and/ or preventing scarring are differentially expressed at later time-points following

cryoinjury and potentially even later in cryoinjury + silica treated fish. However, it is also likely that these genes are expressed at similar time-points to those involved in the final steps of wound healing. Thus, it will be difficult to identify these mediators of successful wound healing solely based on typical clustering analysis. Therefore, secondly, pathway-based analysis will be carried out to infer biological responses from the different temporal expression profiles. Since about 30% of genes identified in zebrafish are not yet annotated, the pathway analysis could be done in combination with a comparative analysis between zebrafish and mammals to predict putative mammalian orthologues in zebrafish based on protein and sequence homology. Thirdly, an extensive comparison of altered gene expression with datasets available at Boehringer Ingelheim is planned to identify mechanisms that lead to successful wound healing in zebrafish while causing scarring in mice. However, the relevance of this comparison to human fibrosis is questionable since mice do not exhibit the truly progressive nature of fibrosis and, like zebrafish, often only form a transient scar that resolves over time [181, 371, 372]. Therefore, datasets available in the literature of human repair processes following injury will be compared with the present datasets to further investigate the similarities in repair processes between zebrafish and humans and to reveal potential differences. However, this analysis will be difficult to perform as a dataset suitable for this comparison would have to be identified, *i.e.* similar tissue, similar time-points following injury etc. Although not ideal, comparisons could also be performed with datasets available from human dermal wound healing processes, since key repair pathways are conserved between different organs [351].

It will be important to clearly define the scientific question and to carefully choose a strategy to perform the bioinformatics analysis. Recently, two large-scale comparative analyses of inflammatory diseases between mouse and humans drew much attention not only from researchers but also from the mass media and the general public [373, 374]. Both studies used the exact same gene expression datasets of inflammatory conditions (trauma, burns and endotoxemia) from humans and mice for a comparative analysis, but came to completely opposite conclusions: whilst Seok *et al.* concluded that mouse models poorly mimic human inflammatory diseases [373], Takao *et al.* concluded that the genomic responses between these two organisms greatly correlate [374]. The opposite outcomes were due to different strategies of selecting the differentially expressed genes they used for the comparison and the different statistical tests used to perform these studies. Hence, it is crucial to define an analysis strategy in an unbiased manner and carefully put the results in context of the question to be answered.

The ultimate goal of this project is to identify specific pathways and genes that are differentially expressed in fish and mammals, offering potential new drugable targets. Following extensive bioinformatics analysis proposed above, *in situ* hybridisation will be carried out to validate identified target genes and reveal spatial resolution to determine which cells and tissues express these particular genes. Finally, identified pathways and genes will be validated *in vivo* by altering their expression and testing for modified outcomes of injury and/or irritants. For these experiments mutant fish available from ZFIN or pharmacological inhibitors could be used. If neither of these is available, targeted gene disruption will be carried out using TALENs or the CRISPR-Cas system [183, 184]. Lastly, identified genes will be validated in mouse models of fibrosis to confirm their relevance to modify fibrotic responses in mammals.

4.6 Conclusion

In this chapter, several models of mucosal injury in zebrafish gills were developed which allowed the study of inflammatory, wound healing and remodelling responses after exposure to irritants and/ or physical injury. Despite the fact that both exposure to irritants and physical injury provoked an inflammatory response and induce remodelling responses, zebrafish gills regenerate and do not develop fibrosis. Preliminary analysis of time series gene expression profiling by RNA-seq of gill tissue following tissue injury demonstrates that the zebrafish gill models of mucosal injury developed in this study represent valuable tools for studying mechanisms of wound-healing versus fibrosis and facilitate a comparative analysis with human wound-healing pathologies in the lung potentially allowing the identification of to new drug targets.

Chapter 5

Final discussion

Chapter 5 | Final discussion

5.1 Significance of the study and key findings

The continuous emergence of new animal models has been driven by an urge to better understand the pathogenesis of mucosal inflammatory diseases and the clinical imperative to find new treatments. Rodent animal models of mucosal inflammatory conditions have contributed much to our understanding of the mechanisms of disease pathology and they are indispensable tools to evaluate different therapeutic options. However, the failure of almost all promising drug candidates to translate into clinical success [47, 66, 137] raises questions over the validity of these animal models for the investigation of human mucosal inflammatory diseases.

Whilst rodent models have undoubtedly provided much of the conceptual framework regarding the involvement of adaptive immune responses as critical drivers of these conditions [91, 96, 121, 122, 167-169], modulation of these responses is not sufficient to effectively treat mucosal inflammatory disease [47, 127, 130, 137]. In fact, a better understanding of the exact disease aetiology is needed to treat these conditions in the future. The recent advances in sequencing techniques have provided new genomic information and the discovery of susceptibility genes through systematic interpretation of genome-wide signatures in human diseases [373, 374]. Various genes involved in PRR signalling and epithelium integrity have been associated with susceptibility to mucosal inflammatory diseases in humans [59, 66, 172, 375]. Indeed, it is becoming increasingly evident that innate immune recognition within the mucosal epithelium is considerably more relevant to mucosal inflammatory conditions of the lung and the intestine than originally envisaged [48, 50-53, 57, 58]. However, functional and mechanistic studies to understand the contribution of these susceptibility genes to mucosal disease are difficult and laborious in rodents and mostly carried out *ex vivo* from isolated primary cells. Thus, there is a need to explore alternative animal models that allow the study of mucosal inflammatory diseases *in vivo*, in an intact organism. Over the last decades, zebrafish has proven an attractive model organism to study aspects of human inflammatory processes [186, 256, 376, 377]. Particularly in recent years, the zebrafish has demonstrated its validity in the study of early inflammatory signals to tissue injury that are conserved in

mammals. For instance, signals that initiate immune cell recruitment to damaged epithelial tissues (H_2O_2 , redox and the Src family kinase Lyn) [378-380] and those that dampen the inflammatory responses (myeloperoxidase of neutrophils) [381] were all discovered in zebrafish. Importantly, the basic composition of mucosal epithelial tissues and molecular pathways are conserved between zebrafish and mammals [187, 188, 190, 191, 206, 207, 212-216, 218, 222, 225-227, 229-231, 233, 234, 236, 238, 242, 250-253, 256, 261, 262, 310, 382]. In the experiments described in this thesis, zebrafish was further explored as a physiologically relevant model to discover and to study mechanisms involved in acute and chronic mucosal inflammatory responses.

The first significant finding was that dietary cholesterol activates the inflammasome in intestinal epithelial cells, which results in immune cell accumulation in the short term and functional impairments of the intestine in the longer-term. These findings confirm the suggestions of previous studies in mice that innate immune recognition within intestinal epithelial cells can contribute to inflammatory conditions of the intestine [50-53, 58]. Thus, this part of the project not only consolidates previous studies in the validity to use zebrafish as a model to study aspects of intestinal physiology and inflammation [222, 233, 251-253, 259, 262, 267, 383], but also demonstrates how zebrafish can be used as a valid tool to discover mechanisms that contribute to intestinal inflammation.

The second significant finding of this study was that zebrafish gills do not develop chronic inflammation or fibrosis despite extending exposure to irritants and/ or severe tissue injury. These results not only confirm previous studies in zebrafish investigating inflammation and wound-healing in different organs such as the brain, the heart, the skin and the tail fin [190, 191, 329, 336, 337, 339, 341, 349, 364-366, 369], but highlight for the first time the relevance of the adult zebrafish gills to explore mechanisms involved in inflammation and tissue remodelling of the mammalian lung.

5.2 Future work

Zebrafish as a tool to gain functional insights in mucosal inflammatory diseases using genome editing

Given the high degree of conservation at the sequence and proteome level between mammals and zebrafish [382, 384] and in particular of genes involved in innate immune recognition [213-215], zebrafish offer the potential to further help the discovery of the

aetiology of mucosal inflammatory disorders. Therefore, here I propose that zebrafish could be an ideal organism to complement mammalian animal models in the study and verification of susceptibility genes and affected pathways identified from GWAS in a high-throughput manner.

One drawback of the zebrafish model has been the lack of easily applicable loss-of-function-techniques; apart from the injection of MO into zebrafish embryos where a transient knock-down of target genes can be achieved up to about 5 dpi [182]. Zinc finger nucleases have been employed [385], but their usefulness has been limited by variations in their different degrees of specificity and off-target toxicity [336, 386]. More recently, the development of TALENs and the CRISPR-Cas system has enabled directed creation of zebrafish gene mutations [183, 184]. However, these techniques are still laborious and so far do not facilitate conditional and tissue-specific gene targeting. In the meantime, to overcome these challenges and to study the function of a gene of interest, researchers still rely on pharmacological or heat shock-inducible dominant negative approaches [362, 363]. Our MO-based technique of selectively inducing target gene knock-down in intestinal epithelial cells might offer the possibility of studying the involvement and mechanisms of PRR signalling at mucosal barriers in a high-throughput manner. However, there is certainly more research needed to fully validate this approach. For instance, the mechanism and kinetics of MO entry, the potential sub-type of epithelial cells that take up the MO and the effect of MO treatment on other cells and tissues need to be investigated. The possibility to knock down target genes in the gill epithelium using this technique could be explored. MO added to the water as performed in experiments with free-swimming larvae is financially not feasible. To overcome this, different delivery techniques could be explored, such as localised application of MO potentially under mild anesthesia that allows survival of fish or injection into the retro-orbital venous sinus of zebrafish. Although the latter has not yet been used to specifically target the zebrafish gills, from an own experience and published literature [387] it seems that fluorescent compounds injected retro-orbitally into zebrafish are directly transported through the bulbus arteriosus into the gills before being distributed throughout the organism [388]. As the gills are rich in capillaries that are in close proximity of the respiratory epithelium, there is a possibility that the gill tissue could be targeted this way. Together, these techniques might have the potential to alter gene expression in a conditional and tissue-specific manner and if established might be of great use to the wider zebrafish community. However, there is emerging criticism of the use of MO in general, most notably due to off-target effects

[389]. Thus, extensive controls are essential, such as non-overlapping MOs yielding identical phenotypes or mRNA rescue. As the latter control is not possible using our delivery technique, the loss of function phenotype should eventually be established independently [390]. Therefore, to facilitate gene targeting in a conditional and tissue-specific manner in the future, a potential approach could be to adapt the recently established ability of inserting site-specific compatible loxP sites targeting a gene of interest using TALENs [391] and combine these with suitable Cre transgenic zebrafish, some of which are already available [258]. In summary, using recent advanced techniques, zebrafish certainly have the potential to discover mechanisms of mucosal inflammation and contribute in defining the function of genes associated with the susceptibility to these conditions.

Zebrafish as a tool to gain “visible” insights in mucosal inflammatory diseases using in vivo microscopy

In addition to the use of zebrafish to perform functional studies, they offer key advantages over rodents to gain insights in the mechanisms of mucosal inflammatory processes using microscopy techniques. This is of particular relevance in view of some key questions that still remain unanswered in the field of mucosal immunology research, as the mucosal organs in rodents are in internal and not easily accessible for *in vivo* imaging. In contrast, the gills of zebrafish are readily exposed to the outside environment and the availability of transparent mutants allows the study of the gastrointestinal tract *in vivo*, even into adulthood.

Higher numbers of macrophages and dendritic cells are found in mucosal organs of patients suffering from IBD and pulmonary inflammatory diseases [1, 2, 45, 47, 66, 72, 96, 138]. The same is true for animal models of these conditions. The two cell types are thought to contribute to pathologies, but whether they are recruited to sites of injury and infection or whether the increase in number reflects a change in resident myeloid cell populations is not yet established in great detail [1, 2, 146]. Similarly, as demonstrated in this study, zebrafish respond to inflammatory stimuli with an accumulation of inflammatory cells to sites of exposure, such as the intestine and the gills. However, it is still unclear whether these cells are recruited to injury sites or whether the increase in leukocyte numbers upon exposure to irritants reflects cells that are retained and/ or activated. Further, the fate of these inflammatory cells is unclear, *i.e.* are they cleared by apoptosis, do they leave the site of injury and if they do so, where do they go? For instance,

CXCR4^{high} neutrophils have been shown to home back to the bone marrow instead of being cleared by apoptosis as originally assumed [392]. Here the zebrafish offers a variety of tools that could be used to elucidate the fate of inflammatory cells. For instance, transgenic zebrafish expressing photo-convertible fluorescent proteins could be used to image and track neutrophils (*Tg(mpx:Dendra2)* [393]) and macrophages (*Tg(mpeg1:Kaede)* [194]) locally in the intestine consequent to HCD or in the gills following exposure to silica and/ or cryoinjury. Although, M1 and M2 macrophage polarisation in zebrafish is yet to be addressed, the heterogeneity of the macrophage cell population could be delineated using single-cell lineage tracing experiments in the recently developed Zebrabow lines [394] that are based on the Brainbow technology [395]. Further, the Dallman lab is currently developing Förster resonant energy transfer-biosensors to map biological processes involved in mucosal inflammation, such as apoptosis and inflammasome activation, *in vivo*. Using advanced imaging techniques such as FLIM and optical projection tomography [345, 346], these biosensors should theoretically allow the dissection of molecular interactions in the complex mucosal tissue at the whole organismal level in real time. Further, the possibility of 2nd harmonic imaging to allow for detection of changes in collagen distribution in the gill tissue following cryoinjury ± silica exposure could be explored [301]. Thus, together with the progressing development of new imaging techniques, the zebrafish has advantages over rodent models to obtain high-resolution information of biological processes at mucosal barriers *in vivo*.

Understanding inflammation and wound healing in zebrafish to identify mechanisms of resolution of inflammation and scar removal

The results of this study demonstrate that zebrafish gills do not develop chronic inflammation or fibrosis in their gills, which is consistent with previous studies reporting similar observations in other organs such as the brain, the heart, the skin and the tail fin [190, 191, 329, 336, 337, 339, 341, 349, 364-366, 369]. Together, these results raise the hypothesis that zebrafish generally do not develop persistent and progressive inflammation. In contrast, the larval zebrafish intestine showed persistent accumulation of myeloid cells following extended HCD, however, key features of chronic IBD such as pro-inflammatory cytokines, decreased number of goblet cells and altered intestinal structure are absent. Therefore, although the integrity of the epithelial barrier still needs to be investigated, it remains unknown whether the sustained accumulation of leukocytes following extended HCD really correlates with chronic inflammation. Although there was a clear correlation

between the number of leukocytes in the intestine and the severity of the functional impairment and although this impairment was dependent on inflammation, the exact mechanisms leading to impaired intestinal peristalsis following extended HCD need to be investigated. Further, whether extended HCD leads to persistent immune cell accumulation in adult zebrafish remains to be defined. It could be argued that at the larval stage the immune system of zebrafish is not fully developed and therefore mechanisms that inhibit chronic inflammation from occurring during adult stages might depend on the presence of an adaptive immune system. It is also unknown whether zebrafish regenerate even severe intestinal epithelial destruction induced by DSS or TNBS treatment [250-253]. Thus, further investigations are required to answer these remaining questions regarding inflammation and regeneration within the intestine. However, given the observations from the gills and other tissues it can be speculated that even in the intestine, zebrafish will not develop chronic inflammation and will recover even from severe tissue destruction.

Thus, understanding the similarities and differences between zebrafish and humans may help identifying new candidate genes and pathways involved in driving detrimental pathologies in mammals.

Zebrafish as a model to facilitate integrated multi-organ analysis of systemic pathophysiological responses

Lastly, the developed models of mucosal inflammation and wound healing in the intestine and in the gills respectively offer the possibility of integrated multi-organ analysis of pathophysiological responses, which should undoubtedly be the focus of future research. Indeed, there is emerging evidence that life-style choices have impacts beyond the directly affected tissues. For instance, smoking has been linked to IBD [128], and conversely, the dietary fiber content and the resulting SCFAs produced by the intestinal microbiota have been shown to influence the susceptibility to asthmatic airway inflammation [164]. Similarly, intestinal inflammation leading to leaky barriers, subsequent translocation of bacterial products and systemic endotoxemia [269, 396] might influence the inflammatory status of the lungs. Indeed, high plasma endotoxin levels in rats achieved by intraperitoneal injection of LPS have been shown to activate NF κ B in the lungs [397]. Given that a cholesterol enriched-diet can induce intestinal inflammation, it would be interesting to investigate the influence of an HCD on inflammation and wound-healing responses in the gills. Similarly, how does an on-going wound-healing process in the gills or smoking affect the intestinal pathologies following acute and extended HCD? Although it is likely that

smoke exposure in zebrafish is systemic due to the means of smoke administration directly to the water, the zebrafish still allows the study of different stimuli within different mucosal organs on the ability of the individual to respond to infection, injury and inflammation. Further, although the bacteria that colonise zebrafish gills are probably different at the molecular level compared to a specific airway microbiota in humans [32], the fundamental principles and pathways involved in responses towards these microorganisms are conserved in zebrafish.

Further, it would be interesting to assess the effect of an acute inflammatory response due to an HCD or exposure to irritants on the overall immune fitness of the organism, *e.g.* the ability to respond to infection. Similarly, the dramatic increased occurrence of mucosal inflammatory disease in the last decades has been linked to changes in diet, the microbiota and exposure to irritants [18, 129, 146, 270]. However, the level of stress is also constantly on the rise and adverse life events, chronic stress and depression have been linked to intestinal pathologies [66], although the mechanisms are far from being understood. Here the zebrafish is an ideal model to combine several parameters such as various types of injury within different mucosal organs and assess the effect of stress on inflammatory outcomes. Further, the behavior of fish could easily be analysed to determine their level of stress they are experience [398].

In summary, I suggest that the zebrafish offers a valuable complement to rodent animal models in the study of the mechanisms that drive mucosal inflammatory conditions. With a particular focus on the innate aspects of mucosal inflammatory diseases including immune recognition at mucosal barriers, the zebrafish will hopefully aid definition of the basic molecular steps involved in disease aetiology. However, bearing in mind that zebrafish do not appear to develop chronic inflammation that is characterised by a diverse range of adaptive immune effectors as seen during mucosal inflammatory pathologies in humans [91, 96, 121, 122, 167-169], it might be reasonable not to try to mimic all aspects of the human disease in zebrafish. Thus, the question remains as to what really constitutes a good animal model for mucosal inflammatory diseases that will provide translational potential to humans.

5.3 Implications and future directions

Current animal models mainly attempt to recreate the entire pathogenesis of human mucosal pathologies, but a comprehensive genomic characterisation of patients has only recently become possible since the development of sequencing techniques. Therefore, to fully achieve the potential benefits of an immunological understanding for human well-being, more emphasis needs to be placed on human studies as it is key to learn more about these conditions from patients directly. For that, more GWAS, gene expression profiling of directly affected tissues, systematic reviews and meta-analysis need to be performed to identify novel susceptibility genes and disease-altered pathways. However, with regards to human data there are caveats yet to overcome. Firstly, as sampling of mucosal tissues in humans is difficult, there is often a lack of control tissues from truly healthy individuals. Further, inflammation as well as the microbial composition of mucosal tissues shows spatial heterogeneity, which are likely result in different gene expression profiles. Moreover, gene expression analysis of tissues from patients with advanced disease pathology might not aid to uncover disease aetiology. Thus, gene expression analysis of patients could be performed in combination with information about the patients' life-styles (*e.g.* smoking, occupational exposure to lung tissue irritants, diet, etc...) and the microbial composition of their intestines and lungs, which are unique to each individual.

Since almost every drug candidate for mucosal inflammatory diseases exerts its function at the molecular level, translational success of preclinical investigations depends on whether the behavior of key genes and intracellular pathways can be replicated in the chosen animal models, and the ability to do so could prove useful quality control criteria. Identified susceptibility genes and disease-altered pathways could therefore be used to decide on the validity of an animal model at the molecular level in addition to the phenotype and serve as a guide to recapitulate the complexity of human conditions. Hence, animal models should be critically evaluated, revised accordingly and those identified that most faithfully mimic human mucosal inflammatory diseases.

Even popular models have clear limitations that are often ignored. For instance, mice exposed to bleomycin might show initial signs of scarring, however, they recover and do not even develop fibrotic pathology [181, 371, 372]. Further, the epithelial injury induced by DSS or TNBS in mouse colitis models does not represent IBD pathology and may therefore not be physiologically relevant [399]. In fact, it is becoming increasingly apparent that current rodent animal models of mucosal inflammatory diseases lack the

chronicity and progressive nature characteristic of those conditions in humans [47, 137, 181]. These observations not only suggest possible discrepancies in the exact disease pathology between rodents and humans but also open up new questions as to whether mucosal inflammatory conditions are purely human diseases. Yet, the ease with which these animal models allow the study of ‘potential’ disease mechanisms leads to the fact that their limited translational potential is often overlooked. A greater understanding of disease aetiology and pathology is needed to critically re-evaluate existing animal models of human mucosal inflammatory diseases.

To conclude, to tackle human mucosal inflammatory diseases it is firstly key to learn more about these conditions from patients directly, secondly to identify disease aetiology potentially with the help of the zebrafish model organism and lastly not to overrely on current mouse models but rather try to revise them accordingly or develop new animal models that better mimic disease pathology to allow drug testing. Here, recent advances on whole organ *in vitro* set-ups, such as the development of synthetic reconstructed human lung tissues [400] that can even be made up from human primary cells [401], might represent a further promising complement to animal models with the potential of high through-put candidate drug screening.

This thesis therefore ends with the proposal that multi-disciplinary approaches combining knowledge from patients and research animals together with a more critical attitude towards the development and use of animal models will help translational applications for patients suffering from mucosal inflammatory diseases.

Bibliography:

1. Holt, P. G., Strickland, D. H., Wikstrom, M. E., Jahnsen, F. L. (2008) Regulation of immunological homeostasis in the respiratory tract. *Nat Rev Immunol* 8, 142-152.
2. Maloy, K. J. and Powrie, F. (2011) Intestinal homeostasis and its breakdown in inflammatory bowel disease. *Nature* 474, 298-306.
3. Cone, R. A. (2009) Barrier properties of mucus. *Advanced drug delivery reviews* 61, 75-85.
4. Frey, A., Giannasca, K. T., Weltzin, R., Giannasca, P. J., Reggio, H., *et al.* (1996) Role of the glycocalyx in regulating access of microparticles to apical plasma membranes of intestinal epithelial cells: implications for microbial attachment and oral vaccine targeting. *The Journal of experimental medicine* 184, 1045-1059.
5. Johansson, M. E., Phillipson, M., Petersson, J., Velcich, A., Holm, L., *et al.* (2008) The inner of the two Muc2 mucin-dependent mucus layers in colon is devoid of bacteria. *Proc Natl Acad Sci U S A* 105, 15064-15069.
6. Johansson, M. E., Sjovall, H., Hansson, G. C. (2013) The gastrointestinal mucus system in health and disease. *Nature reviews. Gastroenterology & hepatology* 10, 352-361.
7. Ehre, C., Worthington, E. N., Liesman, R. M., Grubb, B. R., Barbier, D., *et al.* (2012) Overexpressing mouse model demonstrates the protective role of Muc5ac in the lungs. *Proc Natl Acad Sci U S A* 109, 16528-16533.
8. Koslowski, M. J., Beisner, J., Stange, E. F., Wehkamp, J. (2010) Innate antimicrobial host defense in small intestinal Crohn's disease. *International journal of medical microbiology : IJMM* 300, 34-40.
9. Bals, R. (2000) Epithelial antimicrobial peptides in host defense against infection. *Respiratory research* 1, 141-150.
10. Tenner, A. J., Robinson, S. L., Borchelt, J., Wright, J. R. (1989) Human pulmonary surfactant protein (SP-A), a protein structurally homologous to C1q, can enhance FcR- and CR1-mediated phagocytosis. *J Biol Chem* 264, 13923-13928.
11. Wright, J. R. (2005) Immunoregulatory functions of surfactant proteins. *Nat Rev Immunol* 5, 58-68.
12. Tsukita, S., Furuse, M., Itoh, M. (2001) Multifunctional strands in tight junctions. *Nat Rev Mol Cell Biol* 2, 285-293.
13. Hartsock, A. and Nelson, W. J. (2008) Adherens and tight junctions: structure, function and connections to the actin cytoskeleton. *Biochim Biophys Acta* 1778, 660-669.
14. Shen, L., Weber, C. R., Raleigh, D. R., Yu, D., Turner, J. R. (2011) Tight junction pore and leak pathways: a dynamic duo. *Annu Rev Physiol* 73, 283-309.
15. Turner, J. R. (2009) Intestinal mucosal barrier function in health and disease. *Nat Rev Immunol* 9, 799-809.
16. Masson, C. J., Plat, J., Mensink, R. P., Namiot, A., Kisielewski, W., *et al.* (2010) Fatty acid- and cholesterol transporter protein expression along the human intestinal tract. *PLoS One* 5, e10380.
17. Yu, L., Bharadwaj, S., Brown, J. M., Ma, Y., Du, W., *et al.* (2006) Cholesterol-regulated translocation of NPC1L1 to the cell surface facilitates free cholesterol uptake. *J Biol Chem* 281, 6616-6624.

18. Sekirov, I., Russell, S. L., Antunes, L. C., Finlay, B. B. (2010) Gut microbiota in health and disease. *Physiological reviews* 90, 859-904.
19. Nell, S., Suerbaum, S., Josenhans, C. (2010) The impact of the microbiota on the pathogenesis of IBD: lessons from mouse infection models. *Nature reviews. Microbiology* 8, 564-577.
20. Hooper, L. V. (2004) Bacterial contributions to mammalian gut development. *Trends Microbiol* 12, 129-134.
21. Hooper, L. V. and Gordon, J. I. (2001) Commensal host-bacterial relationships in the gut. *Science* 292, 1115-1118.
22. Hooper, L. V., Wong, M. H., Thelin, A., Hansson, L., Falk, P. G., *et al.* (2001) Molecular analysis of commensal host-microbial relationships in the intestine. *Science* 291, 881-884.
23. Hooper, L. V., Midtvedt, T., Gordon, J. I. (2002) How host-microbial interactions shape the nutrient environment of the mammalian intestine. *Annu Rev Nutr* 22, 283-307.
24. Reeves, A. R., D'Elia, J. N., Frias, J., Salyers, A. A. (1996) A *Bacteroides thetaiotaomicron* outer membrane protein that is essential for utilization of maltooligosaccharides and starch. *Journal of bacteriology* 178, 823-830.
25. Reeves, A. R., Wang, G. R., Salyers, A. A. (1997) Characterization of four outer membrane proteins that play a role in utilization of starch by *Bacteroides thetaiotaomicron*. *Journal of bacteriology* 179, 643-649.
26. Smith, P. M., Howitt, M. R., Panikov, N., Michaud, M., Gallini, C. A., *et al.* (2013) The microbial metabolites, short-chain fatty acids, regulate colonic Treg cell homeostasis. *Science* 341, 569-573.
27. Duncan, S. H., Louis, P., Flint, H. J. (2004) Lactate-utilizing bacteria, isolated from human feces, that produce butyrate as a major fermentation product. *Applied and environmental microbiology* 70, 5810-5817.
28. Bourriaud, C., Robins, R. J., Martin, L., Kozlowski, F., Tenailleau, E., *et al.* (2005) Lactate is mainly fermented to butyrate by human intestinal microfloras but inter-individual variation is evident. *Journal of applied microbiology* 99, 201-212.
29. Sears, C. L., Islam, S., Saha, A., Arjumand, M., Alam, N. H., *et al.* (2008) Association of enterotoxigenic *Bacteroides fragilis* infection with inflammatory diarrhea. *Clinical infectious diseases : an official publication of the Infectious Diseases Society of America* 47, 797-803.
30. Stappenbeck, T. S., Hooper, L. V., Gordon, J. I. (2002) Developmental regulation of intestinal angiogenesis by indigenous microbes via Paneth cells. *Proc Natl Acad Sci U S A* 99, 15451-15455.
31. Dickson, R. P., Erb-Downward, J. R., Huffnagle, G. B. (2013) The role of the bacterial microbiome in lung disease. *Expert review of respiratory medicine* 7, 245-257.
32. Marsland, B. J., Yadava, K., Nicod, L. P. (2013) The airway microbiome and disease. *Chest* 144, 632-637.
33. Herbst, T., Sichelstiel, A., Schar, C., Yadava, K., Burki, K., *et al.* (2011) Dysregulation of allergic airway inflammation in the absence of microbial colonization. *American journal of respiratory and critical care medicine* 184, 198-205.
34. Dutilh, B. E., Cassman, N., McNair, K., Sanchez, S. E., Silva, G. G., *et al.* (2014) A highly abundant bacteriophage discovered in the unknown sequences of human faecal metagenomes. *Nature communications* 5, 4498.
35. Minot, S., Sinha, R., Chen, J., Li, H., Keilbaugh, S. A., *et al.* (2011) The human gut virome: inter-individual variation and dynamic response to diet. *Genome research* 21, 1616-1625.

36. Coombes, J. L. and Powrie, F. (2008) Dendritic cells in intestinal immune regulation. *Nat Rev Immunol* 8, 435-446.
37. Stumbles, P. A., Thomas, J. A., Pimm, C. L., Lee, P. T., Venaille, T. J., *et al.* (1998) Resting respiratory tract dendritic cells preferentially stimulate T helper cell type 2 (Th2) responses and require obligatory cytokine signals for induction of Th1 immunity. *The Journal of experimental medicine* 188, 2019-2031.
38. Schulz, O., Jaensson, E., Persson, E. K., Liu, X., Worbs, T., *et al.* (2009) Intestinal CD103+, but not CX3CR1+, antigen sampling cells migrate in lymph and serve classical dendritic cell functions. *The Journal of experimental medicine* 206, 3101-3114.
39. Laffont, S., Siddiqui, K. R., Powrie, F. (2010) Intestinal inflammation abrogates the tolerogenic properties of MLN CD103+ dendritic cells. *European journal of immunology* 40, 1877-1883.
40. Murai, M., Turovskaya, O., Kim, G., Madan, R., Karp, C. L., *et al.* (2009) Interleukin 10 acts on regulatory T cells to maintain expression of the transcription factor Foxp3 and suppressive function in mice with colitis. *Nat Immunol* 10, 1178-1184.
41. Jakubzick, C., Tacke, F., Llodra, J., van Rooijen, N., Randolph, G. J. (2006) Modulation of dendritic cell trafficking to and from the airways. *J Immunol* 176, 3578-3584.
42. Thorley, A. J., Ford, P. A., Giembycz, M. A., Goldstraw, P., Young, A., *et al.* (2007) Differential regulation of cytokine release and leukocyte migration by lipopolysaccharide-stimulated primary human lung alveolar type II epithelial cells and macrophages. *J Immunol* 178, 463-473.
43. Westphalen, K., Gusarova, G. A., Islam, M. N., Subramanian, M., Cohen, T. S., *et al.* (2014) Sessile alveolar macrophages communicate with alveolar epithelium to modulate immunity. *Nature* 506, 503-506.
44. Otte, J. M., Rosenberg, I. M., Podolsky, D. K. (2003) Intestinal myofibroblasts in innate immune responses of the intestine. *Gastroenterology* 124, 1866-1878.
45. Wynn, T. A. (2008) Cellular and molecular mechanisms of fibrosis. *J Pathol* 214, 199-210.
46. Wynn, T. A. (2011) Integrating mechanisms of pulmonary fibrosis. *The Journal of experimental medicine* 208, 1339-1350.
47. Wynn, T. A. and Ramalingam, T. R. (2012) Mechanisms of fibrosis: therapeutic translation for fibrotic disease. *Nat Med* 18, 1028-1040.
48. Gribar, S. C., Richardson, W. M., Sodhi, C. P., Hackam, D. J. (2008) No longer an innocent bystander: epithelial toll-like receptor signaling in the development of mucosal inflammation. *Mol Med* 14, 645-659.
49. Vaishnava, S., Behrendt, C. L., Ismail, A. S., Eckmann, L., Hooper, L. V. (2008) Paneth cells directly sense gut commensals and maintain homeostasis at the intestinal host-microbial interface. *Proc Natl Acad Sci U S A* 105, 20858-20863.
50. Elinav, E., Henao-Mejia, J., Flavell, R. A. (2013) Integrative inflammasome activity in the regulation of intestinal mucosal immune responses. *Mucosal Immunol* 6, 4-13.
51. Elinav, E., Strowig, T., Kau, A. L., Henao-Mejia, J., Thaiss, C. A., *et al.* (2011) NLRP6 inflammasome regulates colonic microbial ecology and risk for colitis. *Cell* 145, 745-757.
52. Nordlander, S., Pott, J., Maloy, K. J. (2013) NLR4 expression in intestinal epithelial cells mediates protection against an enteric pathogen. *Mucosal Immunol*.
53. Song-Zhao, G. X., Srinivasan, N., Pott, J., Baban, D., Frankel, G., *et al.* (2013) Nlrp3 activation in the intestinal epithelium protects against a mucosal pathogen. *Mucosal Immunol*.

54. Akira, S. and Takeda, K. (2004) Toll-like receptor signalling. *Nat Rev Immunol* 4, 499-511.
55. Abreu, M. T. (2010) Toll-like receptor signalling in the intestinal epithelium: how bacterial recognition shapes intestinal function. *Nature reviews Immunology* 10, 131-144.
56. Schroder, K. and Tschopp, J. (2010) The inflammasomes. *Cell* 140, 821-832.
57. Allen, I. C., Scull, M. A., Moore, C. B., Holl, E. K., McElvania-TeKippe, E., *et al.* (2009) The NLRP3 inflammasome mediates in vivo innate immunity to influenza A virus through recognition of viral RNA. *Immunity* 30, 556-565.
58. Allen, I. C., Wilson, J. E., Schneider, M., Lich, J. D., Roberts, R. A., *et al.* (2012) NLRP12 suppresses colon inflammation and tumorigenesis through the negative regulation of noncanonical NF-kappaB signaling. *Immunity* 36, 742-754.
59. Villani, A. C., Lemire, M., Fortin, G., Louis, E., Silverberg, M. S., *et al.* (2009) Common variants in the NLRP3 region contribute to Crohn's disease susceptibility. *Nature genetics* 41, 71-76.
60. Bauernfeind, F. G., Horvath, G., Stutz, A., Alnemri, E. S., MacDonald, K., *et al.* (2009) Cutting edge: NF-kappaB activating pattern recognition and cytokine receptors license NLRP3 inflammasome activation by regulating NLRP3 expression. *Journal of immunology (Baltimore, Md : 1950)* 183, 787-791.
61. Duewell, P., Kono, H., Rayner, K. J., Sirois, C. M., Vladimer, G., *et al.* (2010) NLRP3 inflammasomes are required for atherogenesis and activated by cholesterol crystals. *Nature* 464, 1357-1361.
62. Wen, H., Gris, D., Lei, Y., Jha, S., Zhang, L., *et al.* (2011) Fatty acid-induced NLRP3-ASC inflammasome activation interferes with insulin signaling. *Nat Immunol* 12, 408-415.
63. Cassel, S. L., Eisenbarth, S. C., Iyer, S. S., Sadler, J. J., Colegio, O. R., *et al.* (2008) The Nalp3 inflammasome is essential for the development of silicosis. *Proc Natl Acad Sci U S A* 105, 9035-9040.
64. Dostert, C., Petricelli, V., Van Bruggen, R., Steele, C., Mossman, B. T., *et al.* (2008) Innate immune activation through Nalp3 inflammasome sensing of asbestos and silica. *Science* 320, 674-677.
65. Hornung, V., Bauernfeind, F., Halle, A., Samstad, E. O., Kono, H., *et al.* (2008) Silica crystals and aluminum salts activate the NALP3 inflammasome through phagosomal destabilization. *Nat Immunol* 9, 847-856.
66. Kaser, A., Zeissig, S., Blumberg, R. S. (2010) Inflammatory bowel disease. *Annual review of immunology* 28, 573-621.
67. Kishimoto, T. (2006) Interleukin-6: discovery of a pleiotropic cytokine. *Arthritis research & therapy* 8 Suppl 2, S2.
68. Dinarello, C. A. (2009) Immunological and inflammatory functions of the interleukin-1 family. *Annual review of immunology* 27, 519-550.
69. Tracey, K. J. and Cerami, A. (1994) Tumor necrosis factor: a pleiotropic cytokine and therapeutic target. *Annu Rev Med* 45, 491-503.
70. Afzali, B., Lombardi, G., Lechler, R. I., Lord, G. M. (2007) The role of T helper 17 (Th17) and regulatory T cells (Treg) in human organ transplantation and autoimmune disease. *Clinical and experimental immunology* 148, 32-46.
71. Mosmann, T. R. and Coffman, R. L. (1989) TH1 and TH2 cells: different patterns of lymphokine secretion lead to different functional properties. *Annual review of immunology* 7, 145-173.

72. Barnes, P. J. (2004) Mediators of chronic obstructive pulmonary disease. *Pharmacological reviews* 56, 515-548.
73. Mantovani, A., Cassatella, M. A., Costantini, C., Jaillon, S. (2011) Neutrophils in the activation and regulation of innate and adaptive immunity. *Nat Rev Immunol* 11, 519-531.
74. Murray, P. J. and Wynn, T. A. (2011) Protective and pathogenic functions of macrophage subsets. *Nat Rev Immunol* 11, 723-737.
75. Snelgrove, R. J., Jackson, P. L., Hardison, M. T., Noerager, B. D., Kinloch, A., *et al.* (2010) A critical role for LTA4H in limiting chronic pulmonary neutrophilic inflammation. *Science* 330, 90-94.
76. Borregaard, N. (2010) Neutrophils, from marrow to microbes. *Immunity* 33, 657-670.
77. Jozsef, L., Zouki, C., Petasis, N. A., Serhan, C. N., Filep, J. G. (2002) Lipoxin A4 and aspirin-triggered 15-epi-lipoxin A4 inhibit peroxynitrite formation, NF-kappa B and AP-1 activation, and IL-8 gene expression in human leukocytes. *Proc Natl Acad Sci U S A* 99, 13266-13271.
78. Faurischou, M. and Borregaard, N. (2003) Neutrophil granules and secretory vesicles in inflammation. *Microbes and infection / Institut Pasteur* 5, 1317-1327.
79. Smith, P. D., Smythies, L. E., Shen, R., Greenwell-Wild, T., Gliozzi, M., *et al.* (2011) Intestinal macrophages and response to microbial encroachment. *Mucosal Immunol* 4, 31-42.
80. Mosser, D. M. and Edwards, J. P. (2008) Exploring the full spectrum of macrophage activation. *Nat Rev Immunol* 8, 958-969.
81. Walker, J. A., Barlow, J. L., McKenzie, A. N. (2013) Innate lymphoid cells--how did we miss them? *Nat Rev Immunol* 13, 75-87.
82. Buonocore, S., Ahern, P. P., Uhlig, H. H., Ivanov, I., Littman, D. R., *et al.* (2010) Innate lymphoid cells drive interleukin-23-dependent innate intestinal pathology. *Nature* 464, 1371-1375.
83. Chang, Y. J., Kim, H. Y., Albacker, L. A., Baumgarth, N., McKenzie, A. N., *et al.* (2011) Innate lymphoid cells mediate influenza-induced airway hyper-reactivity independently of adaptive immunity. *Nat Immunol* 12, 631-638.
84. Gazit, R., Gruda, R., Elboim, M., Arnon, T. I., Katz, G., *et al.* (2006) Lethal influenza infection in the absence of the natural killer cell receptor gene *Ncr1*. *Nat Immunol* 7, 517-523.
85. Kronenberg, M. and Gapin, L. (2002) The unconventional lifestyle of NKT cells. *Nat Rev Immunol* 2, 557-568.
86. Nagarajan, N. A. and Kronenberg, M. (2007) Invariant NKT cells amplify the innate immune response to lipopolysaccharide. *J Immunol* 178, 2706-2713.
87. Akbari, O., Faul, J. L., Hoyte, E. G., Berry, G. J., Wahlstrom, J., *et al.* (2006) CD4+ invariant T-cell-receptor+ natural killer T cells in bronchial asthma. *The New England journal of medicine* 354, 1117-1129.
88. Nieuwenhuis, E. E., Matsumoto, T., Exley, M., Schleipman, R. A., Glickman, J., *et al.* (2002) CD1d-dependent macrophage-mediated clearance of *Pseudomonas aeruginosa* from lung. *Nat Med* 8, 588-593.
89. Tupin, E., Kinjo, Y., Kronenberg, M. (2007) The unique role of natural killer T cells in the response to microorganisms. *Nature reviews. Microbiology* 5, 405-417.
90. De Winter, B. Y., van den Wijngaard, R. M., de Jonge, W. J. (2012) Intestinal mast cells in gut inflammation and motility disturbances. *Biochim Biophys Acta* 1822, 66-73.

91. Wick, G., Grundtman, C., Mayerl, C., Wimpissinger, T. F., Feichtinger, J., *et al.* (2013) The immunology of fibrosis. *Annual review of immunology* 31, 107-135.
92. Miyazawa, S., Hotta, O., Doi, N., Natori, Y., Nishikawa, K., *et al.* (2004) Role of mast cells in the development of renal fibrosis: use of mast cell-deficient rats. *Kidney international* 65, 2228-2237.
93. Malaviya, R., Ikeda, T., Ross, E., Abraham, S. N. (1996) Mast cell modulation of neutrophil influx and bacterial clearance at sites of infection through TNF-alpha. *Nature* 381, 77-80.
94. Galli, S. J., Nakae, S., Tsai, M. (2005) Mast cells in the development of adaptive immune responses. *Nat Immunol* 6, 135-142.
95. Walker, M. M., Warwick, A., Ung, C., Talley, N. J. (2011) The role of eosinophils and mast cells in intestinal functional disease. *Current gastroenterology reports* 13, 323-330.
96. Lambrecht, B. N. and Hammad, H. (2013) Asthma: the importance of dysregulated barrier immunity. *European journal of immunology* 43, 3125-3137.
97. Deckers, J., Branco Madeira, F., Hammad, H. (2013) Innate immune cells in asthma. *Trends in immunology* 34, 540-547.
98. Wakahara, K., Van, V. Q., Baba, N., Begin, P., Rubio, M., *et al.* (2013) Basophils are recruited to inflamed lungs and exacerbate memory Th2 responses in mice and humans. *Allergy* 68, 180-189.
99. Jacobsen, E. A., Zellner, K. R., Colbert, D., Lee, N. A., Lee, J. J. (2011) Eosinophils regulate dendritic cells and Th2 pulmonary immune responses following allergen provocation. *J Immunol* 187, 6059-6068.
100. Al-Haddad, S. and Riddell, R. H. (2005) The role of eosinophils in inflammatory bowel disease. *Gut* 54, 1674-1675.
101. Slack, E., Hapfelmeier, S., Stecher, B., Velykoredko, Y., Stoel, M., *et al.* (2009) Innate and adaptive immunity cooperate flexibly to maintain host-microbiota mutualism. *Science* 325, 617-620.
102. Mora, J. R., Iwata, M., Eksteen, B., Song, S. Y., Junt, T., *et al.* (2006) Generation of gut-homing IgA-secreting B cells by intestinal dendritic cells. *Science* 314, 1157-1160.
103. Lund, F. E., Hollifield, M., Schuer, K., Lines, J. L., Randall, T. D., *et al.* (2006) B cells are required for generation of protective effector and memory CD4 cells in response to *Pneumocystis* lung infection. *J Immunol* 176, 6147-6154.
104. Iwata, M., Hirakiyama, A., Eshima, Y., Kagechika, H., Kato, C., *et al.* (2004) Retinoic acid imprints gut-homing specificity on T cells. *Immunity* 21, 527-538.
105. Kunkel, E. J. and Butcher, E. C. (2003) Plasma-cell homing. *Nature Reviews Immunology* 3, 822-829.
106. Kohlmeier, J. E. and Woodland, D. L. (2006) Memory T cell recruitment to the lung airways. *Curr Opin Immunol* 18, 357-362.
107. Banham, A. H., Powrie, F. M., Suri-Payer, E. (2006) FOXP3+ regulatory T cells: Current controversies and future perspectives. *European journal of immunology* 36, 2832-2836.
108. Sutton, C. E., Lalor, S. J., Sweeney, C. M., Brereton, C. F., Lavelle, E. C., *et al.* (2009) Interleukin-1 and IL-23 induce innate IL-17 production from gammadelta T cells, amplifying Th17 responses and autoimmunity. *Immunity* 31, 331-341.
109. Martin, B., Hirota, K., Cua, D. J., Stockinger, B., Veldhoen, M. (2009) Interleukin-17-producing gammadelta T cells selectively expand in response to pathogen products and environmental signals. *Immunity* 31, 321-330.

110. Lockhart, E., Green, A. M., Flynn, J. L. (2006) IL-17 production is dominated by gammadelta T cells rather than CD4 T cells during Mycobacterium tuberculosis infection. *J Immunol* 177, 4662-4669.
111. Sturm, A. and Dignass, A. U. (2008) Epithelial restitution and wound healing in inflammatory bowel disease. *World journal of gastroenterology : WJG* 14, 348-353.
112. Wynn, T. A. (2007) Common and unique mechanisms regulate fibrosis in various fibroproliferative diseases. *The Journal of clinical investigation* 117, 524-529.
113. van der Flier, L. G. and Clevers, H. (2009) Stem cells, self-renewal, and differentiation in the intestinal epithelium. *Annu Rev Physiol* 71, 241-260.
114. Sun, S., Schiller, J. H., Gazdar, A. F. (2007) Lung cancer in never smokers--a different disease. *Nature reviews. Cancer* 7, 778-790.
115. Irwin, R. S., Augustyn, N., French, C. T., Rice, J., Tedeschi, V., *et al.* (2013) Spread the word about the journal in 2013: from citation manipulation to invalidation of patient-reported outcomes measures to renaming the Clara cell to new journal features. *Chest* 143, 1-4.
116. Camelo, A., Dunmore, R., Sleeman, M. A., Clarke, D. L. (2014) The epithelium in idiopathic pulmonary fibrosis: breaking the barrier. *Frontiers in pharmacology* 4, 173.
117. Beers, M. F. and Morrissey, E. E. (2011) The three R's of lung health and disease: repair, remodeling, and regeneration. *The Journal of clinical investigation* 121, 2065-2073.
118. Crosby, L. M. and Waters, C. M. (2010) Epithelial repair mechanisms in the lung. *Am J Physiol Lung Cell Mol Physiol* 298, L715-731.
119. Ivanov, A. I., Parkos, C. A., Nusrat, A. (2010) Cytoskeletal regulation of epithelial barrier function during inflammation. *Am J Pathol* 177, 512-524.
120. Barbara, G. (2006) Mucosal barrier defects in irritable bowel syndrome. Who left the door open? *Am J Gastroenterol* 101, 1295-1298.
121. Holgate, S. T. (2007) Epithelium dysfunction in asthma. *J Allergy Clin Immunol* 120, 1233-1244; quiz 1245-1236.
122. Barnes, P. J. (2014) Cellular and molecular mechanisms of chronic obstructive pulmonary disease. *Clinics in chest medicine* 35, 71-86.
123. Selman, M. and Pardo, A. (2006) Role of epithelial cells in idiopathic pulmonary fibrosis: from innocent targets to serial killers. *Proc Am Thorac Soc* 3, 364-372.
124. Burisch, J., Jess, T., Martinato, M., Lakatos, P. L., EpiCom, E. (2013) The burden of inflammatory bowel disease in Europe. *Journal of Crohn's & colitis* 7, 322-337.
125. Suenart, P., Bulteel, V., Lemmens, L., Noman, M., Geypens, B., *et al.* (2002) Anti-tumor necrosis factor treatment restores the gut barrier in Crohn's disease. *Am J Gastroenterol* 97, 2000-2004.
126. Slebioda, T. J. and Kmiec, Z. (2014) Tumour necrosis factor superfamily members in the pathogenesis of inflammatory bowel disease. *Mediators of inflammation* 2014, 325129.
127. Sorrentino, D., Nash, P., Viladomiu, M., Hontecillas, R., Bassaganya-Riera, J. (2014) Stopping anti-TNF agents in patients with Crohn's disease in remission: is it a feasible long-term strategy? *Inflam Bowel Dis* 20, 757-766.
128. Kikuchi, H., Itoh, J., Fukuda, S. (2008) Chronic nicotine stimulation modulates the immune response of mucosal T cells to Th1-dominant pattern via nAChR by upregulation of Th1-specific transcriptional factor. *Neuroscience letters* 432, 217-221.

129. Molodecky, N. A., Soon, I. S., Rabi, D. M., Ghali, W. A., Ferris, M., *et al.* (2012) Increasing incidence and prevalence of the inflammatory bowel diseases with time, based on systematic review. *Gastroenterology* 142, 46-54 e42; quiz e30.
130. Bellini, M., Gambaccini, D., Stasi, C., Urbano, M. T., Marchi, S., *et al.* (2014) Irritable bowel syndrome: a disease still searching for pathogenesis, diagnosis and therapy. *World J Gastroentero* 20, 8807-8820.
131. Collins, S. M. (1996) The immunomodulation of enteric neuromuscular function: implications for motility and inflammatory disorders. *Gastroenterology* 111, 1683-1699.
132. Kalff, J. C., Carlos, T. M., Schraut, W. H., Billiar, T. R., Simmons, R. L., *et al.* (1999) Surgically induced leukocytic infiltrates within the rat intestinal muscularis mediate postoperative ileus. *Gastroenterology* 117, 378-387.
133. The, F. O., Boeckxstaens, G. E., Snoek, S. A., Cash, J. L., Bennink, R., *et al.* (2007) Activation of the cholinergic anti-inflammatory pathway ameliorates postoperative ileus in mice. *Gastroenterology* 133, 1219-1228.
134. Tam, C. C., O'Brien, S. J., Tompkins, D. S., Bolton, F. J., Berry, L., *et al.* (2012) Changes in Causes of Acute Gastroenteritis in the United Kingdom Over 15 Years: Microbiologic Findings From 2 Prospective, Population-Based Studies of Infectious Intestinal Disease. *Clinical Infectious Diseases* 54, 1275-1286.
135. Austin, M., Mellow, M., Tierney, W. M. (2014) Fecal Microbiota Transplantation in the Treatment of Clostridium difficile Infections. *Am J Med* 127, 479-483.
136. Global Initiative for Asthma. (2014) <http://www.ginasthma.org>.
137. Holmes, A. M., Solari, R., Holgate, S. T. (2011) Animal models of asthma: value, limitations and opportunities for alternative approaches. *Drug discovery today* 16, 659-670.
138. Hansel, T. T., Johnston, S. L., Openshaw, P. J. (2013) Microbes and mucosal immune responses in asthma. *Lancet* 381, 861-873.
139. Barnes, C. B. and Ulrik, C. S. (2014) Asthma and Adherence to Inhaled Corticosteroids: Current Status and Future Perspectives. *Respiratory care*.
140. World Health Organization. (2014) <http://www.who.int/en/>.
141. Abboud, R. T. and Vimalanathan, S. (2008) Pathogenesis of COPD. Part I. The role of protease-antiprotease imbalance in emphysema. *Int J Tuberc Lung Dis* 12, 361-367.
142. Fischer, B. M., Pavlisko, E., Voynow, J. A. (2011) Pathogenic triad in COPD: oxidative stress, protease-antiprotease imbalance, and inflammation. *Int J Chron Obstruct Pulmon Dis* 6, 413-421.
143. Kadioglu, A., Weiser, J. N., Paton, J. C., Andrew, P. W. (2008) The role of Streptococcus pneumoniae virulence factors in host respiratory colonization and disease. *Nature reviews. Microbiology* 6, 288-301.
144. Ruuskanen, O., Lahti, E., Jennings, L. C., Murdoch, D. R. (2011) Viral pneumonia. *Lancet* 377, 1264-1275.
145. Huaux, F. (2007) New developments in the understanding of immunology in silicosis. *Current opinion in allergy and clinical immunology* 7, 168-173.
146. Friedman, S. L., Sheppard, D., Duffield, J. S., Violette, S. (2013) Therapy for fibrotic diseases: nearing the starting line. *Sci Transl Med* 5, 167sr161.

147. Baumgartner, K. B., Samet, J. M., Coultas, D. B., Stidley, C. A., Hunt, W. C., *et al.* (2000) Occupational and environmental risk factors for idiopathic pulmonary fibrosis: a multicenter case-control study. Collaborating Centers. *Am J Epidemiol* 152, 307-315.
148. Groschwitz, K. R. and Hogan, S. P. (2009) Intestinal barrier function: molecular regulation and disease pathogenesis. *J Allergy Clin Immunol* 124, 3-20; quiz 21-22.
149. Lucas, R., Verin, A. D., Black, S. M., Catravas, J. D. (2009) Regulators of endothelial and epithelial barrier integrity and function in acute lung injury. *Biochem Pharmacol* 77, 1763-1772.
150. Zoz, D. F., Lawson, W. E., Blackwell, T. S. (2011) Idiopathic pulmonary fibrosis: a disorder of epithelial cell dysfunction. *Am J Med Sci* 341, 435-438.
151. Rose, M. C. and Voynow, J. A. (2006) Respiratory tract mucin genes and mucin glycoproteins in health and disease. *Physiological reviews* 86, 245-278.
152. Singer, M., Martin, L. D., Vargaftig, B. B., Park, J., Gruber, A. D., *et al.* (2004) A MARCKS-related peptide blocks mucus hypersecretion in a mouse model of asthma. *Nat Med* 10, 193-196.
153. Van der Sluis, M., De Koning, B. A., De Bruijn, A. C., Velcich, A., Meijerink, J. P., *et al.* (2006) Muc2-deficient mice spontaneously develop colitis, indicating that MUC2 is critical for colonic protection. *Gastroenterology* 131, 117-129.
154. Ju, C. R., Liu, W., Chen, R. C. (2012) Serum surfactant protein D: Biomarker of chronic obstructive pulmonary disease. *Dis Markers* 32, 281-287.
155. Greene, K. E., King, T. E., Kuroki, Y., Bucher-Bartelson, B., Hunninghake, G. W., *et al.* (2002) Serum surfactant proteins-A and -D as biomarkers in idiopathic pulmonary fibrosis. *European Respiratory Journal* 19, 439-446.
156. Arrieta, M. C., Madsen, K., Doyle, J., Meddings, J. (2009) Reducing small intestinal permeability attenuates colitis in the IL10 gene-deficient mouse. *Gut* 58, 41-48.
157. Helbing, T., Herold, E. M., Hornstein, A., Wintrich, S., Heinke, J., *et al.* (2013) Inhibition of BMP activity protects epithelial barrier function in lung injury. *J Pathol* 231, 105-116.
158. Devkota, S., Wang, Y., Musch, M. W., Leone, V., Fehlner-Peach, H., *et al.* (2012) Dietary-fat-induced taurocholic acid promotes pathobiont expansion and colitis in Il10^{-/-} mice. *Nature* 487, 104-108.
159. Ding, S., Chi, M. M., Scull, B. P., Rigby, R., Schwerbrock, N. M., *et al.* (2010) High-fat diet: bacteria interactions promote intestinal inflammation which precedes and correlates with obesity and insulin resistance in mouse. *PLoS One* 5, e12191.
160. Moreira, A. P. B., Texeira, T. F. S., Ferreira, A. B., Peluzio, M. d. C. G., Alfenas, R. d. C. G. (2012) Influence of a high-fat diet on gut microbiota, intestinal permeability and metabolic endotoxaemia. *Br J Nutr* 108, 801-809.
161. Vernia, P., Caprilli, R., Latella, G., Barbetti, F., Magliocca, F. M., *et al.* (1988) Fecal lactate and ulcerative colitis. *Gastroenterology* 95, 1564-1568.
162. Frank, D. N., St Amand, A. L., Feldman, R. A., Boedeker, E. C., Harpaz, N., *et al.* (2007) Molecular-phylogenetic characterization of microbial community imbalances in human inflammatory bowel diseases. *Proc Natl Acad Sci U S A* 104, 13780-13785.
163. Hilty, M., Burke, C., Pedro, H., Cardenas, P., Bush, A., *et al.* (2010) Disordered microbial communities in asthmatic airways. *PLoS One* 5, e8578.

164. Trompette, A., Gollwitzer, E. S., Yadava, K., Sichelstiel, A. K., Sprenger, N., *et al.* (2014) Gut microbiota metabolism of dietary fiber influences allergic airway disease and hematopoiesis. *Nat Med* 20, 159-166.
165. Erb-Downward, J. R., Thompson, D. L., Han, M. K., Freeman, C. M., McCloskey, L., *et al.* (2011) Analysis of the lung microbiome in the "healthy" smoker and in COPD. *PLoS One* 6, e16384.
166. Pragman, A. A., Kim, H. B., Reilly, C. S., Wendt, C., Isaacson, R. E. (2012) The lung microbiome in moderate and severe chronic obstructive pulmonary disease. *PLoS One* 7, e47305.
167. Powrie, F., Leach, M. W., Mauze, S., Menon, S., Caddle, L. B., *et al.* (1994) Inhibition of Th1 responses prevents inflammatory bowel disease in scid mice reconstituted with CD45RBhi CD4+ T cells. *Immunity* 1, 553-562.
168. Saleh, M. and Elson, C. O. (2011) Experimental inflammatory bowel disease: insights into the host-microbiota dialog. *Immunity* 34, 293-302.
169. Cosio, M. G., Saetta, M., Agusti, A. (2009) Immunologic aspects of chronic obstructive pulmonary disease. *The New England journal of medicine* 360, 2445-2454.
170. Asquith, M. J., Boulard, O., Powrie, F., Maloy, K. J. (2010) Pathogenic and Protective Roles of MyD88 in Leukocytes and Epithelial Cells in Mouse Models of Inflammatory Bowel Disease. *Gastroenterology* 139, 519-529.
171. Hugot, J. P., Chamaillard, M., Zouali, H., Lesage, S., Cezard, J. P., *et al.* (2001) Association of NOD2 leucine-rich repeat variants with susceptibility to Crohn's disease. *Nature* 411, 599-603.
172. Pierik, M., Joossens, S., Van Steen, K., Van Schuerbeek, N., Vlietinck, R., *et al.* (2006) Toll-like receptor-1, -2, and -6 polymorphisms influence disease extension in inflammatory bowel diseases. *Inflamm Bowel Dis* 12, 1-8.
173. Matera, M. G., Calzetta, L., Cazzola, M. (2010) TNF-alpha inhibitors in asthma and COPD: we must not throw the baby out with the bath water. *Pulmonary pharmacology & therapeutics* 23, 121-128.
174. Strowig, T., Henao-Mejia, J., Elinav, E., Flavell, R. (2012) Inflammasomes in health and disease. *Nature* 481, 278-286.
175. Denes, A., Lopez-Castejon, G., Brough, D. (2012) Caspase-1: is IL-1 just the tip of the ICEberg? *Cell death & disease* 3, e338.
176. Zosky, G. R. and Sly, P. D. (2007) Animal models of asthma. *Clinical and experimental allergy : journal of the British Society for Allergy and Clinical Immunology* 37, 973-988.
177. Wirtz, S. and Neurath, M. F. (2007) Mouse models of inflammatory bowel disease. *Advanced drug delivery reviews* 59, 1073-1083.
178. Vijay-Kumar, M., Sanders, C. J., Taylor, R. T., Kumar, A., Aitken, J. D., *et al.* (2007) Deletion of TLR5 results in spontaneous colitis in mice. *The Journal of clinical investigation* 117, 3909-3921.
179. Wright, J. L., Cosio, M., Churg, A. (2008) Animal models of chronic obstructive pulmonary disease. *Am J Physiol Lung Cell Mol Physiol* 295, L1-15.
180. Moore, B. B. and Hogaboam, C. M. (2008) Murine models of pulmonary fibrosis. *Am J Physiol Lung Cell Mol Physiol* 294, L152-160.
181. Moeller, A., Ask, K., Warburton, D., Gauldie, J., Kolb, M. (2008) The bleomycin animal model: a useful tool to investigate treatment options for idiopathic pulmonary fibrosis? *Int J Biochem Cell Biol* 40, 362-382.

182. Nasevicius, A. and Ekker, S. C. (2000) Effective targeted gene 'knockdown' in zebrafish. *Nature genetics* 26, 216-220.
183. Sander, J. D., Cade, L., Khayter, C., Reyon, D., Peterson, R. T., *et al.* (2011) Targeted gene disruption in somatic zebrafish cells using engineered TALENs. *Nature biotechnology* 29, 697-698.
184. Hwang, W. Y., Fu, Y., Reyon, D., Maeder, M. L., Tsai, S. Q., *et al.* (2013) Efficient genome editing in zebrafish using a CRISPR-Cas system. *Nature biotechnology* 31, 227-229.
185. White, R. M., Sessa, A., Burke, C., Bowman, T., LeBlanc, J., *et al.* (2008) Transparent adult zebrafish as a tool for in vivo transplantation analysis. *Cell stem cell* 2, 183-189.
186. Lieschke, G. J. and Currie, P. D. (2007) Animal models of human disease: zebrafish swim into view. *Nature reviews. Genetics* 8, 353-367.
187. Trede, N. S., Langenau, D. M., Traver, D., Look, A. T., Zon, L. I. (2004) The use of zebrafish to understand immunity. *Immunity* 20, 367-379.
188. Renshaw, S. A. and Trede, N. S. (2012) A model 450 million years in the making: zebrafish and vertebrate immunity. *Dis Model Mech* 5, 38-47.
189. Lam, S. H., Chua, H. L., Gong, Z., Lam, T. J., Sin, Y. M. (2004) Development and maturation of the immune system in zebrafish, *Danio rerio*: a gene expression profiling, in situ hybridization and immunological study. *Developmental & Comparative Immunology* 28, 9-28.
190. Renshaw, S. A., Loynes, C. A., Elworthy, S., Ingham, P. W., Whyte, M. K. (2007) Modeling inflammation in the zebrafish: how a fish can help us understand lung disease. *Experimental lung research* 33, 549-554.
191. Renshaw, S. A., Loynes, C. A., Trushell, D. M. I., Elworthy, S., Ingham, P. W., *et al.* (2006) A transgenic zebrafish model of neutrophilic inflammation. *Blood* 108, 3976-3978.
192. Hall, C., Flores, M. V., Storm, T., Crosier, K., Crosier, P. (2007) The zebrafish lysozyme C promoter drives myeloid-specific expression in transgenic fish. *BMC Dev Biol* 7, 42.
193. Gray, C., Loynes, C. A., Whyte, M. K., Crossman, D. C., Renshaw, S. A., *et al.* (2011) Simultaneous intravital imaging of macrophage and neutrophil behaviour during inflammation using a novel transgenic zebrafish. *Thromb Haemost* 105, 811-819.
194. Ellett, F., Pase, L., Hayman, J. W., Andrianopoulos, A., Lieschke, G. J. (2011) mpeg1 promoter transgenes direct macrophage-lineage expression in zebrafish. *Blood* 117, e49-56.
195. Balla, K. M., Lugo-Villarino, G., Spitsbergen, J. M., Stachura, D. L., Hu, Y., *et al.* (2010) Eosinophils in the zebrafish: prospective isolation, characterization, and eosinophilia induction by helminth determinants. *Blood* 116, 3944-3954.
196. Langenau, D. M., Ferrando, A. A., Traver, D., Kutok, J. L., Hezel, J. P., *et al.* (2004) In vivo tracking of T cell development, ablation, and engraftment in transgenic zebrafish. *Proc Natl Acad Sci U S A* 101, 7369-7374.
197. Langenau, D. M., Traver, D., Ferrando, A. A., Kutok, J. L., Aster, J. C., *et al.* (2003) Myc-induced T cell leukemia in transgenic zebrafish. *Science* 299, 887-890.
198. Page, D. M., Wittamer, V., Bertrand, J. Y., Lewis, K. L., Pratt, D. N., *et al.* (2013) An evolutionarily conserved program of B-cell development and activation in zebrafish. *Blood* 122, E1-E11.
199. Da'as, S., Teh, E. M., Dobson, J. T., Nasrallah, G. K., McBride, E. R., *et al.* (2011) Zebrafish mast cells possess an Fc ϵ RI-like receptor and participate in innate and adaptive immune responses. *Dev Comp Immunol* 35, 125-134.

200. Dobson, J. T., Seibert, J., Teh, E. M., Da'as, S., Fraser, R. B., *et al.* (2008) Carboxypeptidase A5 identifies a novel mast cell lineage in the zebrafish providing new insight into mast cell fate determination. *Blood* 112, 2969-2972.
201. Meeker, N. D. and Trede, N. S. (2008) Immunology and zebrafish: spawning new models of human disease. *Dev Comp Immunol* 32, 745-757.
202. Willett, C. E., Zapata, A. G., Hopkins, N., Steiner, L. A. (1997) Expression of zebrafish rag genes during early development identifies the thymus. *Dev Biol* 182, 331-341.
203. Yoder, J. A., Turner, P. M., Wright, P. D., Wittamer, V., Bertrand, J. Y., *et al.* (2010) Developmental and tissue-specific expression of NITRs. *Immunogenetics* 62, 117-122.
204. Yoder, J. A., Litman, R. T., Mueller, M. G., Desai, S., Dobrinski, K. P., *et al.* (2004) Resolution of the novel immune-type receptor gene cluster in zebrafish. *Proc Natl Acad Sci U S A* 101, 15706-15711.
205. Mitra, S., Alnabulsi, A., Secombes, C. J., Bird, S. (2010) Identification and characterization of the transcription factors involved in T-cell development, t-bet, stat6 and foxp3, within the zebrafish, *Danio rerio*. *The FEBS journal* 277, 128-147.
206. Lugo-Villarino, G., Balla, K. M., Stachura, D. L., Banuelos, K., Werneck, M. B., *et al.* (2010) Identification of dendritic antigen-presenting cells in the zebrafish. *Proc Natl Acad Sci U S A* 107, 15850-15855.
207. Lin, A. F., Xiang, L. X., Wang, Q. L., Dong, W. R., Gong, Y. F., *et al.* (2009) The DC-SIGN of zebrafish: insights into the existence of a CD209 homologue in a lower vertebrate and its involvement in adaptive immunity. *J Immunol* 183, 7398-7410.
208. Feng, Y., Santoriello, C., Mione, M., Hurlstone, A., Martin, P. (2010) Live imaging of innate immune cell sensing of transformed cells in zebrafish larvae: parallels between tumor initiation and wound inflammation. *PLoS biology* 8, e1000562.
209. Danilova, N., Bussmann, J., Jekosch, K., Steiner, L. A. (2005) The immunoglobulin heavy-chain locus in zebrafish: identification and expression of a previously unknown isotype, immunoglobulin Z. *Nat Immunol* 6, 295-302.
210. Hu, Y. L., Xiang, L. X., Shao, J. Z. (2010) Identification and characterization of a novel immunoglobulin Z isotype in zebrafish: implications for a distinct B cell receptor in lower vertebrates. *Molecular immunology* 47, 738-746.
211. Cannon, J. P., Haire, R. N., Rast, J. P., Litman, G. W. (2004) The phylogenetic origins of the antigen-binding receptors and somatic diversification mechanisms. *Immunological reviews* 200, 12-22.
212. Rombout, J. H., Abelli, L., Picchietti, S., Scapigliati, G., Kiron, V. (2011) Teleost intestinal immunology. *Fish & shellfish immunology* 31, 616-626.
213. Stein, C., Caccamo, M., Laird, G., Leptin, M. (2007) Conservation and divergence of gene families encoding components of innate immune response systems in zebrafish. *Genome biology* 8, R251.
214. van der Vaart, M., Spaink, H. P., Meijer, A. H. (2012) Pathogen recognition and activation of the innate immune response in zebrafish. *Adv Hematol* 2012, 159807.
215. Laing, K. J., Purcell, M. K., Winton, J. R., Hansen, J. D. (2008) A genomic view of the NOD-like receptor family in teleost fish: identification of a novel NLR subfamily in zebrafish. *BMC evolutionary biology* 8, 42.

216. van der Sar, A. M., Stockhammer, O. W., van der Laan, C., Spaik, H. P., Bitter, W., *et al.* (2006) MyD88 innate immune function in a zebrafish embryo infection model. *Infect Immun* 74, 2436-2441.
217. Hall, C., Flores, M. V., Chien, A., Davidson, A., Crosier, K., *et al.* (2009) Transgenic zebrafish reporter lines reveal conserved Toll-like receptor signaling potential in embryonic myeloid leukocytes and adult immune cell lineages. *Journal of leukocyte biology* 85, 751-765.
218. Vojtech, L. N., Scharping, N., Woodson, J. C., Hansen, J. D. (2012) Roles of inflammatory caspases during processing of zebrafish interleukin-1beta in *Francisella noatunensis* infection. *Infect Immun* 80, 2878-2885.
219. Gratacap, R. L., Rawls, J. F., Wheeler, R. T. (2013) Mucosal candidiasis elicits NF-kappaB activation, proinflammatory gene expression and localized neutrophilia in zebrafish. *Disease models & mechanisms* 6, 1260-1270.
220. Brugman, S., Witte, M., Scholman, R. C., Klein, M. R., Boes, M., *et al.* (2014) T lymphocyte-dependent and -independent regulation of Cxcl8 expression in zebrafish intestines. *J Immunol* 192, 484-491.
221. Oehlers, S. H., Flores, M. V., Hall, C. J., O'Toole, R., Swift, S., *et al.* (2010) Expression of zebrafish cxcl8 (interleukin-8) and its receptors during development and in response to immune stimulation. *Dev Comp Immunol* 34, 352-359.
222. Kanther, M., Sun, X., Muhlbauer, M., Mackey, L. C., Flynn, E. J., 3rd, *et al.* (2011) Microbial colonization induces dynamic temporal and spatial patterns of NF-kappaB activation in the zebrafish digestive tract. *Gastroenterology* 141, 197-207.
223. Monson, C. A. and Sadler, K. C. (2010) Inbreeding Depression and Outbreeding Depression Are Evident in Wild-Type Zebrafish Lines. *Zebrafish* 7, 189-197.
224. de Jong, J. L. O., Burns, C. E., Chen, A. T., Pugach, E., Mayhall, E. A., *et al.* (2011) Characterization of immune-matched hematopoietic transplantation in zebrafish. *Blood* 117, 4234-4242.
225. Wallace, K. N., Akhter, S., Smith, E. M., Lorent, K., Pack, M. (2005) Intestinal growth and differentiation in zebrafish. *Mech Dev* 122, 157-173.
226. Ng, A. N., de Jong-Curtain, T. A., Mawdsley, D. J., White, S. J., Shin, J., *et al.* (2005) Formation of the digestive system in zebrafish: III. Intestinal epithelium morphogenesis. *Dev Biol* 286, 114-135.
227. Her, G. M., Chiang, C. C., Wu, J. L. (2004) Zebrafish intestinal fatty acid binding protein (I-FABP) gene promoter drives gut-specific expression in stable transgenic fish. *Genesis* 38, 26-31.
228. Crosnier, C., Vargesson, N., Gschmeissner, S., Ariza-McNaughton, L., Morrison, A., *et al.* (2005) Delta-Notch signalling controls commitment to a secretory fate in the zebrafish intestine. *Development* 132, 1093-1104.
229. Crosnier, C., Stamatakis, D., Lewis, J. (2006) Organizing cell renewal in the intestine: stem cells, signals and combinatorial control. *Nature reviews. Genetics* 7, 349-359.
230. Rawls, J. F., Samuel, B. S., Gordon, J. I. (2004) Gnotobiotic zebrafish reveal evolutionarily conserved responses to the gut microbiota. *Proc Natl Acad Sci U S A* 101, 4596-4601.
231. Semova, I., Carten, J. D., Stombaugh, J., Mackey, L. C., Knight, R., *et al.* (2012) Microbiota regulate intestinal absorption and metabolism of fatty acids in the zebrafish. *Cell Host Microbe* 12, 277-288.
232. Pham, L. N., Kanther, M., Semova, I., Rawls, J. F. (2008) Methods for generating and colonizing gnotobiotic zebrafish. *Nat Protoc* 3, 1862-1875.

233. Bates, J. M., Mittge, E., Kuhlman, J., Baden, K. N., Cheesman, S. E., *et al.* (2006) Distinct signals from the microbiota promote different aspects of zebrafish gut differentiation. *Developmental biology* 297, 374-386.
234. Ferguson, H. W. (2006) *Systemic Pathology of Fish*. Scotian Press.
235. Griffitt, R. J., Weil, R., Hyndman, K. A., Denslow, N. D., Powers, K., *et al.* (2007) Exposure to copper nanoparticles causes gill injury and acute lethality in zebrafish (*Danio rerio*). *Environ Sci Technol* 41, 8178-8186.
236. Rombough, P. (2002) Gills are needed for ionoregulation before they are needed for O₂ uptake in developing zebrafish, *Danio rerio*. *J Exp Biol* 205, 1787-1794.
237. Holinka, C. F., Tseng, Y. C., Finch, C. E. (1978) Prolonged Gestation, Elevated Pre-Parturitional Plasma Progesterone and Reproductive Aging in C57bl-6j Mice. *Biol Reprod* 19, 807-816.
238. Karlsson, L. (1983) Gill morphology of Zebrafish, *Branchydanio rerio*. *Journal of Fish Biology* 23, 511-524.
239. Foskett, J. K., Bern, H. A., Machen, T. E., Conner, M. (1983) Chloride Cells and the Hormonal-Control of Teleost Fish Osmoregulation. *Journal of Experimental Biology* 106, 255-&.
240. Evans, D. H., Piermarini, P. M., Choe, K. P. (2005) The multifunctional fish gill: dominant site of gas exchange, osmoregulation, acid-base regulation, and excretion of nitrogenous waste. *Physiological reviews* 85, 97-177.
241. Chilmonczyk, S. and Monge, D. (1980) Rainbow trout gill pillar cells: demonstration of inert particle phagocytosis and involvement in viral infection. *Journal of the Reticuloendothelial Society* 28, 327-332.
242. Haugarvoll, E., Bjerkas, I., Nowak, B. F., Hordvik, I., Koppang, E. O. (2008) Identification and characterization of a novel intraepithelial lymphoid tissue in the gills of Atlantic salmon. *Journal of anatomy* 213, 202-209.
243. Brooker, R. J. (2011) *Biology text book*. McGraw-Hill.
244. Flores-Lopes, F. and Thomaz, A. T. (2011) Histopathologic alterations observed in fish gills as a tool in environmental monitoring. *Braz J Biol* 71, 179-188.
245. Speare, D. J., Carvajal, V., Horney, B. S. (1999) Growth suppression and branchitis in trout exposed to hydrogen peroxide. *J Comp Pathol* 120, 391-402.
246. Stentiford, G. D., Longshaw, M., Lyons, B. P., Jones, G., Green, M., *et al.* (2003) Histopathological biomarkers in estuarine fish species for the assessment of biological effects of contaminants. *Mar Environ Res* 55, 137-159.
247. Ferguson, H. W., Morrison, D., Ostland, V. E., Lumsden, J., Byrne, P. (1992) Responses of Mucus-Producing Cells in Gill Disease of Rainbow-Trout (*Oncorhynchus-Mykiss*). *Journal of Comparative Pathology* 106, 255-265.
248. Austbo, L., Aas, I. B., Konig, M., Weli, S. C., Syed, M., *et al.* (2014) Transcriptional response of immune genes in gills and the interbranchial lymphoid tissue of Atlantic salmon challenged with infectious salmon anaemia virus. *Dev Comp Immunol* 45, 107-114.
249. Caipang, C. M., Lazado, C. C., Brinchmann, M. F., Kiron, V. (2010) Infection-induced changes in expression of antibacterial and cytokine genes in the gill epithelial cells of Atlantic cod, *Gadus morhua* during incubation with bacterial pathogens. *Comparative biochemistry and physiology. Part B, Biochemistry & molecular biology* 156, 319-325.

250. Oehlers, S. H., Flores, M. V., Hall, C. J., Okuda, K. S., Sison, J. O., *et al.* (2013) Chemically induced intestinal damage models in zebrafish larvae. *Zebrafish* 10, 184-193.
251. Oehlers, S. H., Flores, M. V., Hall, C. J., Crosier, K. E., Crosier, P. S. (2012) Retinoic acid suppresses intestinal mucus production and exacerbates experimental enterocolitis. *Dis Model Mech* 5, 457-467.
252. Oehlers, S. H., Flores, M. V., Okuda, K. S., Hall, C. J., Crosier, K. E., *et al.* (2011) A chemical enterocolitis model in zebrafish larvae that is dependent on microbiota and responsive to pharmacological agents. *Developmental dynamics : an official publication of the American Association of Anatomists* 240, 288-298.
253. Fleming, A., Jankowski, J., Goldsmith, P. (2010) In vivo analysis of gut function and disease changes in a zebrafish larvae model of inflammatory bowel disease: a feasibility study. *Inflamm Bowel Dis* 16, 1162-1172.
254. Brugman, S., Liu, K. Y., Lindenbergh-Kortleve, D., Samsom, J. N., Furuta, G. T., *et al.* (2009) Oxazolone-induced enterocolitis in zebrafish depends on the composition of the intestinal microbiota. *Gastroenterology* 137, 1757-1767 e1751.
255. Goldsmith, J. R., Cocchiaro, J. L., Rawls, J. F., Jobin, C. (2013) Glafenine-induced intestinal injury in zebrafish is ameliorated by mu-opioid signaling via enhancement of Atf6-dependent cellular stress responses. *Disease models & mechanisms* 6, 146-159.
256. Santoriello, C. and Zon, L. I. (2012) Hooked! Modeling human disease in zebrafish. *The Journal of clinical investigation* 122, 2337-2343.
257. Zheng, W., Wang, Z., Collins, J. E., Andrews, R. M., Stemple, D., *et al.* (2011) Comparative transcriptome analyses indicate molecular homology of zebrafish swimbladder and mammalian lung. *PLoS One* 6, e24019.
258. Mosimann, C., Kaufman, C. K., Li, P., Pugach, E. K., Tamplin, O. J., *et al.* (2011) Ubiquitous transgene expression and Cre-based recombination driven by the ubiquitin promoter in zebrafish. *Development* 138, 169-177.
259. Stoletov, K., Fang, L., Choi, S. H., Hartvigsen, K., Hansen, L. F., *et al.* (2009) Vascular lipid accumulation, lipoprotein oxidation, and macrophage lipid uptake in hypercholesterolemic zebrafish. *Circ Res* 104, 952-960.
260. Getz, G. S. and Reardon, C. A. (2006) Diet and murine atherosclerosis. *Arteriosclerosis, thrombosis, and vascular biology* 26, 242-249.
261. Field, H. A., Kelley, K. A., Martell, L., Goldstein, A. M., Serluca, F. C. (2009) Analysis of gastrointestinal physiology using a novel intestinal transit assay in zebrafish. *Neurogastroenterol Motil* 21, 304-312.
262. Walters, J. W., Anderson, J. L., Bittman, R., Pack, M., Farber, S. A. (2012) Visualization of lipid metabolism in the zebrafish intestine reveals a relationship between NPC1L1-mediated cholesterol uptake and dietary fatty acid. *Chem Biol* 19, 913-925.
263. Schloss, P. D., Gevers, D., Westcott, S. L. (2011) Reducing the effects of PCR amplification and sequencing artifacts on 16S rRNA-based studies. *PLoS One* 6, e27310.
264. Parks, D. H. and Beiko, R. G. (2010) Identifying biologically relevant differences between metagenomic communities. *Bioinformatics* 26, 715-721.
265. Langmead, B., Trapnell, C., Pop, M., Salzberg, S. L. (2009) Ultrafast and memory-efficient alignment of short DNA sequences to the human genome. *Genome Biol* 10, R25.

266. Robinson, M. D., McCarthy, D. J., Smyth, G. K. (2010) edgeR: a Bioconductor package for differential expression analysis of digital gene expression data. *Bioinformatics* 26, 139-140.
267. Sangha, N. (2012) Investigating Acute Gastrointestinal Inflammation Associated with Feeding a Fat-Enriched Diet in Zebrafish Larvae. PhD Thesis, Imperial College London.
268. Heno-Mejia, J., Elinav, E., Jin, C., Hao, L., Mehal, W. Z., *et al.* (2012) Inflammasome-mediated dysbiosis regulates progression of NAFLD and obesity. *Nature* 482, 179-185.
269. Cani, P. D., Amar, J., Iglesias, M. A., Poggi, M., Knauf, C., *et al.* (2007) Metabolic endotoxemia initiates obesity and insulin resistance. *Diabetes* 56, 1761-1772.
270. Hou, J. K., Abraham, B., El-Serag, H. (2011) Dietary intake and risk of developing inflammatory bowel disease: a systematic review of the literature. *Am J Gastroenterol* 106, 563-573.
271. Muegge, B. D., Kuczynski, J., Knights, D., Clemente, J. C., Gonzalez, A., *et al.* (2011) Diet drives convergence in gut microbiome functions across mammalian phylogeny and within humans. *Science* 332, 970-974.
272. Wu, G. D., Chen, J., Hoffmann, C., Bittinger, K., Chen, Y. Y., *et al.* (2011) Linking long-term dietary patterns with gut microbial enterotypes. *Science* 334, 105-108.
273. Hara, Y. (2003) Exposure to fatty acids modulates interferon production by intraepithelial lymphocytes. *Immunology Letters* 86, 139-148.
274. Yoshida, H., Miura, S., Kishikawa, H., Hirokawa, M., Nakamizo, H., *et al.* (2001) Fatty acids enhance GRO/CINC-1 and interleukin-6 production in rat intestinal epithelial cells. *The Journal of nutrition* 131, 2943-2950.
275. Suganami, T., Tanimoto-Koyama, K., Nishida, J., Itoh, M., Yuan, X., *et al.* (2007) Role of the Toll-like receptor 4/NF-kappaB pathway in saturated fatty acid-induced inflammatory changes in the interaction between adipocytes and macrophages. *Arteriosclerosis, thrombosis, and vascular biology* 27, 84-91.
276. Oh, D. Y., Talukdar, S., Bae, E. J., Imamura, T., Morinaga, H., *et al.* (2010) GPR120 is an omega-3 fatty acid receptor mediating potent anti-inflammatory and insulin-sensitizing effects. *Cell* 142, 687-698.
277. Lee, J. Y., Plakidas, A., Lee, W. H., Heikkinen, A., Chanmugam, P., *et al.* (2003) Differential modulation of Toll-like receptors by fatty acids: preferential inhibition by n-3 polyunsaturated fatty acids. *Journal of lipid research* 44, 479-486.
278. Fujiyama, Y., Hokari, R., Miura, S., Watanabe, C., Komoto, S., *et al.* (2007) Butter feeding enhances TNF-alpha production from macrophages and lymphocyte adherence in murine small intestinal microvessels. *J Gastroenterol Hepatol* 22, 1838-1845.
279. Ji, Y., Sakata, Y., Tso, P. (2011) Nutrient-induced inflammation in the intestine. *Curr Opin Clin Nutr Metab Care* 14, 315-321.
280. Clifton, J. D., Lucumi, E., Myers, M. C., Napper, A., Hama, K., *et al.* (2010) Identification of novel inhibitors of dietary lipid absorption using zebrafish. *PLoS One* 5, e12386.
281. Hsu, K., Traver, D., Kutok, J. L., Hagen, A., Liu, T. X., *et al.* (2004) The pu.1 promoter drives myeloid gene expression in zebrafish. *Blood* 104, 1291-1297.
282. Lecerf, J.-M. and de Lorgeril, M. (2011) Dietary cholesterol: from physiology to cardiovascular risk. *Br J Nutr* 106, 6-14.
283. Ros, E. (2000) Intestinal absorption of triglyceride and cholesterol. Dietary and pharmacological inhibition to reduce cardiovascular risk. *Atherosclerosis* 151, 357-379.

284. Altmann, S. W., Davis, H. R., Jr., Zhu, L.-J., Yao, X., Hoos, L. M., *et al.* (2004) Niemann-Pick C1 Like 1 protein is critical for intestinal cholesterol absorption. *Science (New York, N Y)* 303, 1201-1204.
285. Betterers, J. L. and Yu, L. (2010) NPC1L1 and cholesterol transport. *FEBS letters* 584, 2740-2747.
286. Seedorf, U., Engel, T., Lueken, A., Bode, G., Lorkowski, S., *et al.* (2004) Cholesterol absorption inhibitor Ezetimibe blocks uptake of oxidized LDL in human macrophages. *Biochem Biophys Res Commun* 320, 1337-1341.
287. Stewart, C. R., Stuart, L. M., Wilkinson, K., van Gils, J. M., Deng, J., *et al.* (2010) CD36 ligands promote sterile inflammation through assembly of a Toll-like receptor 4 and 6 heterodimer. *Nat Immunol* 11, 155-161.
288. Sheedy, F. J., Grebe, A., Rayner, K. J., Kalantari, P., Ramkhelawon, B., *et al.* (2013) CD36 coordinates NLRP3 inflammasome activation by facilitating intracellular nucleation of soluble ligands into particulate ligands in sterile inflammation. *Nat Immunol* 14, 812-820.
289. Karrasch, T., Kim, J.-S., Muhlbauer, M., Magness, S. T., Jobin, C. (2007) Gnotobiotic IL-10^{-/-};NF-kappa B(EGFP) mice reveal the critical role of TLR/NF-kappa B signaling in commensal bacteria-induced colitis. *Journal of immunology (Baltimore, Md : 1950)* 178, 6522-6532.
290. Turnbaugh, P. J., Ridaura, V. K., Faith, J. J., Rey, F. E., Knight, R., *et al.* (2009) The effect of diet on the human gut microbiome: a metagenomic analysis in humanized gnotobiotic mice. *Sci Transl Med* 1, 6ra14.
291. David, L. A., Maurice, C. F., Carmody, R. N., Gootenberg, D. B., Button, J. E., *et al.* (2014) Diet rapidly and reproducibly alters the human gut microbiome. *Nature* 505, 559-563.
292. Sun, Y., Ishibashi, M., Seimon, T., Lee, M., Sharma, S. M., *et al.* (2009) Free cholesterol accumulation in macrophage membranes activates Toll-like receptors and p38 mitogen-activated protein kinase and induces cathepsin K. *Circ Res* 104, 455-465.
293. Ogryzko, N. V., Renshaw, S. A., Wilson, H. L. (2014) The IL-1 family in fish: Swimming through the muddy waters of inflammasome evolution. *Developmental and Comparative Immunology* 46, 53-62.
294. Ogryzko, N. V., Hoggett, E. E., Solaymani-Kohal, S., Tazzyman, S., Chico, T. J., *et al.* (2013) Zebrafish tissue injury causes up-regulation of interleukin-1 and caspase dependent amplification of the inflammatory response. *Dis Model Mech*.
295. Angosto, D., Lopez-Castejon, G., Lopez-Munoz, A., Sepulcre, M. P., Arizcun, M., *et al.* (2012) Evolution of inflammasome functions in vertebrates: Inflammasome and caspase-1 trigger fish macrophage cell death but are dispensable for the processing of IL-1beta. *Innate immunity* 18, 815-824.
296. Franklin, B. S., Bossaller, L., De Nardo, D., Ratter, J. M., Stutz, A., *et al.* (2014) The adaptor ASC has extracellular and 'prionoid' activities that propagate inflammation. *Nat Immunol* 15, 727-737.
297. Xie, C., Zhou, Z. S., Li, N., Bian, Y., Wang, Y. J., *et al.* (2012) Ezetimibe blocks the internalization of NPC1L1 and cholesterol in mouse small intestine. *Journal of lipid research* 53, 2092-2101.
298. Cocchiaro, J. L. and Rawls, J. F. (2013) Microgavage of zebrafish larvae. *J Vis Exp*, e4434.
299. Ichinohe, T., Pang, I. K., Kumamoto, Y., Peaper, D. R., Ho, J. H., *et al.* (2011) Microbiota regulates immune defense against respiratory tract influenza A virus infection. *Proc Natl Acad Sci U S A* 108, 5354-5359.
300. Nadkarni, M. A., Martin, F. E., Jacques, N. A., Hunter, N. (2002) Determination of bacterial load by real-time PCR using a broad-range (universal) probe and primers set. *Microbiology* 148, 257-266.

301. Progzatky, F., Dallman, M. J., Lo Celso, C. (2013) From seeing to believing: labelling strategies for in vivo cell-tracking experiments. *Interface focus* 3, 20130001.
302. Grabarek, J., Amstad, P., Darzynkiewicz, Z. (2002) Use of fluorescently labeled caspase inhibitors as affinity labels to detect activated caspases. *Hum Cell* 15, 1-12.
303. Seiler, C., Davuluri, G., Abrams, J., Byfield, F. J., Janmey, P. A., *et al.* (2012) Smooth muscle tension induces invasive remodeling of the zebrafish intestine. *PLoS biology* 10, e1001386.
304. de Jonge, W. J., van den Wijngaard, R. M., The, F. O., ter Beek, M. L., Bennink, R. J., *et al.* (2003) Postoperative ileus is maintained by intestinal immune infiltrates that activate inhibitory neural pathways in mice. *Gastroenterology* 125, 1137-1147.
305. Ghoshal, S., Witta, J., Zhong, J., de Villiers, W., Eckhardt, E. (2009) Chylomicrons promote intestinal absorption of lipopolysaccharides. *Journal of lipid research* 50, 90-97.
306. Skov, M., Tonnesen, C. K., Hansen, G. H., Danielsen, E. M. (2011) Dietary cholesterol induces trafficking of intestinal Niemann-Pick Type C1 Like 1 from the brush border to endosomes. *Am J Physiol Gastrointest Liver Physiol* 300, G33-40.
307. Masson, C. J., Plat, J., Mensink, R. P., Namiot, A., Kisielewski, W., *et al.* (2010) Fatty acid- and cholesterol transporter protein expression along the human intestinal tract. *PLoS One* 5, e10380.
308. Crawford, P. A., Crowley, J. R., Sambandam, N., Muegge, B. D., Costello, E. K., *et al.* (2009) Regulation of myocardial ketone body metabolism by the gut microbiota during nutrient deprivation. *Proc Natl Acad Sci U S A* 106, 11276-11281.
309. Ley, R. E., Turnbaugh, P. J., Klein, S., Gordon, J. I. (2006) Microbial ecology: human gut microbes associated with obesity. *Nature* 444, 1022-1023.
310. Masumoto, J., Zhou, W., Chen, F. F., Su, F., Kuwada, J. Y., *et al.* (2003) Caspy, a zebrafish caspase, activated by ASC oligomerization is required for pharyngeal arch development. *J Biol Chem* 278, 4268-4276.
311. Muller, P. A., Kosco, B., Rajani, G. M., Stevanovic, K., Berres, M. L., *et al.* (2014) Crosstalk between Muscularis Macrophages and Enteric Neurons Regulates Gastrointestinal Motility. *Cell* 158, 300-313.
312. Kawakami, K., Abe, G., Asada, T., Asakawa, K., Fukuda, R., *et al.* (2010) zTrap: zebrafish gene trap and enhancer trap database. *Bmc Developmental Biology* 10.
313. Hotamisligil, G. S. (2006) Inflammation and metabolic disorders. *Nature* 444, 860-867.
314. Jia, L., Ma, Y., Rong, S., Betters, J. L., Xie, P., *et al.* (2010) Niemann-Pick C1-Like 1 deletion in mice prevents high-fat diet-induced fatty liver by reducing lipogenesis. *Journal of lipid research* 51, 3135-3144.
315. Umemoto, T., Subramanian, S., Ding, Y., Goodspeed, L., Wang, S., *et al.* (2012) Inhibition of intestinal cholesterol absorption decreases atherosclerosis but not adipose tissue inflammation. *Journal of lipid research* 53, 2380-2389.
316. Dancer, R. C., Wood, A. M., Thickett, D. R. (2011) Metalloproteinases in idiopathic pulmonary fibrosis. *The European respiratory journal* 38, 1461-1467.
317. Cowin, A. J., Brosnan, M. P., Holmes, T. M., Ferguson, M. W. (1998) Endogenous inflammatory response to dermal wound healing in the fetal and adult mouse. *Developmental dynamics : an official publication of the American Association of Anatomists* 212, 385-393.

318. Hopkinson-Woolley, J., Hughes, D., Gordon, S., Martin, P. (1994) Macrophage recruitment during limb development and wound healing in the embryonic and foetal mouse. *Journal of Cell Science* 107, 1159-1167.
319. Cowin, A. J., Holmes, T. M., Brosnan, P., Ferguson, M. W. (2001) Expression of TGF-beta and its receptors in murine fetal and adult dermal wounds. *European journal of dermatology : EJD* 11, 424-431.
320. Leask, A. and Abraham, D. J. (2004) TGF-beta signaling and the fibrotic response. *FASEB journal : official publication of the Federation of American Societies for Experimental Biology* 18, 816-827.
321. Martin, P. and Leibovich, S. J. (2005) Inflammatory cells during wound repair: the good, the bad and the ugly. *Trends in cell biology* 15, 599-607.
322. Stramer, B. M., Mori, R., Martin, P. (2007) The inflammation-fibrosis link? A Jekyll and Hyde role for blood cells during wound repair. *J Invest Dermatol* 127, 1009-1017.
323. Martin, P., D'Souza, D., Martin, J., Grose, R., Cooper, L., *et al.* (2003) Wound Healing in the PU.1 Null Mouse—Tissue Repair Is Not Dependent on Inflammatory Cells. *Current Biology* 13, 1122-1128.
324. Mori, R., Shaw, T. J., Martin, P. (2008) Molecular mechanisms linking wound inflammation and fibrosis: knockdown of osteopontin leads to rapid repair and reduced scarring. *The Journal of experimental medicine* 205, 43-51.
325. Peranteau, W. H., Zhang, L., Muvarak, N., Badillo, A. T., Radu, A., *et al.* (2008) IL-10 overexpression decreases inflammatory mediators and promotes regenerative healing in an adult model of scar formation. *J Invest Dermatol* 128, 1852-1860.
326. Liechty, K. W., Kim, H. B., Adzick, N. S., Crombleholme, T. M. (2000) Fetal wound repair results in scar formation in interleukin-10-deficient mice in a syngeneic murine model of scarless fetal wound repair. *J Pediatr Surg* 35, 866-872; discussion 872-863.
327. Frantz, F. W., Bettinger, D. A., Haynes, J. H., Johnson, D. E., Harvey, K. M., *et al.* (1993) Biology of fetal repair: The presence of bacteria in fetal wounds induces an adult-like healing response. *Journal of Pediatric Surgery* 28, 428-434.
328. Godwin, J. W., Pinto, A. R., Rosenthal, N. A. (2013) Macrophages are required for adult salamander limb regeneration. *Proc Natl Acad Sci U S A* 110, 9415-9420.
329. Petrie, T. A., Strand, N. S., Tsung-Yang, C., Rabinowitz, J. S., Moon, R. T. (2014) Macrophages modulate adult zebrafish tail fin regeneration. *Development* 141, 2581-2591.
330. Duffield, J. S., Forbes, S. J., Constandinou, C. M., Clay, S., Partolina, M., *et al.* (2005) Selective depletion of macrophages reveals distinct, opposing roles during liver injury and repair. *The Journal of clinical investigation* 115, 56-65.
331. Eltom, S., Stevenson, C. S., Rastrick, J., Dale, N., Raemdonck, K., *et al.* (2011) P2X7 receptor and caspase 1 activation are central to airway inflammation observed after exposure to tobacco smoke. *PLoS One* 6, e24097.
332. Claussen, C. A. and Long, E. C. (1999) Nucleic Acid recognition by metal complexes of bleomycin. *Chemical reviews* 99, 2797-2816.
333. Schrier, D. J., Kunkel, R. G., Phan, S. H. (1983) The role of strain variation in murine bleomycin-induced pulmonary fibrosis. *Am Rev Respir Dis* 127, 63-66.
334. Mossman, B. T. and Churg, A. (1998) Mechanisms in the pathogenesis of asbestosis and silicosis. *American journal of respiratory and critical care medicine* 157, 1666-1680.

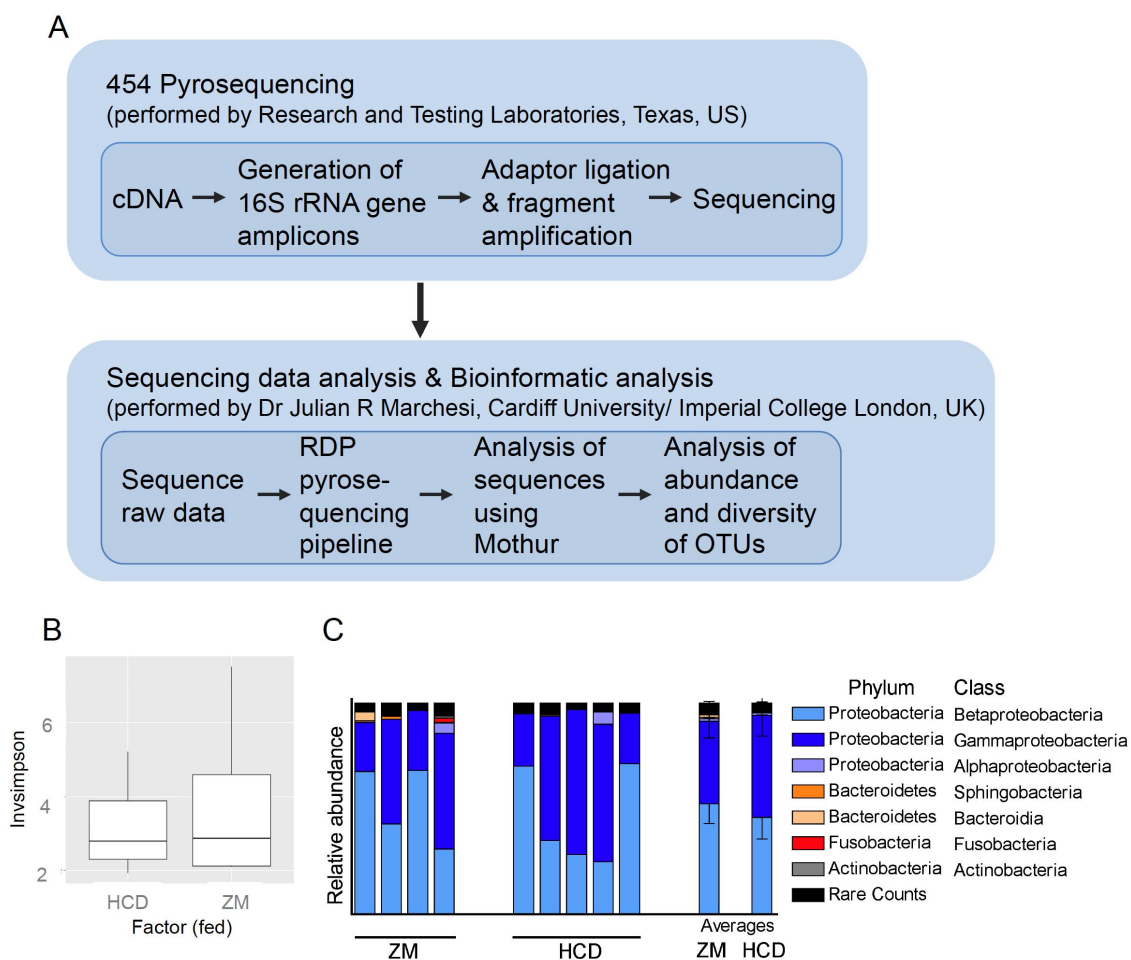
335. Baumgartner, K. B., Samet, J. M., Stidley, C. A., Colby, T. V., Waldron, J. A. (1997) Cigarette smoking: a risk factor for idiopathic pulmonary fibrosis. *American journal of respiratory and critical care medicine* 155, 242-248.
336. Gemberling, M., Bailey, T. J., Hyde, D. R., Poss, K. D. (2013) The zebrafish as a model for complex tissue regeneration. *Trends in Genetics* 29, 611-620.
337. Gonzalez-Rosa, J. M., Martin, V., Peralta, M., Torres, M., Mercader, N. (2011) Extensive scar formation and regression during heart regeneration after cryoinjury in zebrafish. *Development* 138, 1663-1674.
338. Chablais, F., Veit, J., Rainer, G., Jazwinska, A. (2011) The zebrafish heart regenerates after cryoinjury-induced myocardial infarction. *BMC Dev Biol* 11, 21.
339. Richardson, R., Slanchev, K., Kraus, C., Knyphausen, P., Eming, S., *et al.* (2013) Adult Zebrafish as a Model System for Cutaneous Wound-Healing Research. *J Invest Dermatol*.
340. Schnabel, K., Wu, C. C., Kurth, T., Weidinger, G. (2011) Regeneration of cryoinjury induced necrotic heart lesions in zebrafish is associated with epicardial activation and cardiomyocyte proliferation. *PLoS One* 6, e18503.
341. Poss, K. D., Wilson, L. G., Keating, M. T. (2002) Heart Regeneration in Zebrafish. *Science* 298, 2188-2190.
342. Xu, X., Zhang, Y., Williams, J., Antoniou, E., McCombie, W. R., *et al.* (2013) Parallel comparison of Illumina RNA-Seq and Affymetrix microarray platforms on transcriptomic profiles generated from 5-aza-deoxy-cytidine treated HT-29 colon cancer cells and simulated datasets. *BMC bioinformatics* 14 Suppl 9, S1.
343. Mathias, J. R., Dodd, M. E., Walters, K. B., Yoo, S. K., Ranheim, E. A., *et al.* (2009) Characterization of zebrafish larval inflammatory macrophages. *Dev Comp Immunol* 33, 1212-1217.
344. Srivastava, K. D., Rom, W. N., Jagirdar, J., Yie, T. A., Gordon, T., *et al.* (2002) Crucial role of interleukin-1beta and nitric oxide synthase in silica-induced inflammation and apoptosis in mice. *American journal of respiratory and critical care medicine* 165, 527-533.
345. Sharpe, J., Ahlgren, U., Perry, P., Hill, B., Ross, A., *et al.* (2002) Optical projection tomography as a tool for 3D microscopy and gene expression studies. *Science* 296, 541-545.
346. Kumar, S., Alibhai, D., Margineanu, A., Laine, R., Kennedy, G., *et al.* (2011) FLIM FRET technology for drug discovery: automated multiwell-plate high-content analysis, multiplexed readouts and application in situ. *Chemphyschem : a European journal of chemical physics and physical chemistry* 12, 609-626.
347. Le Guellec, D., Morvan-Dubois, G., Sire, J. Y. (2004) Skin development in bony fish with particular emphasis on collagen deposition in the dermis of the zebrafish (*Danio rerio*). *The International journal of developmental biology* 48, 217-231.
348. Doz, E., Noulin, N., Boichot, E., Guenon, I., Fick, L., *et al.* (2008) Cigarette smoke-induced pulmonary inflammation is TLR4/MyD88 and IL-1R1/MyD88 signaling dependent. *J Immunol* 180, 1169-1178.
349. Gonzalez-Rosa, J. M., Peralta, M., Mercader, N. (2012) Pan-epicardial lineage tracing reveals that epicardium derived cells give rise to myofibroblasts and perivascular cells during zebrafish heart regeneration. *Dev Biol* 370, 173-186.
350. Hulsen, T., de Vlieg, J., Alkema, W. (2008) BioVenn - a web application for the comparison and visualization of biological lists using area-proportional Venn diagrams. *BMC genomics* 9, 488.

351. Gurtner, G. C., Werner, S., Barrandon, Y., Longaker, M. T. (2008) Wound repair and regeneration. *Nature* 453, 314-321.
352. Werner, S. and Grose, R. (2003) Regulation of wound healing by growth factors and cytokines. *Physiological reviews* 83, 835-870.
353. Sekine, K., Ohuchi, H., Fujiwara, M., Yamasaki, M., Yoshizawa, T., *et al.* (1999) Fgf10 is essential for limb and lung formation. *Nature genetics* 21, 138-141.
354. Moon, R. T. (2005) Wnt/beta-catenin pathway. *Science's STKE : signal transduction knowledge environment* 2005, cm1.
355. Chilosi, M., Poletti, V., Zamò, A., Lestani, M., Montagna, L., *et al.* (2003) Aberrant Wnt/ β -Catenin Pathway Activation in Idiopathic Pulmonary Fibrosis. *The American Journal of Pathology* 162, 1495-1502.
356. Rock, J. R., Onaitis, M. W., Rawlins, E. L., Lu, Y., Clark, C. P., *et al.* (2009) Basal cells as stem cells of the mouse trachea and human airway epithelium. *Proc Natl Acad Sci U S A* 106, 12771-12775.
357. Dombrowski, Y., Peric, M., Koglin, S., Kammerbauer, C., Goss, C., *et al.* (2011) Cytosolic DNA triggers inflammasome activation in keratinocytes in psoriatic lesions. *Sci Transl Med* 3, 82ra38.
358. Kuipers, M. T., Aslami, H., Janczy, J. R., van der Sluijs, K. F., Vlaar, A. P., *et al.* (2012) Ventilator-induced lung injury is mediated by the NLRP3 inflammasome. *Anesthesiology* 116, 1104-1115.
359. Yucesoy, B., Vallyathan, V., Landsittel, D. P., Sharp, D. S., Matheson, J., *et al.* (2001) Polymorphisms of the IL-1 gene complex in coal miners with silicosis. *American journal of industrial medicine* 39, 286-291.
360. Kinder, B. W., Brown, K. K., Schwarz, M. I., Ix, J. H., Kervitsky, A., *et al.* (2008) Baseline BAL neutrophilia predicts early mortality in idiopathic pulmonary fibrosis. *Chest* 133, 226-232.
361. Chablais, F. and Jazwinska, A. (2012) The regenerative capacity of the zebrafish heart is dependent on TGFbeta signaling. *Development* 139, 1921-1930.
362. Lee, Y., Grill, S., Sanchez, A., Murphy-Ryan, M., Poss, K. D. (2005) Fgf signaling instructs position-dependent growth rate during zebrafish fin regeneration. *Development* 132, 5173-5183.
363. Lepilina, A., Coon, A. N., Kikuchi, K., Holdway, J. E., Roberts, R. W., *et al.* (2006) A dynamic epicardial injury response supports progenitor cell activity during zebrafish heart regeneration. *Cell* 127, 607-619.
364. Jazwinska, A., Badakov, R., Keating, M. T. (2007) Activin-betaA signaling is required for zebrafish fin regeneration. *Current biology : CB* 17, 1390-1395.
365. Kyritsis, N., Kizil, C., Brand, M. (2014) Neuroinflammation and central nervous system regeneration in vertebrates. *Trends in cell biology* 24, 128-135.
366. Kyritsis, N., Kizil, C., Zocher, S., Kroehne, V., Kaslin, J., *et al.* (2012) Acute inflammation initiates the regenerative response in the adult zebrafish brain. *Science* 338, 1353-1356.
367. Cooper, L., Johnson, C., Burslem, F., Martin, P. (2005) Wound healing and inflammation genes revealed by array analysis of 'macrophageless' PU.1 null mice. *Genome Biol* 6, R5.
368. Naik, P. K., Bozyk, P. D., Bentley, J. K., Popova, A. P., Birch, C. M., *et al.* (2012) Periostin promotes fibrosis and predicts progression in patients with idiopathic pulmonary fibrosis. *Am J Physiol Lung Cell Mol Physiol* 303, L1046-1056.

369. Poss, K. D., Shen, J., Nechiporuk, A., McMahon, G., Thisse, B., *et al.* (2000) Roles for Fgf signaling during zebrafish fin regeneration. *Dev Biol* 222, 347-358.
370. Lawson, N. D. and Weinstein, B. M. (2002) In vivo imaging of embryonic vascular development using transgenic zebrafish. *Dev Biol* 248, 307-318.
371. Chua, F., Gauldie, J., Laurent, G. J. (2005) Pulmonary fibrosis: searching for model answers. *Am J Respir Cell Mol Biol* 33, 9-13.
372. Izbicki, G., Segel, M. J., Christensen, T. G., Conner, M. W., Breuer, R. (2002) Time course of bleomycin-induced lung fibrosis. *International journal of experimental pathology* 83, 111-119.
373. Seok, J., Warren, H. S., Cuenca, A. G., Mindrinos, M. N., Baker, H. V., *et al.* (2013) Genomic responses in mouse models poorly mimic human inflammatory diseases. *Proc Natl Acad Sci U S A* 110, 3507-3512.
374. Takao, K. and Miyakawa, T. (2014) Genomic responses in mouse models greatly mimic human inflammatory diseases. *Proc Natl Acad Sci U S A*.
375. Fingerlin, T. E., Murphy, E., Zhang, W., Peljto, A. L., Brown, K. K., *et al.* (2013) Genome-wide association study identifies multiple susceptibility loci for pulmonary fibrosis. *Nature genetics* 45, 613-620.
376. Martin, J. S. and Renshaw, S. A. (2009) Using in vivo zebrafish models to understand the biochemical basis of neutrophilic respiratory disease. *Biochemical Society transactions* 37, 830-837.
377. Ward, A. C. and Lieschke, G. J. (2002) The zebrafish as a model system for human disease. *Frontiers in bioscience : a journal and virtual library* 7, d827-833.
378. Niethammer, P., Grabher, C., Look, A. T., Mitchison, T. J. (2009) A tissue-scale gradient of hydrogen peroxide mediates rapid wound detection in zebrafish. *Nature* 459, 996-999.
379. Yoo, S. K., Freisinger, C. M., LeBert, D. C., Huttenlocher, A. (2012) Early redox, Src family kinase, and calcium signaling integrate wound responses and tissue regeneration in zebrafish. *J Cell Biol* 199, 225-234.
380. Yoo, S. K., Starnes, T. W., Deng, Q., Huttenlocher, A. (2011) Lyn is a redox sensor that mediates leukocyte wound attraction in vivo. *Nature* 480, 109-112.
381. Pase, L., Layton, J. E., Wittmann, C., Ellett, F., Nowell, C. J., *et al.* (2012) Neutrophil-delivered myeloperoxidase dampens the hydrogen peroxide burst after tissue wounding in zebrafish. *Current biology : CB* 22, 1818-1824.
382. Howe, K., Clark, M. D., Torroja, C. F., Torrance, J., Berthelot, C., *et al.* (2013) The zebrafish reference genome sequence and its relationship to the human genome. *Nature* 496, 498-503.
383. Bates, J. M., Akerlund, J., Mittge, E., Guillemin, K. (2007) Intestinal alkaline phosphatase detoxifies lipopolysaccharide and prevents inflammation in zebrafish in response to the gut microbiota. *Cell Host Microbe* 2, 371-382.
384. Kettleborough, R. N., Busch-Nentwich, E. M., Harvey, S. A., Dooley, C. M., de Bruijn, E., *et al.* (2013) A systematic genome-wide analysis of zebrafish protein-coding gene function. *Nature* 496, 494-497.
385. Doyon, Y., McCammon, J. M., Miller, J. C., Faraji, F., Ngo, C., *et al.* (2008) Heritable targeted gene disruption in zebrafish using designed zinc-finger nucleases. *Nature biotechnology* 26, 702-708.
386. Meng, X., Noyes, M. B., Zhu, L. J., Lawson, N. D., Wolfe, S. A. (2008) Targeted gene inactivation in zebrafish using engineered zinc-finger nucleases. *Nature biotechnology* 26, 695-701.

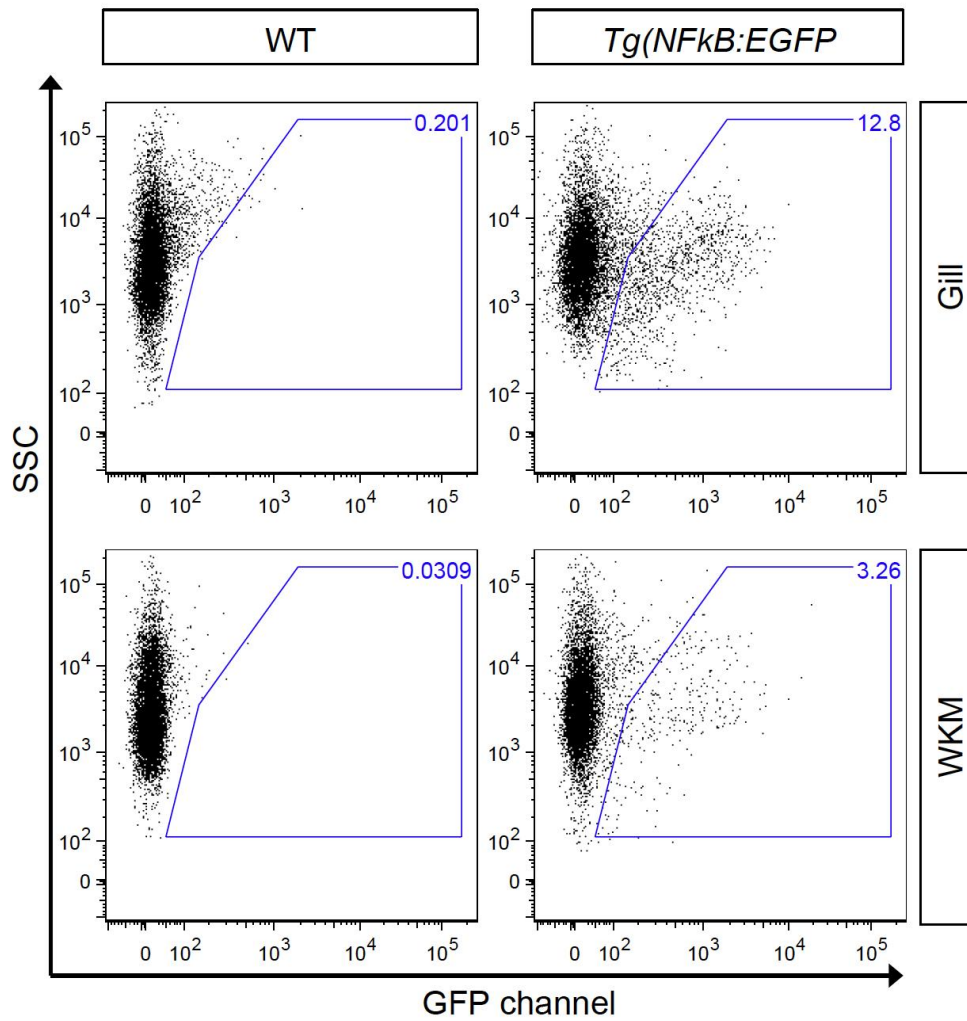
387. Pugach, E. K., Li, P., White, R., Zon, L. (2009) Retro-orbital injection in adult zebrafish. *J Vis Exp*.
388. Hu, N., Yost, H. J., Clark, E. B. (2001) Cardiac morphology and blood pressure in the adult zebrafish. *The Anatomical record* 264, 1-12.
389. Law, S. H. and Sargent, T. D. (2014) The Serine-Threonine Protein Kinase PAK4 Is Dispensable in Zebrafish: Identification of a Morpholino-Generated Pseudophenotype. *PLoS One* 9, e100268.
390. Schulte-Merker, S. and Stainier, D. Y. (2014) Out with the old, in with the new: reassessing morpholino knockdowns in light of genome editing technology. *Development* 141, 3103-3104.
391. Bedell, V. M., Wang, Y., Campbell, J. M., Poshusta, T. L., Starker, C. G., *et al.* (2012) In vivo genome editing using a high-efficiency TALEN system. *Nature* 491, 114-118.
392. Martin, C., Burdon, P. C., Bridger, G., Gutierrez-Ramos, J. C., Williams, T. J., *et al.* (2003) Chemokines acting via CXCR2 and CXCR4 control the release of neutrophils from the bone marrow and their return following senescence. *Immunity* 19, 583-593.
393. Yoo, S. K. and Huttenlocher, A. (2011) Spatiotemporal photolabeling of neutrophil trafficking during inflammation in live zebrafish. *Journal of leukocyte biology* 89, 661-667.
394. Pan, Y. A., Freundlich, T., Weissman, T. A., Schoppik, D., Wang, X. C., *et al.* (2013) Zebrabow: multispectral cell labeling for cell tracing and lineage analysis in zebrafish. *Development* 140, 2835-2846.
395. Livet, J., Weissman, T. A., Kang, H., Draft, R. W., Lu, J., *et al.* (2007) Transgenic strategies for combinatorial expression of fluorescent proteins in the nervous system. *Nature* 450, 56-62.
396. Cani, P. D., Bibiloni, R., Knauf, C., Waget, A., Neyrinck, A. M., *et al.* (2008) Changes in gut microbiota control metabolic endotoxemia-induced inflammation in high-fat diet-induced obesity and diabetes in mice. *Diabetes* 57, 1470-1481.
397. Blackwell, T. S., Blackwell, T. R., Holden, E. P., Christman, B. W., Christman, J. W. (1996) In vivo antioxidant treatment suppresses nuclear factor-kappa B activation and neutrophilic lung inflammation. *J Immunol* 157, 1630-1637.
398. Champagne, D. L., Hoefnagels, C. C., de Kloet, R. E., Richardson, M. K. (2010) Translating rodent behavioral repertoire to zebrafish (*Danio rerio*): relevance for stress research. *Behavioural brain research* 214, 332-342.
399. Perse, M. and Cerar, A. (2012) Dextran sodium sulphate colitis mouse model: traps and tricks. *Journal of biomedicine & biotechnology* 2012, 718617.
400. Huh, D., Matthews, B. D., Mammoto, A., Montoya-Zavala, M., Hsin, H. Y., *et al.* (2010) Reconstituting organ-level lung functions on a chip. *Science* 328, 1662-1668.
401. Sellgren, K. L., Butala, E. J., Gilmour, B. P., Randell, S. H., Grego, S. (2014) A biomimetic multicellular model of the airways using primary human cells. *Lab on a chip* 14, 3349-3358.

Appendices



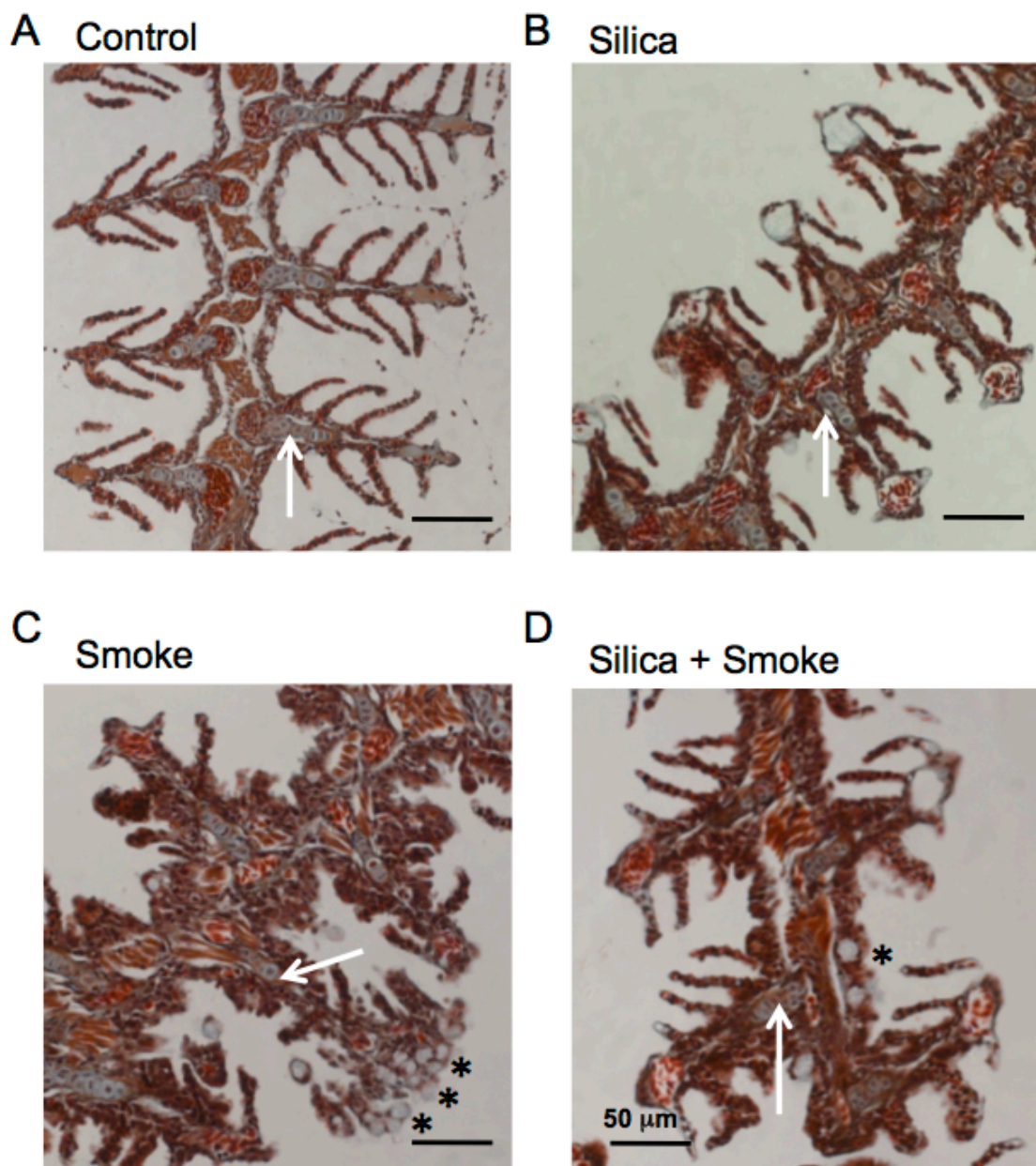
Appendix 1 Effect of HCD on the composition of the commensal microbiota.

Microbiome analysis was performed at the peak of myeloid cell accumulation at 18 hours following ZM or HCD for 6 hours. **(A)** Workflow of 454 pyrosequencing of cDNA samples from intestines. Sample preparation, sequencing and subsequent analysis was performed by Dr Julian R Marchesi (CU, ICL). RDP=Ribosomal Database Project, OTU=Operational taxonomic unit. **(B)** Box plot of the inverse Simpson's alpha index of diversity for the ZM and HCD fed groups, there was no statistical difference between the groups. **(C)** Stacked bar graph showing relative abundance of 16S rRNA gene sequences from different bacterial phyla and classes. (B&C) Each sample is a pool of 20 intestines dissected from larvae fed ZM (n=4) or HCD (n=5).

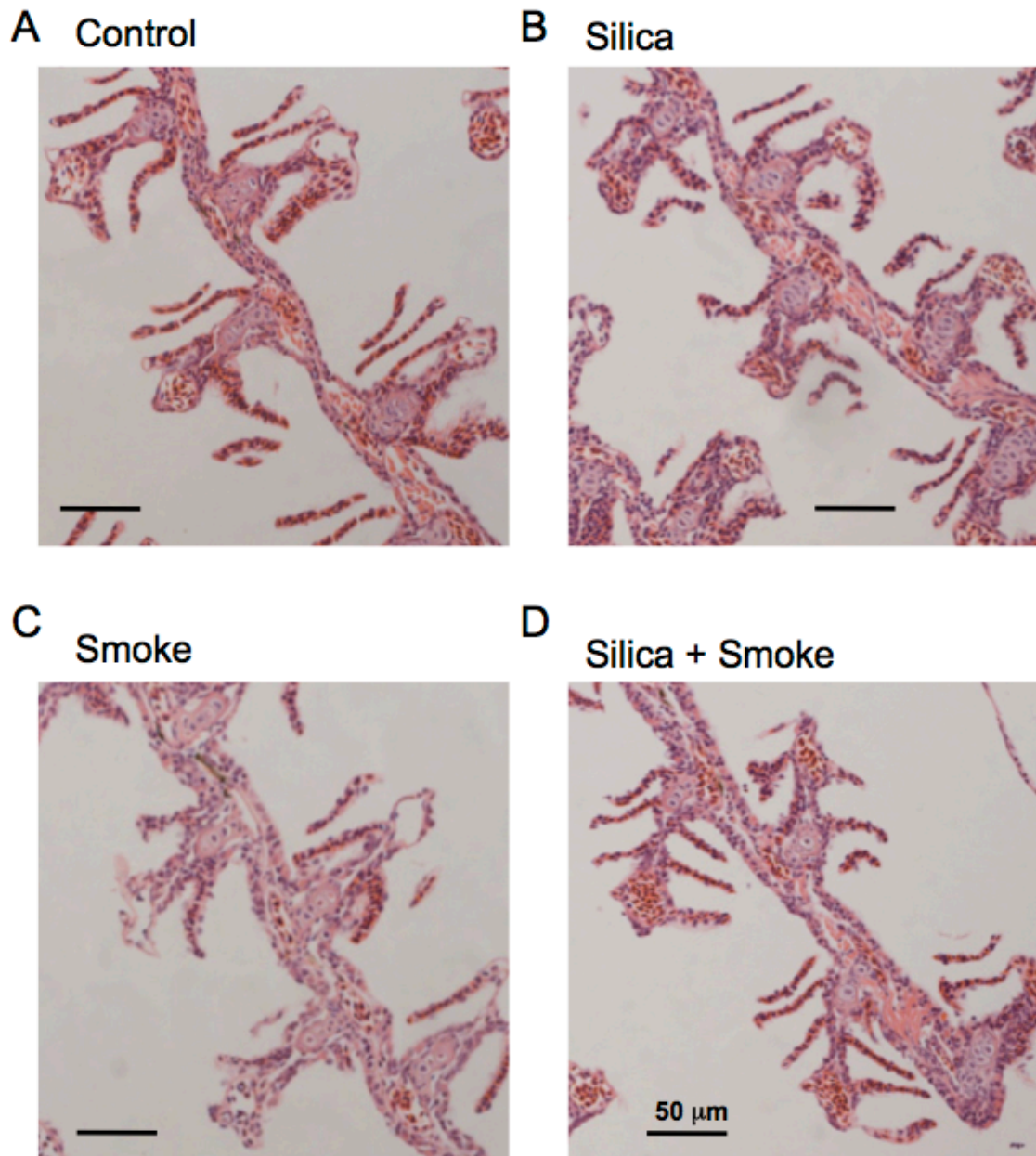


Appendix 2 Analysis of NFkB activation in zebrafish gill at steady state.

Gill tissues (top row) and whole kidney marrow tissues (WKM, bottom row) from WT (left column) and *Tg(NFkB:EGFP)* zebrafish (right column) were dissected, single cell suspensions prepared and analysed by flow cytometry. SSC vs GFP channel dot plots are shown and the gate depict GFP⁺ cells. Representative of n=1.



Appendix 3 Trichrome staining of gill tissue after long-term exposure to silica and cigarette smoke. (A-D) Coronal sections of FFPE zebrafish heads stained with trichrome showing the gills. Fish were exposed to 0.5 mg/L silica or 0.75×10^{-3} c/mL smoke extracts for six hours a day, three days a week, for six weeks. Arrows indicate collagenous structures in a light green colour (A-D) and asterisks indicate mucus cells in smoke and silica + smoke-exposed fish (C&D). Representative images of three experiments are shown.



Appendix 4 Histological analysis of gill tissue after recovery following long-term exposure to silica and cigarette smoke.

(A-D) Coronal sections of FFPE zebrafish heads stained with H&E showing the gills. Fish were exposed to 0.5 mg/L silica or 0.75×10^{-3} c/mL smoke extracts for six hours a day, three days a week, for six weeks and subsequently left to recover in system water for 4 weeks. Representative images of three experiments are shown.